TECHNISCHE UNIVERSITÄT MÜNCHEN

Anorganisch-Chemisches Institut

Late Transition Metal Amido Complexes: Electronic Structure and Reactivity

Björn Birger Askevold

Vollständiger Abdruck der von der Fakultät für Chemie der Technischen Universität München zur Erlangung des akademischen Grades eines

Doktors der Naturwissenschaften (Dr. rer. nat.)

genehmigten Dissertation.

Vorsitzender: Univ.-Prof. Dr. M. Groll

Prüfer der Dissertation:

1. Univ.-Prof. Dr. S. Schneider,
   Georg-August Universität Göttingen

2. Univ.-Prof. Dr. L. Hintermann

3. Univ.-Prof. Dr. K. Köhler

Die Dissertation wurde am 09.05.2012 bei der Technischen Universität München eingereicht und durch die Fakultät für Chemie am 06.06.2012 angenommen.

To my family.
Thanks for all the support,
for having placed your trust in me
and especially for all the love I received,
always and whitout any question.

This thesis originated in the time between January 2009 and April 2012 at the Anorganisch-Chemisches Institut of Technische Universität München and the Friedrich-Alexander-Universität Erlangen-Nürnberg.

I am deeply indebted to my mentor

Professor Dr. Sven Schneider

Thank you for this fascinating topic, your absolute trust in my skills, for the interest which you had in my work and for all these invaluable scientific discussions, which were crucial for the success of this thesis.

I also want to express my gratitude to

Professor Dr. Dr. h. c. mult. Wolfgang A. Herrmann
and
Professor Dr. Karsten Meyer

Thank you very much for the possibility to work in your chair, for the excellent infrastructure which I was allowed to use and for all the support which I was granted.

Abbreviations

Å	angstrom
ACN	acetonitrile
BDE	bond dissociation energy
br	broad
Calcd.	calculated
CO	carbon monoxide
COE	cylcooctene
CV	cyclic voltammetry
DCM	dichloromethane
DFT	density functional theory
DMSO	dimethylsulfoxide
d	doublet
dd	doublet of doublet
δ	chemical shift (ppm)
Eq.	equation
equiv.	equivalent
FT-IR	fourier transform infrared spectroscopy
G	Gibbs energy (J mol^{-1})
H	molar enthalpy (J mol^{-1})
Hz	hertz
HETCOR	heteronuclear correlation, NMR spectroscopic method
HMQC	heteronuclear multiple quantum coherence, NMR spectroscopic method
h	hour(s)
^{i}Pr	isopropyl
J	coupling constant (Hz)
K	equilibrium constant
k	rate constant
KIE	kinetic isotope effect
L	ligand
M	molar (mol L^{-1})
Me	methyl
MHz	megahertz
m	multiplet (NMR), medium (IR)

min	minute(s)
mL	milliliter(s)
μ	micro
NMR	nuclear magnetic resonance
ν	wave number (cm^{-1})
OTf	trifluoromethanfulfonate
PMe_3	trimethylphosphine
Ph	phenyl
PPh_3	triphenylphosphine
ppm	parts per million
q	quarted
R	alkyl or aryl
r	reaction constant
r.d.s	rate determining step
r.t.	room temperature
S	entropy ($J \, mol^{-1} \, K^{-1}$)
s	second(s); singlet (NMR); strong (IR)
sp	septet
THF	tetrahydrofurane
TOF	turnover frequency
TON	turnover number
t	triplet
^{t}Bu	tertiary butyl
vt	virtual triplet
X	halide

Table of Contents

A Introduction

1 Late transition metal amido complexes: metal-ligand bonding and reactivity

In organometallic chemistry considerable effort is being expended on the stabilization and versatile adjustment of the reactivity of the containing metal center, e.g. for the design of homogeneous catalysts. In accordance with Pearson's hard and soft acid and base (HSAB) theory,[1] complexes of early, electron poor transition metals in high oxidation states are well stabilized by covalently bound π-donating ligands, such as alkoxy, oxo, amido, imido or nitrido ligands which adapt for the electronic demand of the high-valent, Lewis acidic metal center.[2] In the 1960s and 1970s, the pioneering studies of Burger, Wannagat, Bradley and Lappart herby established the synthetic strategies and structural motifs of the amido ligand (-NR_2^-) and furthermore explored the reactivity of amido metal bonds.[2a] During the past decades, this type of ligands have developed an increasing dominant role in ligand design due to their unique σ and π donor capabilities and the potential of double substitution at the donor atom.[2b] This development has led to a broad variety of early transition metal complexes with unprecedented reactivity patterns. In contrast, electron rich late transition complexes in low oxidation states (d^6 - d^{10}) with amido ligands were until more recently comparatively rare.[3] Their participation in catalytic transformations, such as C-N coupling reactions, has however stimulated several studies about metal-ligand bonding in late transition metal amido complexes.[4] According to the HSAB theory, a weak $M-NR_2^-$ bonding results for the energetically unfavoured combination of a hard amido ligand with a soft, electron rich metal center.[1] This concept has been useful to explain the relative weakness of the bonding in a qualitative sense.[5] However, bond dissociation energies of M-R (M = Ru^{II}, Pt^{II}; R = alkyl,

---

[1] R. G. Pearson, *J. Am. Chem. Soc.* **1963**, *85*, 3533.

[2] (a) R. Kempe, *Angew. Chem.* **2000**, *112*, 478; *Angew. Chem. Int. Ed.* **2000**, *39*, 468; (b) M. Lappert, P. Power,

A. Protchenko, A. Seeber in *Metal Amide Chemistry*, Wiley, Chichester, **2009**.

[3] a) H. E. Brzynda, W. Tam, *Chem. Rev.* **1988**, *88*, 1163; b) M. D. Fryzuk, C. D. Montgomery, *Coord. Chem.Rev.* **1989**, *95*, 1; b) M. D. Roundhill, *Chem. Rev.* **1992**, *92*, 1; c) R. G. Bergman, *Polyhedron* **1995**, *14*, 3227; d) J. R. Fulton, A. W. Holland, D. J. Fox, R. G. Bergman, *Acc. Chem. Res.* **2002**, *35*, 44; e) T. B. Gunnoe, *Eur.J. Inorg. Chem.* **2007**, 1185.

[4] a) J. F. Hartwig, *Acc. Chem. Res.* **1998**, *31*, 852; b) J. F. Hartwig, *Synlett* **2006**, 1283; c) J. F. Hartwig, *Nature* **2008**, *455*, 314.

[5] R. S. Drago, Applications of Electrostatic-Covalent Models in Chemistry, Surfside, Gainsville, FL. 1994.

aryl, acetylide, hydride, alkoxide and amide)[6] and metal amido hydrogenolysis along the transition series (L_nM-NR_2 + H_2 $\rightleftharpoons$ L_nM-H + HNR_2)[7] provide qualitative information about the M-N bonding, indicating a large polar σ-bond effect which results in a high anionic charge density on the nitrogen atom.[8] The negative charge can be effectively delocalized by N→M π-donation if vacant metal orbitals of suitable symmetry and energy are available, thus triggers a strengthening of the M-N bond.[9] On the other hand, no net M-N π-bond can be established by M-N π-interaction in metal centers without suitable vacant d-orbitals, e.g. in octahedral d^6 or square planar d^8 complexes.[10] The free electron pair at the nitrogen atom can thus not effectively be delocalized, inducing a high basic and nucleophilic character of the amido ligand.[3,11] Hence, similar to main group metal amido complexes, C-N coupling occurs with C-electrophiles such as MeOTf.[11a] Furthermore, weakly acidic molecules, e.g. sp, sp^2, and sp^3 C-H bonds add heterolytically across late transition metal M-N_{amido} bonds.[11b,12] For example, the N-H/D exchange at ruthenium(II) anilido complexes with C_6D_6 e.g. suggests kinetically feasible 1,2-additions of aromatic C-H bonds,[12b] the intramolecular alkane addition was shown in cyclometallation reactions.[12c,d] Fryzuk and co-workers first examined the heterolytic H_2 splitting in their seminal work on late transition amido metal complexes in a series of group 9 and 10 (d^6 and d^8) complexes with the chelating disilylamido PNP pincer ligand $N(SiMe_2CH_2PR_2)_2$.[13] A proton transfer to the amido ligand result upon H_2 heterolysis

[6] H. E. Bryndza, L. K. Fong, R. A. Paciello, W. Tam, J. E. Bercaw, *J. Am. Chem. Soc.* **1987**, *109*, 1444.

[7] J. R. Fulton, A. W. Holland, D. J. Fox, R. G. Bergman, *Acc. Chem. Res.* **2002**, *35*, 44.

[8] P. L. Holland, R. A. Andersen, R. G. Bergman, *Commun. Inorg. Chem.* **1999**, *21*, 115.

[9] L. A. Goj, E. D. Blue, S. A. Delp, T. B. Gunnoe, T. R. Cundari, A. W. Pierpont, J. L. Petersen, P. D. Boyle, *Inorg. Chem.* **2006**, *45*, 9032.

[10] K. G. Caulton, *New J. Chem.* **1994**, *18*, 25.

[11] a) S. Park, A. L. Rheingold, D. M. Roundhill, *Organometallics* **1991**, *10*, 615; b) J. R. Fulton, M. W. Bouwkamp, R. G. Bergman, *J. Am. Chem. Soc.* **2000**, *122*, 8799; c) T. Büttner, F. Breher, H. Grützmacher, *Chem. Commun.* **2004**, 2820; d) P. Maire, F. Breher, H. Schönberg, H. Grützmacher, *Organometallics* **2005**, *24*, 3207; e) T. Büttner, J. Geier, G. Frison, J. Harmer, C. Calle, A. Schweiger, H. Schönberg, H. Grützmacher, *Science* **2005**, *307*, 235.

[12] a) D. Rais, R. G. Bergman, *Chem. Eur. J.* **2004**, *10*, 3970; b) D. Conner, K. N. Jayaprakash, T. R. Cundari, T. B. Gunnoe, *Organometallics* **2004**, *23*, 2724; c) A. N. Walstrom, L. A. Watson, M. Pink, K. G. Caulton, *Organometallics* **2004**, *23*, 4814; d) Y. Feng, M. Lail, N. A. Foley, T. B. Gunnoe, K. A. Barakat, T. R. Cundari, J. L. Petersen, *J. Am. Chem. Soc.* **2006**, *128*, 7982.

[13] a) M. D. Fryzuk, P. A. McNeil, *J. Am. Chem. Soc.* **1981**, *103*, 3592; b) M. D. Fryzuk, P. A. McNeil, *Organometallics* **1983**, *2*, 355; c) M. D. Fryzuk, P. A. McNeil, S. J. Rettig, *Organometallics* **1986**, *5*, 2469.

affording hydrido amine complexes.[14] This extensively studied reaction was later recognized as key step in 'bifunctional' hydrogenation catalysis, denoted initially as 'N-H effect' as well as 'metal-ligand cooperative' or 'Noyori-Morris-type' catalysis.[15,16]
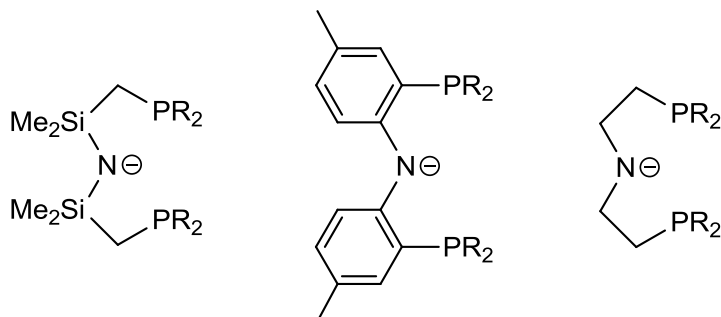
Figure A-1: Amido chelat ligands.

The stabilisation of these late transition metal complexes with disilylamido ligands by Fryzuk points to another common reactivity of this class of compounds: electron rich amido complexes exhibit a strong thermodynamic driving force for extrusion of imines. Accordingly, late transition metal complexes with alkylamido ligands containing β-hydrogen atoms suffer from low thermodynamic stability and typically decompose towards metal hydride complexes.[17] In recent years, different amido ligands without β-hydrogen atoms, e.g. the diarylamido pincer ligand established by Ozerov and co-workers (Figure A-1) were utilized among others to prevent β-hydride-elimination.[18] While the reaction is well

[14] a) M. D. Fryzuk, P. A. McNell, S. J. Rettig, *Organometallics* **1983**, *2*, 682; b) M. D. Fryzuk, P. A. McNeil, *Organometallics* **1985**, *4*, 1145; c) M. D. Fryzuk, P. A. McNeil, S. J. Rettig, *J. Am. Chem. Soc.* **1987**, *109*, 2803.

[15] a) R. Noyori, T. Okhuma, *Angew. Chem.* **2001**, *113*, 40; *Angew. Chem. Int. Ed.* **2001**, *40*, 40; b) S. E. Clapham, A. Hadzovic, R. H. Morris, *Coord. Chem. Rev.* **2004**, *248*, 2201; c) K. Muñiz, *Angew. Chem.* **2005**, *117*, 6780–6785; *Angew. Chem. Int. Ed.* **2005**, *44*, 6622; d) H. Grützmacher, *Angew. Chem.* **2008**, *120*, 1838; *Angew. Chem. Int. Ed.* **2008**, *47*, 1814; e) J. S. M. Samec, J.-E. Bäckvall, P. G. Andersson, P. Brandt, *Chem. Soc. Rev.* **2006**, *35*, 237; f) T. Ikariya, A. J. Blacker, *Acc. Chem. Res.* **2007**, *40*, 1300; g) M. Ito, T. Ikariya, *Chem. Commun.* **2007**, 5134.

[16] S. Schneider, J. Meiners, B. Askevold, *Eur. J. Inorg. Chem.* **2012**, 412.

[17] a) S. E. Diamond, F. Mares, *J. Organomet. Chem.* **1977**, *142*, C55; b) J. F. Hartwig, *J. Am. Chem. Soc.* **1996**, *118*, 7010. c) S. Wagaw, R. A. Rennels, S. L. Buchwald, *J. Am. Chem. Soc.* **1997**, *119*, 8451.

[18] a) O. V. Ozerov, C. Guo, V. A. Papkov, B. M. Foxman, *J. Am. Chem. Soc.* **2004**, *126*, 4792; b) L. Fan, L. Yang, C. Guo, B. M. Foxman, O. V. Ozerov, *Organometallics* **2004**, *23*, 4778; c) W. Weng, C. Guo, C. Muora, L. Yang, B. M. Foxman, O. V. Ozerov, *Organometallics* **2005**, *24*, 3487; d) L. Fan, O. V. Ozerov, *Chem. Commun.* **2005**, 4450; e) L. Fan, S. Parkin, O. V. Ozerov, *J. Am. Chem. Soc.* **2005**, *127*, 16772.

examined for alkyl complexes,[19] only view mechanistic examinations have been reported for the corresponding amido counterparts.[20] Recently, the Ir(III) amides [Ir(H)$_2$(PNP)] (PNP = N(CH$_2$CH$_2$PiPr$_2$)$_2$ and [Ir(H)$_2$(PNN)] (PNN = N(CH$_2$CH$_2$PiPr$_2$)$_2$ (Figure A-1) were presented as rare example for the stabilizing of late transition metal complexes with highly π-acidic dialkylamido ligands, which are active catalysts for the transfer hydrogenation of ketones with 2-propanol.[21] A theoretical study confirmed thereby the participation of the ligand in a proposed Noyori-type mechanism.[21c]

Besides high basicity and nucleophilicity of amido ligands, a mainly *N*-centered HOMO suggests potential ligand redox non-innocence for amido radical complexes. Therefore, the electronic structure should rather be considered by a Lewis formalism as an aminyl (*N*-radical) than an amido (metalloradical) complex (Figure A-2).[22]
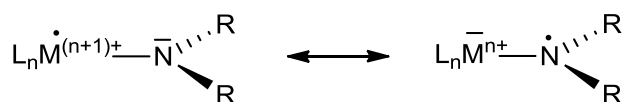
Figure A-2: Canonic Lewis structures for open-shell amido complexes.

The structure of an amido radical complex is albeit important for the reactivity and thus of relevance for catalysis. The enzyme galactose oxidase provides a related example in nature for the catalytic oxidation of alcohols to aldehydes. The overall two-electron redox reaction is accomplished in the active site by a metal- and by a ligand-centered one-electron redox step of the copper phenoxide moiety.[23] Oxidation of a e.g. platinum(II) anilido complex with

[19] a) J. P. Collman, L. S. Hegedus, J. R. Norton, R. G. Finke, In *Principles and Applications of Organotransition Metal Chemistry*, University Science Books, Sausalito, CA, **1987**; b) R. H. Crabtree, In *The Organometallic Chemistry of the Transition Metals*, 3rd ed., Wiley-Interscience, New York, NY, **2001**; c) S. Niu, M. B. Hall, *Chem. Rev.* **2000**, *100*, 353.

[20] a) J. M. Mayer, C. J. Curtis, J. E. Bercaw, *J. Am. Chem. Soc.* **1983**, *105*, 2651; b) Y.-C Tsai, M. J. A. Johnson, D. J. Mindiola, C. C. Cummins, *J. Am. Chem. Soc.* **1999**, *121*, 10426; c) J. Zhao, H. Hesslink, J. F. Hartwig, *J. Am. Chem. Soc.* **2001**, *123*, 7220; e) P. Zhao, J. F. Hartwig, *J. Am. Chem. Soc.* **2005**, *127*, 12066; f) I. Matas, J. Campora, P. Palma, E. Alvarez, *Organometallics* **2009**, *28*, 6515.

[21] a) Z. E. Clarke, P. T. Maragh, T. P. Dasgupta, D. G. Gusev, A. J. Lough, K. Abdur-Rashid, *Organometallics* **2006**, *25*, 4113; b) A. Choualeb, A. J. Lough, D. G. Gusev, *Organometallics* **2007**, *26*, 5224; c) S. Bi, Q. Xie, X. Zhao, Y. Zhao, X. Kong, *J. Organomet. Chem.* **2008**, *693*, 633.

[22] Selected reviews and comments on non-innocent ligands: a) K. Ray, T. Petrenko, K. Wieghardt, F. Neese, *Dalton Trans.* **2007**, 1552; b) R. G. Hicks, *Angew. Chem.* **2008**, *120*, 7503; *Angew. Chem. Int. Ed.* **2008**, *47*, 7393; W. Kaim, *Science* **2005**, *307*, 216; c) W. Kaim, *Inorg. Chem.* **2011**, *50*, 9752.

[23] L. Que Jr., W. B. Tolman, *Nature* **2008**, *455*, 333.

silverhexafluorophosphate results in oxidative *para* C-C coupling of the anilido ligand pointing towards ligand centered radical reactivity.[24] The presence of considerable spin density on the ligand is furthermore confirmed by spectroscopically characterized or even a few isolable persistent late transition metal amido radical complexes.[11e,25,26] Besides, redox chemistry of electron rich amido complexes remains scarcely examined.[16]

These overall observations illustrate a distinct different reactivity of electron rich transition metal complexes with covalently bound π-donor ligands as compared to high valent metal complexes. Their unique properties, application and proposed participation in stoichiometric activation of unreactive bonds or even catalytic reactions have stimulated on the one hand studies of M-E bonding and one the other hand of applied research to afford novel methods for metal mediated catalytic functionalization of organic molecules.

2 Late transition metal amido complexes: relevance for catalysis and MLC

Amido complexes of late transition metals have been successfully applied in several catalytic C-N bond forming reactions. The introduction of these precious metal catalysts in the homogeneous olefin hydroamination represents an interesting alternative to group 4 and lanthanoid based catalysts due to the generally higher functional group tolerance.[27] Two mechanisms are conceivable for this reaction: (1) the olefin is electrophilic activated by coordination of the metal and subsequently attacked by the amine. E.g. hydroamination of olefins catalyzed by electrophilic platinum and palladium complexes proceeds via this route which generally results in Markovnikov addition and is consequently similar to acid catalyzed hydroamination.[27c,28] (2) the olefin inserts after amine oxidative addition into the M-N (or M-

[24] a) N. W. Alcock, R. D. O'Sullivan, A. W. Parkins, *J. Chem. Soc., Chem. Commun.* **1980**, 1216; b) R. D. O'Sullivan, A. W. Parkins, N. W. Alcock, *J. Chem. Soc., Dalton Trans.* **1986**, 571.

[25] a) F. N. Penkert, T. Weyhermüller, E. Bill, P. Hildebrandt, S. Lecomte, K. Wieghardt, *J. Am. Chem. Soc.* **2000**, *122*, 9663. b) D. Adhikari, S. Mossin, F. Basuli, J. C. Huffmann, R. K. Szilagyi, K. Meyer, D. J. Mindiola, *J. Am. Chem. Soc.* **2008**, *130*, 3676.

[26] a) C. Tejel, M. A. Ciriano, M. Pilar del Rio, D. G. H. Hetterscheid, N. Tsichlis i Spithas, J. M. N. Smits, B. de Bruin, *Chem. Eur. J.* **2008**, *14*, 10932; b) C. Tejel, M. P. del Rio, M. A. Ciriano, E. J. Reijerse, F. Hartl, S. Zalis, D. G. H. Hetterscheid, N. Tsichlis I Spithas, B. de Bruin, *Chem. Eur. J.* **2009**, *15*, 11878.

[27] a) T. E. Müller, M. Beller, *Chem. Rev.* **1998**, *98*, 675; b) P. W. Roesky, T. E. Müller, *Angew. Chem.* **2003**, *115*, 2812; *Angew. Chem. Int. Ed.* **2003**, *42*, 2708; c) J. F. Hartwig, *Pure Appl. Chem.* **2004**, *76*, 507; d) K. C. Hultzsch, *Adv. Synth. Catal.* **2005**, *347*, 367.

[28] a) C. Hahn, *Chem Eur. J.* **2004**, *10*, 5888; b) A. M. Johns, M. Utsunomiya, C. D. Incarvito, J. F. Hartwig, *J. Am. Chem. Soc.* **2006**, *128*, 1828; c) B. M. Cochran, F. E. Michael, *J. Am. Chem. Soc.* **2008**, *130*, 2786.

H) bond which is followed by amine reductive elimination. In this case, an *anti*-Markovnikov addition can be expected for the insertion/reductive elimination mechanism, rendering this route particularly interesting due to the potentially different selectivity.[29] However, β-hydride migration from aminoalkyl intermediates is frequently observed prior amine reductive amination affording considerable amounts of side products.[30] The few reported protocols are furthermore highly limited in substrate tolerance.[31]

The electronic structure and the M-E bonding properties of late transition amido complexes results in ligand centered reactivity (s.o.), which renders these compounds as ideal candidates to promote metal-ligand cooperativity (MLC). The participation of such a functional group in the first coordination sphere of the metal center in reversible chemical reactions accelerates absolute and relative rates of bond activation reactions and improves therefore rates and selectivity.[32] This bifunctional (or cooperative) mechanism involves both functional groups of the bifunctional chemical species in the rate-controlling step, affording larger corresponding catalytic coefficient than expected for catalysis by chemical species containing only one of these functional groups.[32b] The pronounced nitrogen centered reactivity of late transition metal amido complexes, such as high basicity and nucleophilicity could be successfully applied in MLC. Noyori obtained tremendously high activities for the hydrogenation and transfer hydrogenation of carbonyl groups with a ruthenium amino pre-catalyst,[33] which was explained by bifunctional mechanisms.[34] Typically, the catalyst is

[29] a) P. Zhao, C. Krug, J. F. Hartwig, *J. Am. Chem. Soc.* **2005**, *127*, 12066; b) J. D. Neukom, N. S. Perch, J. P. Wolfe, *J. Am. Chem. Soc.* **2010**, *132*, 6276; c) P. S. Hanley, D. Markovic, J. F. Hartwig, *J. Am. Chem. Soc.* **2010**, *132*, 6302.

[30] M. Beller, M. Eichberger, H. Trauthwein, *Angew. Chem.* **1997**, *109*, 2306; *Angew. Chem. Int. Ed. Engl.* **1997**, *36*, 2225.

[31] a) A. L. Casalnuovo, J. C. Calabrese, D. Milstein, *J. Am. Chem. Soc.* **1988**, *110*, 6738; b) R. Dorta, P. Egli, F.Züricher, A. Togni, *J. Am. Chem. Soc.* **1997**, *119*, 10857; c) D. Vasen, A. Salzer, F. Gerhards, H.-J. Gais, R. Stürmer, N. H. Bieler, A. Togni, *Organometallics* **2000**, *19*, 539; d) J. Zhou, J. F. Hartwig, *J. Am. Chem. Soc.* **2008**, *130*, 12220.

[32] a) G. J. Rowlands, *Tetrahedron* **2001**, *57*, 1865; b) H. Grützmacher, *Angew. Chem.* **2008**, *120*, 1838; *Angew. Chem. Int. Ed.* **2008**, *47*, 1814; c) D. B. Grotjahn, *Dalton Trans.* **2008**, 6497; d) Y. J. Park, J.-W. Park, C.-H. Jun, *Acc. Chem. Res.* **2008**, *41*, 222; e) J. I. van der Vlugt, J. N. H. Reek, *Angew. Chem.* **2009**, *121*, 8990; *Angew. Chem. Int. Ed.* **2009**, *48*, 8832.

[33] R. Noyori, T. Ohkuma, *Angew. Chem.* **2001**, *113*, 40; *Angew. Chem. Int. Ed.* **2001**, *40*, 40.

[34] a) S. E. Clapham, A. Hadzovic, R. H. Morris, *Coord. Chem. Rev.* **2004**, *248*, 2201; b) K. Muñiz, *Angew. Chem.* **2005**, *117*, 6780; *Angew. Chem. Int. Ed.* **2005**, *44*, 6622; c) J. S. M. Samec, J.-E. Bäckvall, P. G. Andersson, P. Brandt, *Chem. Soc. Rev.* **2006**, *35*, 237.

received by in situ reaction under formation of a hydride complex. This active species reduces the substrate by a concerted, bifunctional proton and hydride transfer from the N-H and Ru-H moieties (Figure A-3).
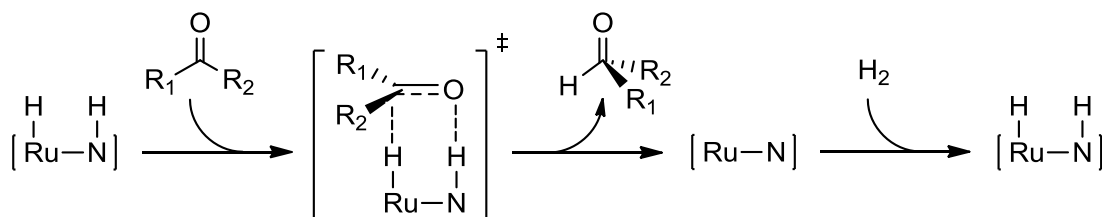
Figure A-3: Detail of the proposed mechanism of the ionic hydrogenation with Noyori-type catalysts: concerted, *bifunctional* proton/hydride transfer to the substrate and catalyst regeneration via non-classical dihydrogen complex.

The utilization of chiral, non racemic catalysts for inasymmetric hydrogenation indicate thereby a highly organized transition state which contributes to an enantioselectiv reaction with high ee's. A near coplanar H-M-N-H *syn*-arrangement is favoured for the transition state and stabilized by intramolecular M-H¨H-N bonding.[35] Regeneration of the catalyst proceeds via an intermediate, non-classical dihydrogen complex by a subsequent proton transfer to the amido moiety. A side-on binding of dihydrogen to the metal atom acidifies the ligand,[36] the heterolytic H_2-activation (with typically higher rates than H_2 oxidative addition) represents the rate determining step of the catalytic cycle.[34a] Experimental and theoretical studies indicate Brønsted-acids and -base assisted H_2 splitting, for example by water, alcohols or alkoxides.[37] To date, a broad variety of MLC hydrogenation catalysts with primary or secondary amine ligands have been reported,[38] few examples even for the reverse reaction, i.e. the oxidation

[35] R. H. Crabtree, P. E. M. Siegbahn, O Eisenstein, A. L. Rheingold, T. H. Koetzle, *Acc. Chem. Res.* **1996**, *29*, 348.

[36] G. J. Kubas, *Chem. Rev.* **2007**, *107*, 4152.

[37] a) R. Hartmann, P. Chen, *Angew. Chem.* **2001**, *113*, 3693; *Angew. Chem. Int. Ed.* **2001**, *40*, 3581; b) M. Ito, M. Hirakawa, K. Murata, T. Ikariya, *Organometallics* **2001**, *20*, 379; c) V. Rautenstrauch, X. Hoang-Cong, R. Churland, K. Abdur-Rashid, R. H. Morris, *Chem. Eur. J.* **2003**, *9*, 4954; d) W. Baratta, K. Siega, P. Rigo, *Chem. Eur. J.* **2007**, *13*, 7479; e) A. Hadzovic, D. Song, C. M. MacLaughlin, R. H. Morris, *Organometallics* **2007**, *26*, 5987; f) A. Friedrich, M. Drees, J. Schmedt auf der Günne, S. Schneider, *J. Am. Chem. Soc.* **2009**, *131*, 17552; g) M. Zimmer-De Iuliis, R. H. Morris, *J. Am. Chem. Soc.* **2009**, *131*, 11263.

[38] Selected recent examples: a) W. Baratta, G. Chelucci, E. Herdtweck, S. Magnolia, K. Siega, P. Rigo, *Angew. Chem.* **2007**, *119*, 7795; *Angew. Chem. Int. Ed.* **2007**, *46*, 7651; b) D. Amoroso, T. W. Graham, R. Guo, C.-W. Tsang, K. Abdur-Rashid, *Aldrichim. Acta* **2008**, *41*, 15; c) A. Mikhailine, A. J. Lough, R. H. Morris, *J. Am. Chem. Soc.* **2009**, *131*, 1394; d) S. D. Phillips, J. A. Fuentes, M. L. Clarke, *Chem. Eur. J.* **2010**, *16*,

of alcohols by acceptorless dehydrogenation to give H_2 and ketones, aldehydes or dehydrocoupling products (e.g. esters).[39,40] The utilization of chelating ligands for MLC helps to suppress amide β-hydrogen elimination.[3a] The formation of imines is however prone for catalyst decomposition in the absence of H_2.[41] A high conformational flexibility of the chelating ligand stabilizes both the pyramidal and planar geometry around the amine and amido nitrogen atom, respectively.[16]

3 Goal and motivation

The initial aim of this thesis was the stabilisation of highly electronically and coordinatively unsaturated late transition metal amido complexes and their utilization for metal-ligand cooperative bond activation. The aliphatic, anionic ethylene bridged PNP ligand $N(CH_2CH_2PR_2)_2$ was chosen to establish a suitable platform for the stabilization and activation of multiple bonded ligands, owing to (1) the chelating effect of the pincer framework and the strong bonding of the phosphine ligands to electron rich metal centers, (2) the possibility for the adjustment of the steric demand of the substituent R, (3) the simple ligand functionalization by oxidation of the ethylene backbone bridge and (4) the highly useful NMR properties of the ^{31}P nucleus (I = 1/2) as a spectroscopic probe[42]. Until more recently, only few studies were reported for the utilization of a dialkylamido PNP ligand in late, electron rich transition metal complexes.[20,43] The synthesis of iridium(I) complexes with a highly electron rich metal center with such a M(PNP) platform was demonstrated in

8002; e) T. Irrgang, D. Friedrich, R. Kempe, *Angew. Chem. Int. Ed.* **2011**, *123*, 2231; *Angew. Chem. Int. Ed.* **2011**, *50*, 2183.

[39] a) J. Zhao, J. F. Hartwig, *Organometallics* **2005**, *24*, 2441-2446; b) N. Andrushko, V. Andrushko, P. Roose, K. Moonen, A. Börner, *ChemCatChem* **2010**, *2*, 640; c) M. Bertoli, A. Choualeb, A. J. Lough, B. Moore, D. Spasyuk, D. G. Gusev, *Organometallics* **2011**, *30*, 3479; d) M. Bertoli, A. Choualeb, D. G. Gusev, A. J. Lough, Q. Major, B. Moore, *Dalton Trans.* **2011**, *40*, 8941; e) M. Nielsen, A. Kammer, D. Cozzula, H. Junge, S. Gladiali, M. Beller, *Angew. Chem.* **2011**, *123*, 9767;

[40] A. Friedrich, S. Schneider, *ChemCatChem* **2009**, *1*, 72.

[41] R. Abbel, K. Abdur-Rashid, M. Faatz, A. Hadzovic, A. J. Lough, R. H. Morris, *J. Am. Chem. Soc.* **2005**, *127*, 1870.

[42] P. S. Pregosin, R. W. Kunz, in *31P and 13C NMR of Transition Metal Phosphine Complexes*, Springer, **1979**.

[43] a) K. Abdur-Rashid, WO2004/096735, **2004**; b) D. Amoroso, T: W. Graham, R. Guo, C. W. Tsang, K. Abdur-Rashid, *Aldrichim. Acta* **2008**, *41*, 15; c) X. Chen, W. Jia, R. Guo, T. W. Graham, M. A. Gullons, K. Abdur-Rashid, *Dalton Trans.* **2009**, 1407.

preliminary work.[44] Additionally, important information about the M-N bonding and reactivity could be obtained by the study of electron rich four-coordinate d_8 palladium complexes, including N-H pK_a values or one-electron oxidation reactions.[45] The expansion to d_6 ruthenium PNP complexes, with the possibility of backbone ligand functionalization to amino, amido, imino and enamido complexes, showed MLC in a reversible, heterolytic H_2 activation at the nitrogen atom and the ligand backbone. Furthermore, the high potential of this Ru(PNP) platform was proven in a highly efficient catalytic acceptorless dehydrogenation of alcohols and borane-amines via a bifunctional mechanism.[46]

The focus of this thesis is the versatile fine-tuning of the electronic properties and reactivities of late transition metal PNP dialkylamido complexes by simple dehydrogenation of the ethylene backbone to control stability and reactivity, with respect to unusual, electronically and coordinatively unsaturated 14 VE complexes as suitable platforms for the stabilization of multiple bonded ligands, e.g. terminal nitrido ligands. The expected high donor ability of the nitrogen atom in combination with possible MLC should be beneficial for the activation of these ligands. The hydrogenolysis of nitrido complexes could thus serve as model compounds to examine ammonia formation en route to a highly desirable homogeneous catalyst for a *Haber-Bosch* like process at ambient conditions.
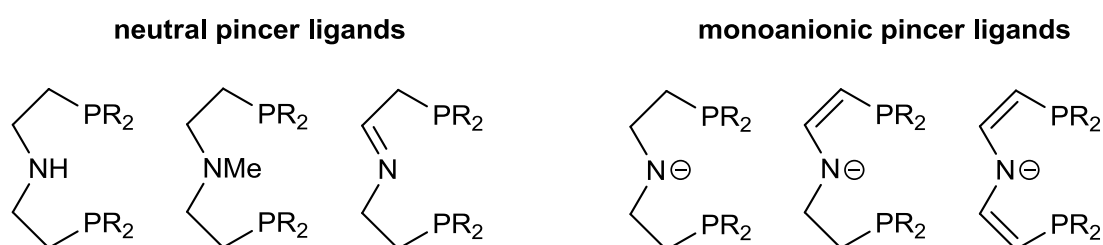
Figure A-4: used PNP pincer ligands.

The coordination chemistry of several ruthenium and iridium complexes with amino, amido, imino, enamido and dienamido ligands will be presented (Figure A-4). The simple ligand backbone functionalization with their impact on donor properties and electronic structure and reactivity of the respective complexes are discussed, particularly with respect to their use for multiple bond stabilization and metal-ligand cooperative activation.

[44] A. Friedrich, *Synthesis and Characterization of Iridium Complexes with chelating Amine and Amido Phosphine Ligands*, diploma thesis, TU München, **2007**.

[45] A. N. Marziale, E. Herdtweck, J. Eppinger, S. Schneider *Inorg. Chem.* **2009**, *48*, 3699.

[46] A. Friedrich, Bifunctional *Transition Metal Amido Complexes: Cooperative H2 Activation and Catalytic Dehydrogenation, disertation*, TU München, **2010**.

B Results and discussion

1 Reactivity of iridium(I) PNP amido complex towards protonation and oxidation

Unpublished results:

B. Askevold, A. Friedrich, E. Herdtweck, A. C. Filippou, S. Schneider

1.1 Introduction

Covalently bound π-donating ligands, e.g. alkoxy, oxo, amido, imido, or nitrido ligands, are frequently used to stabilize complexes of electron poor, early transition metal centers (TM's) in high oxidation states (d^0 - d^4).[1] In contrast, stable, late TM amido complexes in low oxidation states ($d^6 - d^{10}$) are comparatively rare. However, the involvement of such compounds in catalytic processes, such as C-N cross coupling or bifunctional (cooperative) hydrogenation of ketones and imines,[2,3] have stimulated several fundamental studies about M–N bonding and reactivity to rationalize their distinctly different reactivity.[4] The M–N σ-bond polarity results in high anionic charge density on the nitrogen,[5] which is effectively reduced by N$\rightarrow$M π-donation in the case of high valent, early TM's. On the other hand, electron rich metal centers are generally lacking vacant metal orbitals of suitable symmetry and energy for charge delocalization by M–N π-bonding.[6] The reactivity of such compounds can therefore be attributed to the high electron density on the ligand, and *N*-centered nucleophilicity and ligand non-innocence upon oxidation can be expected.[31,7,8] In fact, the few well characterized precious metal amido radical complexes confirm the presence of

[1] a) R. Kempe, *Angew. Chem.* **2000**, *112*, 478; b) M. Lappert, P. Power, A. Protchenko, A. Seeber in *Metal Amide Chemistry*, Wiley, Chichester, **2009**.

[2] a) J.-P. Corbet, G. Mignani, *Chem. Rev.* **2006**, *106*, 2651; b) J. F. Hartwig, *Acc. Chem. Res.* **1998**, *31*, 852; c) J. F. Hartwig, *Synlett* **2006**, 1283; d) J. F. Hartwig, *Nature* **2008**, *455*, 314.

[3] a) R. Noyori, T. Ohkuma, *Angew. Chem. Int. Ed.* **2001**, *40*, 40; b) S. E. Clapham, A. Hadzovic, R. H. Morris, *Coord. Chem. Rev.* **2004**, *248*, 2201; c) K. Muñiz, *Angew. Chem. Int. Ed.* **2005**, *44*, 6622; d) J. S. M. Samec, J.-E. Bäckvall, P. G. Andersson, P. Brandt, *Chem. Soc. Rev.* **2006**, *35*, 237.

[4] a) H. E. Brzynda, W. Tam, *Chem. Rev.* **1988**, *88*, 1163; b) M. D. Fryzuk, C. D. Montgomery, *Coord. Chem. Rev.* **1989**, *95*, 1; c) M. D. Roundhill, *Chem. Rev.* **1992**, *92*, 1; c) R. G. Bergman, *Polyhedron* **1995**, *14*, 3227; d) J. R. Fulton, A. W. Holland, D. J. Fox, R. G. Bergman, *Acc. Chem. Res.* **2002**, *35*, 44; e) T. B. Gunnoe, *Eur. J. Inorg. Chem.* **2007**, 1185.

[5] P. L. Holland, R. A Andersen, R. G. Bergman, *Comm. Inorg. Chem.* **1999**, *21*, 115.

[6] K. G. Caulton, *New J. Chem.* **1994**, *18*, 25.

[7] a) S. Park, A. L. Rheingold, D. M. Roundhill, *Organometallics* **1991**, *10*, 615; b) J. R. Fulton, M. W. Bouwkamp, R. G. Bergman, *J. Am. Chem. Soc.* **2000**, *122*, 8799; c) T. Büttner, F. Breher, H. Grützmacher, *Chem. Commun.* **2004**, 2820; d) P. Maire, F. Breher, H. Schönberg, H. Grützmacher, *Organometallics* **2005**, *24*, 3207; e) T. Büttner, J. Geier, G. Frison, J. Harmer, C. Calle, A. Schweiger, H. Schönberg, H. Grützmacher, *Science* **2005**, *307*, 235.

[8] K. Ray, T. Petrenko, K. Wieghardt, F. Neese, *Dalton Trans.* **2007**, 1552.

considerable spin density on the ligand.[7e,9,10] Accordingly, the radical reactivity of late TM amido complexes has been utilized, e.g. oxidative C-C coupling of anilido ligands or catalytic amine and alcohol oxidation.[11,12,13] While these general reactivity trends with electrophiles and oxidizing agents are well understood, a lack of comprehensive studies is apparent which allow for the estimation of secondary ligand effects.

Anionic, aryl based PCP pincer ligands have been popularized for catalysis owing to the high thermal stability and versatile control over steric and electronic properties.[14] The introduction of amido π-donor groups, such as in disilylamido, diarylamido, or pyridine based PNP pincer ligands, allows for further variation.[4b,15,16,17] However, these ligands are relatively weak π-donors compared with dialkylamides, such as Grützmacher's CNC pincer ligands.[7c,d,e,13] Hence, we set out to explore the chemistry of electron rich complexes with strongly π-basic PNP dialkylamido ligands,[18,19,20] starting from amine ligand

[9] a) F. N. Penkert, T. Weyhermüller, E. Bill, P. Hildebrandt, S. Lecomte, K. Wieghardt, *J. Am. Chem. Soc.* **2000**, *122*, 9663; b) D. Adhikari, S. Mossin, F. Basuli, J. C. Huffmann, R. K. Szilagyi, K. Meyer, D. J. Mindiola, *J. Am. Chem. Soc.* **2008**, *130*, 3676.

[10] a) C. Tejel, M. A. Ciriano, M. Pilar del Rio, D. G. H. Hetterscheid, N. Tsichlis i Spithas, J. M. N. Smits, B. de Bruin, *Chem. Eur. J.* **2008**, *14*, 10932; b) C. Tejel, M. P. del Rio, M. A. Ciriano, E. J. Reijerse, F. Hartl, S. Zalis, D. G. H. Hetterscheid, N. Tsichlis I Spithas, B. de Bruin, *Chem. Eur. J.* **2009**, *15*, 11878.

[11] a) N. W. Alkock, R. D. O'Sullivan, A. W. Parkins, *J. Chem. Soc., Chem. Commun.* **1980**, 1216; b) R. D. O'Sullivan, A. W. Parkins, N. W. Alkock, *J. Chem. Soc., Dalton Trans.* **1986**, 571.

[12] F. R. Keele, *Coord. Chem. Rev.* **1999**, *187*, 121.

[13] M. Königsmann, N. Donati, D. Stein, H. Schönberg, J. Harmer, A. Sreekanth, H. Grützmacher *Angew. Chem.* **2007**, *119*, 3637.

[14] a) M. E. van der Boom, D. Milstein, *Chem. Rev.* **2003**, *103*, 1759; b) A. S. Goldman, K. B. Renkema, M. Czerw, K. Krogh-Jespersen, In *Activation and Functionalization of C-H Bonds*; K. I. Goldberg, A. S. Goldman, Eds.; ACS Symposium Series 885; American Chemical Society: Washington, DC, **2004**; pp 198-215.

[15] a) O. V. Ozerov, C. Guo, V. A. Papkov, B. M. Foxman, *J. Am. Chem. Soc.* **2004**, *126*, 4792; b) L. Fan, L. Yang, C. Guo, B. M. Foxman, O. V. Ozerov, *Organometallics* **2004**, *23*, 4778; c) W. Weng, C. Guo, C. Muora, L. Yang, B. M. Foxman, O. V. Ozerov, *Organometallics* **2005**, *24*, 3487; d) L. Fan, O. V. Ozerov, *Chem. Commun.* **2005**, 4450; e) L. Fan, S. Parkin, O. V. Ozerov, *J. Am. Chem. Soc.* **2005**, *127*, 16772; f) C. D. Fafard, D. Adhikari, B. M. Foxman, D. J. Mindiola, O. V. Ozerov, *J. Am. Chem. Soc.* **2007**, *129*, 10318; h) M. T. Whited, M. T. Grubbs, *J. Am. Chem. Soc.* **2008**, *130*, 5874.

[16] J. I. van der Vlugt, J. N. H. Reek, *Angew. Chem. Int. Ed.* **2009**, *48*, 8832.

[17] a) M. Feller, A. Karton, G. Leitus, J. M. L. Martin, D. Milstein, *J. Am. Chem. Soc.* **2006**, *128*, 12400; b) E. Ben-Ari, G. Leitus, L. J. Shimon, D. Milstein, *J. Am. Chem. Soc.* **2006**, *128*, 15390.

[18] a) M. Käß, A. Friedrich, M. Drees, S. Schneider *Angew. Chem. Int. Ed.* **2009**, *48*, 905; b) A. Friedrich, M. Drees, S. Schneider *Chem. Eur. J.*, **2009**, *15*, 10339; c) A. Friedrich, M. Drees, J. Schmedt auf der Günne, S.

HN(CH$_2$CH$_2$PR$_2$)$_2$ (*H*PNP^R; R = *i*-Pr, *t*-Bu).[21] We recently reported the synthesis of the *d*^{8} amine complexes [ML(*H*PNP^{iPr})]$^+$ (M = Ir, L = CO (**1^{CO}**), cyclooctene (**1^{COE}**), C$_2$H$_4$ (**1^{C_2H_4}**); M = Pd, L = Cl (**2^{Cl}**), Me (**2^{Me}**), Ph (**2^{Ph}**)), and the corresponding amido complexes [ML(PNP^{iPr})] (M = Ir, L = CO (**3^{CO}**), cyclooctene (**3^{COE}**), C$_2$H$_4$ (**3^{C_2H_4}**); M = Pd, L = Cl (**4^{Cl}**), Me (**4^{Me}**), Ph (**4^{Ph}**)).[19,20] In the present paper we present a study which is aimed at assessing reactivity trends with electrophiles and oxidizing agents as dependent on further secondary ligands.

1.2 Results and discussion

Synthesis and structural characterization of 3^{PMe_3}. Amine complexes [Ir(L)(*H*PNP^{iPr})]PF$_6$ (**1^{PMe_3}**: L = PMe$_3$; **1^{dmso}**: L = OSMe$_2$) can be synthesized in high yield from ethylene complex **1^{C_2H_4}** and PMe$_3$ (Scheme B-1.1) and from [IrCl(dmso)$_2$]$_2$ with *H*PNP^{iPr}, respectively.[22] The NMR spectroscopic features of **1^{PMe_3}** and **1^{dmso}** strongly resemble those of the related amine complexes **1^{CO}** and **1^{C_2H_4}**, indicating *C$_s$* symmetry on the NMR timescale as a result of the pyramidally coordinated nitrogen atom. The $^2J_{PP}$ coupling constant of **1^{PMe_3}** is in agreement with a mutual *cis* configuration of the PMe$_3$ ligand and the pincer ligand phosphine atoms, respectively. Reaction of **1^{PMe_3}** with KO^{t}Bu gives the corresponding amido complex [Ir(PMe$_3$)(PNP^{iPr})] (**3^{PMe_3}**) in high yield. Deprotonation of the amine ligand effects *C$_{2v}$* symmetry on the NMR timescale. All attempts to synthesize [Ir(O=SMe$_2$)(PNP^{iPr})] resulted in complex mixtures of products which could not be further characterized.

The square-planar coordination geometry of complexes **1^{PMe_3}** and **3^{PMe_3}** was confirmed by single crystal X-ray diffraction (Supporting Information and Figure B-1.1). Most structural

Schneider *J. Am. Chem. Soc.* **2009**, *131*, 17552; d) A. Friedrich, M. Drees, M. Käß, E. Herdtweck, S. Schneider, *Inorg. Chem.*, **2010**, *49*, 5482; e) B. Askevold, M. M. Khusniyarov, E. Herdtweck, K. Meyer, S. Schneider *Angew. Chem. Int. Ed.* **2010**, *49*, 7566; f) A. Staubitz, M. Sloan, A. Robertson, A. Friedrich, S. Schneider, P. Gates, J. Schmedt auf der Günne, I. Manners *J. Am Chem. Soc.* **2010**, *132*, 13332.

[19] a) A. Friedrich, R. Ghosh, R. Kolb, E. Herdtweck, S. Schneider, *Organometallics* **2009**, *28*, 708; b) J. Meiners, A. Friedrich, E. Herdtweck, S. Schneider *Organometallics* **2009**, *28*, 6331.

[20] A. Marziale, E. Herdtweck, J. Eppinger, S. Schneider, *Inorg. Chem.* **2009**, *48*, 3699.

[21] Other authors that have reported late TM metal complexes with this ligand: a) Z. E. Clarke, P. T. Maragh, T. P. Dasgupta, D. G. Gusev, A. J. Lough, K. Abdur-Rashid, *Organometallics* **2006**, *25*, 4113; b) D. Amoroso, T. W. Graham, R. Guo, C. W. Tsang, K. Abdur-Rashid, *Aldrichim. Acta* **2008**, *41*, 15; c) X. Chen, W. Jia, R. Guo, T. W. Graham, M. A. Gullons, K. Abdur-Rashid, *Dalton Trans.* **2009**, 1407; d) T. W. Graham, C.-W. Tsang, X. Chen, R. Guo, W. Jia, S.-M. Lu, C. Sui-Seng, C. B. Ewart, A. Lough, D. Amoroso, K. Abdur-Rashid, *Angew. Chem. Int. Ed.* **2010**, *49*, 8708.

[22] For synthetic, crystallographic, or computational details, *c.f.*, Supporting Information.

parameters of **1**[PMe₃] and **3**[PMe₃] strongly resemble the respective ethylene and CO complexes.[19a] The molecular structures of **3**[L] (L = PMe₃, C₂H₄, CO) feature considerably more planarized amido nitrogen atoms (Σ_{angles}(N): 355.7° (**3**[CO]), 356.6° (**3**[C₂H₄]), 353.0° (**3**[PMe₃])) as compared with pyramidal nitrogen observed for Pd-amido complexes **4**[R] (R = Cl (337.4°), Me (345.7°)) and [Pd(CNtBu){N(CH₂CH₂PiPr₂)₂}]PF₆ (343.2°).[19a,20] Planarization of the nitrogen atom is a structural prerequisite for N-M π-bonding, possibly indicating stronger π-interactions for **3**[L] as compared with **4**[R] in the solid state.
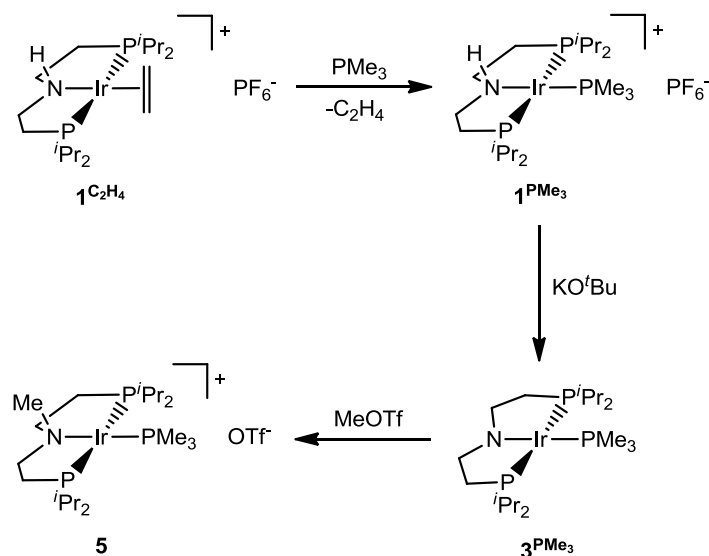
Scheme B-1.1: Synthesis of amido complex **3**[PMe₃] and reaction with MeOTf.
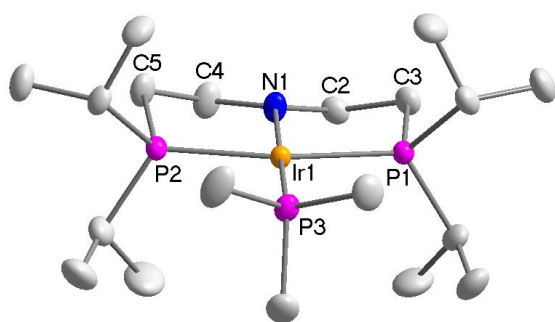
Figure B-1.1: Molecular structure of amido complex **3**[PMe₃] with thermal ellipsoids drawn at the 50% probability level (hydrogen atoms omitted for clarity). Selected bond lengths (Å) and angles (deg): Ir–N1 2.069(X), Ir–P1 2.289(X), Ir–P2 2.276(X), Ir–P3 2.223(X); P1–Ir–N1 81.29(X), P2–Ir–N1 81.67(X), P3–Ir–N1 178.48(X), P1–Ir1–P2 162.89(X).

Reaction of 3^L with electrophiles. Complex 3^{PMe_3} reacts with MeOTf to give [Ir(PMe₃){MeN(CH₂CH₂PiPr₂)₂}]OTf (**5**) in high yield (Scheme B-1.1). The same reactivity was found for 4^{Cl} and other palladium(II) amido complexes.[20,23] However, in case of iridium(I), oxidative addition of the electrophile at the metal center instead attack at the amido nitrogen atom could be a viable alternative, but no indication for the formation of an iridium(III) methyl complex was found. **5** was fully characterized including single crystal X-ray diffraction (Supporting Information).

The basicity of 3^L (L = PMe₃, COE, CO) was quantified by derivation of the corresponding 1^L pK_a values from equilibrium constants of 3^L with suitable Brønsted acids. d_6-dmso was chosen as solvent to prevent contact ion formation and make use of the extensive reference pK_a data available for this solvent.[24,25] The ligand in *trans*-position to the PNP nitrogen atom exhibits a strong influence on amine acidity which varies over a range of more than 7 orders of magnitude (Table B-1.1). The data follows the expected trend, since the π-acceptor ligands COE (olefin) and CO should stabilize the corresponding electron rich amido complexes more efficiently than the strong σ-donor ligand PMe₃. However, the large range of the pK_a values is somewhat surprising if compared with Pd complexes 2^R (R = Me, Ph) which show almost identical pK_a values (2^{Me}: 24.2(1), 2^{Ph}: 23.2(1)), respectively.[20] As indicated by the molecular structures, a stronger π-bonding for iridium(I) could be responsible. Accordingly, the three orbitals of a 3^{CO} DFT model (B3LYP/6-311+G**) that mainly arise from mixing of the nitrogen lone pair, the d_{xz}(Ir)-orbital,[26] and the respective in-plane π*(CO)-orbital are occupied by four electrons (HOMO-3, HOMO, and LUMO).[22] Due to the N-Ir π-antibonding character of the HOMO no net N-Ir π-bond results. However, d_{xz}(Ir)→π*(CO) backbonding stabilizes this orbital in terms of a 3c-4e N-Ir-L *push-pull* π-interaction. The striking differences in the pK_a range for the iridium(I) and palladium(II) complexes are therefore attributed to the different propensity for π-bonding. The more contracted palladium d-orbitals possibly provide a qualitative rationale for this observation. Despite the higher formal oxidation state of 4^R considerably lower N-H acidities result.

[23] S. Park, A. L. Rheingold, M. Roundhill, *Organometallics* **1991**, *10*, 615.

[24] a) F. G. Bordwell, *Acc. Chem. Res.* **1988**, *21*, 456; b) K. Abdur-Rashid, T. P. Fong, B. Greaves, D. G. Gusev, J. G. Hinman, S. E. Landau, A. J. Lough, R. H. Morris, *J. Am. Chem. Soc.* **2000**, *122*, 9155.

[25] http://www.chem.wisc.edu/areas/reich/pkatable/

[26] The coordinate system is defined by the vector which is perpendicular to the coordination plane (z-axis) and by the Ir-N bond vector (x-axis).

Table B-1.1: pK_a values of $\mathbf{1^L}$ in d^6-dmso and oxidation potentials of $\mathbf{3^L}$ (*vs.* FeCp$_2$/FeCp$_2^+$) at room temperature (electrolyte: THF, 0.1 M NBu$_4$PF$_6$; scan rate: 100 mV/s; $E_{1/2}$: half wave potential; I_a / I_c: anodic / cathodic current).

IrL(PNP)	pK_a	$E_{1/2}^I$ [V]	I_a^I / I_c^I	$E_{1/2}^{II}$ [V]	I_a^{II} / I_c^{II}	$E_{1/2}^{III}$ [V]	I_a^{III} / I_c^{III}
PMe$_3$	22.0(1)	-1.09	2.8	-0.69	1.0	0.10	1.8
COE	16.0(4)	-0.49	4.2	-0.26	1.0	0.25	2.0
CO	14.8(2)	-0.39	3.1	0.03	2.0	0.41	1.0

Oxidation of 3^L. We recently reported that chemical oxidation of palladium(II) amide $\mathbf{4^{Ph}}$ with AgPF$_6$ in THF gives amine complex $\mathbf{2^{Ph}}$ as major product and minor quantities of imine [PdPh{N(CHCH$_2$P*i*Pr$_2$)(CH$_2$CH$_2$P*i*Pr$_2$)}] ($\mathbf{6^{Ph}}$).[20] Deuterium labelling suggested the formation of transient radical cation [PdPh(PNP^{iPr})]$^{+\bullet}$ ($\mathbf{7^{Ph}}$) which decomposes by hydrogen abstraction from the solvent THF and by competitive disproportionation of $\mathbf{7^{Ph}}$ towards $\mathbf{2^{Ph}}$ and $\mathbf{6^{Ph}}$. Similarly, the reaction of iridium(I) amide $\mathbf{3^{PMe_3}}$ with AgPF$_6$, [FeCp$_2$]PF$_6$, or CPh$_3$PF$_6$ in THF results in the formation of $\mathbf{1^{PMe_3}}$ as major product. Small amounts of a minor product are assigned to imine complex [Ir(PMe$_3$){N(CHCH$_2$P*i*Pr$_2$)(CH$_2$CH$_2$P*i*Pr$_2$)}] ($\mathbf{8^{PMe_3}}$) by ^{31}P and ^{1}H NMR spectroscopy.

The oxidation of square-planar d^8 iridium PNP amides $\mathbf{3^L}$ (L = PMe$_3$, COE, CO) was further examined by cyclic voltammetry (CV) in a THF/N(*n*Bu)$_4$PF$_6$ electrolyte. The first oxidation (1e$^-$) is characterized by an anodic wave at $E_{1/2}^I$ (Table B-1.1). The potential is strongly dependent on the ligand in *trans*-position to the amide. As expected, electron rich $\mathbf{3^{PMe_3}}$ is oxidized at considerably more negative potential compard with $\mathbf{3^{COE}}$ and $\mathbf{3^{CO}}$. Irreversibility of this oxidation process at scan rates of 100 mVs^{-1} is indicated by the ratios of the anodic and cathodic currents (I_a^I / I_c^I), becoming quasireversible upon increasing the scan rate (Supporting Information). Furthermore, two oxidation waves $E_{1/2}^{II}$ and $E_{1/2}^{III}$ are observed at higher potential (Table B-1.1). $E_{1/2}^{II}$ is quasi-reversible at scan rates of 100 mVs^{-1} and higher for $\mathbf{3^{PMe3}}$ and $\mathbf{3^{COE}}$ but irreversible for $\mathbf{3^{CO}}$ at experimental conditions (100 – 600 mVs^{-1}). In contrast, $E_{1/2}^{III}$ is irreversible for all three complexes even at high scan rates (600 mVs^{-1}).
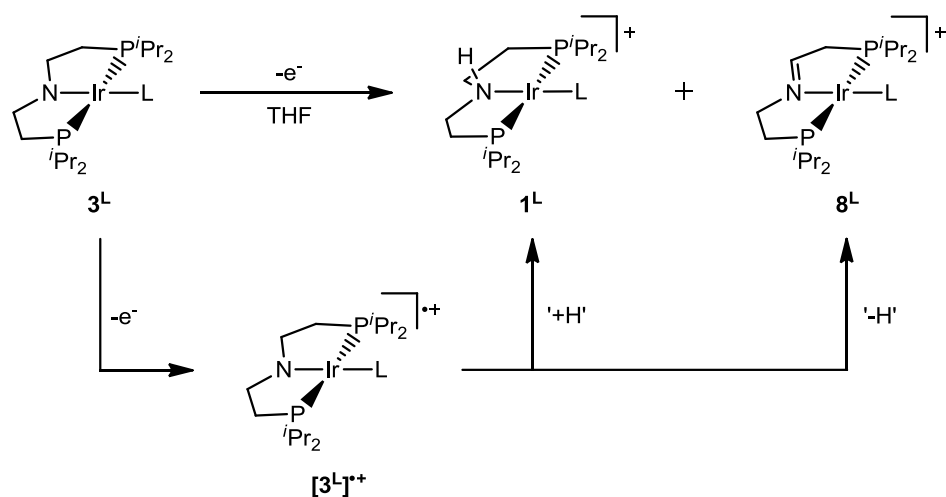
Scheme B-1.2: Oxidation of amido complexes 3^L in THF.

The wave at $E_{1/2}^{III}$ in case of 3^{PMe_3} could be ascribed to one electron oxidation of amine 1^{PMe3} by comparison with the cyclic voltammogram of an original sample (Supporting Information). In contrast, it is not yet possible to unambigously assign the subsequent wave at $E_{1/2}^{II}$ to a redox couple. However it is reasonable to assume the competitive disproportionation of $[3^{PMe_3}]^{\bullet+}$ towards amine 1^{PMe_3} and imine 8^{PMe_3} complex within the electrochemical timescale, too (vide supra). Thus, an Ir^I/Ir^{II} redox couple should emerge for the imine complex, while further oxidation of the amine ligand is expected at considerably higher potentials.[27] To date, all attempts to selectively isolate 8^{PMe_3} afforded product mixtures and comparison of the oxidation potentials remains hence still missing.

The results from electrochemical and chemical oxidation are in agreement with an ECE mechanism within the electrochemical timescale.[28] Initial formation of $[3^L]^{\bullet+}$ radical cation is followed by competitive hydrogen abstraction from THF or disproportionation reaction (Scheme B-1.2). This reactivity suggests strongly *N*-centered radicals, which is supportd by DFT calculations:[22] For 3^{CO}, NPA charge density on the nitrogen atom is strongly reduced by oxidation ($\Delta q = +0.29e$) as compared with the metal center ($\Delta q = +0.18e$), the phosphorous atoms ($\Delta q = +0.00$), or the CO-carbon ($\Delta q = +0.05e$) or -oxygen atoms ($\Delta q = +0.11e$). Accordingly, considerable spin density is located at the nitrogen atom of $[3^{CO}]^{\bullet+}$ (0.63)

[27] N. G. Connelly, W. E. Geiger, *Chem. Rev.* **1996**, *96*, 877.

[28] J. Heinze, *Angew. Chem.* **1984**, *96*, 823.

1.3 Conclusion

Electron rich metal amido complexes are particularly interesting compounds owing to their distinct ligand centered basicity and redox chemistry. In this context, a series of square planar iridium(I) dialkylamido complexes **3^L** (L = PMe$_3$, COE, CO) was examined with respect to the reactivity with electrophiles and oxidizing agents. **3^L** readily reacts with strong *C*-electrophiles or proton sources upon *N*-alkylation or -protonation respectively. However, in contrast to analogous palladium complexes their *p*K$_b$ values are strongly dependent on the *N*-trans ligand allowing for facile tuning of this property. Similarly, the *N*-centered oxidation of **3^L** exhibits a strong dependence on the π-acceptor ability of L. Hence, our results emphasize the strong dependence of the iridium amido complex reactivity on π-bonding, attributed to an N-M-L 3*c*-4*e* push-pull interaction, providing valuable information for the design of cooperative or redox-catalysts.

1.4 Experimental section

Materials and methods

All experiments were carried out under an atmosphere of argon using Schlenk and glove-box techniques. The solvents were dried over Na/benzophenone/tetraglyme (benzene) or Na/benzophenone (THF) and distilled under argon or dried and deoxygenated by passing through columns packed with activated alumina and Q5, respectively. C$_6$D$_6$ and d^8-THF were dried by distillation from Na/K alloy. d_6-acetone and dmso were stirred over 4 A molecular sieve and distilled from B$_2$O$_3$ (d_6-acetone) or CaH$_2$ (dmso). All deuterated solvents were deoxygenated by three *freeze-pump-thaw* cycles. KO^{t}Bu was purchased from VWR and sublimed prior to use. AgPF$_6$ (ABCR), [FeCp$_2$]PF$_6$ (Aldrich), CPh$_3$PF$_6$ (VWR) and MeOTf (Aldrich) were used as purchased. [IrCl(dmso)$_2$]$_2$[29] and [Ir(C$_2$H$_4$)$_2$(PNP)^H][PF$_6$] (1^{C_2H_4})[30] were prepared according to published procedures.

Analytical methods

Elemental analyses were obtained from the Microanalytical Laboratory of Technische Universität München. The IR spectra were recorded on a Jasco FT/IR-460 PLUS spectrometer as nujol mulls between KBr plates. NMR spectra were recorded on Jeol Lambda 400, Bruker DMX 500, and Bruker DMX 600 spectrometers at room temperature and were calibrated to the residual proton resonance and the natural abundance ^{13}C resonance of the

---

[29] R. Dorta, H. Rozenberg, L. J. W. Shimon, D. Milstein, *Chem. Eur. J.* **2003**, *9*, 5237.

[30] A. Friedrich, R. Ghosh, R. Kolb, E. Herdtweck, S. Schneider *Organometallics* **2009**, *28*, 708.

solvent (C_6D_6, δ_H = 7.16 ppm, δ_C = 128.06 ppm; d^6-dmso, δ_H = 2.50 ppm, δ_C = 39.52 ppm, d^8-THF, δ_H = 1.73 and 3.58 ppm, δ_C = 25.31 and 61.21 ppm, d_6-acetone δ_H = 2.05 ppm, δ_C = 29.84 ppm and 206.26). ^{31}P NMR NMR chemical shifts are reported relative to external phosphoric acid (δ = 0.0 ppm). IR peak intensities are abbreviated as: m (medium), s (strong). NMR Signal multiplicities are abbreviated as: s (singlet), d (dublet), t (triplet), vt (virtual triplet), sp (septet), m (multiplet), br (broad).

Syntheses

*[Ir(PMe₃)(HPNP^{iPr})]PF₆ (**1^{PMe_3}**).* [Ir(C₂H₄)(PNP)^H][PF₆] (**1^{C_2H_4}**) (0.029 g; 0.043 mmol) is dissolved in THF (5 mL) and PMe₃ (1.0 M in THF; 0.060 mL; 1.4 eq) added via syringe. The yellow solution is stirred for 10 min, filtered, and pentanes (20 mL) added to give a yellow precipitate. The product is filtered off, washed with 10 mL pentanes and dried *i. vac.* Yield: 0.030 g (0.042 mmol, 98%). Anal. Calcd. for $C_{19}H_{46}F_6IrNP_4$ (718.68): C, 31.75; H, 6.45; N, 1.95. Found: C, 31.65; H, 6.06; N, 1.88. IR (Nujol, cm^{-1}) ν = 3240 (m, N-H). NMR (C_6D_6/d_8-THF, r.t., [ppm]) ^{1}H NMR (399.8 MHz): δ = 0.93 (m, 18H, CH_3), 1.09 (dvt, $^3J_{HH}$ = 7.2 Hz, $^3J_{HP}$ = 16.4 Hz, 6H, CH_3), 1.24 (d, 9H, $^2J_{HP}$ = 8.0 Hz, P(CH_3)₃), 1.63 (m, 2H, PCH_2), 1.72-1.98 (m, 8H, PCH_2, CH(CH₃)₂, NCH_2), 3.21 (m, 2H, NCH_2), 4.50 (br, 1H, NH). ^{13}C {^{1}H} NMR (100.6 MHz): δ = 17.6 (s, CH₃), 18.4 (s, CH₃), 20.1 (s, CH₃), 20.4 (s, CH₃), 23.2 (d, J_{CP} = 36.0 Hz, P(CH₃)₃), 25.1 (dvt, J_{CP} = 3.1 Hz, J_{CP} = 12.2 Hz, PCH₂), 26.1 (vt, J_{CP} = 14.5 Hz, CH(CH₃)₂), 27.7 (vt, J_{CP} = 13.8 Hz, CH(CH₃)₂), 55.4 (s, NCH₂). ^{31}P {^{1}H} NMR (161.8 MHz): δ = 56.5 (d, $^2J_{PP}$ = 18.8 Hz, P^iPr₂), -45.5 (d, $^2J_{PP}$ = 18.8 Hz, P(CH₃)₃), -143.0 (sp, $^1J_{PF}$ = 712.0 Hz, PF₆).

*[Ir(SOMe₂)(HPNP^{iPr})]BPh₄ (**1^{DMSO}**).* H(CH₂CH₂P^{i}Pr₂)₂ (0.135 g; 0.443 mmol) in THF (5 mL) is added to a mixture of [IrCl(dmso)₂]₂ (0.170 g; 0.221 mmol) and NaBPh₄ (0.152 g; 0.443 mmol) in THF (5 mL). The solution is stirred for 1 h at room temperature and filtered. The yellow, microcrystalline product is precipitated by addition of diethylether (10 mL) and pentanes (5 mL), filtered off, and dried *i. vac.* Yield: 0.318g (0.355 mmol, 80 %). Anal. Calcd. for $C_{42}H_{63}BIrNOP_2S$ (895.00): C, 56.36; H, 7.10; N, 1.57. Found: C, 56.86; H, 6.99; N, 1.30. IR (Nujol, cm^{-1}) ν = 3181 (s, N-H). NMR (d^8-THF, r.t., [ppm]) ^{1}H NMR (399.8 MHz): δ = 1.16 (dd, $^3J_{HH}$ = 7.2 Hz, $^3J_{HP}$ = 14.0 Hz, 6H, CH_3), 1.24 (dd, $^3J_{HH}$ = 7.2 Hz, $^3J_{HP}$ = 14.0 Hz, 6H, CH_3), 1.31 (pseudo qu, J = 8.0 Hz, 12H, CH_3), 1.46 (m, 2H, PCH_2), 1.96 (m, 2H, PCH_2), 2.15 (m, 2H, NCH_2), 2.35 (m, 2H, CH(CH₃)₂), 2.45 (m, 2H, CH(CH₃)₂), 2.78 (m, 2H, NCH_2), 3.36 (s, 6H, OS(CH_3)₂), 4.47 (br, 1H, NH), 6.72 (t, $^3J_{HH}$ = 7.2 Hz, 4H, B(C₆H_5)₄), 6.86 (t, $^3J_{HH}$ = 7.2 Hz, 8H, B(C₆H_5)₄), 7.28 (br, 8H, B(C₆H_5)₄). ^{13}C {^{1}H} NMR

(100.6 MHz): δ = 17.1 (s, CH_3), 17.9 (s, CH_3), 19.3 (s, CH_3), 19.6 (s, CH_3), 23.6 (vt, J_{CP} = 13.0 Hz, PCH_2), 24.4 (vt, $CH(CH_3)_2$), 26.7 (vt, J_{CP} = 14.5 Hz, $CH(CH_3)_2$), 53.3 (s, OS($CH_3)_2$), 55.7 (br, NCH_2), 120.99 (s, B($C_6H_5)_4$), 124.8 (s, B($C_6H_5)_4$), 136.3 (s, B($C_6H_5)_4$), 164.3 (dd, J_{CP} = 48.9 Hz, B($C_6H_5)_4$). ^{31}P {^{1}H} NMR (161.8 MHz): δ = 58.13 (s, P^iPr_2). ^{11}B {^{1}H} NMR (128.3 MHz): δ = -7.54 (s, B(C$_6$H$_5)_4$).

*[Ir(PMe₃)(PNP^{iPr})] (**3^{PMe_3}**).* [Ir(PMe₃)(*H*PNP^{iPr})]PF₆ (**1^{PMe_3}**) (0.200 g; 0.224 mmol) and KO^{t}Bu (0.025 g; 0.223 mmol) in THF (10 mL) and stirred for 10 min at room temperature. The solvent is evaporated and the residue is extracted with pentanes. After filtration crystallization at -40°C gives **3^{PMe_3}** as orange crystals, which are filtered off and dried *i. vac.* Yield: 0.115 g (0.201 mmol, 90 %). Anal. Calcd. for $C_{19}H_{45}IrNP_3$ (572.71): C, 39.85; H, 7.92; N, 2.45. Found: C, 40.00; H, 8.46; N, 2.49. NMR (C_6D_6, r.t., [ppm]) ^{1}H NMR (399.8 MHz): δ (399.78 MHz, C_6D_6, r.t., ppm): δ = 1.11 (dvt, $^3J_{HH}$ = 6.8 Hz, J_{HP} = 12.8 Hz, 12H, CH(C$H_3)_2$), 1.20 (dvt, $^3J_{HH}$ = 7.6 Hz, J_{HP} = 15.2 Hz, 12H, CH(C$H_3)_2$), 1.54 (d, $^2J_{HP}$ = 6.8 Hz, 9H, P(C$H_3)_3$), 1.85 (m, 4H, PCH_2), 1.96 (m, 4H, CH(CH$_3)_2$), 3.43 (m, 4H, NCH_2). ^{13}C {^{1}H} NMR (100.6 MHz): δ = 18.1 (s, CH_3), 20.3 (s, CH_3), 25.9 (d, $^1J_{CP}$ = 29.2 Hz, P($CH_3)_3$), 26.6 (vt, J_{CP} = 13.1 Hz, CH(CH$_3)_2$), 28.6 (dvt, J_{CP} = 5.3 Hz, J_{CP} = 12.3 Hz, PCH_2), 62.6 (s (br), NCH_2). ^{31}P {^{1}H} NMR (161.8 MHz): δ = 68.1 (d, $^2J_{PP}$ = 18.3 Hz, P^iPr_2), -55.2 (t, $^2J_{PP}$ = 18.3 Hz, P(CH$_3)_3$).

*[Ir(PMe₃)(MePNP^{iPr})]OTf (**5**).* MeOTf (4.7 mg, 3.2 µL, 28 µmol) is added to a solution of [Ir(PMe₃)(PNP^{iPr})] (**3^{PMe_3}**) (15.3 mg, 28 µmol) in toluene (2 mL) and stirred for 30 min until a yellow solid is formed. After removing of all volatiles, the product is washed twice with diethylether and dried *i. vac.* to give microcrystalline, yellow **5**. Yield 19 mg (0.026 mmol; 91%). Anal. Calcd. for $C_{21}H_{48}F_3IrNO_3P_3S$ (736.81): C, 34.23; H, 6.57; N, 1.90; S, 4.35. Found: C, 33.79; H, 6.20; N, 1.91; S, 4.32. NMR (d_6-acetone, r.t., [ppm]) ^{1}H NMR (399.8 MHz): δ = 1.24-1.43 (m, 24 H, CH_3), 1.71 (d, $^2J_{PH}$ = 8.8 Hz, 9H, P(C$H_3)_3$), 2.25-2.31 (m, 4H, PCH_2), 2.25-2.31 (m, 4H, PCH_2), 2.34-2.41 (m, 2H, CH(CH$_3)_2$), 2.46-2.54 (m, 2H, CH(CH$_3)_2$), 2.70 (s, 3H, NCH_3), 2.81-2.91 (m, 2H, NCH_2), 2.99-3.11 (m, 2H, NCH_2). ^{13}C{^{1}H} NMR (100.6 MHz): δ = 16.7 (s, CH_3), 18.8 (s, CH_3), 20.0 (s, CH_3), 20.8 (m, PCH_2), 22.6 (d, PCH_3, $^1J_{CP}$ = 37.6 Hz), 23.1 (m, CH(CH$_3)_2$), 25.1 (m, CH(CH$_3)_2$), 44.9 (s, NCH_3), 64.4 (s, NCH_2). ^{31}P{^{1}H} NMR (161.8 MHz): δ = -47.6 (t, $^2J_{PP}$ = 18.8 Hz, P(CH$_3$)), 53.8 (d, $^2J_{PP}$ = 18.8 Hz, P^iPr_2), ^{19}F NMR (376.2 MHz): δ = -78.7 (s, SO$_3$CF$_3$).

Oxidation of [Ir(PMe₃)(PNP^iPr)] (3^PMe₃). **3^PMe₃** (5 mg, 8.7 μmol) is dissolved in THF (0.5 mL) in a J-Young NMR tube and AgPF₆ (2.2 mg, 8.7 μmol), [FeCp₂]PF₆ (2.9 mg, 8.7 μmol) or CPh₃PF₆ (3.4 mg, 8.7) added at room temperature. Immediately, the orange solution turns dark red. In the case of AgPF₆ a black precipitate forms. The starting material is quantitatively converted to a mixture of **1^PMe₃** (85%) and [Ir(PMe₃)(N(CHCH₂P*i*Pr₂)(CH₂CH₂P*i*Pr₂)] (**7^PMe₃**) (15%). Selected NMR data of (**7^PMe₃**): (d_8-THF, r.t., [ppm]) ^{1}H NMR (399.8 MHz): 3.51 (m, 2H, NCHC*H₂*), 8.31 (d, $^3J_{HH}$ = Hz, 1H, NC*H*CH₂). ^{31}P{^{1}H} NMR (161.8 MHz): δ = -43.5 (t, $^2J_{PP}$ = 18.8 Hz, *P*(CH₃)), 53.8 (dd, $^2J_{PP}$ = 18.8 Hz, 300 Hz, *P^i*Pr₂), 53.8 (dd, $^2J_{PP}$ = 18.8 Hz, 300 Hz, *P^i*Pr₂).

1.5 Cyclic voltammetry

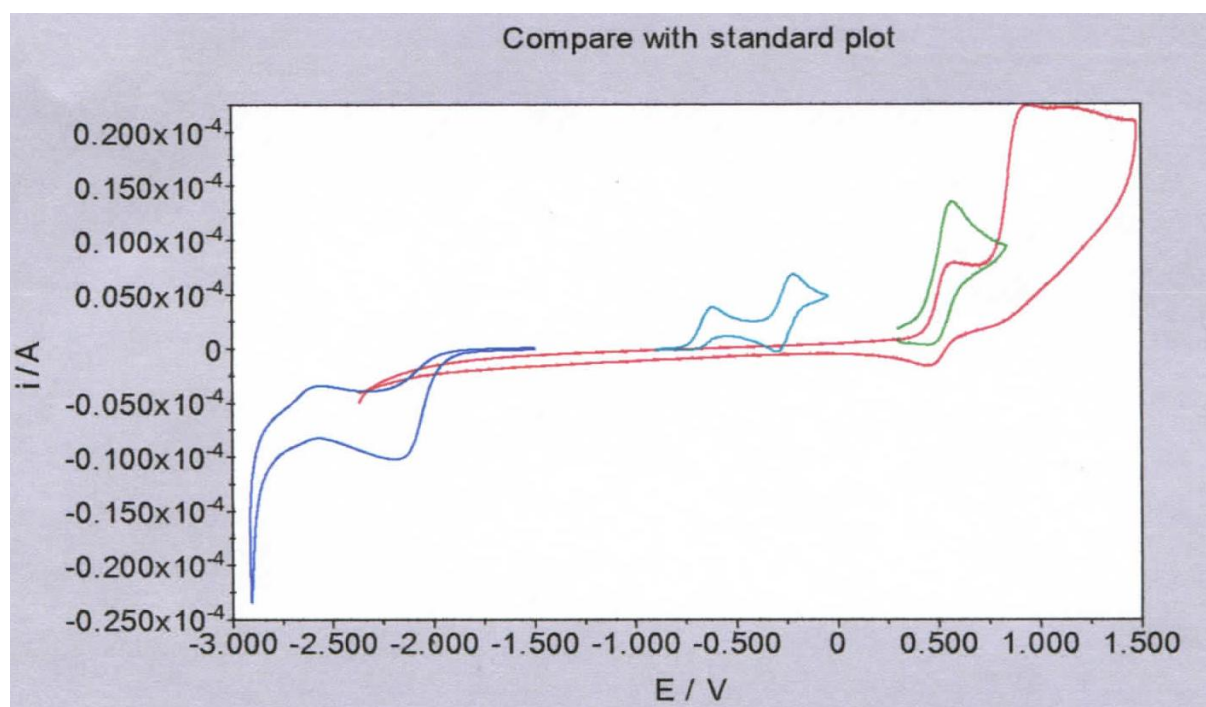**Figure B-1.2:** Comparison of oxidation potential of **1^PMe₃** (red and dark blue) at -25 °C with **3^PMe₃** (light blue and green) at r.t. (THF, 0.1 M NBu₄PF₆; scan rate: 100 mV/s).

1.6 Computational methods

DFT calculations on complex 3^{CO} were performed with GAUSSIAN03 RevC.02 using the B3LYP functional.[31,32] Geometry optimizations were run without symmetry or internal coordinate constraints using the Stuttgart-RSC-ECP and corresponding valence basis set for iridium and all-electron split valence triple-ζ basis set 6-311+G** for all other elements.[33,34] The optimized structure is in good agreement with the experimental molecular structure from X-ray diffraction and was verified as being a true minimum on the potential surface by the absence of negative eigenvalues in the vibrational frequency analysis. NPA analysis was performed with NBO V3.1 as implemented in the G03 software package.[35] Orbital expressions were visualized with GaussView via cube files generated from formatted checkpoint files.[36]

[31] M. J. Frisch, G. W. Trucks, H. B. Schlegel, G. E. Scuseria, M. A. Robb, J. R. Cheeseman, J. Montgomery, J. A. , T. Vreven, K. N. Kudin, J. C. Burant, J. M. Millam, S. S. Iyengar, J. Tomasi, V. Barone, B. Mennucci, M. Cossi, G. Scalmani, N. Rega, G. A. Petersson, H. Nakatsuji, M. Hada, M. Ehara, K. Toyota, R. Fukuda, J. Hasegawa, M. Ishida, T. Nakajima, Y. Honda, O. Kitao, H. Nakai, M. Klene, X. Li, J. E. Knox, H. P. Hratchian, J. B. Cross, V. Bakken, C. Adamo, J. Jaramillo, R. Gomperts, R. E. Stratmann, O. Yazyev, A. J. Austin, R. Cammi, C. Pomelli, J. W. Ochterski, P. Y. Ayala, K. Morokuma, G. A. Voth, P. Salvador, J. J. Dannenberg, V. G. Zakrzewski, S. Dapprich, A. D. Daniels, M. C. Strain, O. Farkas, D. K. Malick, A. D. Rabuck, K. Raghavachari, J. B. Foresman, J. V. Ortiz, Q. Cui, A. G. Baboul, S. Clifford, J. Cioslowski, B. B. Stefanov, G. Liu, A. Liashenko, P. Piskorz, I. Komaromi, R. L. Martin, D. J. Fox, T. Keith, M. A. Al-Laham, C. Y. Peng, A. Nanayakkara, M. Challacombe, P. M. W. Gill, B. Johnson, W. Chen, M. W. Wong, C. Gonzalez, J. A. Pople *Gaussian03 Rev. C.02*; Gaussian Inc.: Wallingford, CT, **2004**.

[32] J. P. Perdew, K. Burke, M. Ernzerhof, *Phys Rev. Lett.* **1996**, *77*, 3865.

[33] a) D. Andrae, U. Häußermann, M. Dolg, H. Stoll, H. Preuß, *Theor. Chim. Acta* **1990**, *77*, 123; b) J. M. L. Martin, A. Sundermann, *J. Chem. Phys.* **2001**, *114*, 3408.

[34] a) W. J. Hehre, R. Ditchfield, J. A. Pople, *J. Chem. Phys.* **1972**, *56*, 2257; b) M. M. Francl, W. J. Pietro, W. J. Hehre, J. S. Binkley, D. J. DeFrees, J. A. Pople, M. S. Gordon, *J. Chem. Phys.* **1982**, *77*, 3654. c) T. Clark, J. Chandrasekhar, G. W. Spitznagel, P. v. R. Schleyer, *J. Comp. Chem.* **1983**, *4*, 294.

[35] NBO Version 3.1, E. D. Glendening, A. E. Reed, J. E. Carpenter, and F. Weinhold.

[36] R. Dennington, T. Keith, J. Millam, *GaussView V4.1*; *Semichem Inc.*: Shawnee Mission, KS, **2007**.
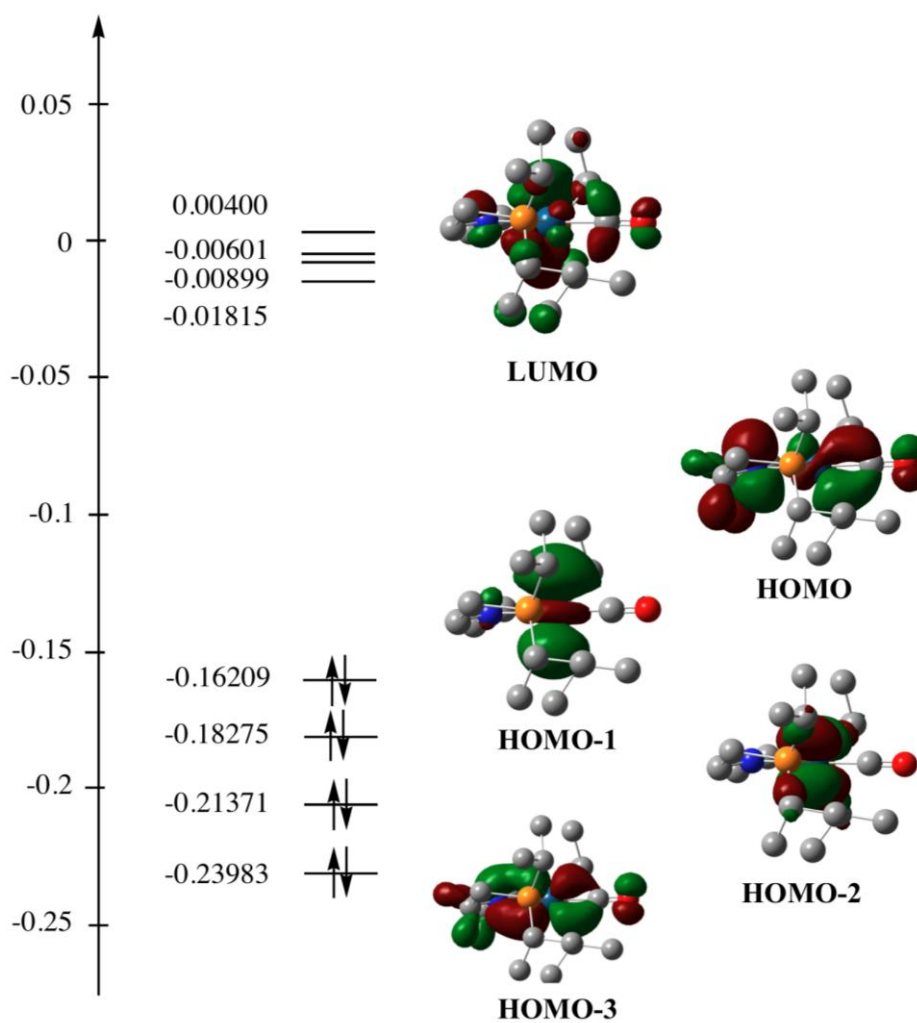
Figure B-1.3: Frontier Kohn-Sham orbital scheme for 3^{CO}.

Coordinates of optimized structures

[IrCO(PNP^{iPr})] (3^{CO}) Absolute energy: HF= -1586.9754469

```
---------------------------------------------------------------------
Center     Atomic    Atomic          Coordinates (Angstroms)
Number     Number    Type        X         Y         Z
---------------------------------------------------------------------
   1         77        0      0.000022  -0.052837  -0.146169
   2         15        0      2.309594  -0.026510   0.161850
   3         15        0     -2.309529  -0.026529   0.161955
   4          8        0     -0.000088  -0.297706  -3.154651
   5          7        0      0.000070   0.093763   1.923053
   6          6        0     -0.000054  -0.217640  -1.991510
   7          6        0      1.198883   0.447666   2.667829
   8          1        0      1.132732   0.050958   3.695099
   9          1        0      1.304725   1.543059   2.783337
  10          6        0      2.464830  -0.119793   2.011571
  11          1        0      2.557635  -1.179946   2.260195
  12          1        0      3.366786   0.387365   2.365957
  13          6        0     -1.198690   0.447794   2.667851
  14          1        0     -1.304465   1.543202   2.783283
```

15	1	0	-1.132518	0.051158	3.695147
16	6	0	-2.464705	-0.119640	2.011693
17	1	0	-3.366597	0.387643	2.366060
18	1	0	-2.557590	-1.179754	2.260442
19	6	0	3.271848	1.496606	-0.359219
20	1	0	4.278048	1.383896	0.060738
21	6	0	3.376541	1.594569	-1.888218
22	1	0	3.913172	0.750775	-2.328271
23	1	0	3.915681	2.506119	-2.164570
24	1	0	2.384971	1.640438	-2.345817
25	6	0	2.639274	2.767742	0.227066
26	1	0	2.633160	2.761722	1.319175
27	1	0	1.607507	2.879190	-0.115574
28	1	0	3.207149	3.646029	-0.096355
29	6	0	3.314105	-1.464519	-0.506257
30	1	0	3.258750	-1.333572	-1.592362
31	6	0	2.642372	-2.804608	-0.169382
32	1	0	1.591251	-2.806440	-0.462475
33	1	0	2.692627	-3.023898	0.901242
34	1	0	3.154520	-3.617033	-0.694557
35	6	0	4.790778	-1.456327	-0.083021
36	1	0	5.314390	-0.551370	-0.398562
37	1	0	5.310767	-2.307758	-0.533691
38	1	0	4.897504	-1.549151	1.001999
39	6	0	-3.271950	1.496443	-0.359207
40	1	0	-4.278134	1.383619	0.060763
41	6	0	-2.639529	2.767695	0.226985
42	1	0	-2.633173	2.761647	1.319093
43	1	0	-3.207660	3.645870	-0.096286
44	1	0	-1.607858	2.879368	-0.115869
45	6	0	-3.376645	1.594270	-1.888213
46	1	0	-3.913331	0.750463	-2.328176
47	1	0	-2.385076	1.640031	-2.345828
48	1	0	-3.915723	2.505829	-2.164657
49	6	0	-3.313915	-1.464686	-0.506036
50	1	0	-3.257936	-1.334223	-1.592168
51	6	0	-2.642570	-2.804726	-0.168187
52	1	0	-1.590935	-2.806376	-0.459448
53	1	0	-3.153668	-3.617150	-0.694377
54	1	0	-2.694696	-3.024166	0.902317
55	6	0	-4.790827	-1.456039	-0.083633
56	1	0	-5.314496	-0.551930	-0.401490
57	1	0	-4.898188	-1.546508	1.001521
58	1	0	-5.310306	-2.308608	-0.532736

$[IrCO(PNP^{iPr})]^{+}$ ($[\mathbf{3^{CO}}]^{+}$) Absolute energy: HF= -1586.7683795

Center Number	Atomic Number	Atomic Type	Coordinates (Angstroms)		
			X	Y	Z

1	77	0	0.000010	0.086752	-0.102700
2	15	0	-2.352482	-0.051371	0.128444
3	15	0	2.352498	-0.051352	0.128420
4	8	0	-0.000232	2.111242	-2.372805
5	7	0	0.000021	-0.767793	1.716699
6	6	0	-0.000081	1.310797	-1.552604
7	6	0	-1.216750	-1.238516	2.390491
8	1	0	-1.101070	-1.118466	3.473812
9	1	0	-1.302691	-2.319961	2.209865
10	6	0	-2.482960	-0.517243	1.921871

11	1	0	-2.598500	0.416197	2.476812
12	1	0	-3.369524	-1.125471	2.115345
13	6	0	1.216801	-1.238520	2.390473
14	1	0	1.302741	-2.319963	2.209838
15	1	0	1.101135	-1.118477	3.473797
16	6	0	2.483005	-0.517243	1.921842
17	1	0	3.369572	-1.125473	2.115294
18	1	0	2.598555	0.416191	2.476791
19	6	0	-3.204669	-1.392419	-0.854345
20	1	0	-4.228549	-1.435540	-0.467891
21	6	0	-3.251396	-1.039321	-2.349100
22	1	0	-3.781326	-0.105105	-2.545737
23	1	0	-3.773657	-1.829963	-2.894023
24	1	0	-2.245747	-0.957141	-2.770691
25	6	0	-2.540785	-2.758397	-0.623128
26	1	0	-2.597723	-3.078393	0.419756
27	1	0	-1.489200	-2.745345	-0.922965
28	1	0	-3.049885	-3.518196	-1.221813
29	6	0	-3.378774	1.496004	-0.092799
30	1	0	-3.268454	1.724530	-1.158641
31	6	0	-2.800896	2.676797	0.703732
32	1	0	-1.738934	2.830921	0.505374
33	1	0	-2.929371	2.541635	1.781012
34	1	0	-3.331858	3.591707	0.429045
35	6	0	-4.870947	1.289639	0.213478
36	1	0	-5.332520	0.530006	-0.419738
37	1	0	-5.407744	2.226026	0.039658
38	1	0	-5.036038	1.012892	1.258700
39	6	0	3.204685	-1.392385	-0.854391
40	1	0	4.228569	-1.435503	-0.467948
41	6	0	2.540813	-2.758370	-0.623180
42	1	0	2.597762	-3.078374	0.419702
43	1	0	3.049914	-3.518161	-1.221875
44	1	0	1.489227	-2.745324	-0.923009
45	6	0	3.251392	-1.039273	-2.349143
46	1	0	3.781314	-0.105052	-2.545778
47	1	0	2.245737	-0.957095	-2.770721
48	1	0	3.773653	-1.829906	-2.894080
49	6	0	3.378780	1.496031	-0.092818
50	1	0	3.268459	1.724558	-1.158660
51	6	0	2.800889	2.676817	0.703714
52	1	0	1.738928	2.830935	0.505346
53	1	0	3.331849	3.591731	0.429037
54	1	0	2.929353	2.541650	1.780994
55	6	0	4.870954	1.289676	0.213460
56	1	0	5.332533	0.530050	-0.419760
57	1	0	5.036047	1.012926	1.258680
58	1	0	5.407744	2.226068	0.039644

----

2 A square-planar ruthenium(II) complex with low-spin configuration

This chapter originated the following publication:

B. Askevold, M. M. Khusniyarov, E. Herdtweck, K. Meyer, S. Schneider

Angew. Chem. **2010**, *122*, 7728; *Angew. Chem. Int. Ed.* **2010**, *49*, 7566.

A   KO*t*Bu   **B**
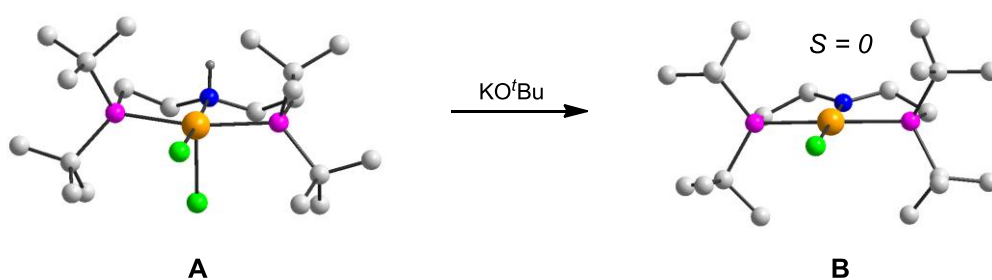
2.1 Introduction

The coordination chemistry of d^6 ions of group 8 is dominated by octahedral complexes. Four-coordination is mainly observed in case of tetrahedral iron complexes, which exhibit an electronic high-spin configuration (S = 2, HS). With macrocyclic, chelating, and few monodentate ligands, square-planar, intermediate-spin (S = 1, IS) iron(II) complexes are known (Scheme B-2.1, left).[1,2,3] On the contrary, four-coordinate ruthenium(II) compounds are typically found to exhibit a butterfly-shaped molecular geometry with an electronic low-spin configuration (S = 0, LS). However, owing to the energetically low-lying LUMO, such complexes exhibit C-H agostic interactions with the metal at the vacant coordination sites.[4] Only recently, true four-coordination was described for this geometry for the first time.[5] However, according to DFT calculations, the PCP pincer complex $[RuCl\{HC(CH_2NHP^tBu_2)_2\}]$ (**A**) was postulated to be an unstable intermediate with square-planar coordination geometry and a triplet ground state (IS).[6] Therefore, the related PNP pincer complexes $[RuX\{N(SiMe_2CH_2P^tBu_2)_2\}]$ (X = F (**B^F**), Cl (**B^{Cl}**), OTf (**B^{OTf}**)) remain the only square-planar ruthenium(II) compounds being experimentally accessible. Likewise, **B^X** exhibit an IS ground state configuration.[7] DFT calculations showed that the highest SOMO of **B^{Cl}** exhibits strong d_{xz}-orbital character owing to the p-interaction with the disilylamido π-donor (Scheme B-2.1, middle). However, this interaction is not sufficient to effect spin pairing. Accordingly, square-planar d^6 14-electron complexes with an electronic low-spin configuration are not known, to date.[8,9]

[1] a) B. W. Dale, R. J. P. Williams, C. E. Johnson, T. L. Thorp, *J. Chem. Phys.* **1968**, *49*, 3441; b) H. Geoff, G. N. La Mar, C. A. Reed, *J. Am. Chem. Soc.* **1977**, *99*, 3641.

[2] K. Ray, A. Begum, T. Weyhermüller, S. Piligkos, J. van Slageren, F. Neese, K. Wieghardt, *J. Am. Chem. Soc.* **2005**, *127*, 4403.

[3] E. J. Hawrelak, W. H. Bernskoetter, E. Lobkovsky, G. T. Yee, E. Bill, P. J. Chirik, *Inorg. Chem.* **2005**, *44*, 3103.

[4] a) Y. Jean in *Molecular Orbitals of Transition Metal Complexes*, Oxford University Press, Oxford, **2005**; b) W. Baratta, E. Herdtweck, P. Rigo, *Angew. Chem.* **1999**, *111*, 1733; *Angew. Chem. Int. Ed.* **1999**, *38*, 1629.

[5] J. P. Lee, Z. Ke, M. A. Ramirez, T. B. Gunnoe, T. R. Cundari, P. D. Boyle, J. L. Petersen, *Organometallics* **2009**, *28*, 1758.

[6] V. F. Kuznetsov, K. Abdur-Rashid, A. J. Lough, D. G. Gusev, *J. Am. Chem. Soc.* **2006**, *128*, 14388.

[7] a) L. A. Watson, O. V. Ozerov, M. Pink, K. G. Caulton, *J. Am. Chem. Soc.* **2003**, *125*, 8246; b) A. Walstrom, M. Pink, N. P. Tsvetkov, H. Fan, M. Ingleson, K. G. Caulton, *J. Am. Chem. Soc.* **2005**, *127*, 16780; c) X. Yang, A. Walstrom, N. Tsvetkov, M. Pink, K. G. Caulton, *Inorg. Chem.* **2007**, *46*, 4612.

[8] S. Alvarez, J. Cirera, *Angew. Chem.* **2006**, *118*, 3078; *Angew. Chem. Int. Ed.* **2006**, *45*, 3012.

Starting from the chelating amino ligand $HN(CH_2CH_2P^iPr_2)_2$ (HPNP^{iPr}), we recently reported the synthesis of octahedral ruthenium(II) amino complexes and the corresponding five-coordinate amides.[10] In this context, the comparison of **A** and **B**^{Cl} (vide supra) raises the question whether the expected even stronger π-donation of the dialkylamido PNP ligand,[11] as compared with the disilylamido ligand in **B**^{Cl}, enables the stabilization of an unprecedented square-planar d^6 complex with a low-spin ground state (Scheme B-2.1, right).
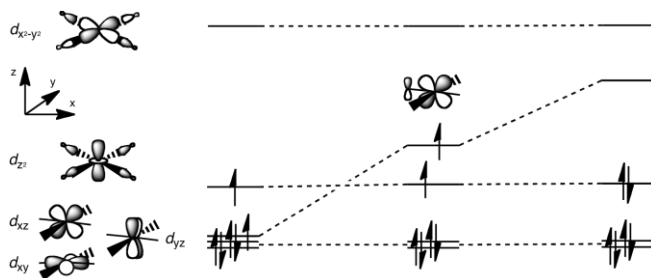
Scheme B-2.1: Qualitative d-orbital splitting of square-planar d^6 complexes with pure σ-donor ligands (left), with one weak π-donor ligand (middle), and one strong π-donor ligand (right), respectively.

2.2 Results and discussion

The reaction of $[RuCl_2(PPh_3)_3]$ (**1**) with HPNP^{tBu} in THF gives amine complex $[RuCl_2(H$PNP$^{tBu})]$ (**2**) in quantitative yield (Scheme B-2.2).[12] The two sets of broadened signals in the ^{31}P and ^{1}H NMR spectra und the exchange signals in the ^{1}H NOESY NMR spectrum (CD$_2$Cl$_2$) of **2** at room temperature, respectively, are in agreement with two C_s symmetric, square-pyramidally coordinated diastereomers, which exhibit exchange on the NMR time scale. Accordingly, below 0 °C sharp peaks are observed in the ^{1}H NMR spectrum allowing for signal assignment by ^{1}H COSY und ^{1}H-^{13}C HMQC NMR spectroscopy. Further cooling to −80 °C leads to broadening and splitting of one *tert*-butyl ^{1}H NMR signal per diastereomer, respectively (Supporting Information). This observation points towards C-H

[9] Most recently, a square-planar iridium(III) 18-electron nitrido complex was reported: J. Schöffel, A. Y. Rogachev, S. D. George, P. Burger, *Angew. Chem.* **2009**, *121*, 4828; *Angew. Chem. Int. Ed.* **2009**, *48*, 4737.

[10] a) M. Käß, A. Friedrich, M. Drees, S. Schneider, *Angew. Chem.* **2009**, *121*, 922; *Angew. Chem. Int. Ed.* **2009**, *48*, 905; b) A. Friedrich, M. Drees, S. Schneider, S. *Chem. Eur. J.*, **2009**, *15*, 10339; c) A. Friedrich, M. Drees, J. Schmedt auf der Günne, S. Schneider, *J. Am. Chem. Soc.* **2009**, *131*, 17552; d) A. Friedrich, M. Drees, M. Käß, E. Herdtweck, S. Schneider, *Inorg. Chem.* **2010**, *49*, 5482.

[11] A. Friedrich, R. Ghosh, R. Kolb, E. Herdtweck, S. Schneider, *Organometallics* **2009**, *28*, 708.

[12] For experimental details see Supporting Information.

agostic interactions with the metal center at the vacant coordination site. The molecular structure of one diastereomer with square-pyramidal coordination geometry was derived by single-crystal X-ray diffraction (Figure B-2.1).[12,13] The short Ru–H^{tBu} (2.39 Å) distances at the vacant coordination site confirm stablilization of the coordinatively unsaturated metal center by C-H agostic interactions in the solid state, as well.
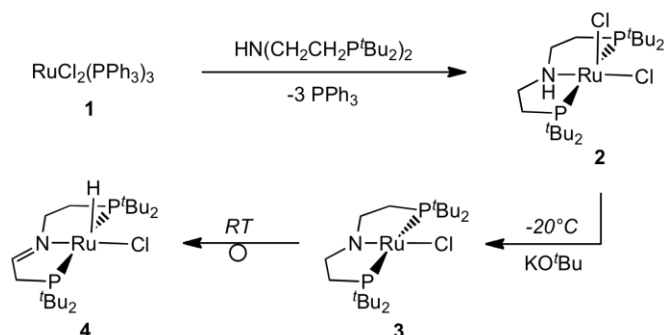
Scheme B-2.2: Synthesis of amido complex 3 and β-hydrogen elimination towards compound 4 (RT = room temperature).

Deprotonation of **2** with KO^{t}Bu at –78 °C and isolation at –20 °C gives amido complex [RuCl(PNP^{tBu})] (**3**) in over 80 % yield (Scheme B-2.2). Complex **3** is thermally unstable towards β-hydrogen elimination. At room temperature in solution, **3** is quantitatively converted to [RuHCl{N(CHCH$_2$P^{t}Bu$_2$)(CH$_2$CH$_2$P^{t}Bu$_2$)}] ([RuHCl(PN=P^{tBu})]; **4**) over the course of 2 days. However, **3** can be stored for several days without decomposition at temperatures below –30 °C in solution or at room temperature in the solid state, allowing for full characterization. Integration and chemical shift of the ^{1}H NMR hydride signal of **4** confirm the absence of further H$_2$ ligands at the vacant coordination site. Furthermore,

[13] **2**: turquoise columns, C$_{20}$H$_{45}$Cl$_2$NP$_2$Ru, M_r=533.48; monoclinic, space group $P2_1/c$ (Nr. 14), a=19.389(1), b=13.420(1), c=22.854(2) Å, β=91.103(4)°, V=5945.5(7) Å^3, Z=8, λ(Mo$_{K\alpha}$)=0.71073 Å, μ=0.820 mm^{-1}, ρ_{calcd}=1.192 gcm^{-3}, T=153(1) K, F(000)=2240, crystal dimensions 0.08 × 0.13 × 0.61 mm. $R1$=0.0291 (observed reflexes), $wR2$=0.0719 (all reflexes), GOF=1.041, 493 parameters, $\Delta\rho_{max/min}$=0.65/-0.56 eÅ^{-3}. **3**: brown needles, C$_{20}$H$_{44}$ClNP$_2$Ru, M_r=497.02; monoclinic, space group $P2_1/c$ (Nr. 14), a=12.0574(6), b=16.0573(7), c=13.0190(6) Å, β=104.438(2)°, V=2441.0(2) Å^3, Z=4, λ(Mo$_{K\alpha}$)=0.71073 Å, μ=0.887 mm^{-1}, ρ_{calcd}=1.352 gcm^{-3}, T=123(1) K, F(000)= 1048, crystal dimensions 0.02 × 0.02 × 0.15 mm. $R1$=0.0239 (observed reflexes), $wR2$=0.0587 (all reflexes), GOF=1.074, 402 parameters, $\Delta\rho_{max/min}$=0.59/-0.31 eÅ^{-3}. CCDC-771336 (**2**) and CCDC-771337 (**3**) contain the crystallographic data and can be ordered free of charge from the Cambridge Crystallographic Data Centre.

monitoring the β-hydrogen elimination in **3** towards **4** by [^1]H NMR spectroscopy in a sealed tube at room temperature in d^8-THF provides no indication for further free or coordinated H_2.

In the crystal, the metal center of **3** exhibits a planar, slightly distorted coordination geometry with a typical PNP bite angle P1–Ru1–P2 of 168.13(2)° and an almost linear N1–Ru1–Cl1 arrangement (179.63(6)°) (Figure B-2.1).[12,13] Planar coordination of the nitrogen atom (Σ_{angles} = 360.0°) and the particularly short Ru–N1 distance (1.890(2) Å), as compared with, e.g., square-planar **B**^{Cl} (2.050(1) Å) or the five-coordinate ruthenium(II) alkylamides [RuHPMe$_3$(PNP^{iPr})] (2.023(1) Å) or [RuH(HNCMe$_2$CMe$_2$NH$_2$) (PPh$_3$)$_2$] (1.967(1) Å), respectively, point towards a strong N→Ru π-bonding contribution.[7a,10d,14] Likewise, a relatively short Ru1–Cl1 distance (2.3805(6) Å) is found, e.g., as compared with the basal Ru–Cl bond in **2** (2.4506(6) bzw. 2.4478(6) Å).
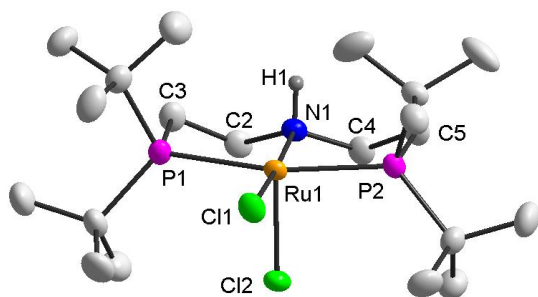

Figure B-2.1: DIAMOND plot of the molecular structure of complex **2** in the crystal (one of two cristallographically independent molecules; thermal ellipsoids drawn at the 50% probability level). Hydrogen atoms except for H1 are omitted for clarity. Selected bond lengths [Å] and angles [°]: Ru1–Cl1 2.4506(6) (2.4478(6)), Ru1–Cl2 2.3438(6) (2.3579(8)), Ru1–N1 2.130(2) (2.131(2)), Ru1–P1 2.3854(6) (2.3888(7)), Ru1–P2 2.3405(6) (2.3397(7)); N1–Ru1–Cl1 175.79(5) (176.47(6)), N1–Ru1–Cl2 90.52(5) (91.19(6)), P1–Ru1–P2 164.08(2) (163.81(2)). Values for the second independent molecule in parantheses.

Neither the IR nor the [^1]H NMR spectrum (180 - 280 K) of **3** provides evidence for the presence of hydrido ligands. Therefore, the reactivity (vide supra) and the spectroscopic characterization exclude the assignment of a hydride complex, such as [Ru(H)$_2$Cl(PNP^{tBu})]. The [^31]P, [^1]H and [^13]C NMR spectra point towards C_{2v} symmetry on the NMR time scale in solution. However, particularly the [^31]P signal (C$_6$D$_6$: –22.58 ppm; $\Delta\nu_{1/2}$ = 8 Hz) and the NCH$_2$

[14] K. Abdur-Rashid, S. E. Clapham, A. Hadzovic, J. N. Harvey, A. J. Lough, R. H. Morris, *J. Am. Chem. Soc.* **2002**, *124*, 15104.

[1]H signal (C$_6$D$_6$: 14.41 ppm; $\Delta\nu_{1/2}$ = 12 Hz) are slightly broadened and exhibit unusual chemical shifts with a strong temperature dependence.[12,15] As an example, the NCH$_2$ ^{1}H NMR signal is shifted by 3.64 ppm towards higher field upon cooling from 280 K to 180 K in d^8-THF. These NMR spectroscopic properties of **3** can be rationalized with the presence of a LS ground state and an energetically low lying, IS excited state. The ^{13}C NMR signals, which are not significantly paramagnetically shifted,[11,16] therefore point towards hyperconjugation as the predominant transfer mechanism of spin density.[17] However, in the solid state (SQUID) no magnetic moment could be detected (μ_{eff} < 0.01 μ_B) in the temperature range of 2 - 300 K. Therefore, the thermodynamic parameters of the singlet-triplet transition were estimated in solution by fitting the chemical shifts as a function of temperature to the equation: $\delta = \delta^{dia} + C / (T \cdot e^{(\Delta H + T\Delta S)})$.[12,18] The relatively small experimentally accessible temperature range does not permit a very precise assessment (d^8-toluene: ΔH^0 = 10.6 $\pm$ 0.3 kJ/mol; ΔS^0 = 4.2 $\pm$ 0.8 J/molK). However, the result is in agreement with the observation that the population of the triplet state is not sufficient to be detected by magnetometry.[19] Interestingly, for the related complex [IrCl{=C(CH$_2$CH$_2$P^{t}Bu$_2$)$_2$}] unusual chemical shifts were found for the Ir=C—CH_2 protons by ^{1}H NMR spectroscopy, as well (δ = –2.77 ppm).[20] However, this observation was not closely examined.

[15] For example, the ^{31}P NMR signals of the iridium(I) amido complex [Ir(COE)(PNP^{tBu})] were found at +56.4 and +52.4 ppm, respectively: J. Meiners, S. Schneider *in preparation*.

[16] A. N. Marziale, E. Herdtweck, J. Eppinger, S. Schneider, *Inorg. Chem.* **2009**, *48*, 3699.

[17] F. H. Köhler in *Magnetism: Molecules to Materials, Vol. 1* (Hrsg.: J. S. Miller, M. Drillon), Wiley-VCH, Weinheim, **2001**, p. 379-430.

[18] a) P. Gütlich, B. R. McGarvey, W. Kläui, *Inorg. Chem.* **1980**, *19*, 3704; b) M. E. Smith, R. A. Andersen, *J. Am. Chem. Soc.* **1996**, *118*, 11119.

[19] Based on the fitted thermodynamic parameters, a population of the triplet state of less than 2.5 % can be estimated for the spin equilibrium in d^8-Toluol at 300 K.

[20] H. D. Empsall, E. M. Hyde, R. Markham, W. S. McDonald, M. C. Norton, B. L. Shaw, B. Weeks, *J. Chem. Soc., Chem. Comm.* **1977**, 589.
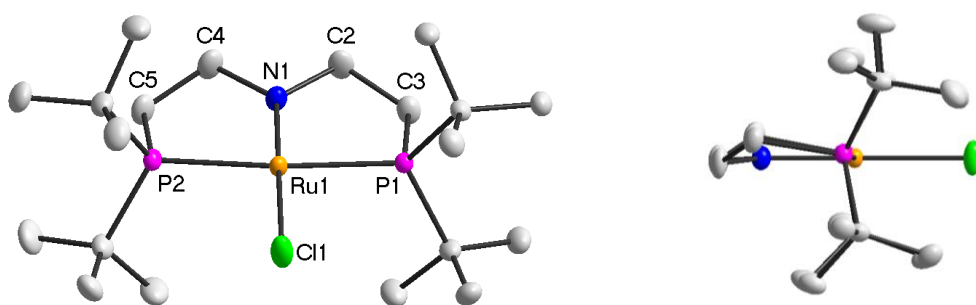
Figure B-2.2: DIAMOND plot of the molecular structure of complex **3** (left: front view; right: side view) in the crystal (thermal ellipsoids drawn at the 50% probability level). Hydrogen atoms are omitted for clarity. Selected bond lengths [Å] and angles [°]: Ru1–N1 1.890(2), Ru1–Cl1 2.3805(6), Ru1–P1 2.3316(5), Ru1–P2 2.3240(6); N1–Ru1–Cl1 179.63(6), P1–Ru1–P2 168.13(2).

The experimental results were reassessed by DFT calculations. Geometry optimizations of a full model of **3** in the singlet state (6-31+G**) with different functionals (B3LYP and BP86) were in excellent agreement with the experimentally derived molecular structure by X-ray diffraction.[12] However, simplified models with PMe_2- instead of P^tBu_2-substituents resulted in minimum structures exhibiting butterfly conformations (N–Ru–Cl < 160°), as typically found for four-coordinate ruthenium(II) compounds (vide supra). This result suggests that the square-planar molecular geometry is mainly stabilized by the large steric pressure of the bulky chelating ligand.[21] A comparison of the electronic structures in the singlet and triplet states, respectively, confirms the simplified bonding model (Scheme B-2.1). The strong metal d_{z^2}-character of the HOMO in the singlet state explains the absence of C-H agostic interactions at the vacant axial coordination sites of **3** (Figure B-2.3), reminiscent of square-planar d^8-complexes.[22] Furthermore, in the singlet state the antibonding combination of the Ru–N und Ru–Cl π-bonds is not occupied (LUMO). Hence, strong Ru–N π-bonding results and explains the short Ru–N distance, as compared with the triplet state ($\Delta d_{S\text{-}T} = -0.1$ Å; BP86) which exhibits strong Ru–N π*-character for the highest occupied SOMO. Accordingly, in the singlet state less negative NPA charges at the N ($\Delta q_{S\text{-}T} = +0.14$ e; B3LYP) and Cl ($\Delta q_{S\text{-}T} = +0.08$ e; B3LYP) atoms, a more negative charge at the metal ($\Delta q_{S\text{-}T} = -0.29$ e; B3LYP) and larger Wiberg-bond-indices for the Ru–N ($\Delta WBI_{S\text{-}T} = +0.43$; B3LYP) and Ru–

---

[21] All efforts to synthesize a four-coordinate complex analogous to **3** with the amido ligand PNP^{iPr} were without success.

[22] Y. Zhang, J. C. Lewis, R. G. Bergman, J. A. Ellman, E. Oldfield, *Organometallics* **2006**, *25*, 3515.

Cl (ΔWBI_{S-T} = +0.15; B3LYP) bonds are found. The calculated small energy gap between the singlet and triplet states (ΔE_{S-T} = −2.0 kcal/mol (BP86); +2.3 kcal/mol (B3LYP)) does not permit a reliable assignment of the electronic ground state on the applied level of theory.[23] However, within the error of the method, this result is in agreement with the experimentally derived singlet ground state and an energetically low lying excited triplet state.[24]
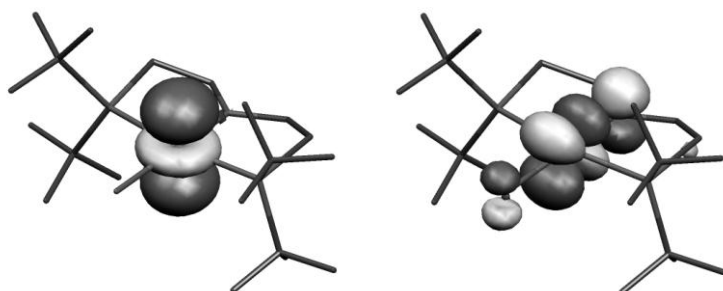

Figure B-2.3: Kohn-Sham HOMO (left) and LUMO (right) plots of complex **3** in the singlet state (B3LYP/6-31+G**).

2.3 Conclusion

The experimental and quantum chemical results of **3** demonstrate, that the unprecedented electronic LS configuration in this coordination geometry can be attributed to a combination of the steric bulk and the strong π-donation caused by the chelating amido ligand.[25,26] Therefore, the simple variation of the M–N π-interaction by replacing a disilyl amido with a dialkyl amido ligand in the related compounds $\mathbf{B}^{\mathbf{Cl}}$ (IS) and **3** (LS) allows for control of the electronic ground state, consequently offering an interesting approach for the design of novel spin-crossover materials. The high thermal stability of the 14-electron complex $\mathbf{B}^{\mathbf{Cl}}$ and concomitant absence of C–H agostic stabilization was attributed by Caulton *et al.* to the triplet character of the compound.[7a] However, the singlet state can also be efficiently stabilized, if

---

[23] Singel point calculations with the triple-ζ basis 6-311+G** resulted in almost identical energies (see Supporting Information).

[24] Typically, hybrid functionals (e.g. B3LYP) tend to favor the higher and pure (GGA) functionals (e.g. BP86) the lower spin state: H. Paulson, A. X. Trautwein in *Topics in Current Chemistry, Vol. 235* (Eds.: P. Gütlich, H. A. Goodwin), Springer, Berlin, **2004**, S. 197.

[25] Likewise, the diamagnetic ground state of the ruthenium(IV) nitrido complex [Ru($\equiv$N){N(SiMe$_2$CH$_2$P^{t}Bu$_2$)$_2$}] can be attributed to the strong π-donation by the nitrido ligand.[8,26]

[26] A. Walström, M. Pink, X. Yang, J. Tomaszewski, M.-H. Baik, K. G. Caulton, *J. Am. Chem. Soc.* **2005**, *127*, 5330.

possible decomposition pathways, such as β-hydrogen elimination or C-H oxidative addition, can be effectively suppressed by the chelate effect and the high charge density at the vacant coordination sites.

2.4 Synthetic and analytical details

Materials and methods

All experiments were carried out under an atmosphere of argon using Schlenk and glove-box techniques. Solvents were dried over Na/benzophenone/tetraglyme (benzene) or Na/benzophenone (THF), distilled under argon, and deoxygenated prior to use. Deuterated solvents were obtained from Euriso-Top GmbH, dried over Na/K (d_8-THF, C_6D_6, d_8-toluene) or CaH_2 (CD_2Cl_2), distilled by trap-to-trap transfer in vacuo, and degassed by three freeze-pump-thaw cycles, respectively. KO^tBu was purchased from VWR and sublimed prior to use. Ruthenium(III)chloride hydrate (ABCR) was used as purchased. **1** and $HN(CH_2CH_2P^tBu_2)_2$ were prepared according to published procedures.[27]

Analytical methods

Elemental analyses were obtained from the Microanalytical Laboratory of Technische Universität München. The IR spectra were recorded as nujol mulls between KBr plates. NMR spectra were recorded on a Bruker Avance III 400 spectrometer and were calibrated to the residual proton resonance and the natural abundance ^{13}C resonance of the solvent (CD_2Cl_2: δ_H = 5.32 and δ_C = 54.00 ppm; C_6D_6: δ_H = 7.16 and δ_C = 128.06 ppm; d_8-THF: δ_H = 3.58 and δ_C = 67.57 ppm; d_8-toluene: δ_H = 2.09). ^{31}P NMR chemical shifts are reported relative to external phosphoric acid (δ = 0.0 ppm). Signal multiplicities are abbreviated as: s (singlet), d (dublet), t (triplet), q (quartet), m (multiplet), br (broad). Temperature-dependent magnetic susceptibility data were recorded on an MPMS Quantum Design SQUID magnetometer at 1 T in the temperature range 2 – 300 K.

---

27 a) M. A. Fox, J. E. Harris, S. Heider, V. Perez-Gregorio, M. E. Zakrzewska, J. D. Farmer, D. S. Yufit, J. A. Howard, P. Low, *J. Organomet. Chem.* **2009**, *694*, 2350; b) J. Meiners, A. Friedrich, E. Herdtweck, S. Schneider, *Organometallics* **2009**, *28*, 6331.

Syntheses

[RuCl$_2$(HPNP^{tBu})] *(2)*: HN(CH$_2$CH$_2$P^{t}Bu$_2$)$_2$ (0.101 g; 0.279 mmol) is added to a suspension of **1** (0.268 g; 0.279 mmol) in 10 mL THF. **2** slowly precipitates from solution as a green solid. After 2 h at r.t., the solid is filtered off, washed with pentane (2 x 10 mL) and diethyl ether (2x 10 mL), and dried *i. vac.* Yield: 0.136 g of diastereomeres **2a** and **2b** (0.254 mmol, 91%). Anal. Calc. for C$_{20}$H$_{45}$Cl$_2$NP$_2$Ru (533.51): C, 45.03; H, 8.50; N, 2.63. Found: 45.62; H, 8.59; N, 2.59. IR (cm^{-1}) $\tilde{\nu}$ = 3131 (N-H). NMR (CD$_2$Cl$_2$, RT, [ppm]) ^{1}H NMR (399.8 MHz): δ = 10.29 (s (br), 1H, N*H*, **2a**), 5.90 (s (br), 1H, N*H*, **2b**), 3.58-3.36 (m, 2H, PC*H*$_2$, **2a**), 3.36-3.15 (m, 2H, PC*H*$_2$, **2b**), 2.87-2.75 (m, 2H, NC*H*$_2$, **2a**), 2.74-2.64 (m, 2H, NC*H*$_2$, **2a**), 2.63-2.53 (m, 2H, NC*H*$_2$, **2b**), 2.53-2.43 (m, 2H, NC*H*$_2$, **2b**), 2.40-2.32 (m, 2H, PC*H*$_2$, **2b**), 2.31-2.17 (m, 2H, PC*H*$_2$, **2a**), 1.57 (s (br), 18H, C*H*$_3$, **2a**), 1.47 (s (br), 18H, C*H*$_3$, **2b**), 0.59 (s (br), 18H, C*H*$_3$, **2a**), 0.39 (s, (br), 18H, C*H*$_3$, **2b**). ^{13}C {^{1}H} NMR (100.6 MHz): δ = 56.2 (s (br), N*C*H$_2$, **2a**), 55.4 (s (br), N*C*H$_2$, **2b**), 41.4 (s (br), P*C*(CH$_3$)$_3$), 38.6 (s (br), P*C*(CH$_3$)$_3$), 37.6 (s (br), P*C*(CH$_3$)$_3$), 36.8 (s (br), P*C*(CH$_3$)$_3$), 30.9 (s, *C*H$_3$, **2a**), 30.0 (s, *C*H$_3$, **2b**), 28.5 (s, *C*H$_3$, **2a**), 25.8 (s, *C*H$_3$, **2b**), 25.3 (s (br), *C*H$_2$P, **2a**), 23.7 (s (br), *C*H$_2$P, **2b**). ^{31}P{^{1}H} NMR (161.83 MHz): δ = 45.2 (s (br), *P*^{t}Bu$_2$), 32.1 (s, *P*^{t}Bu$_2$).

[RuCl(PNP^{tBu})] *(3)*. A mixture of **2** (28.5 mg, 0.053 mmol) and KO^{t}Bu (6 mg, 0.053, 1.0 equiv.) are dissolved in THF (5 mL) at -78 °C. The ligth brown suspension is warmed to -20 °C, filtered, and the solvent is evaporated *i. vac.* The residue is washed with pentane at -78 °C to give a tan, highly air sensitive solid. Yield: 21.8 mg (0.044 mmol, 82%). Anal. Calc. for C$_{20}$H$_{44}$ClNP$_2$Ru (497.05): C, 48.33; H, 8.92; N, 2.82. Found: C, 49.16; H, 8.64; N, 2.71. NMR ([D$_8$]THF, 260 K, [ppm]) ^{1}H NMR (399.8 MHz): δ = 10.63 (br, NC*H*$_2$, 4H), 1.50 (A$_{18}$XX´A´$_{18}$, N = |^{3}J(H,P) + ^{5}J(H,P)| = 12.0 Hz, C*H*$_3$, 36H), 0.86 (br, PC*H*$_2$, 4H). ^{13}C{^{1}H} NMR (100.53 MHz): d = 58.9 (AXX´A´, N = |^{2}J(C,P) + ^{4}J(C,P)| = 13.0 Hz, N*C*H$_2$), 34.8 (s, *C*H$_3$), 30.3 (A$_2$XX´A´$_2$, N = |^{1}J(C,P) + ^{3}J(C,P)| = 12.2 Hz, *C*(CH$_3$)$_3$), 21.6 (AXX´A´, N = |^{1}J(C,P) + ^{3}J(C,P)| = 10.0 Hz, P*C*H$_2$). ^{31}P{^{1}H} NMR (161.83 MHz) δ = -4.3 (s, *P*^{t}Bu$_2$). ([D$_6$]benzene, RT, [ppm]) ^{1}H NMR (399.8 MHz): δ = 14.41 (br, NC*H*$_2$, 4H), 1.48 (A$_{18}$XX´A´$_{18}$, N = |^{3}J(H,P) + ^{5}J(H,P)| = 12.4 Hz, C*H*$_3$, 36H), 0.13 (br, PC*H*$_2$, 4H). ^{31}P{^{1}H} NMR (161.83 MHz) δ = -22.6 (s, *P*^{t}Bu$_2$).

[RuHCl(PN=P^{tBu})] *(4)*. A solution of **3** (44.7 mg, 0.084 mmol) in THF (5 mL) is stirred over 2 days at room temperature. Upon evaporation of the solvent, **5** is obtained as a dark red, microcristalline solid. Yield: 40.7 mg (0.033 mmol, 98%). Anal. Calc. for C$_{20}$H$_{44}$ClNP$_2$Ru (497.05): C, 48.33; H, 8.92; N, 2.82. Found: C, 48.53; H, 8.47; N, 2.54. IR (cm^{-1}) $\tilde{\nu}$ = 2068 (s, Ru-H), 1566 (s, N=C). NMR ([D$_6$]benzene, RT, [ppm]) ^{1}H NMR (399.8 MHz): δ = 7.37

(d, ^3J(H,P) = 20.3 Hz, 1H, NCH), 3.37 – 3.19 (m, 1H, NCH_2), 2.91 – 2.76 (m, 1H, NCH_2), 2.15 – 1.97 (m, 2H, PCH_2), 1.47 – 1.40 (m, 2H, PCH_2), 1.38-1.34 (m, 18H, CH_3), 1.32 (d, ^3J(H,P) = 9.7 Hz, 9H, CH_3), 1.27 (d, ^3J(H,P) = 10.0 Hz, 9H, CH_3), -32.25 (dd, ^3J(H,P) = ^3J(H,P) = 20.0 Hz, 1H). ^{13}C{^{1}H} NMR (100.53 MHz): δ = 162.1 (dd, ^3J(C,P) = 2.7 Hz, ^2J(C,P) = 6.9 Hz, NCH), 65.9 (dd, ^3J(C,P) = 2.8 Hz, ^2J(C,P) = 5.9 Hz, NCH_2), 36.2 (dd, ^3J(C,P) = 4.0 Hz, ^1J(C,P) = 6.8 Hz, C(CH$_3$)$_3$), 36.0 (AXY, N = |^1J(C,P) + ^3J(C,P)| = 10.0 Hz, C(CH$_3$)$_3$), 34.3 (dd, ^3J(C,P) = 5.3 Hz, ^1J(C,P) = 7.6 Hz, C(CH$_3$)$_3$), 33.9 (dd, ^3J(C,P) = 4.5 Hz, ^1J(C,P) = 6.1 Hz, C(CH$_3$)$_3$), 32.3 (d, ^1J(C,P) = 8.8 Hz, PCH_2), 28.6 (dd, ^4J(C,P) = 1.9 Hz, ^2J(C,P) = 4.5 Hz, CH$_3$), 28.5 (dd, ^4J(C,P) = 2.1 Hz, ^2J(C,P) = 4.9 Hz, CH$_3$), 28.4 (dd, ^4J(C,P) = 2.2 Hz, ^2J(C,P) = 4.9 Hz, CH$_3$), 28.1 (dd, ^4J(C,P) = 2.0 Hz, ^2J(C,P) = 4.9 Hz, CH$_3$), 23.7 (d, ^1J(C,P) = 9.9 Hz, PCH_2). ^{31}P{^{1}H} NMR (161.83 MHz) δ = 84.1 (d, ^2J(P,P) = 317.2 Hz, P^tBu$_2$), 81.6 (d, ^2J(P,P) = 317.2 Hz, P^tBu$_2$).

2.5 Single crystal X-ray diffraction

Suitable single-crystals for the X-ray diffraction studies were grown by diffusion of pentane into a CH$_2$Cl$_2$ solution at room temperature (**2**) or diffusion of pentane into a toluene solution at -78 °C (**3**). Crystals were stored under perfluorinated ether, transferred to a Lindemann capillary, fixed, and sealed. Preliminary examinations and data collection were carried out with an APEX II (Bruker AXS) area detecting system and a rotating anode X-ray source (Bruker AXS, FR591) using graphite-monochromated Mo-K$_α$ radiation ($λ$ = 0.71073 Å). The unit cell parameters were obtained from 9998 (**2**) and 9913 (**3**) reflexes, respectively, by full-matrix least-squares refinements during the scaling procedures.[28] 199966 reflexes (**2**; $θ_{max}$: 25.35°, 10 s per frame, 4855 frames, $Δφ/ΔΩ$: 0.50°, dx: 45.0 mm) and 66229 reflexes (**3**; $θ_{max}$: 25.34°, 20 s per frame, 3240 frame, $Δφ/ΔΩ$: 0.50°, dx: 40.0 mm), respectively, were measured. Intensities were integrated and the raw data were corrected for Lorentz, polarization, and arising from the scaling procedure for latent decay.[29] Upon averaging, (**2**: R_{int}=0.075; **3**: R_{int}=0.054) 10871 (**2**; all data) and 4463 (**3**; all data) independent reflexes (9715 (**2**) and 3824 (**3**) with $I>2σ(I)$), respectively, were used for further calculations. The structures were solved by direct methods (SIR-92).[30] Full-matrix least-squares refinements were

---

[28] APEX suite of crystallographic software. APEX 2 Version 2008.4. Bruker AXS Inc., Madison, Wisconsin, USA, **2008**.

[29] SAINT, Version 7.56a and SADABS Version 2008/1. Bruker AXS Inc., Madison, Wisconsin, USA, **2008**.

[30] A. Altomare, G. Cascarano, C. Giacovazzo, A. Guagliardi, M. C. Burla, G. Polidori, M. Camalli, *J. Appl. Cryst.* **1994**, *27*, 435.

carried out by minimizing $\Sigma w(F_o^2 - F_c^2)^2$ with the SHELXL-97 weighting scheme.[31] The final residual electron density maps showed no remarkable features. Neutral atom scattering factors for all atoms and anomalous dispersion corrections for the non-hydrogen atoms were taken from *International Tables for Crystallography*.[32] All non-hydrogen atoms were refined with anisotropic displacement parameters. All hydrogen atoms of **2** were placed in ideal positions and refined using a riding model. All hydrogen atoms of **3** could be localized in the last refinement cycles and were refined with individual isotropic displacement parameters. Two solvent molecules in the structure of **2** (dichloromethane) could not be modeled satisfactory and were treated by the "calc squeeze" algorithm.[33] The asymmetric unit of **2** contains two crystallographically independent molecules. Figures were prepared with the program DIAMOND.[34]

2.6 Spectroscopic results
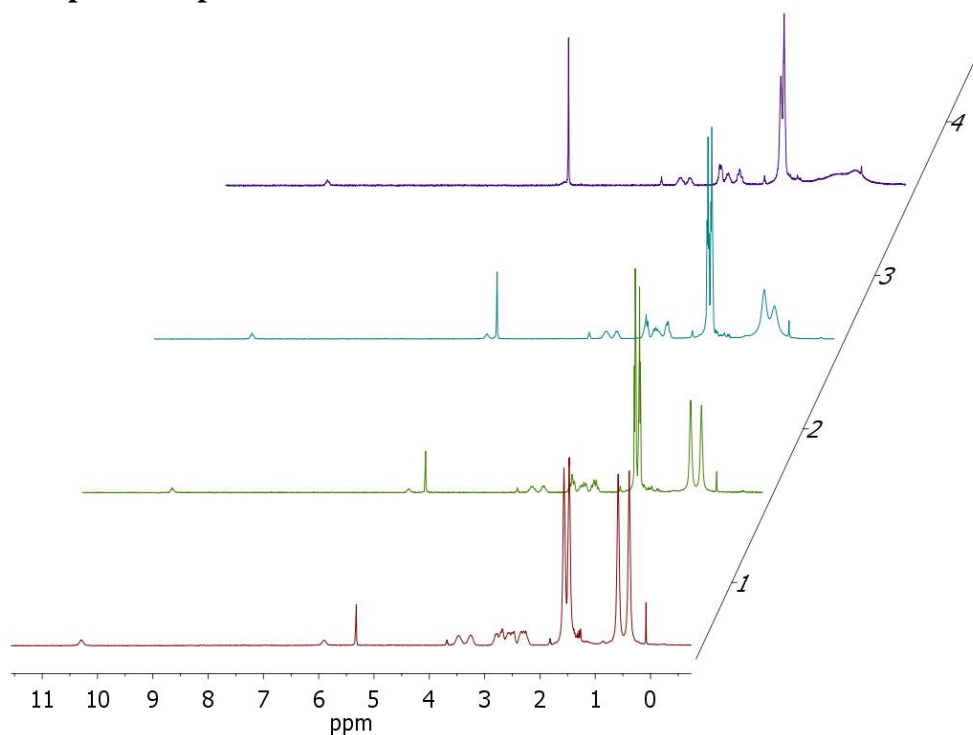
Figure B-2.4: Temperature dependent ^{1}H NMR spectra of complex **2** in CD_2Cl_2 (300 K (1), 270 K (2), 250 K (3), 230 K (4)).

31 G. M. Sheldrick, SHELXL-97, University of Göttingen, Göttingen, Germany, **1998**;

32 International Tables for Crystallography, Vol. C, Tables 6.1.1.4 (pp. 500-502), 4.2.6.8 (pp. 219-222), and 4.2.4.2 (pp. 193-199) (Hrsg.: A. J. C. Wilson), Kluwer Academic Publishers, Dordrecht, The Netherlands, **1992**.

33 a) A. L. Spek, PLATON, A Multipurpose Crystallographic Tool, Utrecht University, Utrecht, The Netherlands, **2010**; b) L. J. Farrugia, *J. Appl. Cryst.* **1999**, *32*, 837.

34 Brandenburg, K.; Diamond, Version 3.1d, Crystal Impact GbR, Bonn, Germany, **2006**.

Figure B-2.5: ^{1}H NOESY NMR spectrum (CD$_2$Cl$_2$, 300 K) of complex **2**.

Figure B-2.5: ^{1}H COSY NMR spectrum (CD$_2$Cl$_2$, 270 K) of complex **2**.
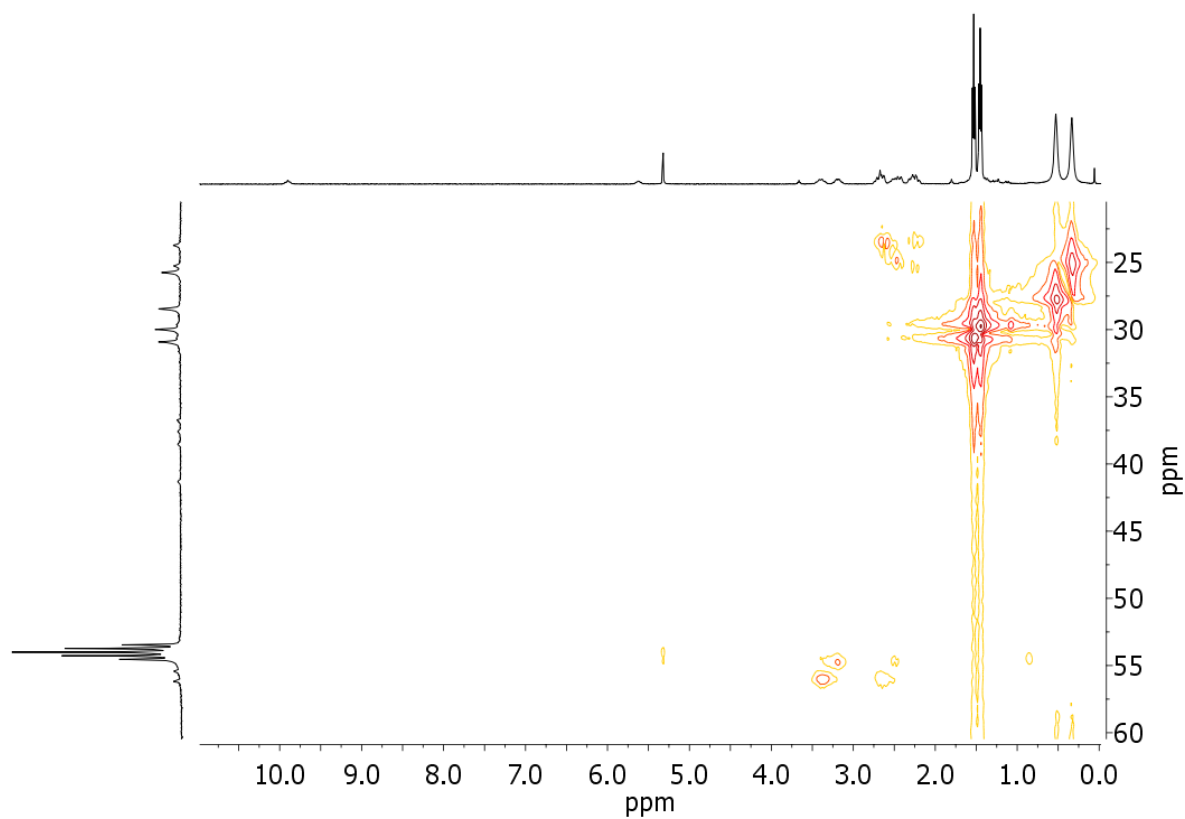
Figure B-2.6: ^{1}H-^{13}C HMQC NMR spectrum (CD$_2$Cl$_2$, 270 K) of complex **2**.
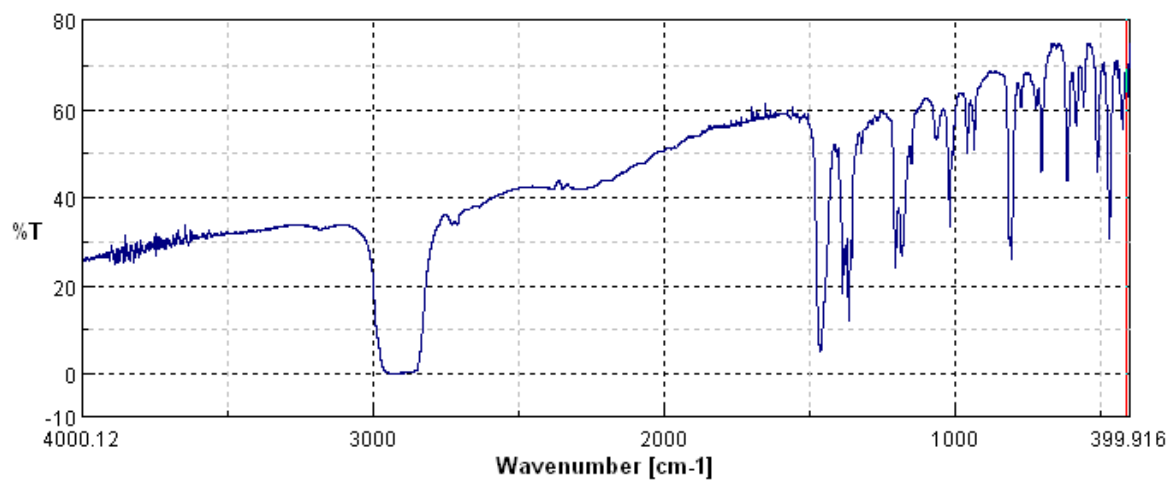
Figure B-2.7: IR-spectrum (Nujol mull) of complex **3**.
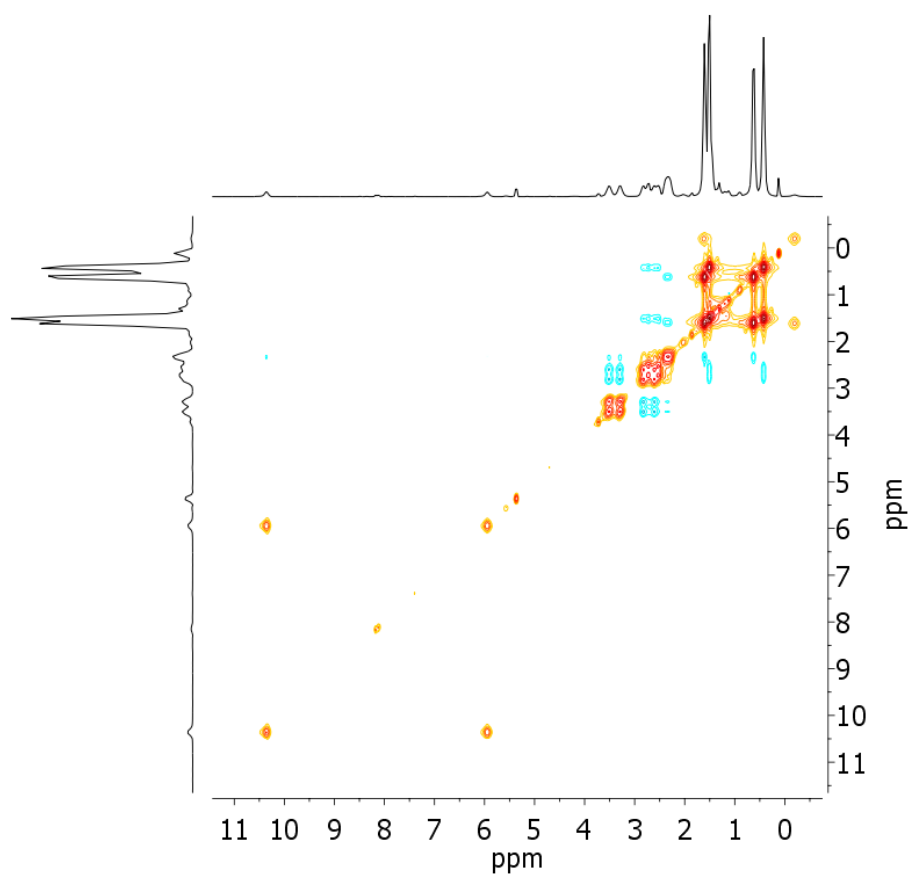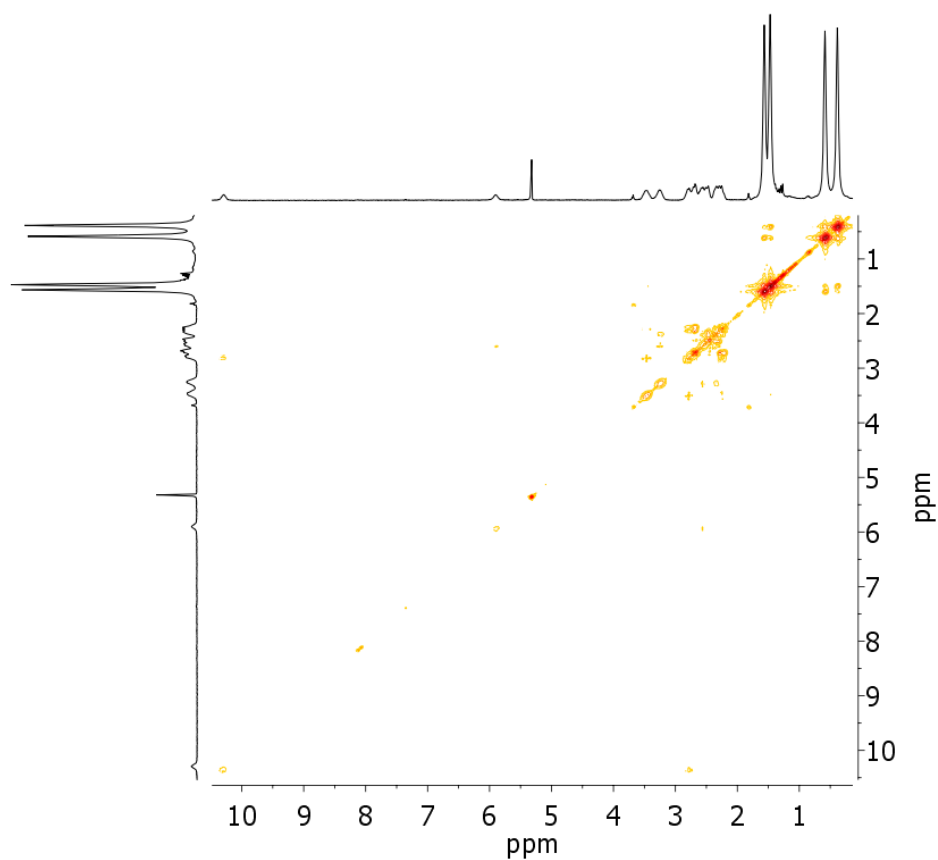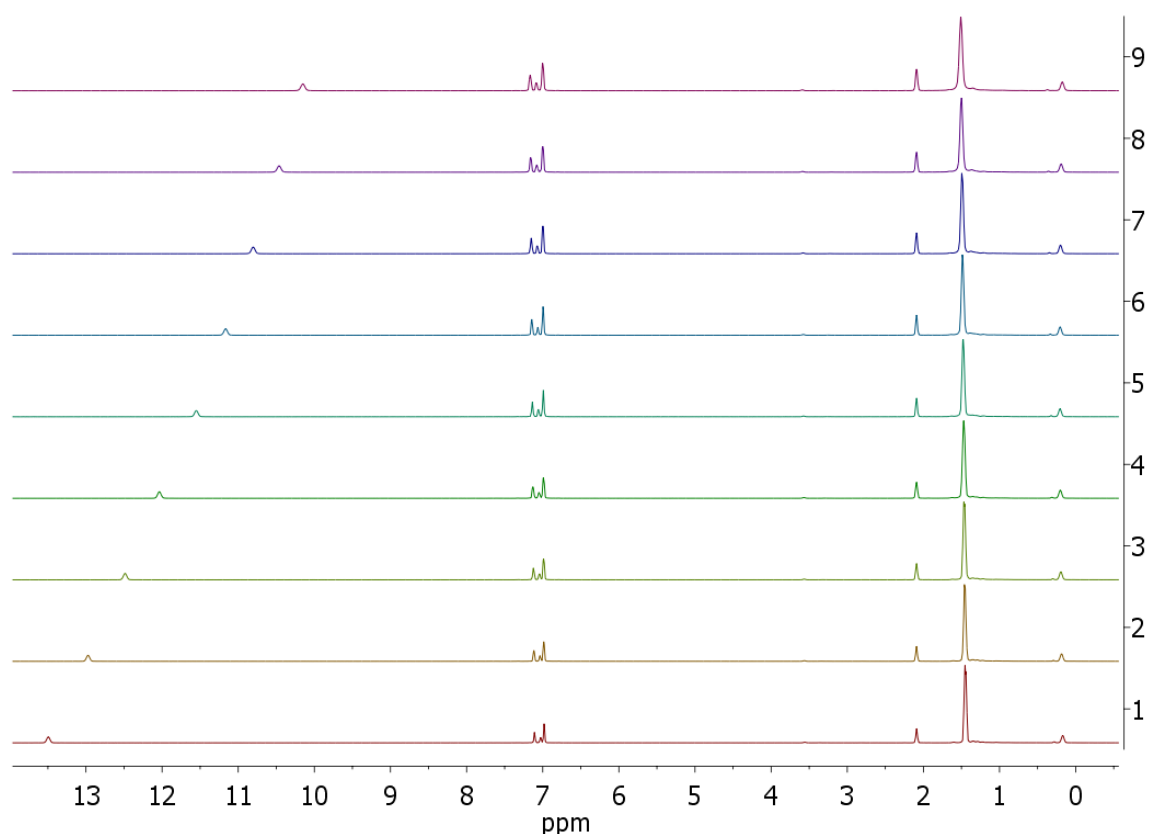
Figure B-2.8: VT-^{1}H NMR of complex **3** (d_8-toluene; 280 K (1), 270 K (2), 260 K (3), 250 K (4), 240 K (5), 230 K (6), 220 K (7), 210 K (8), 200 K (9)).

Least-squares fitting of the temperature dependent [1]H(NCH_2) and ^{31}P signals of complex **3** in d_8-toluene was performed using the Microsoft Excel tool Solver.[35] Chemical shifts were fitted to the formula:

$$\delta = \delta^{\mathrm{dia}} + C / (T \cdot e^{(\Delta H + T\Delta S)}) \; {}^{[36]}$$

Fitting results:

T [K]	δ(NCH_2) exp [ppm]	δ(NCH_2) fit [ppm]	δ(P) exp [ppm]	δ(P) fit [ppm]
200	10.15	10.17	-5.23	-5.27
210	10.46	10.46	-6.47	-6.45
220	10.80	10.79	-7.86	-7.80
230	11.16	11.16	-9.28	-9.31
240	11.55	11.56	-10.89	-10.97
250	12.04	12.01	-12.88	-12.78
260	12.49	12.48	-14.73	-14.72
270	12.97	12.98	-16.78	-16.77
280	13.49	13.50	-18.91	-18.92

[35]   D. C. Harris, *J. Chem. Ed.* **1998**, *75*, 119.
[36]   a) P. Gütlich, B. R. McGarvey, W. Kläui, *Inorg. Chem.* **1980**, *19*, 3704; b) M. E. Smith, R. A. Andersen, *J. Am. Chem. Soc.* **1996**, *118*, 11119.

Fit parameters from fitting of both curves:

Parameter	Result	Std. dev	Std. error
ΔH [J/mol]	10578	64	256
ΔS [J/molK]	4.2	0.2	0.8
$\delta_{LS}(NCH_2)$ [ppm]	9.17	0.02	0.07
$C(NCH_2)$ [K]	70307	1	6
$\delta_{LS}(P)$ [ppm]	-1.18	0.07	0.27
$C(P)$ [K]	-287910	1	1
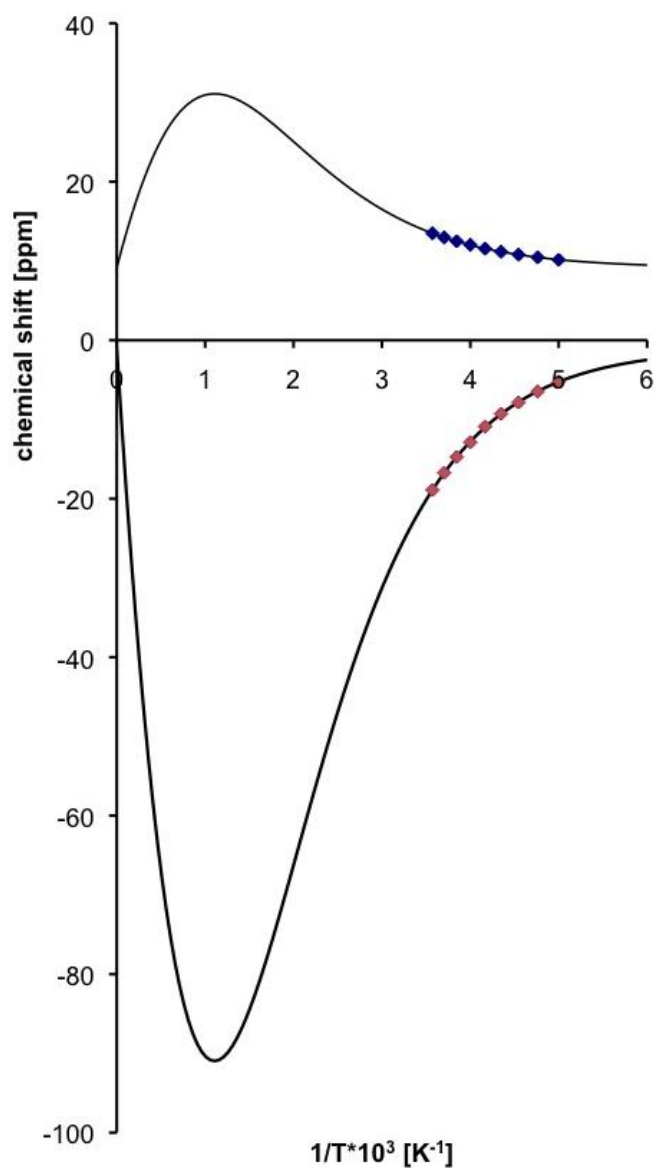
Figure B-2.9: Least squares fits (black lines) of the ^{1}H(NCH_2) (◆) and ^{31}P (◆) shifts of complex **3**.
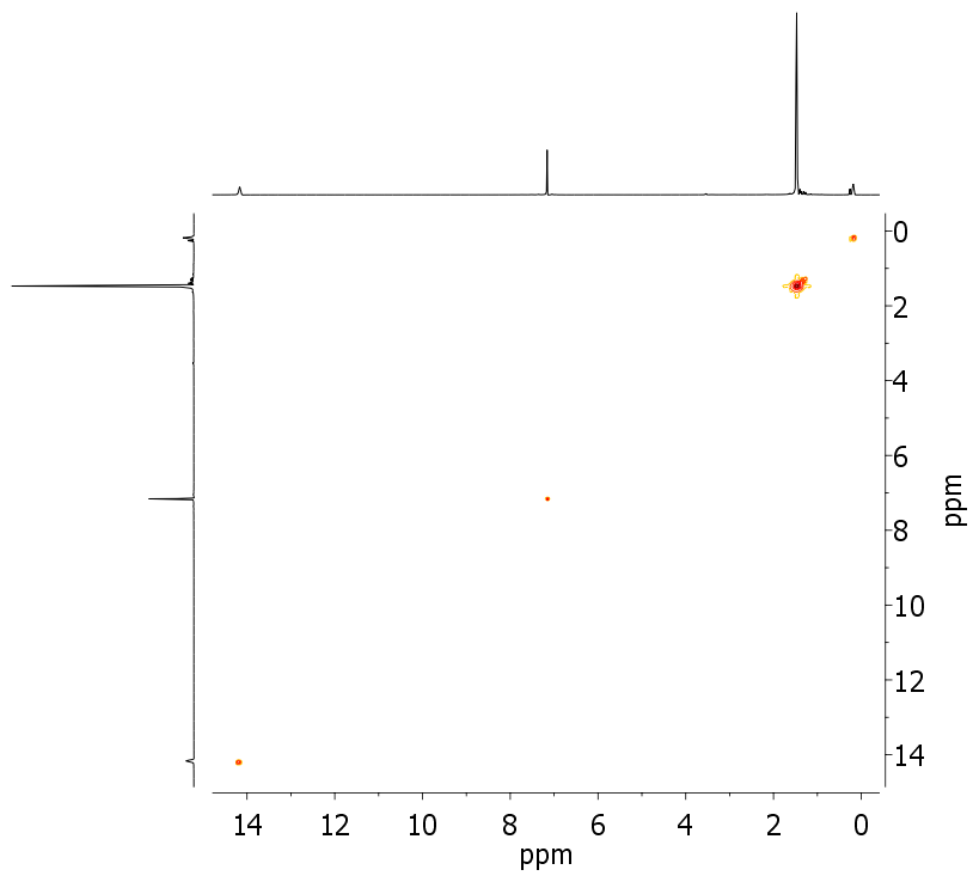
Figure B-2.10: ^{1}H COSY NMR spectrum (d^6-benzene, r.t.) of complex **3**.
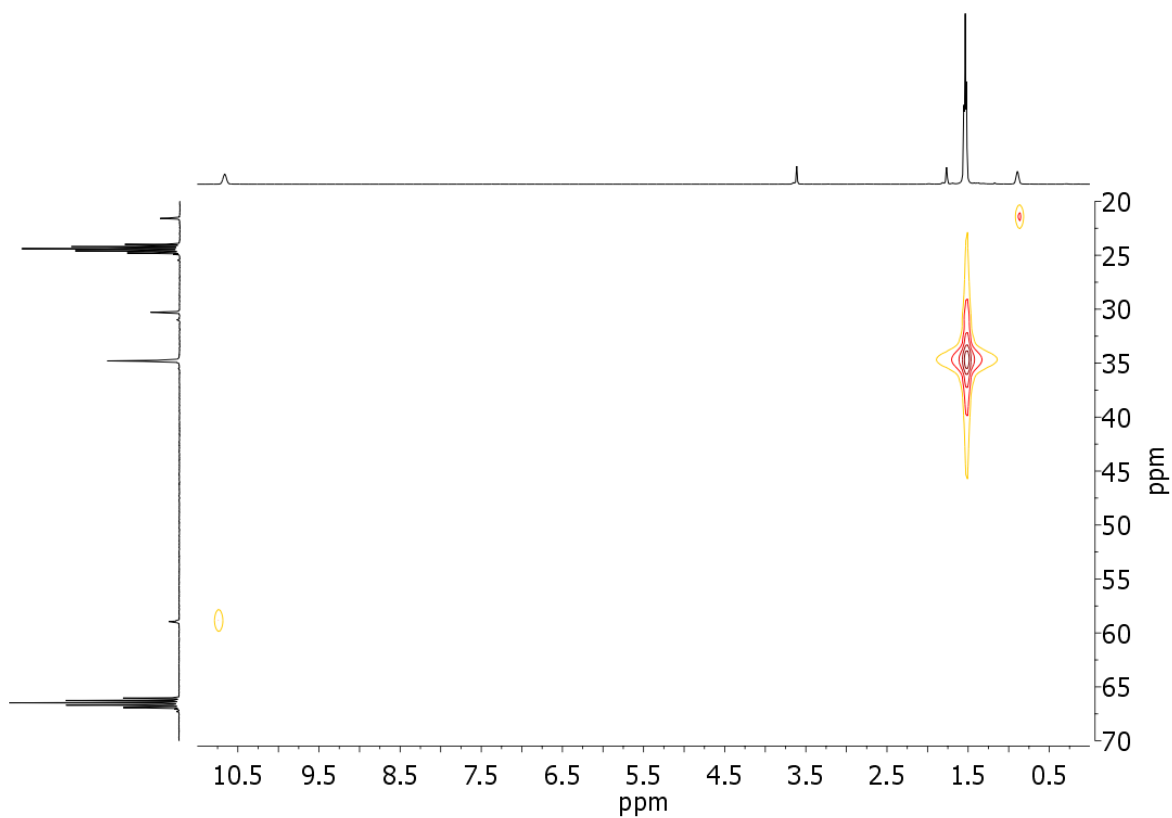
Figure B-2.11: ^{1}H-^{13}C HMQC NMR spectrum (d^8-THF, 260 K) of complex **3**.
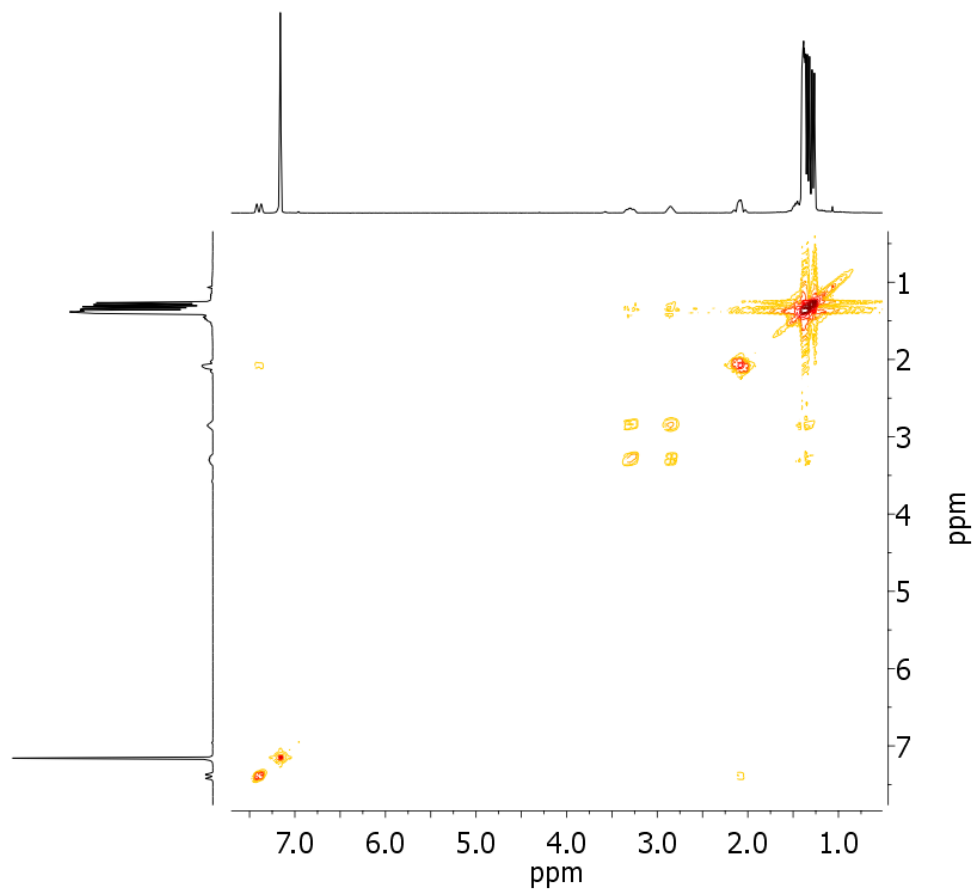
Figure B-2.12: ^{1}H COSY NMR spectrum (d^6-benzene, r.t.) of complex **4**.
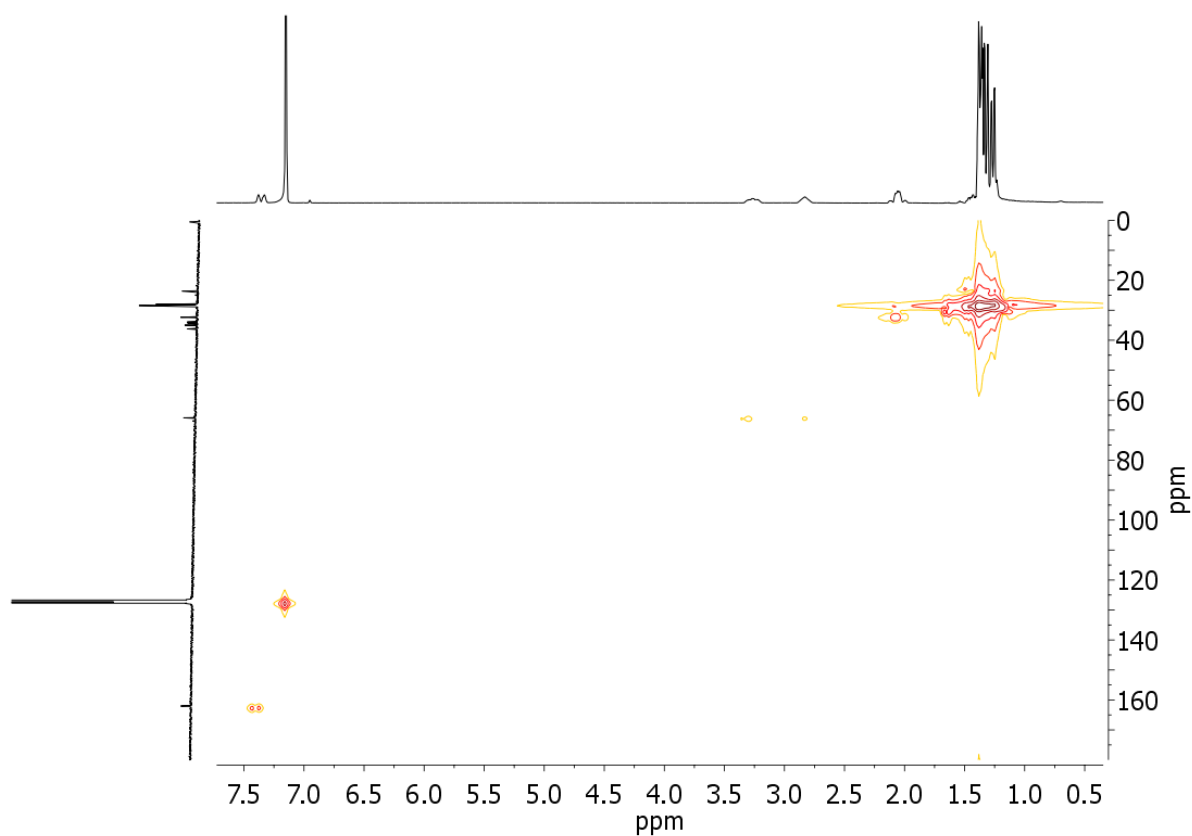
Figure B-2.13: ^{1}H-^{13}C HMQC NMR spectrum (d^6-benzene, r.t.) of complex **4**.

2.7 Computational results

Geometry optimizations without symmetry restrictions were executed with the program Gaussian-03 using the functionals B3LYP and BP86, respectively.[37,38] Stuttgart-Dresden-ECP and respective basisset were used for ruthenium and split valence double-ζ basisset 6-31+G** for all other atoms.[39,40] Single-point calculations with the triple-ζ basisset 6-311+G** were obtained using the optimized geometries as input structures. All optimized geometries were verified as being true minima by the absence of negative eigenvalues in the vibrational frequency analysis. NBO analyses were obtained with the program NBO V3.1 as implemented in the program package Gaussian-03.[41]

37   M. J. Frisch, G. W. Trucks, H. B. Schlegel, G. E. Scuseria, M. A. Robb, J. R. Cheeseman, J. A. Montgomery, Jr., T. Vreven, K. N. Kudin, J. C. Burant, J. M. Millam, S. S. Iyengar, J. Tomasi, V. Barone, B. Mennucci, M. Cossi, G. Scalmani, N. Rega, G. A. Petersson, H. Nakatsuji, M. Hada, M. Ehara, K. Toyota, R. Fukuda, J. Hasegawa, M. Ishida, T. Nakajima, Y. Honda, O. Kitao, H. Nakai, M. Klene, X. Li, J. E. Knox, H. P. Hratchian, J. B. Cross, V. Bakken, C. Adamo, J. Jaramillo, R. Gomperts, R. E. Stratmann, O. Yazyev, A. J. Austin, R. Cammi, C. Pomelli, J. W. Ochterski, P. Y. Ayala, K. Morokuma, G. A. Voth, P. Salvador, J. J. Dannenberg, V. G. Zakrzewski, S. Dapprich, A. D. Daniels, M. C. Strain, O. Farkas, D. K. Malick, A. D. Rabuck, K. Raghavachari, J. B. Foresman, J. V. Ortiz, Q. Cui, A. G. Baboul, S. Clifford, J. Cioslowski, B. B. Stefanov, G. Liu, A. Liashenko, P. Piskorz, I. Komaromi, R. L. Martin, D. J. Fox, T. Keith, M. A. Al-Laham, C. Y. Peng, A. Nanayakkara, M. Challacombe, P. M. W. Gill, B. Johnson, W. Chen, M. W. Wong, C. Gonzalez, and J. A. Pople, *Gaussian03 Rev. D.01*; Gaussian Inc.: Wallingford, CT, **2004**.

38   a) S. H. W. L. Vosko, M. Nusair, *Can. J. Phys.* **1980**, *58*, 1200; b) J. P. Perdew, *Phys. Rev. B* **1986**, *33*, 8822; c) C. Lee, W. Yang, R. G. Parr, *Phys. Rev. B* **1988**, *37*, 785; d) A. D. Becke, *Phys. Rev. A* **1988**, *38*, 3098; e) A.D. Becke, *J. Chem. Phys.* **1993**, *98*, 5648; f) P. J. Stephens, F. J. Devlin, C.F. Chabalowski, M. J. Frisch, *J. Phys. Chem.* **1994**, *98*, 11623.

39   M. Dolg, H. Stoll, H. Preuss, R.M. Pitzer, *J. Phys. Chem.* **1993**, *97*, 5852.

40   a) W. J. Hehre, R. Ditchfield, J. A. Pople, *J. Chem. Phys.* **1972**, *56*, 2257; b) M. M. Francl, W. J. Petro, W. J. Hehre, J. S. Binkley, M. S. Gordon, D. J. DeFrees and J. A. Pople, *J. Chem. Phys.* **1982**, *77*, 3654.

41   E. D. Glendening, A. E. Reed, J. E. Carpenter, F. Weinhold, NBO Version 3.1.

Table B-2.1: Comparison of computational results.

	X-ray	**DFT**			
Functional		**B3LYP**		**BP86**	
Spinstate		Singlet	Triplet	Singlet	Triplet
Basiset		**6-31+G****			
Geometry					
Ru-N [Å]	1.890(2)	1.901	1.991	1.897	1.986
Ru-Cl [Å]	2.3805(6)	2.395	2.445	2.380	2.428
N-Ru-Cl [°]	179.63(6)	179.4	177.2	179.5	175.9
Energy					
ΔE_{S-T} [kcal/mol]		+1.8		-2.9	
ΔE_{S-T} [kcal/mol] (with ZPE)		+2.3		-2.0	
ΔS_{S-T} [cal/molK]		-1.4		-6.3	
ΔG_{S-T}^{300K} [kcal/mol]		+3.1		-0.5	
NPA-Analysis					
q_{Ru} [e]		-0.35	-0.06	-0.52	-0.21
q_{N} [e]		-0.43	-0.57	-0.35	-0.50
q_{Cl} [e]		-0.42	-0.50	-0.34	-0.44
q_{P} [e]		+1.17	+1.13	+1.16	+1.13
WBI_{RuN}		+1.17	+0.73	+1.19	+0.74
WBI_{RuCl}		+0.77	+0.62	+0.82	+0.65
Basiset		**6-311+G****			
ΔE_{S-T} [kcal/mol]		+2.2		-2.9	

Table B-2.2: Coordinates of **3** (singlet state, B3LYP).

Center Number	Atomic Number	Atomic Type	Coordinates (Angstroms)		
			X	Y	Z
1	44	0	0.000000	0.056276	0.030759
2	17	0	0.000007	1.181458	-2.083372
3	15	0	2.351005	-0.042367	0.208304
4	15	0	-2.351002	-0.042365	0.208312
5	7	0	0.000001	-0.855514	1.698395
6	6	0	1.207096	-1.352124	2.396362
7	6	0	2.484949	-0.616057	1.983553
8	6	0	-1.207093	-1.352124	2.396365
9	6	0	-2.484945	-0.616052	1.983561
10	6	0	3.358295	1.595789	0.206937
11	6	0	3.656283	2.038903	-1.240651
12	6	0	2.439276	2.658656	0.852815
13	6	0	4.674190	1.535059	1.011470
14	6	0	3.245025	-1.398553	-0.820843
15	6	0	2.620115	-2.749432	-0.402826
16	6	0	4.768201	-1.480231	-0.608139
17	6	0	2.939470	-1.182283	-2.318972
18	6	0	-3.358286	1.595791	0.206935
19	6	0	-2.439254	2.658676	0.852767
20	6	0	-3.656291	2.038861	-1.240665
21	6	0	-4.674163	1.535082	1.011497
22	6	0	-3.245038	-1.398539	-0.820839
23	6	0	-2.620358	-2.749462	-0.402622
24	6	0	-4.768254	-1.480019	-0.608350
25	6	0	-2.939238	-1.182417	-2.318939
26	1	0	1.297682	-2.431106	2.200245
27	1	0	1.062601	-1.248994	3.482277
28	1	0	3.371016	-1.230953	2.174452
29	1	0	2.583098	0.287910	2.591456
30	1	0	-1.062594	-1.248998	3.482279
31	1	0	-1.297684	-2.431105	2.200244
32	1	0	-2.583087	0.287918	2.591462
33	1	0	-3.371015	-1.230942	2.174464
34	1	0	2.751972	2.043966	-1.856079
35	1	0	4.405582	1.403200	-1.720990
36	1	0	4.060347	3.059517	-1.224399
37	1	0	2.972466	3.617871	0.885520
38	1	0	2.159341	2.402317	1.880315
39	1	0	1.519619	2.792588	0.278312
40	1	0	4.510172	1.277977	2.062817
41	1	0	5.145153	2.526739	0.993609
42	1	0	5.393615	0.826563	0.597293
43	1	0	1.528395	-2.726800	-0.477566
44	1	0	2.896038	-3.036689	0.617099
45	1	0	2.990212	-3.535768	-1.072718
46	1	0	5.039547	-1.587983	0.447773
47	1	0	5.290145	-0.608302	-1.010420

48	1	0	5.157187	-2.361335	-1.135586
49	1	0	3.351697	-2.023451	-2.891873
50	1	0	3.385174	-0.265824	-2.710903
51	1	0	1.864000	-1.130763	-2.505916
52	1	0	-1.519605	2.792588	0.278248
53	1	0	-2.159308	2.402365	1.880271
54	1	0	-2.972442	3.617893	0.885451
55	1	0	-4.405611	1.403159	-1.720971
56	1	0	-2.751989	2.043882	-1.856107
57	1	0	-4.060327	3.059487	-1.224444
58	1	0	-5.393588	0.826559	0.597368
59	1	0	-5.145136	2.526756	0.993602
60	1	0	-4.510116	1.278050	2.062853
61	1	0	-1.528624	-2.726977	-0.477214
62	1	0	-2.990457	-3.535805	-1.072506
63	1	0	-2.896461	-3.036604	0.617285
64	1	0	-5.039760	-1.587662	0.447532
65	1	0	-5.157265	-2.361121	-1.135784
66	1	0	-5.290043	-0.608063	-1.010770
67	1	0	-1.863736	-1.131017	-2.505726
68	1	0	-3.384789	-0.265938	-2.711001
69	1	0	-3.351465	-2.023585	-2.891839

Table B-2.3: Coordinates of **3** (triplet state, B3LYP).

Center Number	Atomic Number	Atomic Type	Coordinates (Angstroms)		
			X	Y	Z
1	44	0	-0.000001	0.031924	-0.011068
2	17	0	0.000008	1.291832	-2.106800
3	15	0	2.360416	-0.067651	0.217331
4	15	0	-2.360417	-0.067650	0.217329
5	7	0	-0.000003	-0.907488	1.743642
6	6	0	1.205518	-1.481211	2.348197
7	6	0	2.477608	-0.708224	1.972584
8	6	0	-1.205524	-1.481215	2.348194
9	6	0	-2.477614	-0.708229	1.972578
10	6	0	3.316431	1.594948	0.285090
11	6	0	3.614024	2.104476	-1.140515
12	6	0	2.353176	2.601228	0.958277
13	6	0	4.624836	1.544873	1.102559
14	6	0	3.277802	-1.359625	-0.863277
15	6	0	2.667087	-2.736103	-0.513876
16	6	0	4.799185	-1.427279	-0.633581
17	6	0	2.985914	-1.075313	-2.352695
18	6	0	-3.316428	1.594951	0.285094
19	6	0	-2.353097	2.601275	0.958107
20	6	0	-3.614188	2.104390	-1.140508
21	6	0	-4.624738	1.544924	1.102718

22	6	0	-3.277803	-1.359619	-0.863285
23	6	0	-2.667266	-2.736130	-0.513695
24	6	0	-4.799220	-1.427104	-0.633765
25	6	0	-2.985707	-1.075462	-2.352691
26	1	0	1.309824	-2.543042	2.061870
27	1	0	1.103286	-1.479404	3.446723
28	1	0	3.373409	-1.314723	2.146158
29	1	0	2.556916	0.173741	2.614980
30	1	0	-1.103294	-1.479409	3.446720
31	1	0	-1.309826	-2.543045	2.061865
32	1	0	-2.556927	0.173733	2.614978
33	1	0	-3.373413	-1.314732	2.146146
34	1	0	2.715901	2.104999	-1.765173
35	1	0	4.389960	1.513559	-1.635687
36	1	0	3.984313	3.136127	-1.078374
37	1	0	2.856013	3.572906	1.046281
38	1	0	2.057341	2.293220	1.967049
39	1	0	1.447873	2.743332	0.361356
40	1	0	4.460311	1.233497	2.138896
41	1	0	5.059774	2.552361	1.134128
42	1	0	5.373384	0.882059	0.663970
43	1	0	1.575100	-2.730846	-0.597532
44	1	0	2.933933	-3.066796	0.494582
45	1	0	3.051312	-3.485646	-1.216867
46	1	0	5.056752	-1.580952	0.419906
47	1	0	5.308920	-0.526582	-0.984960
48	1	0	5.211709	-2.274179	-1.197779
49	1	0	3.400547	-1.890940	-2.959485
50	1	0	3.438069	-0.143750	-2.697863
51	1	0	1.912872	-1.007530	-2.550096
52	1	0	-1.447857	2.743331	0.361081
53	1	0	-2.057158	2.293338	1.966870
54	1	0	-2.855921	3.572962	1.046093
55	1	0	-4.390232	1.513487	-1.635527
56	1	0	-2.716153	2.104809	-1.765292
57	1	0	-3.984402	3.136070	-1.078393
58	1	0	-5.373343	0.882096	0.664246
59	1	0	-5.059664	2.552416	1.134293
60	1	0	-4.460095	1.233593	2.139049
61	1	0	-1.575270	-2.730992	-0.597235
62	1	0	-3.051492	-3.485696	-1.216662
63	1	0	-2.934254	-3.066705	0.494762
64	1	0	-5.056929	-1.580619	0.419711
65	1	0	-5.211753	-2.274038	-1.197905
66	1	0	-5.308829	-0.526405	-0.985320
67	1	0	-1.912635	-1.007778	-2.549964
68	1	0	-3.437748	-0.143894	-2.697998
69	1	0	-3.400328	-1.891110	-2.959461

Table B-2.4: Coordinates of **3** (singlet state, BP86).

Center Number	Atomic Number	Atomic Type	Coordinates (Angstroms)		
			X	Y	Z
1	44	0	0.000003	0.040360	0.029062
2	17	0	-0.000039	1.120522	-2.084214
3	15	0	2.324987	-0.040708	0.204956
4	15	0	-2.324965	-0.040721	0.205075
5	7	0	0.000038	-0.842380	1.707779
6	6	0	1.212976	-1.329918	2.421803
7	6	0	2.492822	-0.604279	1.991286
8	6	0	-1.212873	-1.329889	2.421876
9	6	0	-2.492725	-0.604218	1.991429
10	6	0	3.326857	1.611557	0.192562
11	6	0	3.589923	2.051514	-1.266533
12	6	0	2.403881	2.663973	0.857900
13	6	0	4.662230	1.568378	0.973266
14	6	0	3.240544	-1.402698	-0.814939
15	6	0	2.616708	-2.750323	-0.374782
16	6	0	4.766444	-1.464085	-0.597918
17	6	0	2.925958	-1.201071	-2.316067
18	6	0	-3.326844	1.611514	0.192515
19	6	0	-2.404094	2.663936	0.858162
20	6	0	-3.589421	2.051453	-1.266680
21	6	0	-4.662470	1.568277	0.972782
22	6	0	-3.240594	-1.402679	-0.814787
23	6	0	-2.615627	-2.750228	-0.375992
24	6	0	-4.766271	-1.465059	-0.596496
25	6	0	-2.927425	-1.199887	-2.316050
26	1	0	1.295239	-2.421155	2.236269
27	1	0	1.058697	-1.211835	3.514324
28	1	0	3.384742	-1.231917	2.166324
29	1	0	2.611041	0.311103	2.595327
30	1	0	-1.058530	-1.211805	3.514387
31	1	0	-1.295180	-2.421123	2.236345
32	1	0	-2.610881	0.311185	2.595451
33	1	0	-3.384657	-1.231818	2.166534
34	1	0	2.663804	2.046814	-1.866312
35	1	0	4.337956	1.411329	-1.763962
36	1	0	3.992379	3.082729	-1.264745
37	1	0	2.915360	3.645929	0.848839
38	1	0	2.174245	2.420693	1.910613
39	1	0	1.447541	2.758529	0.318221
40	1	0	4.525741	1.283508	2.031066
41	1	0	5.107992	2.581776	0.967834
42	1	0	5.400814	0.885075	0.526832
43	1	0	1.514485	-2.717667	-0.438426
44	1	0	2.905441	-3.028754	0.654202
45	1	0	2.978645	-3.552665	-1.045268
46	1	0	5.037783	-1.548710	0.469421

47	1	0	5.281985	-0.585294	-1.018733
48	1	0	5.171626	-2.357065	-1.112271
49	1	0	3.331556	-2.057996	-2.887701
50	1	0	3.377774	-0.283642	-2.723895
51	1	0	1.839826	-1.143263	-2.493792
52	1	0	-1.447595	2.758533	0.318771
53	1	0	-2.174765	2.420640	1.910937
54	1	0	-2.915596	3.645879	0.848972
55	1	0	-4.337098	1.411104	-1.764443
56	1	0	-2.663054	2.046958	-1.866077
57	1	0	-3.992094	3.082582	-1.265043
58	1	0	-5.400906	0.884997	0.526071
59	1	0	-5.108238	2.581673	0.967261
60	1	0	-4.526319	1.283353	2.030613
61	1	0	-1.513482	-2.716952	-0.440672
62	1	0	-2.977754	-3.552370	-1.046612
63	1	0	-2.903244	-3.029422	0.653095
64	1	0	-5.036612	-1.550687	0.471016
65	1	0	-5.171415	-2.357856	-1.111198
66	1	0	-5.282664	-0.586215	-1.016150
67	1	0	-1.841479	-1.141459	-2.494694
68	1	0	-3.380011	-0.282354	-2.722816
69	1	0	-3.333153	-2.056588	-2.887929

Table B-2.5: Coordinates of **3** (triplet state, BP86).

Center Number	Atomic Number	Atomic Type	Coordinates (Angstroms)		
			X	Y	Z
1	44	0	0.000000	0.046898	0.009112
2	17	0	0.000002	1.369440	-2.027404
3	15	0	2.332307	-0.066611	0.215025
4	15	0	-2.332307	-0.066610	0.215024
5	7	0	-0.000001	-0.913518	1.747136
6	6	0	1.210636	-1.486000	2.360169
7	6	0	2.483888	-0.715681	1.973868
8	6	0	-1.210637	-1.485998	2.360170
9	6	0	-2.483889	-0.715678	1.973868
10	6	0	3.321413	1.587042	0.278377
11	6	0	3.615513	2.086485	-1.154749
12	6	0	2.365216	2.600076	0.957636
13	6	0	4.634439	1.511283	1.091092
14	6	0	3.223212	-1.370914	-0.888968
15	6	0	2.585625	-2.736903	-0.532153
16	6	0	4.748847	-1.464340	-0.678820
17	6	0	2.907852	-1.067371	-2.373297
18	6	0	-3.321412	1.587043	0.278376
19	6	0	-2.365216	2.600077	0.957636
20	6	0	-3.615512	2.086486	-1.154750
21	6	0	-4.634439	1.511284	1.091089

22	6	0	-3.223212	-1.370914	-0.888968
23	6	0	-2.585624	-2.736902	-0.532156
24	6	0	-4.748847	-1.464343	-0.678816
25	6	0	-2.907856	-1.067371	-2.373297
26	1	0	1.310457	-2.559300	2.076944
27	1	0	1.101080	-1.478127	3.467546
28	1	0	3.389719	-1.328156	2.131472
29	1	0	2.575779	0.174621	2.620028
30	1	0	-1.101081	-1.478123	3.467547
31	1	0	-1.310460	-2.559298	2.076947
32	1	0	-2.575779	0.174626	2.620026
33	1	0	-3.389720	-1.328152	2.131472
34	1	0	2.703079	2.094494	-1.775490
35	1	0	4.385915	1.476622	-1.656086
36	1	0	4.003189	3.121925	-1.101536
37	1	0	2.873674	3.579916	1.039121
38	1	0	2.075625	2.291387	1.977987
39	1	0	1.446489	2.737806	0.362414
40	1	0	4.465870	1.214395	2.140521
41	1	0	5.101164	2.514992	1.109401
42	1	0	5.367414	0.816790	0.652099
43	1	0	1.483503	-2.702533	-0.601731
44	1	0	2.860296	-3.076514	0.481223
45	1	0	2.945059	-3.501661	-1.246265
46	1	0	5.019975	-1.635823	0.378012
47	1	0	5.272529	-0.560202	-1.029951
48	1	0	5.145132	-2.317960	-1.262207
49	1	0	3.281558	-1.900098	-2.999597
50	1	0	3.388484	-0.142018	-2.725972
51	1	0	1.823856	-0.958180	-2.544722
52	1	0	-1.446487	2.737805	0.362416
53	1	0	-2.075627	2.291388	1.977988
54	1	0	-2.873673	3.579918	1.039119
55	1	0	-4.385930	1.476639	-1.656080
56	1	0	-2.703081	2.094474	-1.775497
57	1	0	-4.003165	3.121935	-1.101538
58	1	0	-5.367416	0.816795	0.652092
59	1	0	-5.101161	2.514994	1.109403
60	1	0	-4.465871	1.214389	2.140517
61	1	0	-1.483501	-2.702527	-0.601724
62	1	0	-2.945049	-3.501657	-1.246276
63	1	0	-2.860303	-3.076522	0.481216
64	1	0	-5.019972	-1.635838	0.378016
65	1	0	-5.145134	-2.317956	-1.262212
66	1	0	-5.272530	-0.560200	-1.029934
67	1	0	-1.823860	-0.958180	-2.544725
68	1	0	-3.388489	-0.142018	-2.725972
69	1	0	-3.281563	-1.900098	-2.999596

----

3 Square-planar ruthenium(II) PNP pincer complexes: control of electronic structure by tunig of N→M π-donation

Unpublishes results:

B. Askevold, M. M. Khusniyarov, J. Meiners, E. Herdtweck, F. Heinemann, S. Schneider

S = 0   **S = 1**
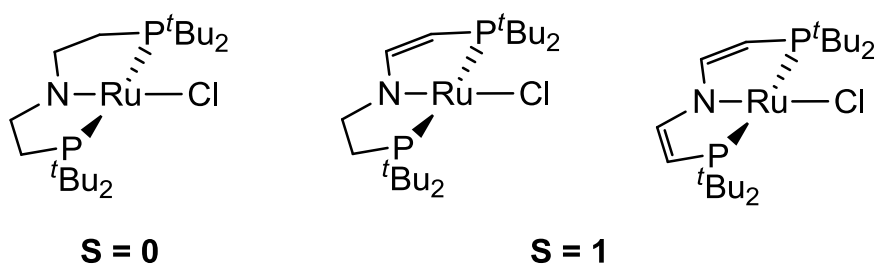
3.1 Introduction

The spin multiplicity of transition metal complexes strongly determines their molecular structure, physical properties, and chemical reactivity. Complexes of $3d$ metal ions generally favour higher spin states, as compared with homologous 2nd and 3rd row metals owing to higher ligand field stabilization and smaller interelectronic repulsion.[1] Metal ions with d^6 valence electron configurations represent an interesting case, because three possible spin-states, i.e. low-spin (LS, S = 0), intermediate-spin (IS, S = 1), and high-spin (HS, S = 2), have to be considered. In fact, for four-coordinate ions, all three spin-states are known, strongly depending on the nature of the metal, the ligands and their geometrical arrangement. Tetrahedral coordination (T_d) of $3d$ ions results in comparatively small ligand field splitting and electronic high spin configuration. In contrast, four-coordinate complexes of $4d$ and $5d$ ions are generally found to exhibit a butterfly-shape (sawhorse or *cis*-divacant octahedral) molecular geometry. The resulting electronic low-spin configuration is, however, usually stabilized by C-H agostic interactions owing to the energetically low-lying LUMO which is localized at the vacant coordination sites.[2] Hence, higher effective coordination numbers than four are obtained, except for very few examples.[3]
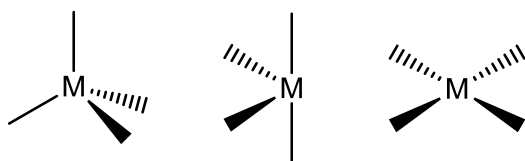
Figure B-3.1: Configuration of 4-coordinate complexes: tetrahedral (left), butterfly-shape (middle) and square-planar (right).

If the ligands are coordinated in a square-planar coordination geometry (D_{4h}), the d-orbital manifold is split into three energetically low lying orbitals, d_{xy} (b_{2g}) and d_{xz}, d_{yz} (e_g), one orbital with intermediate energy, d_{z^2} (a_{1g}), and one high lying orbital, $d_{x^2-y^2}$ (b_{1g}) (Figure B-3.2). In case of $3d^6$ ions with weak-field ligands, electronic high-spin configurations were reported, e.g. iron(II) and cobalt(III) complexes with macrocyclic or chelating N_4 or O_4

[1] S. Alvarez, J. Cirera, *Angew. Chem.* **2006**, *118*, 3078–3087; S. Alvarez, J. Cirera, *Angew. Chem. Int. Ed.* **2006**, *45*, 3012.

[2] a) Y. Jean in *Molecular Orbitals of Transition Metal Complexes*, Oxford University Press, Oxford, **2005**; b) W. Baratta, E. Herdtweck, P. Rigo, *Angew. Chem.* **1999**, *111*, 1733; *Angew. Chem. Int. Ed.* **1999**, *38*, 1629.

[3] J. P. Lee, Z. Ke, M. A. Ramirez, T. B. Gunnoe, T. R. Cundari, P. D. Boyle, J. L. Petersen, *Organometallics* **2009**, *28*, 1758.

ligands.[4,5] Stronger ligand fields can afford an intermediate-spin electronic configuration, $(d_{xy},d_{yz},d_{xz})^5(d_{z^2})^1(d_{x^2-y^2})^0$ (Figure B-3.2, **A**). Ferrous complexes with macrocyclic and rigid chelating ligands, such as iron(II)porphyrinates or iron(II)bis(dithiolates), and in some cases also with monodentate ligands, represent well studied examples.[6,7,8] In contrast, square-planar complexes with 4*d* and 5*d* ions are particularly rare. Gusev and co-workers proposed that the square-planar PCP pincer complex [RuCl{HC(CH$_2$NHP^{t}Bu$_2$)$_2$}] **1** is a transient intermediate in the equilibrium formed by its α− and β−elimination products [Ru(H)Cl{=C(CH$_2$NHP^{t}Bu$_2$)$_2$}] and [Ru(H)Cl{^{t}Bu$_2$PNHCH=CHCH$_2$NHP^{t}Bu$_2$}].[9] DFT calculations, in fact, indicated an intermediate spin ground state for **1**, providing a basis to rationalize the rapid carbene/olefin-complex equilibrium in terms of two-state reactivity.[10] Experimental evidence for an IS square-planar ruthenium(II) complex was first given by Caulton and co-workers which reported the isolation of disilylamide [RuCl{L$_C^{tBu}$}] (**2**; L$_C^{tBu}$ = {N(SiMe$_2$CH$_2$P^{t}Bu$_2$)$_2$}).[11] The magnetic data could be fitted to a model with an S = 1 state, yet an essentially non-magnetic ground state owing to extraordinarily large zero-field splitting. Since then, further examples of such square-planar, paramagnetic 14 valence-electron complexes, such as [Ru(OTf){L$_C^{tBu}$}], [OsI{L$_C^{tBu}$}], or hydrolysis product [Ru(OSiMe$_2$CH$_2$P^{t}Bu$_2$)$_2$], were reported, albeit their magnetic properties were not examined in detail.[12] We recently presented the synthesis of strongly related, square-planar

[4] a) J. Jubb, D. Jacoby, C. Floriani, A. Chiesi-Villa, C. Rizzoli, *Inorg. Chem.* **1992**, *31*, 1306; b) C. A. Nijhuis, E. Jellema, T. J. J. Sciarone, A. Meetsma, P. H. M. Budzclaar, B. Hessen, *Eur. J. Inorg. Chem.* **2005**, 2089; c) S. De Angelis, E. Solari, C. Floriani, A. Chiesi-Villa, C. Rizzoli, *J. Am. Chem. Soc.* **1994**, *116*, 5702.

[5] a) V. Esposito, E. Solari, C. Floriani, N. Re, C. Rizzoli, A. Chiesi-Villa, *Inorg. Chem.* **2000**, *39*, 2604; b) X. Wurzenberger, H. Piotrowski, P. Klüfers, *Angew. Chem.* **2011**, 123, 5078; *Angew. Chem. Int. Ed.* **2011**, *50*, 4974; c) S. A. Cantalupo, S. R. Fiedler, M. P. Shores, A. L. Rheingold, L. H. Doerrer, *Angew. Chem.* **2012**, 124, 1024; *Angew. Chem. Int. Ed.* **2012**, *51*, 1000.

[6] a) B. W. Dale, R. J. P. Williams, C. E. Johnson, T. L. Thorp, *J. Chem. Phys.* **1968**, *49*, 3441; b) H. Goff, G. N. La Mar, C. A. Reed, *J. Am. Chem. Soc.* **1977**, *99*, 3641.

[7] K. Ray, A. Begum, T. Weyhermüller, S. Piligkos, J. van Slageren, F. Neese, K. Wieghardt, *J. Am. Chem. Soc.* **2005**, *127*, 4403.

[8] E. J. Hawrelak, W. H. Bernskoetter, E. Lobkovsky, G. T. Yee, E. Bill, P. J. Chirik, *Inorg. Chem.* **2005**, *44*, 3103.

[9] V. F. Kuznetsov, K. Abdur-Rashid, A. J. Lough, D. G. Gusev, *J. Am. Chem. Soc.* **2006**, *128*, 14388.

[10] Literatur 2-state reactivity (Schwarz, Shaik)

[11] L. A. Watson, O. V. Ozerov, M. Pink, K. G. Caulton, *J. Am. Chem. Soc.* **2003**, *125*, 8426.

[12] a) A. Walstrom, M. Pink, K. G. Caulton, *Inorg. Chem.* **2006**, *45*, 5617; b) X. Yang, A. Walstrom, N. Tsvetkov, M. Pink, K. G. Caulton, *Inorg. Chem.* **2007**, *46*, 4612; c) N. Tsvetkov, M. Pink, H. Fan, J.-H. Lee,

ruthenium(II) dialkylamide [RuCl{L1^{tBu}}] (**3**, {L1^{tBu}} = {N(CH$_2$CH$_2$P^{t}Bu$_2$)$_2$}).[13] In contrast to **2**, NMR data and magnetic measurements indicated diamagnetism, hence an LS ground state for **3**. However, unusual ^{1}H and ^{31}P NMR chemical shifts with strong temperature dependence were rationalized by proposing a spin equilibrium with an energetically low lying triplet (IS) state and fitting of the NMR spectroscopic data to this model afforded an estimate of the thermodynamic parameters (ΔH = 10.6 ± 0.3 kJ mol^{-1}; ΔS = 4.2 ± 0.8 J mol^{-1} K^{-1}). Computational results also indicated a small singlet/triplet gap for **3**, in agreement with the experimental findings.

The strikingly different electronic structures of the related dialkyl- and disilylamido complexes **3** and **2** (and similarly of alkylcomplex **1**) were attributed to the π-donor properties of the central donor atom within the pincer ligand framework. The pure σ-donor in **1** (alkyl) does not affect the degeneracy of the nonbonding e_g set (idealized D_{4h} symmetry) (see Figure B-3.2). Introduction of a perpendicular π-donor should raise the d_{xz} orbital owing to mixing with the ligand lone pair with π*-antibonding character, however, for disilylamide (**2**) not to an extend that the spin-pairing energy is overcome. Finally, in accord with having the strongest π-donor in this series (dialkylamide), **3** adopts a LS ground state owing to further destabilization of the d$_{xz}$ orbital. In fact, computations confirmed a $(d_{xy},d_{yz},d_{z^2})^6(d_{xz})^0(d_{x^2-y^2})^0$ configuration for **3** and structural parameters, such as Ru-N bond distances (**3**: 1.890(2) Å; **2**: 2.050(1) Å), are in agreement with this explanation. However, it remains open whether this qualitative and highly simplified picture can be probed with more examples for this rare class of compounds.

Recently, we showed the versatile ligand modification of {L1^{tBu}}$^-$ by dehydrogenation of the chelate backbone bridges towards enamido {L3^{tBu}}$^-$ and dienamido {L4^{tBu}}$^-$ ligands. Octahedral PNP imine complex [RuHCl(PMe$_3$){L2^{iPr}}] {L2^{iPr}} = {N(CHCH$_2$P^{t}Bu$_2$) (CH$_2$CH$_2$P^{i}Pr$_2$)} is deprotonated by KO^{t}Bu in α-position to the imine carbon affording five-coordinate enamide [RuH(PMe$_3$){L3^{iPr}}].[14] Similarly, related pyridine based PNP pincer

K. G. Caulton, *Eur. J. Inorg. Chem.* **2010**, 4790; d) N. Tsvetkov, H. Fan, K. G. Caulton, *Dalton Trans.* **2011**, *40*, 1105.

[13] B. Askevold, M. M. Khusniyarov, E. Herdtweck, K. Meyer, S. Schneider, *Angew. Chem.* **2010**, *122*, 7728; *Angew. Chem. Int. Ed.* **2010**, *49*, 7566.

[14] a) M. Käß, A. Friedrich, M. Drees, S. Schneider, *Angew. Chem.* **2009**, *121*, 922; *Angew. Chem. Int. Ed.* **2009**, *48*, 905; b) A. Friedrich, M. Drees, M. Käß, E. Herdtweck, S. Schneider, *Inorg. Chem.* **2010**, *49*, 5482.

complexes can be deprotonated in the benzylic position.[15] Finally, the novel dienamido ligand L4 could be synthesised by template ligand backbone dehydrogenation with benzoquinone as hydrogen acceptor. Oxidation of $[Ir(H)Cl(C_8H_{13})\{L1^{tBu}\}]$ afforded square-planar iridium(II) complex $[IrCl\{L4^{tBu}\}]$.[16] Partial or full dehydrogenation of the PNP pincer backbone should have a profound impact on the ligand (π-)donor properties owing to N–C=C π-conjugation, which was demonstrated for $[RuH(PMe_3)\{L1^{iPr}\}]$ *vs*. $[RuH (PMe_3)\{L2^{iPr}\}]$.[14] Hence, we were interested if the simple model described above for such square-planar 14 VE ruthenium(II) pincer complexes can be further substantiated by oxidative ligand backbone functionalization reactions. In this contribution, the synthesis and characterization of novel square-planar ruthenium(II) complexes by PNP pincer dehydrogenation is reported, and the impact on electronic structure, in particular ground state spin multiplicity, is discussed.
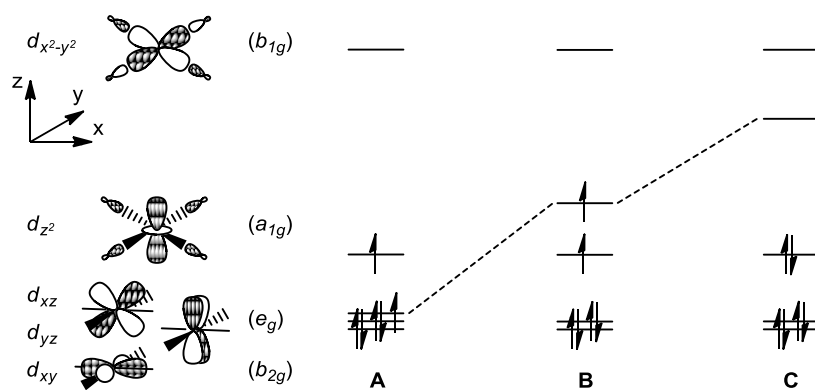
Figure B-3.2: Valence *d*-orbital splitting in square-planar coordination geomertry (D_{4h}) for a d^6 ion with pure σ-donor ligands (**A**) and one weak (**B**) or strong (**C**) single faced, perpendicular π-donor, respectively.

[15] a) J. Zhang, G. Leitus, Y. Ben-David, D. Milstein, *J. Am. Chem. Soc.* **2005**, *127*, 10840; b) J. Zhang, G. Leitus, Y. Ben-David, D. Milstein, *Angew. Chem.* **2006**, *118*, 1131; J. Zhang, G. Leitus, Y. Ben-David, D. Milstein, *Angew. Chem. Int. Ed.* **2006**, *45*, 1113; c) D. Vuzman, E. Poverenov, L. J. W. Shimon, Y. Diskin-Posner, D. Milstein, *Organometallics* **2008**, *27*, 2627; d) J. I. van der Vlugt, M. Lutz, E. A. Pidko, D. Vogt, A. L. Spek, *Dalton Trans.* **2009**, 1016; e) J. I. van der Vlugt, E. A. Pidko, D. Vogt, M. Lutz, A. L. Spek, *Inorg. Chem.* **2009**, *48*, 7513; f) J. van der Vlugt, J. N. H. Reek, *Angew. Chem.* **2009**, *121*, 8990; J. I. van der Vlugt, J. N. H. Reek, *Angew. Chem. Int. Ed.* **2009**, *48*, 8832.

[16] J. Meiners, M. G. Scheibel, M.-H. Lemée-Cailleau, S. A. Mason, M. B. Boeddinghaus, T. F. Fässler, E. Herdtweck, M. M. Khusniyarov, S. Schneider, *Angew. Chem.* **2011**, *123*, 8334; *Angew. Chem. Int. Ed.* **2011**, *50*, 8184.
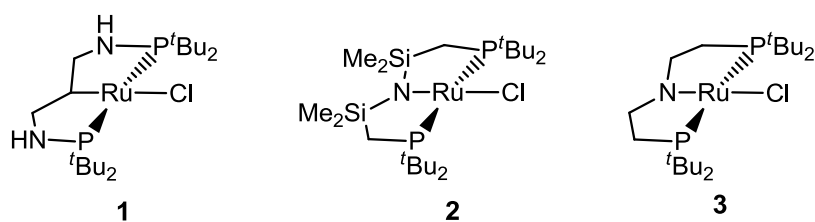
Figure B-3.3: Square-planar ruthenium(II) complexes with IS (**1** and **2**) and LS (**3**) ground states, respectively.
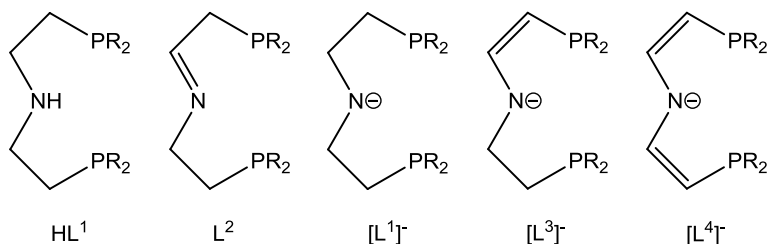

Figure B-3.4: PNP chelating ligands derived from $HN(CH_2CH_2PR_2)_2$.

3.2 Results and discussion

Synthesis and spectroscopic characterization of square-planar ruthenium(II) complexes. Thermolysis of five-coordinate amine complex $[RuCl_2\{HL1^{tBu}\}]$ (**4**) over several weeks in THF results in selective dehydrogenation of one PNP ligand backbone ethylene bridge (Scheme B-3.1). The long reaction time could not be reduced by addition of potential hydrogen acceptors (e.g., acetone, $H_2C=CH^{t}Bu$). However, resulting imine complex $[RuCl_2\{L2^{tBu}\}]$ (**5**) was isolated in 84% yield and fully characterized. Multinuclear NMR characterization of **5** is in agreement with a C_1 symmetric, square-pyramidal molecular structure (see ESI). The ^{31}P NMR spectrum exhibits two signals with a typical $^2J_{PP}$ *trans*-coupling constant (341 Hz) suggesting a meridional arrangement of the $\{L2^{tBu}\}$ ligand. The ^1H NMR at r.t. in CD_2Cl_2 features a signal at 8.16 ppm with a characteristic downfield shift for the imine proton similar to analogous hydrido imine complex $[RuCl(H)\{L2^{tBu}\}]$ (7.37 ppm).[13] ^1H COSY measurement allowed for assignment of all inequivalent backbone protons resulting in six multiplets between 4.23 to 2.05 ppm. Contrary to $[RuCl(H)\{L2^{tBu}\}]$, the weaker chloride vs. hydride *trans* influence effects stabilization by C-H agostic interactions at the vacant coordination site as indicated by a strong highfield shift of one single ^{t}Bu ^1H signal and further confirmed by single crystal X-ray diffraction (see below). Broadening of the ^1H signals at room temperature suggests rapid dynamic behaviour of the ethylene backbone bridge which can be frozen by cooling to 250 K in CD_2Cl_2.
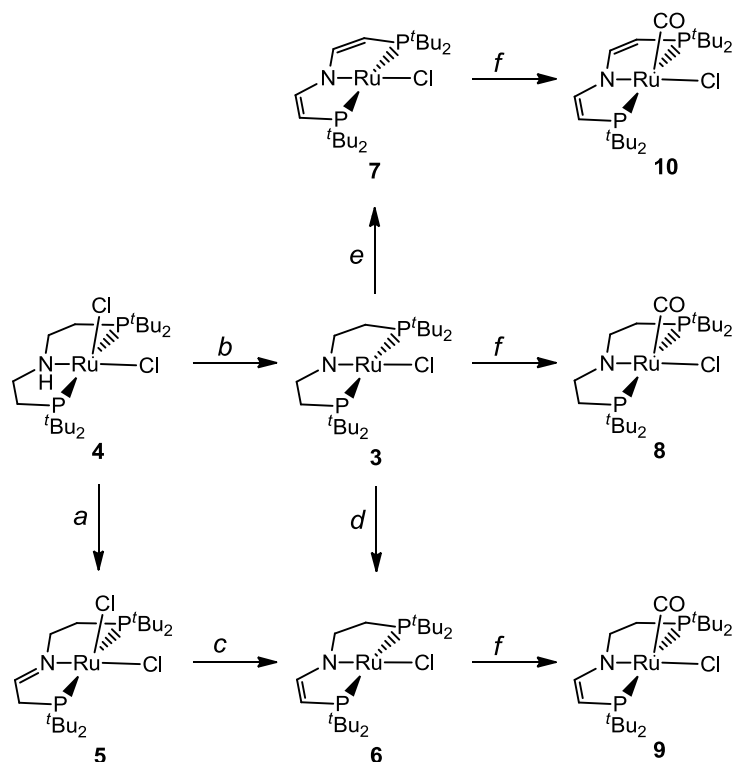
Scheme B-3.1: *Conditions*: (*a*) ΔT, -H$_2$, THF, several weeks; (*b*) -20 °C, KO^{t}Bu, THF; (*c*) 5 °C, KN(SiMe$_3$)$_2$, benzene; (*d*) -78°C to r.t., benzoquinone, THF, partial oxidation to **7** (e) -78°C to r.t., 2 equiv. benzoquinone, THF; (*f*) -78°C to r.t., CO, THF.

5 reacts selectively with KN(SiMe$_3$)$_2$ to give deep purple enamido complex [RuCl{L3^{tBu}}] (**6**) in 80 % yield (Scheme B-3.1). Oxidation of **3** with benzoquinone affords complex **6**, too. However, the product from full backbone dehydrogenation, dienamido complex [RuCl{L4^{tBu}}] (**7**; for selective synthesis see below), is also obtained even at low temperature and separation of **6** and **7** by recrystallization was unsuccessful, to date. Accordingly, a mixture of both compounds was detected by ^{1}H NMR after crystallization. Therefore, this route is not suitable for the selective synthesis of **6**. However, **3** can be oxidized with 2 equiv. benzoquinone affording green dienamido complex **7** in 34 % spectroscopic and 16 % analytically pure yield after crystallization from pentane at -35 °C (Scheme B-3.1).

Both complexes show characteristic absorptions in the infrared spectrum for the C=C double bond at 1532 cm^{-1} (**6**) and 1524 cm^{-1} (**7**), respectively, similar to [IrCl{L4^{tBu}}] (1524 cm^{-1}) and no sign for the presence of additional hydride ligands.[16] The absence of signals in the ^{31}P NMR spectra and the paramagnetically strongly shifted ^{1}H NMR signals indicate an open shell electronic structure for both complexes. The ^{1}H NMR spectrum of **7** in d_6-benzene shows three broad and strongly paramagnetic shifted signals which can be assigned to the ^{t}Bu substituents (-5.70 ppm) and the two sets of ligand backbone C-H protons (44.1 and -190

ppm), respectively and is in agreement with a C_{2v}-symmetric molecular structure on the NMR timescale. As a consequence of the lower symmetry, complex **6** exhibits two signals for the ^{t}Bu substituents (-0.69 and -7.69 ppm) and four signals assignable to the ethylene (460 and 48.7 ppm) and vinylene (-275 and -15.3 ppm) backbone protons, respectively, by peak integrals. Curie-plots (Figure B-3.5) for the proton NMR signals of **6** and **7** show linear relation with 1/T. This result suggests that only one electronic configuration is thermally populated within the examined temperature range (193 and 333 K) in solution. Furthermore, magnetic moments of 2.8 μ_B (**6**) and 2.7 μ_B (**7**) were derived by Evans' method which is close to the spin-only values for two unpaired electrons (2.83 μ_B).
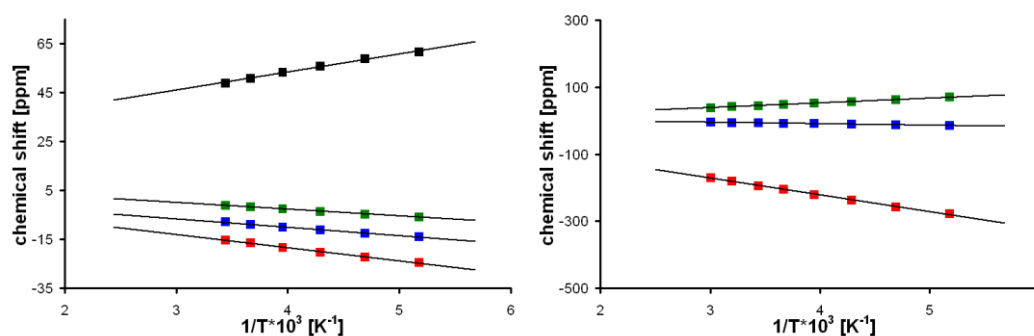
Figure B-3.5: Curie-plots for complexes **6** and **7**.

Crystal structures. The molecular structure of **5** was derived by single-crystal X-ray diffraction (Figure B-3.4). Deviation from an ideal square-pyramidal geometry arises from a PNP bite angle of 159.79(2)°, approximately 5° smaller than for the amine and amido complexes [RuCl$_2${HL1^{tBu}}] and [RuCl{L1^{tBu}}], respectively.[13] The Ru-N1 distance (2.056(1) Å) lies between five-coordinate ruthenium(II) alkylamide [Ru(H)PMe$_3${L1^{iPr}}] (2.023(1) Å) and amine complex [RuCl$_2${HL1^{tBu}}] (2.13(2) Å), attributed to the lower coordination number of imine vs. amine nitrogen.[12a,14b] The sum of bond angles around N (359.4°) and the N1-C2 distance (1.28(1) Å) are also in agreement with the formation of an imine complex, comparing well with C=N bond lengths found in the literature.[17] Furthermore, a short Ru$\cdots$H^{tBu} (2.135(1) Å) distance at the vacant coordination site confirms a C-H agostic interaction with the coordinatively unsaturated metal center in the solid state.

[17] a) J.-S. Huang, S. K.-Y. Leung, K.-K. Cheung, C.-M. Che, *Chem. Eur. J.* **2000**, *6*, 2971; b) A. L. R. Silva, M. O. Santiago, I. C.N. Diogenes, S. O. Pinheiro, E. E. Castellano, J. Ellena, A. A. Batista, F. B. do Nascimento, I. S. Moreira, Inorg. Chem. Commun. **2005**, *8*, 1154.
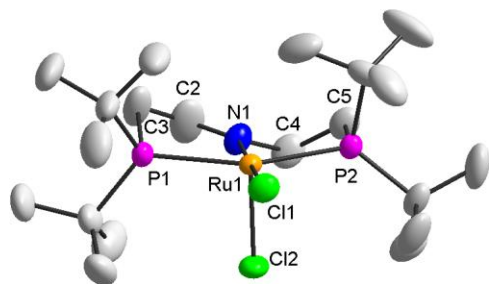
Figure B-3.6: DIAMOND plot of the molecular structure of complex **5** in the crystal (thermal ellipsoids drawn at the 50% probability level). Hydrogen atoms are omitted for clarity. Selected bond lengths [Å] and angles [°]: Ru1–Cl1 2.4444(1), Ru1–N1 2.0564(1), Ru1–P1 2.4024(1), Ru1–P2 2.3267(1), N1–C2 1.2769(0), N1–C4 1.4764(1), C2–C3 1.4769(1), C4–C5 1.5098(1); N1-Ru1-Cl1 176.49(1), N1-Ru1-Cl2 91.63(1), P1-Ru1-P2 159.80(2).

The molecular structure of **6** was derived by single crystal X-ray diffraction (Figure B-3.4). All crystallization attempts gave crystals that exhibited statistical disorder with respect to the location of the C-C single and double bonds in the ligand backbone which was refined by application of a crystallographic split model. Hence, the structural discussion of **6** has to be taken with care. However, the structural model clearly confirms the planar coordination mode of the metal and one single (C2–C3 1.52(2) Å) and one double C-C bond (C4–C5 1.37(4) Å) in the ligand backbone, respectively. Furthermore, the Ru–N bond length (1.972(2) Å) is considerably longer as compared with **3** (1.890(2) Å), indicative of weaker N→Ru π-donation (*vide infra*).

The metal center in complex **7** exhibits a square-planar geometry with an ideally linear N1-Ru1-Cl1 axis (180.0°) and a typical PNP bite angle P1-Ru1-P2 of 165.13(0) (Figure B-3.4). The Ru1-N1 bond length (1.997(16) Å) compares well with, for example **2** (2.050(1) Å) and **6** (1.972(2) Å)**,** and is considerably longer as found in **3** (1.890(2) Å).[12a,13] The planar coordination of the nitrogen atom (sum of angles 360.0°) and the short C1-C2 (1.359(19) Å) and N1-C1 (1.392(15)) Å) distances confirm dehydrogenation of both pincer backbone bridges (table B-3.1). Five-coordinate diaryl PNP pincer complex [Ru(H)CO{L$_A^{iPr}$}] exhibits almost identical N1-C1 distances (1.399 (5) Å) but exhibits remarkable longer C=C bonds in the aryl ligand (1.405(6) and 1.423(5) Å).[18] Note that for both **6** and **7** the shortest intermolecular Ru-Ru distances are considerably larger than 7 Å.

---

[18] R. Çelenligil-Çetin, L. A. Watson, C. Guo, B. M. Foxman, O. V. Ozerov, O*rganometallics*, **2005**, *24*, 186.
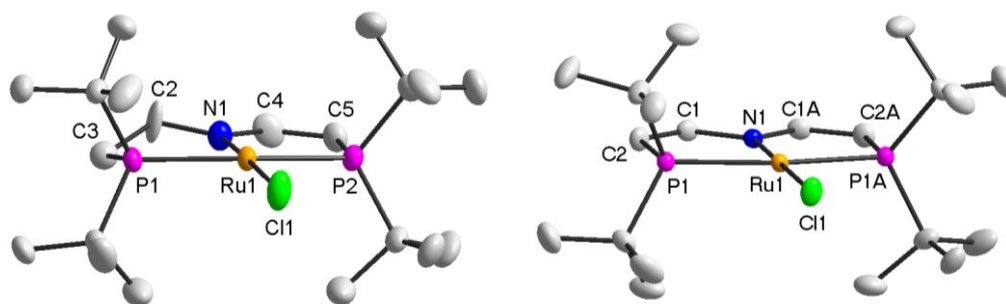
Figure B-3.7: DIAMOND plot of the molecular structure of complex **6** (left) and **7** (right) in the crystal (thermal ellipsoids drawn at the 50% probability level), respectively. Hydrogen atoms are omitted for clarity. Only one set of the split model for the backbone carbon atoms is drawn for complex **6**.

Table B-3.1: Selected bond lengths and angles of square planar ruthenium(II) complexes **2,3,6** and **7**.[12a,13]

bond lengths [Å]	2	3	6	7
Ru–Cl	2.361(1)	2.381(6)	2.395(6)	2.378(3)
Ru–N	2.050(1)	1.890(2)	1.972(2)	1.997(2)
Ru–P	2.384(4)	2.332(5)	2.358(6)	2.360(2)
	2.376(4)	2.324(6)	2.353(6)	2.360(2)
C–C backbone		1.513(4)	1.52(2)	
		1.517(4)		
C=C backbone			1.37(4)	1.350(1)
angles [°]				
N1–Ru1–Cl1	177.9(4)	179.63(6)	177.85(6)	180.0
P1–Ru1–P2	175.1(2)	168.13(2)	165.93(2)	165.13(3)

The temperature dependence of the structural parameters of **7** was examined by single-crystal X-ray diffraction at several temperatures between 30 and 200 K. Notably, all bond lengths and angles are invariant within standard deviation of the structural model. According to DFT calculations, especially the Ru–N distance is a sensitive probe for the electronic configuration (see below).

Bulk magnetization measurements. The magnetic susceptibility of Caulton's disilylamido complex **2** at room temperature is in agreement with two unpaired electrons ($\chi_M T = 1.03$ at 300 K).[11] The triplet state was also calculated by DFT to be favored by about 10 kcal/mol.[12d] Nevertheless, $\chi_M T$ drops at low temperatures to near zero suggesting a non-magnetic ground state. The isotropic magnetic data was parametrized by fitting to a zero-field-splitting (ZFS) spin-hamiltonian (SH) model.[12a] The resulting positive axial ZFS parameter ($D = +273$ cm^{-1}) indicated that the spin triplet ground state is further split into the non-magnetic $| S = 1, M_S = 0 \rangle$ microstate and the Kramer's doublet $| S = 1, M_S = \pm 1 \rangle$ at higher energies.[19] Such unusually high axial ZFS parameters were formerly reported for diruthenium tetracarboxylato and tetraformamidato paddlewheel complexes, which host two (Ru^{II}/Ru^{II}) or three (Ru^{II}/Ru^{III}) unpaired electrons, respectively, within the three almost degenerate ($\pi^*_x \pi^*_y \delta^*$) manifold of the Ru_2^{n+} (n = 4, 5) core.[20] Limitations within the SH formalism arise here owing to increased spin-orbit coupling in heavier late transition metal complexes which is only considered as a minor perturbation.[19] Alternatively, the electronic structures and magnetic properties can be described by ligand field theory. The introduction of spin-orbit coupling in this model may however cause extensive mixing of several close-lying states, making it difficult to assign a particular ground state.[21] Therefore, the SH formalism remains a common approach to describe electronic and magnetic properties of transition metal complexes even with distinct spin-orbit coupling.[12a]

As reported for complex **2**, both **6** and **7** exhibit magnetic moments in the solid state (powder) at room temperature that are in agreement with two unpaired electrons (Figure B-3.5). In analogy, $\chi_M T$ drops to near zero upon lowering the temperature, indicating a non-magnetic ground state. The magnetic data could be satisfactorily fitted to a ZFS-SH, giving large, positive axial ZFS parameters (**6**: g = 2.05, $D = +392$ cm^{-1}; **7**: g = 2.20, $D = +232$ cm^{-1}), respectively. E/D was fixed at 0 because the fit was insensitive towards variation of the rhombic ZFS parameter E. Small levels of paramagnetic (S = 1/2) impurity (**6**: 6 %; **7**: 2 %) were assumed, which is particularly apparent at very low temperatures: While the susceptibility χ_M vs. T initially plateaus at temperatures below 100 K as expected for a magnetically pure sample, the sharp rise below 20 K can be attributed to an impurity with

[19] R. Boca, *Coord. Chem. Rev.* **2004**, *248*, 757.

[20] Representative examples: a) F. A. Cotton, V. M. Miskowski, B. Zhong, *J. Am. Chem. Soc.* **1989**, *111*, 6177; b) W.-Z. Chen, F. A. Cotton, N. S. Dalal, C. A. Murillo, C. M. Ramsey, T. Ren, X. Wang, *J. Am. Chem. Soc.* **2005**, *127*, 12691.

[21] Boyd, P. D. W.; Buckingham, D. A.; McMeeking, R. F.; Mitra, S. *Inorg. Chem.* **1979**, *18*, 3585.

Curie-law behavior (Figure B-3.8, right).[20a] Small impurity levels with non-integer spin were also indicated by the detection of a rhombic signal in the EPR spectrum of **6**. However, the nature of the impurities could not be clarified, to date and the magnetic data of **6** should therefore be treated with caution. Furthermore, it is noted that some ambiguity remains regarding the sign of *D* which is difficult to derive accurately from powder samples.[20b]
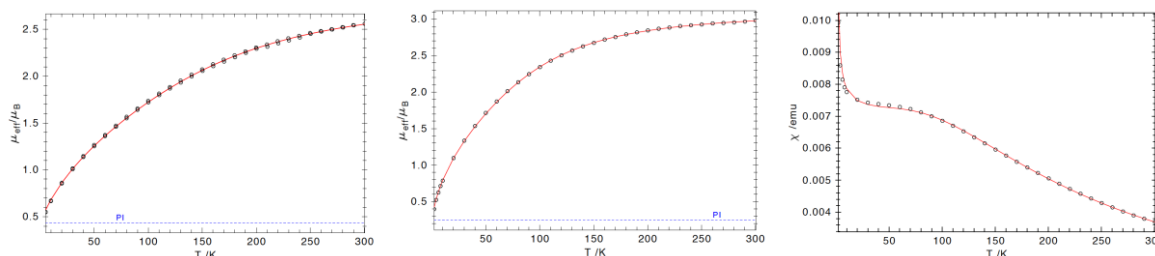

Figure B-3.8: Temperature dependence of the magnetic moment for complexes **6** (left) and **7** (center) and of the molar suxceptibility χ_M of **7** (right) at 0.1 T. The red lines represent the best fits (fit parameters: S = 1, g = 2.05, D = 392 cm^{-1}, E/D = 0, TIP = 10.3 x 10^{-6} emu (**6**) and S = 1, g = 2.20, *D* = 232 cm^{-1}, E/D = 0, TIP = 69.2 x 10^{-6} emu (**7**)). Levels of paramagnetic impurities (S = 1/2) included in the fit denoted by blue lines (**6**: 6 %; **7**: 2 %).

Syntheses of carbonyl complexes [Ru(Cl)CO{LX^{tBu}}] (X = 1, 2, 3). The CO stretching vibrations of the corresponding five-coordinate complexes [Ru(Cl)(CO){L1^{tBu}}] (**8**), [Ru(Cl)(CO){L2^{tBu}}] (**9**), and [Ru(Cl)(CO){L3^{tBu}}] (**10**) were used as probe in trying to rationalize the electronic structures of **3**, **6**, and **7** on the basis of the ligand donor properties. The square-planar complexes **3**, **6**, and **7** react at low temperature (-78 °C) under CO atmosphere (1 bar) quantitatively to the corresponding carbonyl complexes **8**, **9**, and **10**, respectively (Scheme B-3.1). Complexes **8**-**10** are diamagnetic as evidenced by a single ^{31}P NMR signal for symmetric **8** and **10** and two ^{31}P NMR signals ($^2J_{PP}$ = 260 Hz) for asymmetric **9**. ^{31}P, ^{1}H, and ^{13}C NMR spectra are in agreement with a square-pyramidal molecular geometry and meridional coordination of the pincer ligand, hence C_s (**8**, **10**) and C_1 (**9**) symmetry, respectively. The ^{1}H NMR spectra of **9** and **10** show characteristic signals in the olefinic region (δ_{NCH} = 7.18 (**9**), 7.01 (**10**) ppm; δ_{PCH} = 3.95 (**9**), 4.10 (**10**) ppm), assignable to the vinylene bridges. This coordination geometry was confirmed for **8** and **10** in the solid state by single-crystal X-ray diffraction (see ESI). However, the low qualities of the structural solutions do not permit a detailed discussion.

The corresponding CO stretching vibrations are observed within a range of around 30 cm^{-1} (ν_{CO} = 1888 cm^{-1} (**8**), 1896 cm^{-1} (**9**), 1916 cm^{-1} (**10**)), indicating decreasing electron density at the metal center within the series **8** > **9** > **10**. Remarkably, the four-coordinate iridium(I)

complexes [IrCO{L1^{iPr}}] (ν_{CO} = 1908 cm^{-1}) and [IrCO{L4^{tBu}}] (ν_{CO} = 1937 cm^{-1}) show an almost identical shift upon full dehydogenation of the dialkylamido backbone suggesting similar electronic effects despite the different metal centers, coordination geometries, and phosphine substituents.[22] Note that disilylamido complex [IrCO{L$_C^{iPr}$}] (ν_{CO} = 1930 cm^{-1}) also ranges within this window, yet closer to the dehydrogenated complexes.[23] The observed shift of the CO stretching vibration can be qualitatively attributed to decreasing N→Ru electron donation. The dialkylamido ligand is the strongest σ- and particularly π-donor within this series, hence showing the lowest value. Note that **8** exhibits an almost identical CO stretching vibration as alkyl complex [RuCl(CO){CH(CH$_2$CH$_2$P^{t}Bu$_2$)$_2$}] (ν_{CO} = 1887 cm^{-1}), indicating that the weaker expected N→Ru vs. C→Ru σ-donation is offset by N→Ru π-donation.[24] Dehydrogenative backbone functionalization of the amido ligand results in mixing of the *N*-lone-pair with *C*-p-orbitals (see below), tantamount to stabilization by conjugation with C=C double bonds and, in turn, reduced N→Ru π-donation. In contrast, the effect on N→Ru σ-donation is expected to be of minor relevance. Similarly, Fryzuk's disilylamido ligand {L$_C$} will be a weaker π-donor owing to the electron accepting properties of the silyl substituents, which is in agreement with the observed CO stretching vibration of [IrCO{L$_C^{iPr}$}], as compared to [IrCO{L1^{iPr}}] and [IrCO{L3^{tBu}}].

DFT calculations. As previously reported for **3**,[13] the electronic structures of **6** and **7** were examined by DFT calculations. Geometry optimizations of **6** and **7** in the singlet and triplet states, respectively, (B3LYP/6-31+G**) indicate better agreement of the minimum structures for S = 1. Particularly two parameters are regarded as sensitive indicators: the Ru–N bond length and the Cl–Ru–N bond angle. The calculated Ru–N bond length are considerably longer in the triplet state (Δd = 0.07 – 0.09 Å). In case of **3** an excellent agreement with the singlet minimum structure was found.[13] For **6** and **7** the experimental Ru–N bond lengths from X-ray diffraction are right between the calculated values for singlet and triplet states, hence not indicative enough to make a clear assignment. However, contrary to **3**, the calculated structures of **6** and particularly of **7** in the singlet state exhibit considerable deviation from square-planar geometry by bending of the Cl–Ru–N angle (**6**: 173°; **7**: 161°),

[22] a) A. Friedrich, R. Ghosh, R. Kolb, E. Herdtweck, S. Schneider, *Organometallics* **2009**, *28*, 708; b) S. Schneider, J. Meiners, B. Askevold, *Eur. J. Inorg. Chem.* **2012**, 412-429; c) M. Scheibel, S. Schneider, *unpublished results*.

[23] M. D. Fryzuk, P. A. McNeil, S. J. Rettig, *Organometallics* **1986**, *5*, 2469.

[24] D. G. Gusev, A. J. Lough, *Organometallics* **2002**, *21*, 5091.

approaching sawhorse geometry, which is not observed in the experimental structure. Besides these structural arguments, the calculated energies further support assignment of an S = 1 ground state for **6** and **7**: While the calculated singlet/triplet-gap at that level of theory was well within the error of the method (ΔE = 2.3 kcal/mol),[13] considerably higher energy differences were found for **6** (9.3 kcal/mol) and **7** (14.6 kcal/mol) in favour of the triplet state.

| | **3** | | | **6** | | | **7** | | |
	X-ray	DFT[a]		X-ray	DFT[a]		X-ray	DFT[a]	
Spin		0	1		0	1		0	1
Geometry									
Ru-N [Å]	1.89	1.90	1.99	1.97	1.93	2.01	2.00	1.97	2.04
Ru-Cl [Å]	2.38	2.40	2.45	2.40	2.38	2.42	2.38	2.42	2.40
Cl-Ru-N [°]	180	179	177	178	173	178	180	161	176
Energy (S-T)									
ΔE [kcal/mol][b]		+2.3			+9.3			+14.6	
ΔG [kcal/mol][c]		+3.1			+10.6			+16.2	

[a] B3LYP/6-31+G** [b] including Zero-Point Energy [c] at 298.15 K

This trend can be qualitatively rationalized by analysis of the frontier orbitals. Comparison of **3**, **6**, and **7** in the singlet state displays a decreasing HOMO-LUMO gap upon going from **3** (2.7 eV) to **6** (2.3 eV) and to **7** (2.1 eV), attributable to gradual stabilization of the LUMO (Figure B-3.9). The LUMOs displays a strong Ru–N π* antibonding contribution (Figure B-3.9), explaining the considerably longer Ru–N bonds in the triplet state where this orbital is singly occupied. The LUMO stabilization within the series **3**, **6**, **7** is a consequence of mixing with C(p)-orbitals tantamount to the vinyl groups acting as π-acceptors with respect to the N-lone-pair. Consequently, Ru–N π-donation is gradually diminished upon going from the dialkylamido (**3**) to the enamido (**6**) and dienamido (**7**) ligands with the effect that electron pairing becomes energetically more unfavourable.
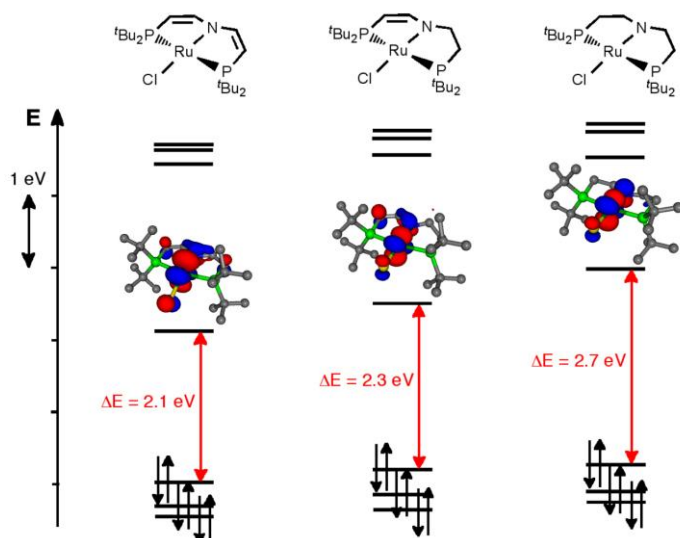
Figure B-3.9: Frontier orbital scheme of complexes **7** (left), **6** (center), and **3** (right) in the singlet state and graphic representation of the respective LUMOs.

3.3 Conclusions

The strikingly different spin multiplicity of reported square-planar ruthenium complexes **3** and **2** can be related to the stronger N→M π-donation of the central donor atom within the pincer ligand framework. The increased π-donation directly influences the singlet-triplet gap, favoring a low-spin over intermediate-spin ground state if the spin pairing energy is overcompensated. The versatile ligand functionalization of **3** enables the direct comparison of the related enamido and dienamido complexes, respectively. The utilization of the weaker donating ligand L3 or L4 results in an open shell electronic structure for both complexes. A weaker π-donation reduces the d_{xz}/d_{yz} degeneracy and favours an intermediate spin ground state. Hence, the electronic structure of enamido and dienamido complexes **6** and **7** scale closer to disilylamides in terms of N→M π-donor properties.

Magnetometry and DFT studies of **6** and **7** are in agreement with two unpaired electrons at room temperature. Nevertheless, $\chi_M T$ drops to near zero at low temperatures suggesting a non-magnetic ground-state. Fitting of the magnetic data to a zero-field-splitting (ZFS) spin-hamiltonian (SH) model results in unusual high positive axial ZFS parameters (**6**: $D = +392$ cm^{-1}; **7**: $D = +232$ cm^{-1}). This indicates that the spin triplet ground state is further split into the non-magnetic $| S = 1, M_S = 0 \rangle$ microstate and the Kramer's doublet $| S = 1, M_S = \pm 1 \rangle$ at higher energies. However, limitations within this SH formalism arise owing to increased spin-orbit coupling in heavier late transition metal complexes which is only considered as a minor perturbation and may lead to unusual high values for the axial ZFS parameter.

Nevertheless, the SH formalism remains a common approach to describe electronic and magnetic properties of transition metal complexes even with distinct spin-orbit coupling.

The utilization of a CO probe allowed the rationalization of the electronic structures of **3**, **6**, and **7** on the basis of the ligand donor properties. The observed shift of CO stretching vibration can be qualitatively attributed to a decrease in N→M electron donation. The simplified and highly qualitative model with a distinct influence of the π-donor ability explains thus the experimental findings. This work demonstrates how the spin ground-state of square-planar ruthenium(II) amido complexes can be controlled by tuning the extend of N→Ru π-donation. Further research efforts will account for the translation of the adjustable electronic structure into diverse reactivities.

3.4 Synthetic and analytical details

Materials and methods

All experiments were carried out under an atmosphere of argon using Schlenk and glovebox techniques. Solvents were dried over Na/benzophenone/tetraglyme (benzene), Na/benzophenone (THF), distilled under argon and deoxygenated prior to use. Aceton, Pentane and Et_2O were dried by passing through colums packed with activated alumina. Deuterated solvents were obtained from Euriso-Top GmbH, dried over Na/K (d_8-THF, C_6D_6) or CaH_2 (CD_2Cl_2), distilled by trap-to-trap transfer in vacuo, and degassed by three freezepump-thaw cycles, respectively. KO^tBu (VWR) and 1,4-Benzoquinone (Merck) were sublimed prior to use and Ruthenium(III)chloride hydrate (ABCR) used as purchased. $RuCl_2(PPh_3)_3$, $HN(CH_2CH_2P^tBu_2)_2$ and $KN(SiMe_3)_2$ were prepared according to published procedures.[25]

Analytical methods

Elemental analyses were obtained from the Microanalytical Laboratory of Technische Universität München. The IR spectra were recorded as nujol mulls between KBr plates. NMR spectra were recorded on a Bruker Avance III 400 spectrometer and were calibrated to the residual proton resonance and the natural abundance 13C resonance of the solvent (CD_2Cl_2: $\delta H = 5.32$ and $\delta C = 54.00$ ppm; C_6D_6: $\delta H = 7.16$ and $\delta C = 128.06$ ppm; d_8-THF: $\delta H = 3.58$ and $\delta C = 67.57$ ppm). 31P NMR chemical shifts are reported relative to external phosphoric acid ($\delta = 0.0$ ppm). Signal multiplicities are abbreviated as: s (singlet), d (dublet), t (triplet), q (quartet), m (multiplet), br (broad). Temperature-dependent magnetic susceptibility data were

---

[25] J. Meiners, A. Friedrich, E. Herdtweck, S. Schneider, *Organometallics* **2009**, *28*, 6331.

recorded on an MPMS XL Quantum Design SQUID magnetometer in the temperature range of 5 – 300 K. The experimental magnetic susceptibility data were corrected for underlying diamagnetism and temperature-independent paramagnetism (TIP). The program JulX v.1.5 was used to fit experimental data.[26]

Synthesis

Preparation of [RuCl$_2${L2^{tBu}}] (5). [RuCl$_2${HL1^{tBu}}] **4** (0.150 g; 0.281 mmol) is suspended in THF (10 mL) and refluxed for four weeks. The solvent is removed *i. vac.*, the resulting solid dissolved in methylenchloride and precipitated with pentane. The solution is filtered off and the pale grey solid washed with pentane (2x 10 mL) and dried *i. vac.* Yield: 0.126 g (0.173 mmol, 84%). Anal. Calcd. for C$_{20}$H$_{43}$Cl$_2$NP$_2$Ru (531.49): C, 45.20; H, 8.15; N, 2.64. Found: 44.65; H, 8.59; N, 2.41. IR (cm^{-1}) $\tilde{v}$ = 1616 (C=N). NMR (CD$_2$Cl$_2$, 230 K, [ppm]) ^{1}H NMR (399.8 MHz): δ = 8.16 (d, $^3J_{HH}$ = 21.7 Hz, 1H, NCH), 4.23 – 4.07 (m, 1H, NCH_2), 3.78 – 3.74 (m, 1H, NCH_2), 3.36 (dd, $^2J_{HH}$ = 7.4 Hz, $^3J_{HH}$ = 17.3 Hz, 1H, CHCH_2P), 2.94 – 2.83 (m, 1H, CHCH_2P), 2.49 (m, 1H, PCH_2), 2.05 (m, 1H, PCH_2), 1.52 (d, $^3J_{HP}$ = 13.1 Hz, 9H, CH_3), 1.32 (d, $^3J_{HP}$ = 12.5 Hz, 9H, CH_3), 1.13 (d, $^3J_{HP}$ = 12.2 Hz, 9H, CH_3), -0.61 (s (br), 9H, CH_3). ^{13}C{^{1}H} NMR (100.53MHz): δ = 176.1 (dd, $^2J_{CP}$ = 6.5 Hz, $^3J_{CP}$ = 1.0 Hz, NCH), 66.1 (dd, $^2J_{CP}$ = 5.3 Hz, $^3J_{CP}$ = 1.6 Hz, NCH$_2$), 32.4 (dd, $^1J_{CP}$ = 11.9 Hz, $^3J_{CP}$ = 2.3 Hz, PCH$_2$CH), 29.0 (m, CH_3), 23.2 (dd, $^1J_{CP}$ = 15.7 Hz, $^3J_{CP}$ = 1.7 Hz, PCH$_2$), (PC(CH$_3$)$_3$) not detected due to low solubility. ^{31}P{^{1}H} NMR (161.83 MHz): δ = 62.0 (d, $^2J_{PP}$ = 341.2 Hz, P^tBu$_2$), 38.1 (d, $^2J_{PP}$ = 340.8 Hz, P^tBu$_2$).

Preparation of [RuCl(L3^{tBu})] (6). A mixture of **5** (42.8 mg, 0.080 mmol) and Kbtsa (20.9 mg, 0.080 mmol, 1.0 equiv.) is cooled to 5 °C and dissolved in benzene (5 mL). Immediately, the suspension turns dark blue. After stirring for 5 minutes, the solution is filtered of and the white residue extracted twice with benzene. The solvent is removed *i. vac.* affording **6** in high yield. Yield: 32.7 mg (0.066 mmol, 82%). Anal. Calcd. for C$_{20}$H$_{42}$ClNP$_2$Ru (495.02): C, 48.53; H, 8.55; N, 2.83. Found: C, 48.94; H, 8.40; N, 2.85. IR (cm^{-1}) $\tilde{v}$ = 1532 (C=C). NMR (C$_6$D$_6$, r.t., [ppm]) ^{1}H NMR (399.8 MHz): δ = 459.33 (s, CH_2, 2H), 48.69 (s, CH, 1H), -0.69 (s, C(CH_3)$_3$, 18H), -7.69 (s, C(CH_3)$_3$, 18H), -15.34 (s, CH_2, 2H), -275.31 (s, CH, 1H). No signal was found by ^{31}P NMR spectroscopy.

Preparation of [RuCl(L4^{tBu})] (7). THF (5 mL) is added to a mixture of **3** (50.0 mg, 0.10 mmol) and benzoquinone (21.7 mg, 0.20 mmol, 2.0 equiv.) at -78 °C. Immediately, the suspension turns dark purple. After stirring for 30 minutes, the reaction mixture is slowly

[26] E. Bill, *JulX version 1.5*, MPI for Bioinorganic Chemistry, Mülheim an der Ruhr, Germany, **2008**.

allowed to warm up to r.t. The colour changes to black and the solvent removed *i. vac* after 30 minutes. The residue is extracted with Et_2O (4x 5mL), the solvent removed *i. vac.* and the crude product extracted with pentane (3x 5mL). Concentration of the green solution *i. vac.* and cristallisation at -35 °C affords dark green **7**. Yield: 7.8 mg (0.015 mmol, 16%). Anal. Calcd. for $C_{20}H_{40}NClNP_2Ru$ (493.01): C, 48.72; H, 8.18; N, 2.84. Found: C, 48.41; H, 8.19; N, 2.85. IR (cm^{-1}) $\tilde{\nu}$ = 1524 (C=C). NMR $(C_6D_6$, r.t., [ppm]) ^1H NMR (399.8 MHz): δ = 44.11 (s, C*H*, 2H), -5.70 (s, C(C*H*$_3$)$_3$, 36H), -189.48 (s, C*H*, 2H). No signal was found by ^{31}P NMR spectroscopy.

Preparation of [RuCl(CO)(L1^{tBu})] (8). A solution of **3** (36.7 mg, 0.074 mmol) in THF (5 mL) is frozen, evacuated and backfilled with CO. The solution is slowly warmed up to -50 °C and stirred for additionally 15 min. The solvent is removed *i. vac.* at low temperature giving red **8** quantitatively. Yield: 38.1 mg (0.073 mmol, 98%). Anal. Calcd. for $C_{21}H_{44}ClNOP_2Ru$ (525.05): C, 48.04; H, 8.45; N, 2.67. Found: 48.03; H, 8.62; N, 2.55. IR (cm^{-1}) $\tilde{\nu}$ = 1888 (C≡O). NMR $(C_6D_6$, r.t., [ppm]) ^1H NMR (399.8 MHz): δ = 3.04 – 2.85 (m, 2H, NC*H*$_2$), 2.68 – 2.61 (m, 2H, NC*H*$_2$), 1.68 – 1.48 (m, 4H, PC*H*$_2$), 1.38 (A$_9$XX'A'$_9$, N = $|{}^3J_{HP} + {}^5J_{HP}|$ = 13.4 Hz, 18H, C*H*$_3$), 1.32 (A$_9$XX'A'$_9$, N = $|{}^3J_{HP} + {}^5J_{HP}|$ = 13.4 Hz, 18H, C*H*$_3$). $^{13}C\{^1H\}$ NMR (100.53MHz): δ = 214.4 (br, *C*O), 66.7 (AXX'A', N = $|{}^2J_{CP} + {}^3J_{CP}|$ = 10.2 Hz, NC*H*$_2$), 37.0 (A$_2$XX'A$_2$', N = $|{}^1J_{CP} + {}^3J_{CP}|$ = 16.8 Hz, P*C*(CH$_3$)$_3$), 36.8 (A$_2$XX'A$_2$', N = $|{}^1J_{CP} + {}^3J_{CP}|$ = 15.4 Hz, P*C*(CH$_3$)$_3$), 29.6 (A$_6$XX'A$_6$', N = $|{}^1J_{CP} + {}^3J_{CP}|$ = 4.0 Hz, *C*H$_3$), 29.2 (A$_6$XX'A$_6$', N = $|{}^1J_{CP} + {}^3J_{CP}|$ = 5.0 Hz, *C*H$_3$), 24.9 (AXX'A', N = $|{}^1J_{CP} + {}^3J_{CP}|$ = 16.6 Hz, P*C*H$_2$). $^{31}P\{^1H\}$ NMR (161.83 MHz): δ = 87.8 (s, *P*^{t}Bu$_2$).

Preparation of [RuCl(CO)(L3^{tBu})] (9). Synthesis analogue to the preparation of complex **8**. A solution of **6** (10 mg, 0.020 mmol) in THF is set under CO atmosphere at -50 °C and stirred for 15 min; removing of the solvent *i. vac.* affords quantitative violet complex **9**. Yield: 10.5 mg (0.020 mmol, 100%). Anal. Calcd. for $C_{21}H_{42}ClNOP_2Ru$ (523.03): C, 48.22; H, 8.09; N, 2.68. Found: C, 48.19; H, 7.62; N, 2.62. IR (cm^{-1}) $\tilde{\nu}$ = 1896 (C≡O), 1542 (C=C). NMR $(C_6D_6$, r.t., [ppm]) ^1H NMR (399.8 MHz): δ = 7.18 (dd, $^3J_{HH}$ = 40.0 Hz, $^3J_{HP}$ = 4.0 Hz, 1H, NC*H*), 4.00 – 3.95 (m, 1H, PC*H*), 3.16 (ddd, $^2J_{HH}$ = 36.0 Hz, $^3J_{HH}$ = 8.0 Hz, $^3J_{HH}$ = 12.0, Hz, 1H, NC*H*$_2$), 2.98 – 2.89 (m, 1H, NC*H*$_2$), 1.46 (d, $^3J_{HP}$ = 13.7 Hz, 9H, C*H*$_3$), 1.38 (d, $^3J_{HP}$ = 12.9 Hz, 10H, C*H*$_3$ and PC*H*$_2$), 1.24 (d, $^3J_{HP}$ = 13.0 Hz, 10 H, C*H*$_3$ and PC*H*$_2$), 1.17 (d, $^3J_{HP}$ = 12.9 Hz, 9H, C*H*$_3$). $^{13}C\{^1H\}$ NMR (100.53MHz): δ = 208.9 (dd, $^2J_{CP}$ = 13.8 Hz, $^2J_{CP}$ = 10.6 Hz, *C*O), 169.4 (dd, $^3J_{CP}$ = 15.7 Hz, $^3J_{CP}$ = 2.5 Hz, N*C*H), 80.9 (d, $^1J_{CP}$ = 40.2 Hz, P*C*H), 61.8 (d, $^2J_{CP}$ = 5.4 Hz, N*C*H$_2$), 40.3 (dd, $^1J_{CP}$ = 16.2 Hz, $^3J_{CP}$ = 3.0 Hz, P*C*(CH$_3$)$_3$), 36.6 (dd, $^1J_{CP}$ = 12.0 Hz, $^3J_{CP}$ = 1.9 Hz, P*C*(CH$_3$)$_3$), 36.0 (dd, $^1J_{CP}$ = 19.0 Hz, $^3J_{CP}$ = 3.6 Hz, P*C*(CH$_3$)$_3$), 35.6

(dd, $^1J_{CP}$ = 11.3 Hz, $^3J_{CP}$ = 4.5 Hz, PC(CH$_3$)$_3$), 29.8 (d, $^2J_{CP}$ = 3.6 Hz, CH_3), 29.1 (d, $^2J_{CP}$ = 3.8 Hz, CH_3), 28.9 (d, $^2J_{CP}$ = 3.7 Hz, CH_3), 28.8 (d, $^2J_{CP}$ = 3.1 Hz, CH_3), 25.1 (d, $^1J_{CP}$ = 17.9 Hz, PCH_2). ^{31}P{^{1}H} NMR (161.83 MHz): δ = 78.6 (d, $^2J_{PP}$ = 259.9 Hz, P^tBu$_2$), 72.0 (d, $^2J_{PP}$ = 259.8 Hz, P^tBu$_2$).

*Preparation of [RuCl(CO)(L4^{tBu})] (10).*Synthesis analogue to the preparation of complex **8** (10 mg, 0.020 mmol), A solution of **7** (10 mg, 0.020 mmol) in THF is set under CO atmosphere at -50 °C and stirred for 15 min; removing of the solvent *i. vac.* and cristallisation in pentane affords complex **10** in high yield. Yield: 8.3 mg (0.020 mmol, 79%). Anal. Calcd. for C$_{21}$H$_{40}$ClNOP$_2$Ru (521.02): C, 48.41; H, 7.74; N, 2.69. Found: C, 48.62; H, 7.51; N, 2.62. IR (cm^{-1}) $\tilde{\nu}$ = 1917 (C≡O), 1528 (C=C). NMR (C$_6$D$_6$, r.t., [ppm]) ^{1}H NMR (399.8 MHz): δ = 7.00 (AMXX', N = $\left| ^3J_{HH} + {}^3J_{HP} + {}^4J_{HP} \right|$ = 42.4 Hz, 2H, NCH), 4.10 – 4.07 (m, 2H, PCH), 1.38 (A$_9$XX'A'$_9$, N = $\left| ^3J_{HP} + {}^5J_{HP} \right|$ = 14.1 Hz, 18H, CH_3), 1.21 (A$_9$XX'A'$_9$, N = $\left| ^3J_{HP} + {}^5J_{HP} \right|$ = 13.7 Hz, 18H, CH_3). ^{13}C{^{1}H} NMR (100.53MHz): δ = 205.1 (br, CO), 163.8 (AXX'A', N = $\left| ^2J_{CP} + {}^3J_{CP} \right|$ = 17.0 Hz, NCH), 86.0 (AXX'A', N = $\left| ^1J_{CP} + {}^3J_{CP} \right|$ = 37.6 Hz, PCH), 38.2 (A$_2$XX'A$_2$', N = $\left| ^1J_{CP} + {}^3J_{CP} \right|$ = 19.2 Hz, PC(CH$_3$)$_3$), 36.3 (A$_2$XX'A$_2$', N = $\left| ^1J_{CP} + {}^3J_{CP} \right|$ = 20.6 Hz, PC(CH$_3$)$_3$), 29.9 (A$_6$XX'A$_6$', N = $\left| ^1J_{CP} + {}^3J_{CP} \right|$ = 5.0 Hz, CH_3), 28.6 (A$_6$XX'A$_6$', N = $\left| ^1J_{CP} + {}^3J_{CP} \right|$ = 5.6 Hz, CH_3). ^{31}P{^{1}H} NMR (161.83 MHz): δ = 69.4 (s, P^tBu$_2$).
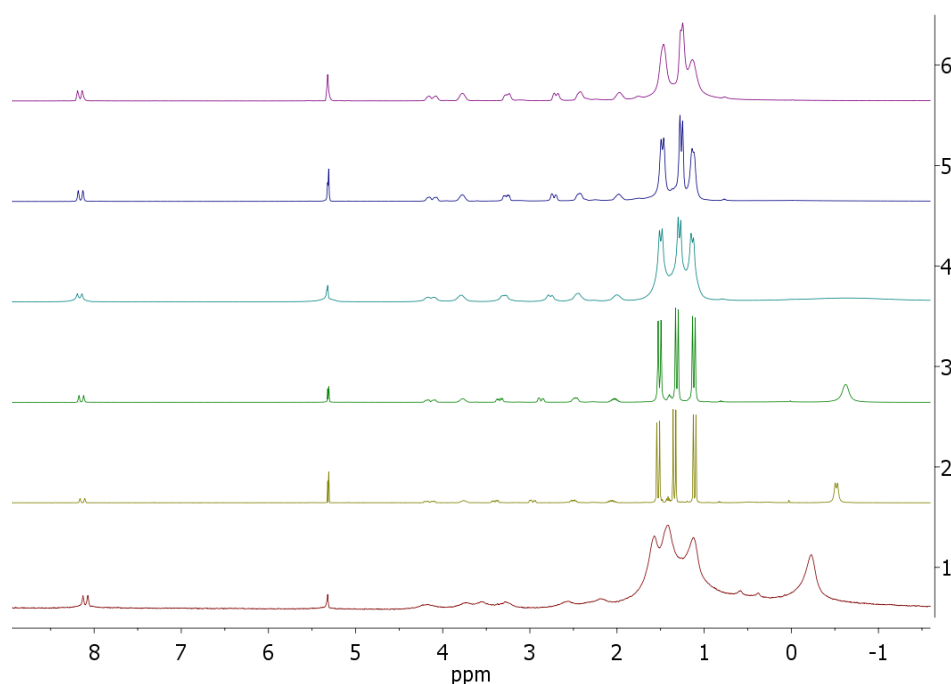
3.5 Spectroscopic results

Figure B-3.10: Temperature dependent ^{1}H NMR spectra of complex **2** in CD$_2$Cl$_2$ (180K, 190K, 200K, 250K, 300K).
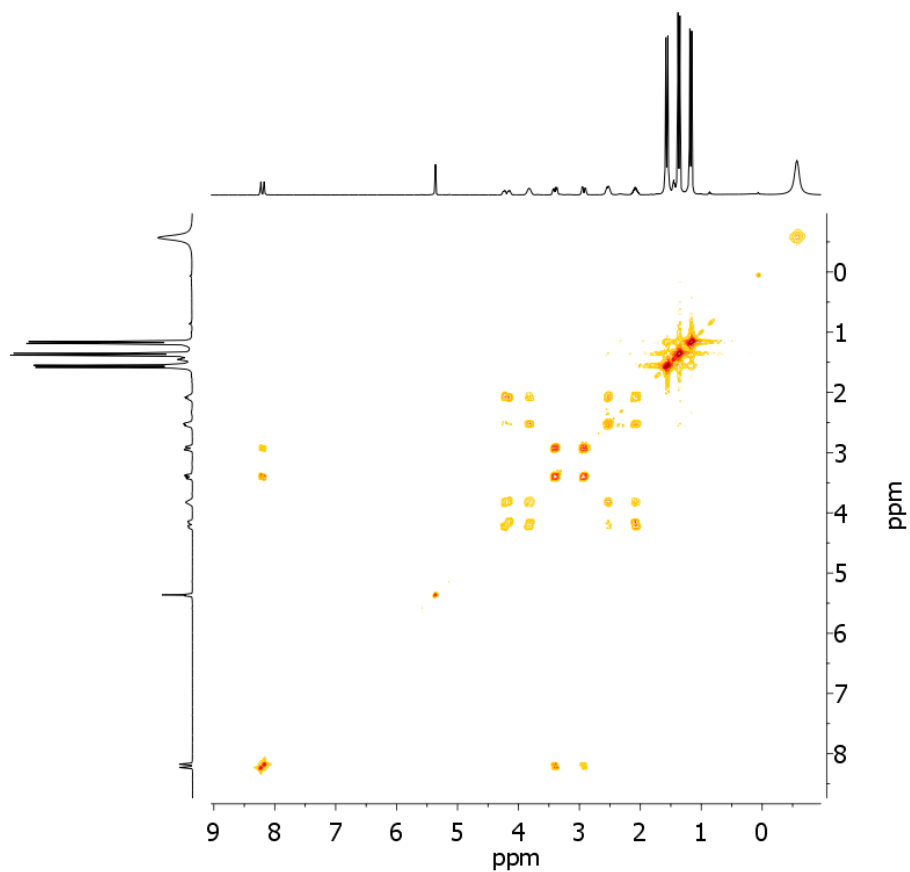
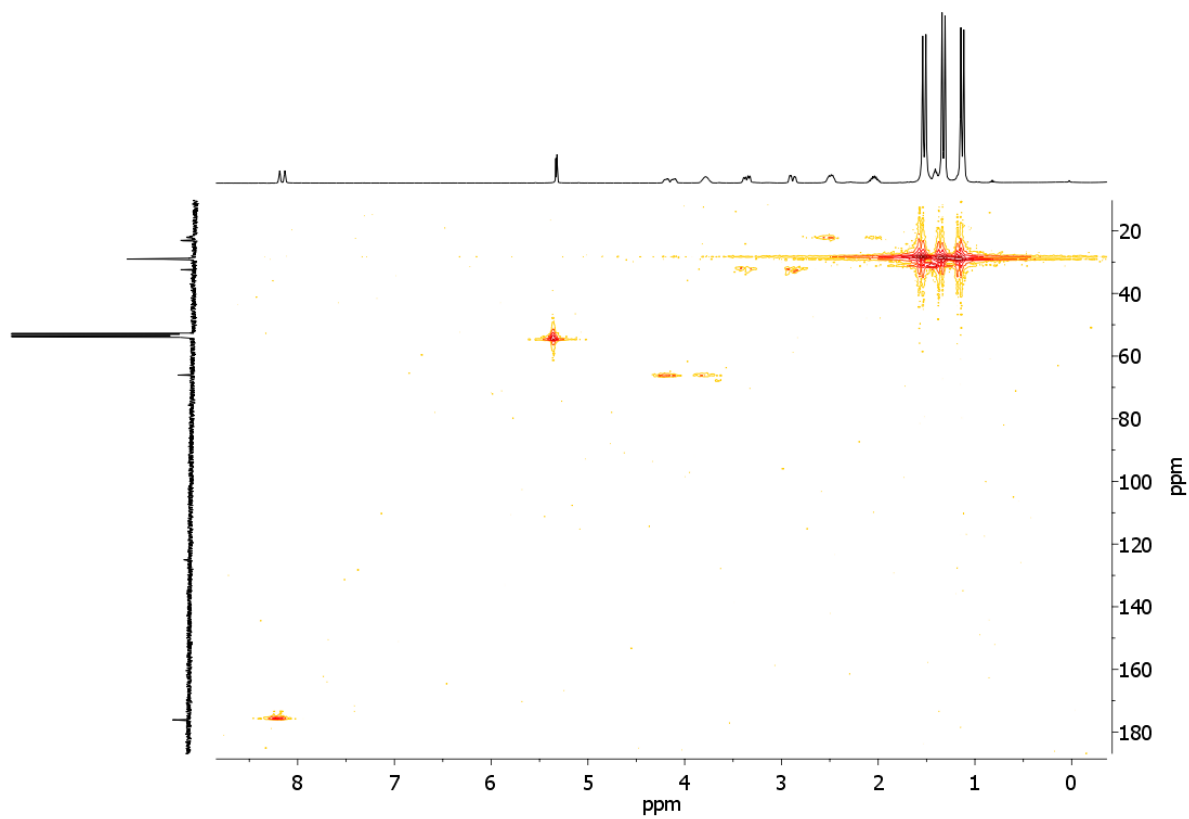**Figure B-3.11:** ^{1}H COSY NMR (CD$_2$Cl$_2$, 230K) of complex **5**.

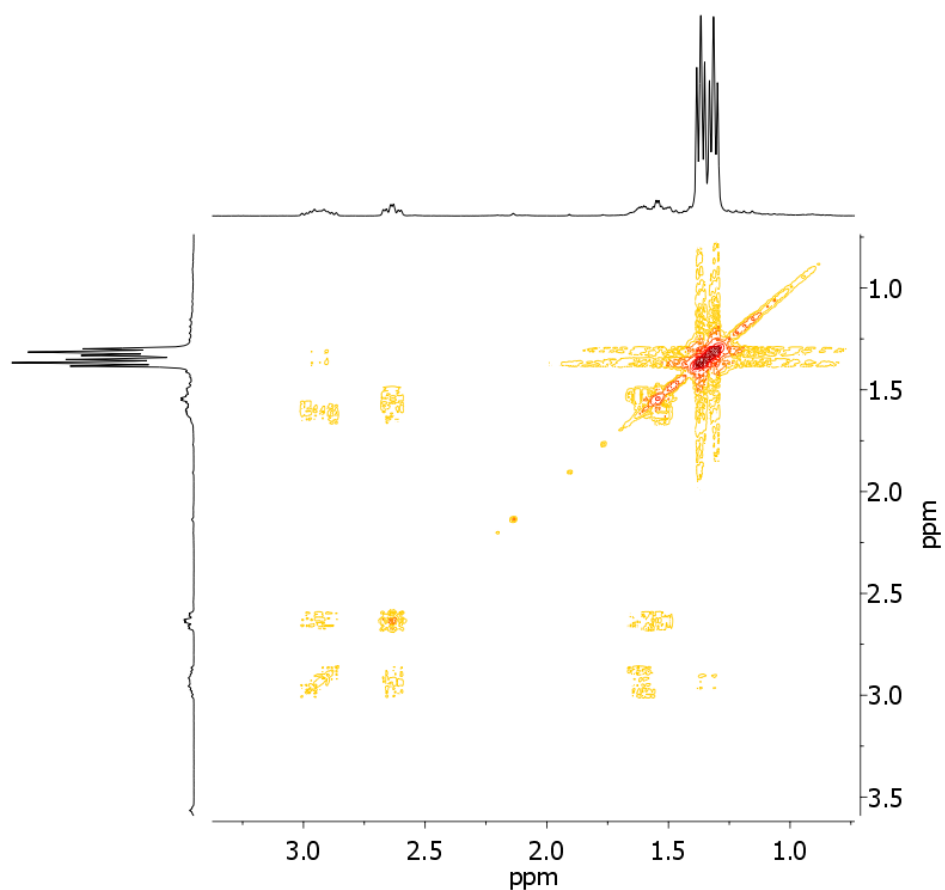**Figure B-3.12:** ^{1}H-^{13}C HMQC NMR (CD$_2$Cl$_2$, 230K) of complex **5**.

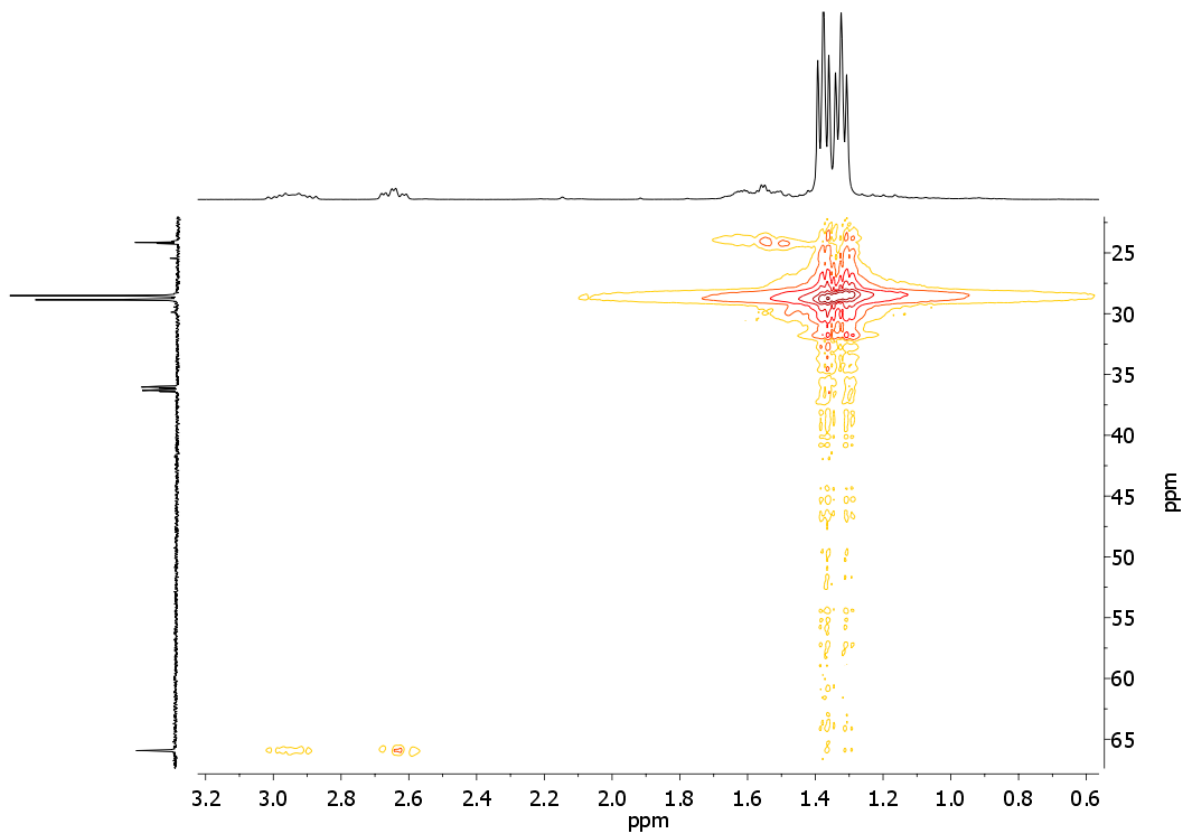**Figure B-3.13:** ¹H COSY NMR (d^6-benzene, r.t.) of complex **8**.

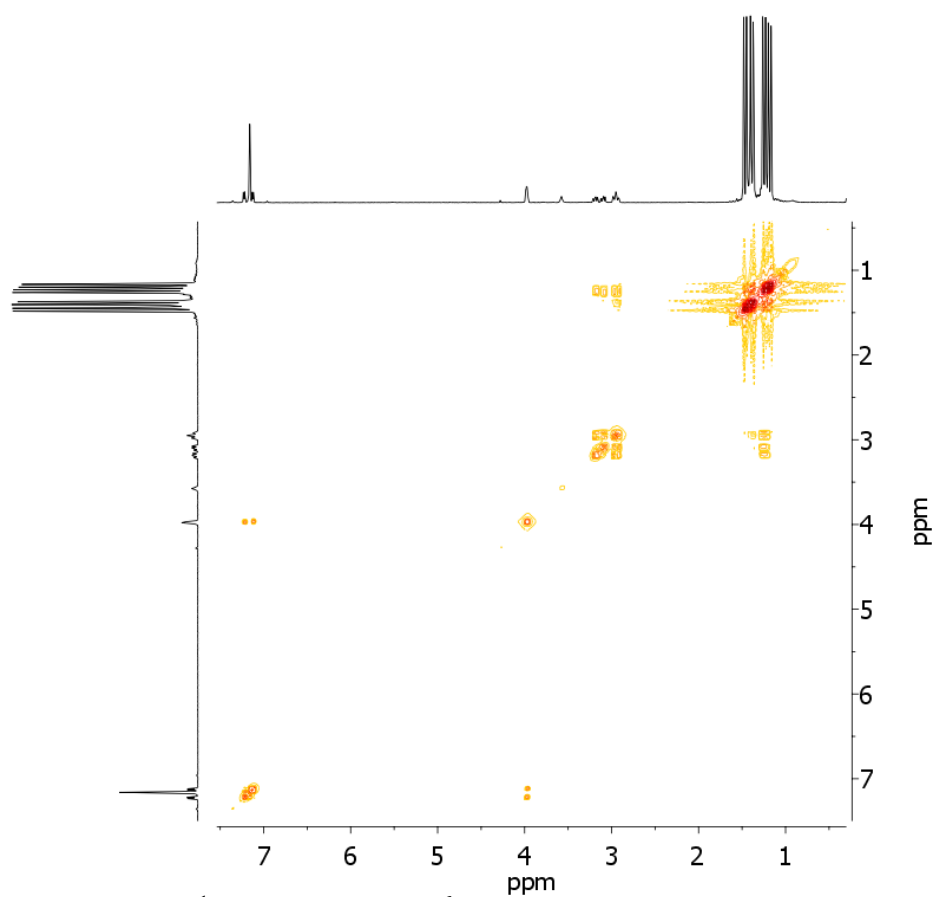**Figure B-3.14:** ¹H-¹³C HMQC NMR (d^6-benzene, r.t.) of complex **8**.

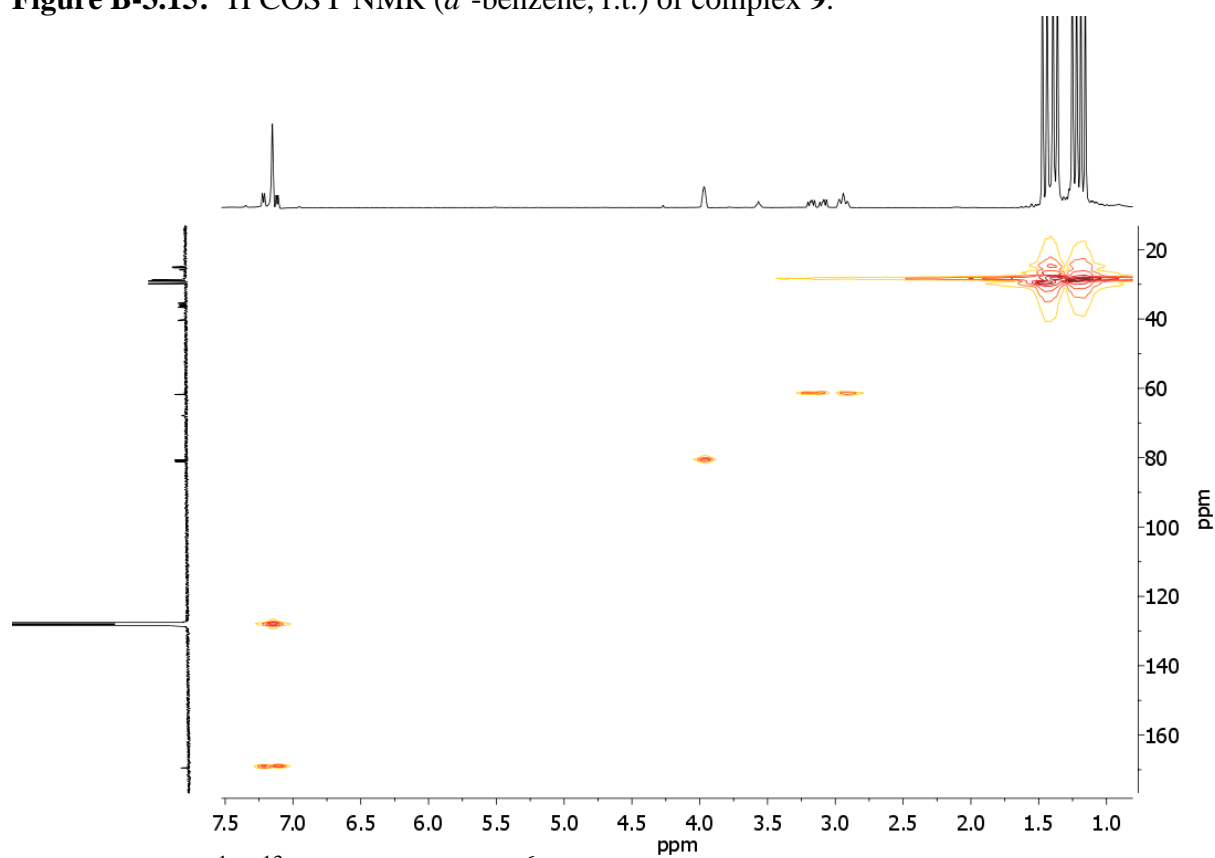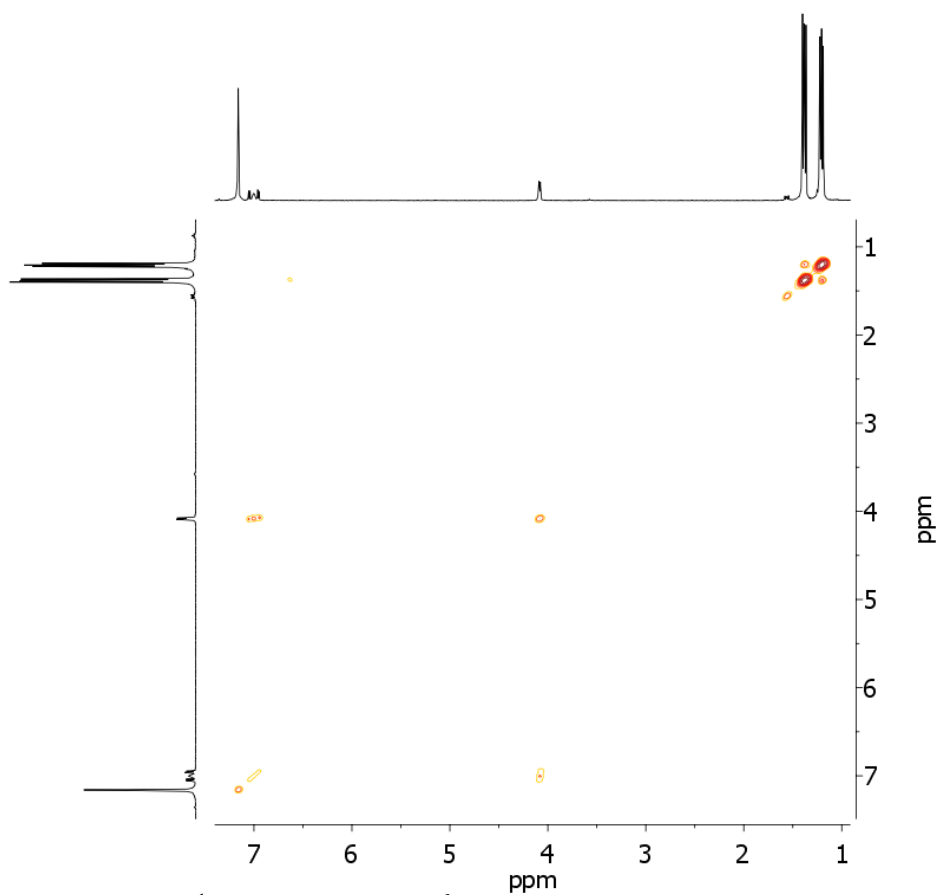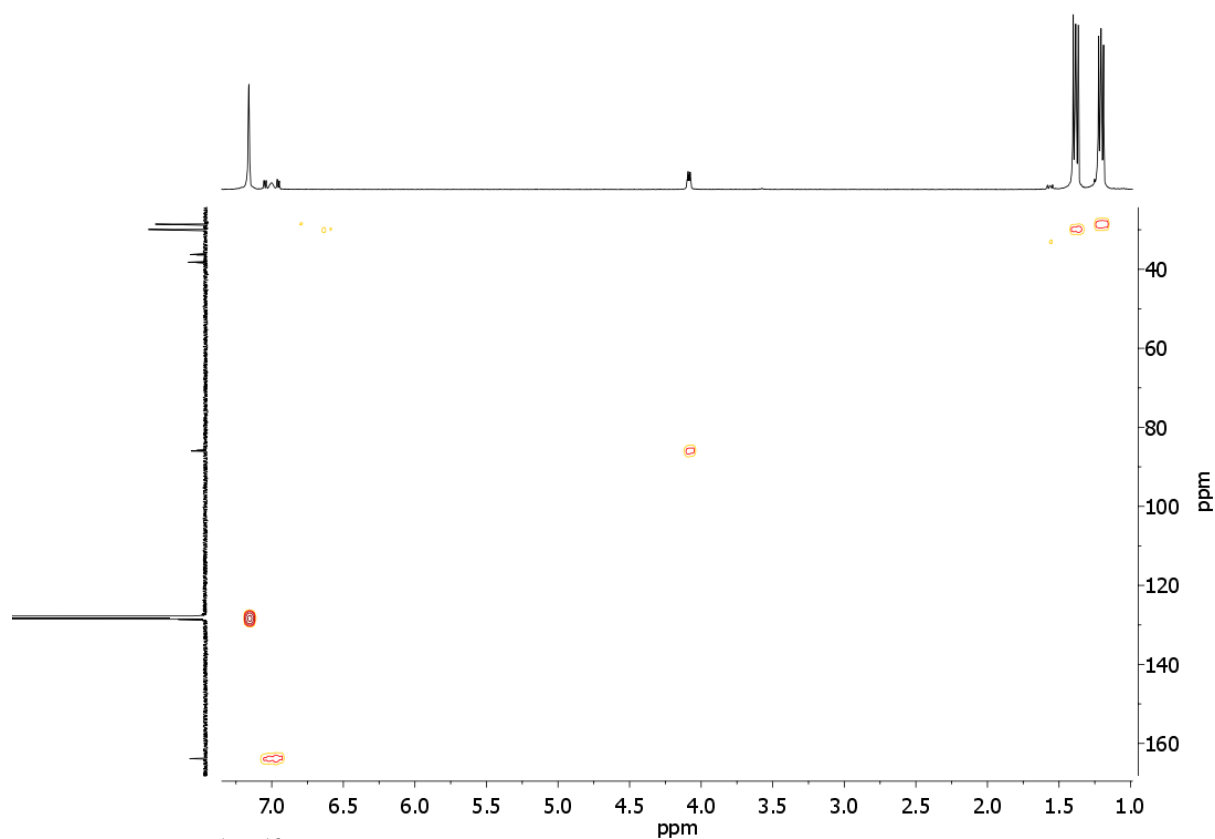**Figure B-3.15:** ^{1}H COSY NMR (d^6-benzene, r.t.) of complex **9**.

Figure B-3.16: ^{1}H-^{13}C HMQC NMR (d^6-benzene, r.t.) of complex **9**.

Figure B-3.17: ^{1}H COSY NMR (d^6-benzene, r.t.) of complex **10**.

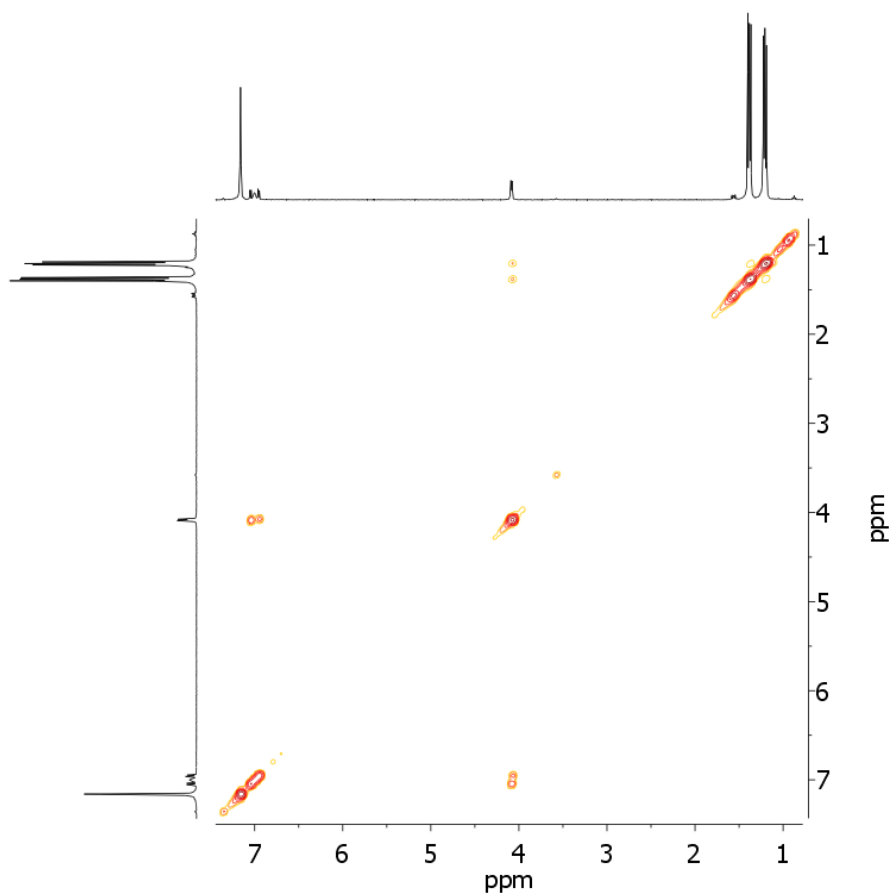**Figure B-3.18:** ^{1}H-^{13}C HMQC NMR (d^6-benzene, r.t.) of complex **10**.

Figure B-3.19: ^{1}H NOESY NMR (d^6-benzene, r.t.) of complex **10**.

3.6 Computational results

Geometry optimizations without symmetry restrictions were executed with the program Gaussian-09 using the functionals B3LYP.[27,28] Stuttgart-Dresden-ECP and respective

27 M. J. Frisch, G. W. Trucks, H. B. Schlegel, G. E. Scuseria, M. A. Robb, J. R. Cheeseman, J. A. Montgomery, Jr., T. Vreven, K. N. Kudin, J. C. Burant, J. M. Millam, S. S. Iyengar, J. Tomasi, V. Barone, B. Mennucci, M. Cossi, G. Scalmani, N. Rega, G. A. Petersson, H. Nakatsuji, M. Hada, M. Ehara, K. Toyota, R. Fukuda, J. Hasegawa, M. Ishida, T. Nakajima, Y. Honda, O. Kitao, H. Nakai, M. Klene, X. Li, J. E. Knox, H. P. Hratchian, J. B. Cross, V. Bakken, C. Adamo, J. Jaramillo, R. Gomperts, R. E. Stratmann, O. Yazyev, A. J. Austin, R. Cammi, C. Pomelli, J. W. Ochterski, P. Y. Ayala, K. Morokuma, G. A. Voth, P. Salvador, J. J. Dannenberg, V. G. Zakrzewski, S. Dapprich, A. D. Daniels, M. C. Strain, O. Farkas, D. K. Malick, A. D. Rabuck, K. Raghavachari, J. B. Foresman, J. V. Ortiz, Q. Cui, A. G. Baboul, S. Clifford, J. Cioslowski, B. B. Stefanov, G. Liu, A. Liashenko, P. Piskorz, I. Komaromi, R. L. Martin, D. J. Fox, T. Keith, M. A. Al-Laham, C. Y. Peng, A. Nanayakkara, M. Challacombe, P. M. W. Gill, B. Johnson, W. Chen, M. W. Wong, C. Gonzalez, and J. A. Pople, *Gaussian03 Rev. D.01*; Gaussian Inc.: Wallingford, CT, **2004**.

28 a) S. H. W. L. Vosko, M. Nusair, *Can. J. Phys.* **1980**, *58*, 1200; b) J. P. Perdew, *Phys. Rev. B* **1986**, *33*, 8822; c) C. Lee, W. Yang, R. G. Parr, *Phys. Rev. B* **1988**, *37*, 785; d) A. D. Becke, *Phys. Rev. A* **1988**, *38*, 3098; e) A.D. Becke, *J. Chem. Phys.* **1993**, *98*, 5648; f) P. J. Stephens, F. J. Devlin, C.F. Chabalowski, M. J. Frisch, *J. Phys. Chem.* **1994**, *98*, 11623.

basisset were used for ruthenium and split valence double-ζ basisset 6-31+G** for all other atoms.[29,30] All optimized geometries were verified as being true minima by the absence of negative eigenvalues in the vibrational frequency analysis.[31]

29   M. Dolg, H. Stoll, H. Preuss, R.M. Pitzer, *J. Phys. Chem.* **1993**, *97*, 5852.

30   a) W. J. Hehre, R. Ditchfield, J. A. Pople, *J. Chem. Phys.* **1972**, *56*, 2257; b) M. M. Francl, W. J. Petro, W. J. Hehre, J. S. Binkley, M. S. Gordon, D. J. DeFrees and J. A. Pople, *J. Chem. Phys.* **1982**, *77*, 3654.
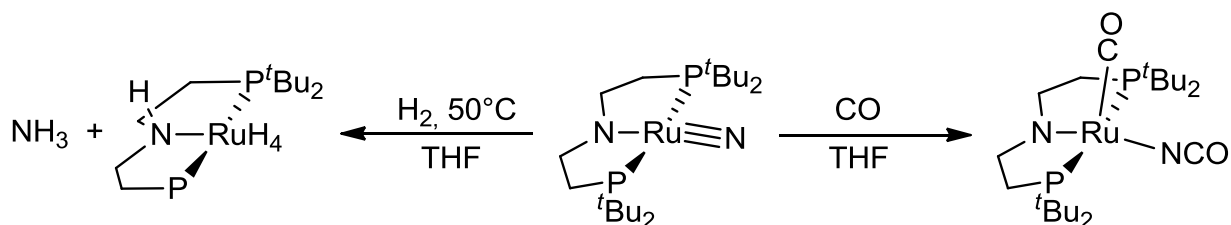
31   E. D. Glendening, A. E. Reed, J. E. Carpenter, F. Weinhold, NBO Version 3.1.

4 Ammonia formation by metal-ligand cooperative hydrogenolysis of a nitrido ligand

This chapter originated the following publication:

B. Askevold, J. T. Nieto, S. Tussupbayev, M. Diefenbach, E. Herdtweck, M.C. Holthausen,

S. Schneider

Nature Chem. **2011**, *3*, 532.

4.1 Abstract

Bioinspired hydrogenation of N_2 to ammonia at ambient conditions by stepwise nitrogen protonation/reduction with metal complexes in solution experienced remarkable success in recent years. In contrast, the highly desirable direct hydrogenation with H_2 remains scarce. In analogy to the heterogeneously catalysed *Haber-Bosch* process, such a reaction is conceivable via metal centered N_2 splitting and unprecedented hydrogenolysis of the nitrido ligands to ammonia. We report the synthesis of a ruthenium(IV) nitrido complex. The high nucleophilicity of the nitrido ligand is demonstrated by unusual N-C coupling with π-acidic CO. Furthermore, the terminal nitrido ligand undergoes facile hydrogenolysis with H_2 at ambient conditions to produce ammonia in high yield. Kinetic and quantum-chemical examinations for this reaction suggest cooperative behaviour of the PNP pincer ligand in rate determining heterolytic hydrogen splitting.

4.2 Introduction

More than 40 years after the characterization of the first dinitrogen complex,[1] the functionalization of N_2 under mild reaction conditions still represents a major challenge.[2] While nitrogen fixation to ammonia at ambient temperature and pressure is performed by bacteria and archeae for millions of years, the heterogeneously catalysed industrial process (*Haber-Bosch*) requires harsh conditions (ca. 450 °C and 300 bar) and consumes more than 1% of the world's annual energy supply. Despite recent improvements in structural models for the [Fe,Mo]-nitrogenase active site from crystallographic, spectroscopic, and theoretical studies, the mechanism of biological nitrogen fixation is not fully understood to date.[3] Few functional models afforded sub-stoichiometric amounts of ammonia by protonation or

---

[1] A. D. Allen, C. V. Senoff, *Chem. Commun.* **1965**, 621

[2] a) J. Chatt, J. R. Dilworth, R. L. Richards, *Chem. Rev.* **1978**, *78*, 589; b) S. Gambarotta, *J. Organomet. Chem.* **1995**, *500*, 117; c) T. A. Bazhenova, A. E. Shilov, *Coord. Chem. Rev.* **1995**, *144*, 69; d) M. Hidai, Y. Mizobe, *Chem. Rev.* **1995**, *95*, 1115; e) M. D. Fryzuk, S. A. Johnson, *Coord. Chem. Rev.* **2000**, *200-202*, 379; f) S. Gambarotta, J. Scott, *Angew. Chem. Int. Ed.* **2004**, *43*, 5298; g) B. A. MacKay, M. D. Fryzuk, *Chem. Rev.* **2004**, *104*, 385; h) Y. Ohki, M. D. Fryzuk, *Angew. Chem. Int. Ed.* **2007**, *46*, 3180; i) R. R. Schrock, *Angew. Chem. Int. Ed.* **2008**, *47*, 5512.

[3] a) O. Einsle, F. A. Tezcan, S. L. A. Andrade, B. Schmid, M. Yoshida, J. B. Howard, D. C. Rees, *Science* **2002**, *297*, 1696; b) T.-C. Yang, N. K. Maeser, M. Laryukhin, H.-I. Lee, D. R. Dean, L. C. Seefeldt, B. M. Hoffman, *J. Am. Chem. Soc.* **2005**, *127*, 12804; c) I. Dance, *J. Am. Chem. Soc.* **2007**, *129*, 1076;

hydrogen atom transfer to N_2- or nitrido-ligands.[4] Two landmark studies reported catalytic ammonia formation at ambient conditions by N_2 hydrogenation with acid and electrochemical or organometallic reduction equivalents, respectively.[5] Most recently, Mo(PNP) pincer complexes were successfully employed, as well.[6] However, turn over numbers remain low and the presence of Brønsted acid and reducing agents renders H_2 formation difficult to suppress − a side reaction which in fact reduces the energy efficiency of biological nitrogen fixation as well. Hence, N_2 hydrogenation using dihydrogen defines a highly desirable goal, but only few accounts for stoichiometric examples have been reported and a catalytic version remains elusive.[7]

Experimental and theoretical examinations of the *Haber-Bosch* process indicate that the reaction commences with the initial splitting of N_2 to adsorbed *N*-atoms featuring bridging binding modes to the metal surface, followed by stepwise hydrogenation to form ammonia.[8] In recent years, substantial research efforts have beeen devoted to the design of an analogous, *Haber-Bosch*-like homogeneous process. However, while metal-mediated splitting of the N_2 to nitrido ligands has been demonstrated,[9] the resulting high-valent complexes do not react with H_2, as best described by Shaver and Fryzuk: *"The problem with developing a viable process coupling nitride formation with the production of useful nitrogen-containing materials is the inherent stability of the metal nitrides generated. Reactions of nitrides employ*

[4] a) J. Chatt, A. J. Pearman, R. L. Richards, *Nature* **1975**, *253*, 39; b) Y. Nishibayashi, S. Iwai, M. Hidai, *Science* **1998**, *279*, 540; c) T. A. Betley, J. C. Peters, *J. Am. Chem. Soc.* **2004**, *126*, 6252; d) J. J. Scepaniak, J. A. Young, R. P. Bontchev, J. M. Smith, *Angew. Chem. Int. Ed.* **2009**, *48*, 3158.

[5] a) C. J. Pickett, J. Talarmin, *Nature* **1985**, *317*, 652; b) D. V. Yandulov, R. R. Schrock, *Science* **2003**, *301*, 76;

[6] K. Arashiba, Y. Miyake, Y. Nishibayashi, *Nat. Chem.* **2011**, *3*, 120; b)

[7] a) M. D. Fryzuk, J. B. Love, S. J. Rettig, V. G. Young, *Science* **1997**, *275*, 1445; b) J. A. Pool, E. Lobkovsky, P. J. Chirik, *Nature* **2004**, *427*, 527.

[8] a) R. Schlögl, *Angew. Chem. Int. Ed.* **2003**, *42*, 2004; b) G. Ertl, *Angew. Chem. Int. Ed.* **2008**, *47*, 3524; c) K. Honkala, A. Hellman, I. N. Remediakis, A. Logadottir, A. Carlsson, S. Dahl, C. H. Christensen, J. K. Norskov, *Science* **2005**, *307*, 555.

[9] C. E. Laplaza, C. C. Cummins, *Science* **1995**, *268*, 861; b) A. Zanotti-Gerosa, E. Solari, L. Giannini, C. Floriani, A. Chiesi-Villa, C. Rizzoli, *J. Am. Chem. Soc.* **1998**, *120*, 437; c) G. K. B. Clentsmith, V. M. E. Bates, P. B. Hitchcock, F. G. N. Cloke, *J. Am. Chem. Soc.* **1999**, *121*, 10444; d) E. Solari, C. Da Silva, B. Iacono, J. Hesschenbrouck, C. Rizzoli, R. Scopelliti, C. Floriani, *Angew. Chem. Int. Ed.* **2001**, *40*, 3907; e) H. Kawaguchi, T. Matsuo, *Angew. Chem. Int. Ed.* **2002**, *41*, 2792; f) I. Korobkov, S. Gambarotta, G. P. A. Yap, *Angew. Chem. Int. Ed.* **2002**, *41*, 3433; g) G. B. Nikiforov, I. Vidyaratne, S. Gambarotta, I. Korobkov, *Angew. Chem. Int. Ed.* **2009**, *48*, 7415.

harsh reagents to affect moderate changes."[10] In search of a platform that affords the hydrogenolysis of intermediate nitrido complexes formed after N_2 bond cleavage, an increased formal metal *d*-electron count (d^n, n ≥ 4) should generally be beneficial both for metal-centered H_2 activation and for subsequent reductive proton transfer to a nitride ligand which decreases unfavorable π-interactions of the ligand with the low-valent metal center.[11] Such nitrido complexes are, however, particularly rare, [4c,d,12] and only partial M-N bond hydrogenolysis has been reported.[12b,e] To date, no example exists for the complete hydrogenolysis of a nitrido ligand by H_2 to ammonia. As part of our ongoing efforts to utilize cooperative metal-ligand complexes,[13] we report here the synthesis of a ruthenium(IV) complex with a nucleophilic nitrido ligand which undergoes facile nitride-CO coupling as well as hydrogenolysis with H_2 to ammonia at moderate temperatures, assisted by the PNP amido pincer ligand.

4.3 Results and discussion

Synthesis and characterization of ruthenium(IV) nitrido complex [Ru(N)(PNP)]

We recently presented the synthesis of four-coordinate ruthenium(II) complex [RuCl(PNP)] (**2**; PNP = $N(CH_2CH_2PtBu_2)_2$) (Figure B-4.1).[14] The steric bulk of the PNP pincer ligand enforces a square-planar coordination geometry, while the unexpected singlet ground state is stabilised by strong N→Ru π-donation. In comparison, Caulton and co-workers have reported the closely related square-planar complex [RuCl(PNP^{Si})] (**3**; PNP^{Si} = $N(SiMe_2CH_2PtBu_2)_2$), which exhibits an intermediate spin ground state, attributal to the weaker π-donation of the disilylamido ligand.[15] The low coordination number and formal 14-

---

[10] M. P. Shaver, M. D. Fryzuk, *Adv. Synth. Catal.* **2003**, *345*, 1061.

[11] a) G. J. Kubas, *Chem. Rev.* **2007**, *107*, 4152; b) K. G. Caulton, *New J. Chem.* **1994,** *18*, 25-41;

[12] a) A. Walstrom, M. Pink, X. Yang, J. Tomaszewski, M.-H. Baik, K. G. Caulton, *J. Am. Chem. Soc.* **2005**, *127*, 5330; b) S. D. Brown, M. P. Mehn, J. C. Peters, *J. Am. Chem. Soc.* **2005**, *127*, 13146; c) C. Vogel, F. W. Heinemann, J. Sutter, C. Anthon, K. Meyer, *Angew. Chem. Int. Ed.* **2008**, *47*, 2681; d) J. J. Scepaniak, M. D. Fulton, R. P. Bontchev, E. N. Duesler, M. L. Kirk, J. M. Smith, *J. Am. Chem. Soc.* **2008**, *130*, 10515; e) J. Schöffel, A. Y. Rogachev, S. DeBeer George, P. Burger, *Angew. Chem.* **2009**, *121*, 4828, *Angew. Chem. Int. Ed.* **2009**, *48*, 4734.

[13] M. Käß, A. Friedrich, M. Drees, S. Schneider, *Angew. Chem.* **2009**, *121*, 922, *Angew. Chem. Int. Ed.* **2009**, *48*, 905;

[14] B. Askevold, M. M. Khusniyarov, E. Herdtweck, K. Meyer, S. Schneider, *Angew. Chem.* **2010**, *122*, 7728, *Angew. Chem. Int. Ed.* **2010**, *49*, 7566;

[15] L. A. Watson, O. V. Ozerov, M. Pink, K. G. Caulton, *J. Am. Chem. Soc.* **2003**, *125*, 8426.

valence-electron count of these complexes suggests the Ru(PNP) fragment as a suitable platform for the stabilisation of multiply bonded ligands. In fact, the Caulton group synthesized ruthenium(IV) nitrido complex [Ru($\equiv$N)(PNP^{Si})] (**4**)[12a] from **3**, encouraging us to examine the preparation of analogous [Ru($\equiv$N)(PNP)] (**5**). Dissolving **2** and an equimolar amount of [PPN]N$_3$ (PPN$^+$ = N(PPh$_3$)$_2^+$) in acetone at room temperature instantaneously affords **5** in quantitative yield (Figure B-4.1). No reaction intermediates are detected by NMR spectroscopy. The exclusion of light gives identical results. For an intermediate low-spin azide complex, thermal N$_2$-elimination would be spin-allowed. Low N$_3^-$ concentrations, e.g., as a result of less polar solvents (e.g. benzene, THF) or sparingly soluble azides (NaN$_3$), afford considerable amounts of side products attributed to competitive amide β-hydrogen elimination.[14]

The NMR spectrum of diamagnetic complex **5** at room temperature in solution is in agreement with a C_{2v}-symmetric structure on the NMR time scale. While considerable distortion from square-planar molecular geometry is found in the solid state (*vide infra*), density functional theory (DFT) calculations predict low barriers of this distorted global minimum with a square-planar conformation (*vide infra*). 1-^{15}N-azide was used to prepare a sample 50 % enriched in the ^{15}N-**5** isotopomer. The nitrido ligand was found at 832.0 ppm in the ^{15}N NMR spectrum (C$_6$D$_6$).
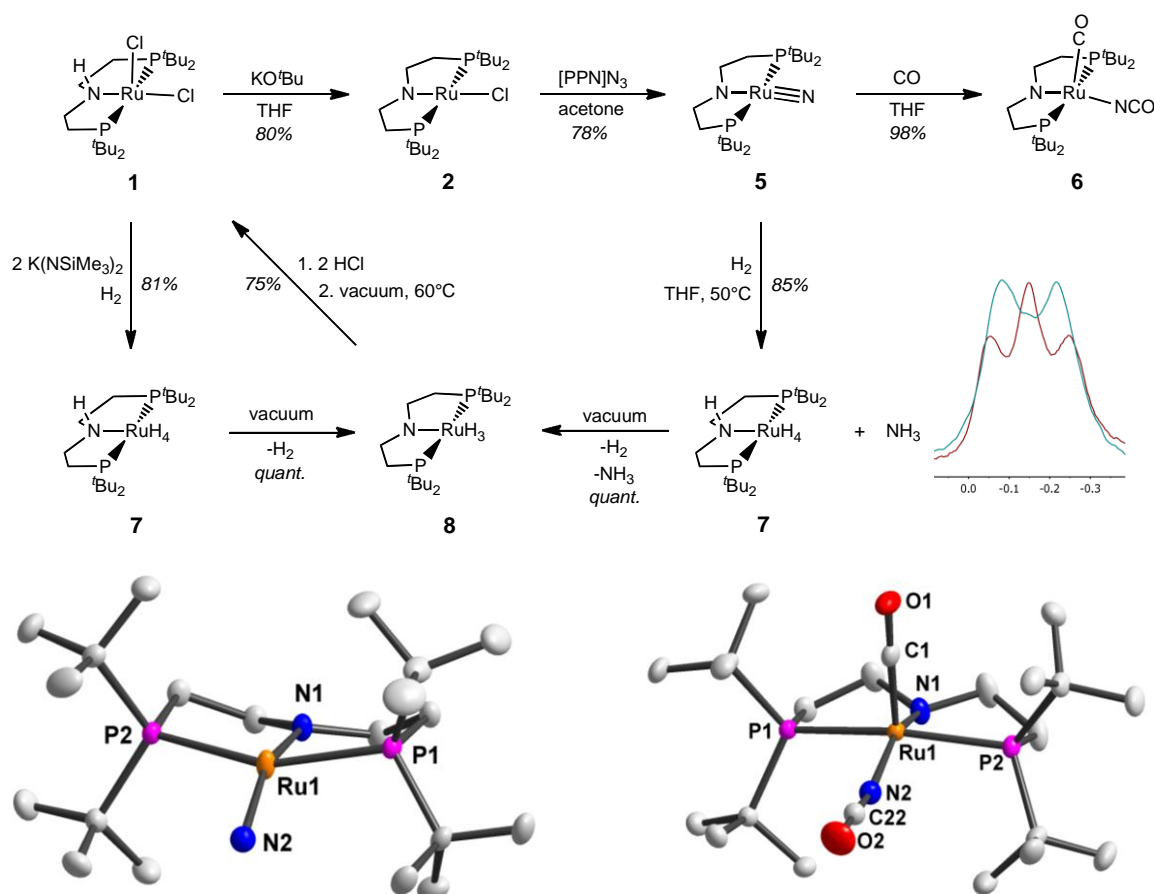
Figure B-4.1: *Top*: Synthetic pathways for the formation of **2**, **5**, **6**, **7**, and **8** (*Inset*: Superimposition of ^{1}H-NMR spectra (NH$_3$ region) after hydrogenolysis of ^{14}N-**5** (red) and ^{14}N/^{15}N-**5** (green), respectively). *Bottom left*: Molecular structure of **5** in the crystal. Selected bond lengths [Å] and angles [°]: Ru1–N1 2.051(1), Ru1–N2 1.688(3) (Ru–N3 1.628(4)), Ru1–P1 2.3796(5), Ru1–P2 2.3724(5); N1–Ru1–N2 147.3(2) (N1–Ru1–N3 165.6(3)), P1–Ru1–P2 155.70(2) (thermal ellipsoids drawn at 50 % probability; hydrogen atoms and N3 omitted for clarity). *Bottom right*: Molecular structure of **6** in the crystal. Selected bond lengths [Å] and angles [°]: Ru1–N1 1.970(2), Ru1–N2 2.124(2), Ru1–C1 1.790(3), Ru1–P1 2.3760(7), Ru1–P2 2.3750(6); N1–Ru1–N2 157.25(7), N1–Ru1–C1 110.94(9), N2–Ru1–C1 91.81(9), P1–Ru1–P2 162.53(2) (thermal ellipsoids drawn at 50 % probability; hydrogen atoms omitted for clarity).

The molecular structure of **5** was derived from single crystal X-ray diffraction and solved applying a split model for the nitride ligand (N2/N3) owing to considerable disorder regarding the nitride ligand position (Figure B-4.1). This observation is easily explained by a flat bending potential for the N1-Ru1-N2 angle as confirmed by DFT calculations (*vide infra*). However, both N2/N3 positions found in the crystal indicate considerable distortion from

square-planar geometry (N1–Ru1–N2 147.3(2)°; N1–Ru1–N3 165.6(3)°) attributable to destabilization by competitive π-bonding of the nitrido and amido ligands. Note that Caulton's nitride **4** exhibits the same type of distortion (N–Ru–N 155.86(13)°).[12a] The shorter ruthenium amide distance of **5** (N1–Ru1 2.051(1) Å) compared with **4** (2.137(2) Å) possibly indicates stronger metal-ligand π-bonding in the dialkylamido complex. In reverse, the *trans*-nitrido ligand exhibits a longer bond with the metal (**5**: 1.688(3) and 1.628(4) Å; **4**: 1.627(2) Å). Owing to the crystallographic disorder with respect to the nitride position, this value has to interpreted with caution. However, IR spectroscopy indicates weaker Ru≡N bonding for **5**, as well. The Ru≡N stretching vibration of **5** was assigned to an absorption at 976 cm^{-1} by comparison with the ^{15}N-**5** isotopomer (945 cm^{-1}, Supporting Information) which is in agreement with the theoretical isomeric shift of 32 cm^{-1}. The Ru≡N stretching vibrations for Ru^{IV} nitrides **5** and **4** (1030 cm^{-1}), several Ru^{VI} nitrido complexes (> 1020 cm^{-1}), and a dinuclear, mixed valent Ru(III)/Ru(IV) nitrido complex (847 cm^{-1}) exhibit a linear correlation with the respective bond lengths (Supporting Information). Please note that the only complex with a lower Ru≡N stretching vibration than **5** is unstable at ambient temperatures.[16]

Reactivity of [Ru(N)(PNP)]: nitride N-CO coupling

The general trends for nitride reactivity have been rationalized in terms of the energies of metal d-orbitals involved in M≡N π-bonding, which are directly influenced by the formal oxidation state of the metal and its position in the periodic table.[17] For example, d^0 tungsten(VI) nitrido complexes exhibit nucleophilic reactivity, while d^2 ruthenium(VI) nitrides are generally electrophilic. Accordingly, osmium(VI) nitrides are intermediate and reactions with nucleophiles and electrophiles have been demonstrated, strongly depending on the ancillary ligand set. In this context, the prediction of reactivity for extremely rare terminal nitrido complexes with d^n (n ≥ 4), such as **5**, is not straightforward. Caulton's ruthenium(IV) nitrido complex **4** does not react with CO or H$_2$ but only reactivity with strong electrophiles was reported.[18] In contrast, Burger's nitride [Ir(≡N)(pyN$_2$)] (**6**; pyN$_2$ = NC$_5$H$_3$-2,6-(CCH$_3$NC$_6$H$_3$-2,6-iPr$_2$)$_2$) exhibits electrophilic reactivity, exemplified by nitride oxidation

[16] a) J. S. Pap, S. DeBeer George, J. F. Berry, *Angew. Chem. Int. Ed.* **2008**, *47*, 10102; b) A. K. Musch Long, R. P. Yu, G. H. Timmer, J. F. Berry, *J. Am. Chem. Soc.* **2010**, *132*, 12228.

[17] a) w. A. Nugent, J. M. Mayer, *Metal Ligand Multiple Bonds*, Wiley, New York, **1988**; b) R. A. Eikey, M. M. Abu-Omar, *Coord. Chem. Rev.* **2003**, *243*, 83.

[18] A. Walstrom, H. Fan, M. Pink, K. G. Caulton, *Inorg. Chim. Acta* **2010**, *363*, 633.

with amine oxide to a nitrosyl complex.[12e] Furthermore, the formation of amido complex [Ir(NH$_2$)(pyN$_2$)] from **6** was described as a nucleophilic attack of H$_2$ at the nitrido ligand.

Complex **5** does not react with PMe$_3$, suggesting nucleophilicity of the nitride. In contrast to **4**, **5** readily reacts with CO at room temperature to form isocyanate complex [Ru(NCO)(CO)(PNP)] (**6**) in high yield (Figure B-4.1). Peaks in the IR spectrum at 1893 and 2209 cm^{-1} and in the ^{13}C NMR spectrum at 213.1 and 132.1 ppm can be assigned to the carbonyl and isocyanate ligands, respectively.[19] The structural assignment of **6** was further confirmed by single crystal X-ray diffraction featuring the metal centre in square pyramidal coordination geometry with CO occupying the apical position (Figure B-4.1). While imide-CO coupling is frequently observed,[20] nitride-CO coupling is particularly rare.[19] The reaction of π-acidic CO with **5** (*vs* **4**) points towards enhanced nitride nucleophilicity of the nitrido ligand owing to the strongly π-donating PNP dialkylamido pincer ligand. Hence we were interested whether the suspected high nucleophilicity promotes H$_2$ addition, as well.

Reactivity of [Ru(N)(PNP)]: nitride hydrogenolysis

Complex **5** reacts under H$_2$ (1 bar) at 50 °C over 48 h to form the tetrahydrido amine complex [RuH$_4$(*H*PNP)] (**7**; *H*PNP = HN(CH$_2$CH$_2$P*t*Bu$_2$)$_2$) in about 85 % yield (Figure B-4.1). Small amounts of unidentified decomposition products and free ligand *H*PNP are also observed by ^{31}P NMR but no reaction intermediate is detected. Lower reaction temperatures result in higher yields of **7** at the expense of smaller reaction rates. Furthermore, a small equilibrium concentration of amido complex [RuH$_3$(PNP)] (**8**) is detected under H$_2$. The fate of the nitride ligand is revealed by ^{1}H NMR spectroscopy. The triplet signal at -0.15 ppm is assigned to ^{14}NH$_3$ by comparison with an original sample of dry ammonia in C$_6$D$_6$. Accordingly, this signal is absent upon hydrogenolysis with D$_2$ and hydrogenation of ^{14}N-**5**/^{15}N-**5** (1:1) with H$_2$ gives an equimolar mixture of ^{14}NH$_3$/^{15}NH$_3$ evidenced by the superimposed triplet (^1J(^{1}H-^{14}N) = 38.1 Hz) and doublet (^1J(^{1}H-^{15}N) = 53.7 Hz) signals (Figure B.4-1). The ratio of the *J*-coupling constants (1.41) is in agreement with the expected value (γ(^{15}N)/γ(^{14}N) = -1.40). Both integration of the ^{1}H NMR signal and indophenolic titration indicate more than 80% formation of ammonia pointing towards quantitative hydrogenolysis of the nitride ligand upon formation of **7**. NMR monitoring of the reaction

---

[19] a) J. S. Silvia, C. C. Cummins, *J. Am. Chem. Soc.* **2008**, *131*, 446; b) B. L. Tran, M. Pink, X. Gao, H. Park, D. J. Mindiola, *J. Am. Chem. Soc.* **2010**, *132*, 1458.

[20] D. J. Mindiola, *Angew. Chem. Int. Ed.* **2008**, *47*, 1557.

suggests pseudo first order kinetics in [**5**] ($k_{298K} = 5.1 \cdot 10^{-3} \pm 0.1$ h^{-1}) and a kinetic isotope effect (KIE) $k_H/k_D = 1.3 \pm 0.2$ was estimated upon use of D_2.

Evaporation of the solvent and redissolving results in H_2 elimination from **7** and selective formation of **8**. Alternatively, **7** and **8** can be synthesised starting from **1** by reaction with base ($KN(SiMe_3)_2$) under an atmosphere of H_2 (Figure B-4.1), allowing for more convenient isolation and full characterization. Both polyhydride complexes **7** and **8** exhibit only one ^1H NMR signal for the hydride ligands, respectively, at temperatures down to 190K indicating high fluxionality on the NMR timescale. According to T_1^{min} (113 ms (**7**), 41 ms (**8**); 400 MHz, d^8-THF) and DFT calculations ($d_{HH}^{min} = 1.57$Å (**7**), 1.31Å (**8**)), molecular structures with one compressed dihydride ligand pair ($d_{HH} = 1.3 - 1.6$ Å), respectively, are tentatively assigned to **7** ([$Ru(H)_2(H_2)(H$PNP)]) and **8** ([$Ru(H)(H_2)(PNP)$]) (Supporting Information).[11a] Further examinations will be subject to a more detailed study. Most importantly, the versatile heterolytic addition and elimination of H_2 across the $Ru-N_{PNP}$ bond possibly points towards the importance of this reactivity for nitride hydrogenolysis.[13]

Finally, hydride complex **8** is easily recycled by reaction with 2 equiv. HCl (Figure B-4.1). Gas evolution and quantitative precipitation of dihydrogen complex [$Ru(Cl)_2(H_2)(H$PNP)] (**9**) is observed which was characterized spectroscopically. Heating a solid sample of **9** at 60°C over night in vacuo recovers the overall starting material **1** in over 75% yield. Hence, the formal formation of NH_3 from azide and H_2 ($HN_3 + H_2 \rightarrow NH_3 + N_2$) is demonstrated in a Ruthenium mediated synthetic cycle.

Quantum-chemical examination.

Various reaction pathways were investigated for the hydrogenolysis of **5** at the PBE/def2-SVP(PP) level of DFT employing the full molecular model. The excellent performance of this functional/basis set combination was validated for the present system by comparison to coupled-cluster reference calculations. For the sake of conciseness, only the energetically most favourable reaction path is reported below (see Supporting Information for computational details and a full presentation of results). Relative energies relate to Gibbs free energies at 298.15 K.[21]

Two isomers of **5** were identified which differ in the conformation of the ethylene bridges in the PNP ligands and in the N-Ru-N bending angle (145.5° (**5**), 173.5° (**5a**); Supporting

---

[21] Following the clear analysis of (R. W. Ashcraft, S. Raman, W. H. Green, *J. Phys. Chem. B* **2007**, *111*, 11968), we used 1 mol·L^{-1} as standard reference state in solution by adding the corresponding free energy corrections (see Supporting Information).

Information). Both isomers are close in energy and separated by a minute barrier suggesting that crystal packing forces allow for facile interconversion, which provides a straightforward explanation for the observed disorder in the solid state.

The lowest free energy path for the hydrogenolysis of **5** is shown in Scheme B-4.1. All intermediates and transition states shown are located on the singlet surface. Reaction steps involving triplet species are substantially higher in energy (Supporting Information). Hence, reactivity contributions of high-spin species, which dominate the nature of rate-limiting steps in the sense of a two-state reactivity scenario, can be safely excluded.[22] Initial H_2 activation is accomplished by heterolytic splitting across the Ru-N_{PNP} bond in **5** to form the hydrido nitride intermediate **I1** with a computed activation barrier of $\Delta G^{\ddagger} = 26.4$ kcal·mol^{-1}. Conceivable alternative steps, such as H_2 oxidative addition at the metal centre, H_2 addition to the nitride, or addition across the Ru≡N bond, all exhibit considerably higher barriers (Supporting Information). From **I1**, an intramolecular reductive proton transfer from the metal to the nitride ligand leads to the ruthenium(II) imido complex **I2** with a slightly smaller activation barrier of 26.1 kcal·mol^{-1}. Subsequent oxidative addition of a second H_2 molecule to **I2** leads to intermediate **I3** with a moderate activation barrier of 9.9 kcal·mol^{-1}, followed by an essentially barrierless proton transfer to yield the complex **I4** in a strongly exoergic step. Release of ammonia is completed by proton transfer from the non-classical H_2 complex **I5** after further H_2 addition, and subsequent barrierless dissociation from dihydride complex **I6**. The resulting dihydrido amine **I7** readily isomerizes to the thermodynamically more stable amido complex **8**. Alternatively, the formation of the energetically slightly preferred amine complex **7** occurs after addition of a fourth H_2 molecule. The computed thermodynamic and kinetic parameters for H_2 elimination from complex **7** are in accordance with the reversible, competitive formation of **7** and **8** under experimental conditions.

The mechanistic scenario evolving from our quantum-chemical study provides a rationale for the multistep reaction sequence of nitride hydrogenolysis. It is characterised by a rate limiting initial heterolytic activation of H_2. Given the estimated error limits of our computational procedure (3 kcal·mol^{-1}, Supporting Information), it is not meaningful to discriminate between the first and second reaction step as being rate limiting. Therefore, the reaction sequence **5**→**I1**→**I2** is considered rate determining with an overall free energy of activation around 26 kcal·mol^{-1}. This value is in agreement with a barrier of 22.3 kcal/mol which was estimated from the experimental pseudo first order rate constant ($k_{298K} = 5.1 \cdot 10^{-3} \pm$

---

[22] a) H. Schwarz, *Int. J. Mass Spectrom.* **2004**, *237*, 75; b) R. Poli, J. N. Harvey, *Chem. Soc. Rev.* **2003**, *32*, 1; c) D. Schröder, S. Shaik, H. Schwarz, *Acc. Chem. Res.* **2000**, *33*, 139.

0.1 h^{-1}) by normalization to standard conditions ([H_2] = 1 M: k = 1.4 h^{-1}) using the solubility of H_2 in THF (3.7·10^{-3} M at 25 °C and 1 atm).[23] All subsequent reaction steps have substantially lower barriers. This picture is in agreement with the absence of observable intermediates by NMR spectroscopy. The computed H/D KIE's for the initial two transition states (1.02 and 1.92) are unexpectedly small for transition states involving dihydrogen bond cleavage or a reductive proton shift, but this finding is in agreement with the experimentally determined KIE of 1.3. Most importantly, our quantum-chemical results emphasize the role of the cooperating PNP amido ligand in rate determining H_2 activation.
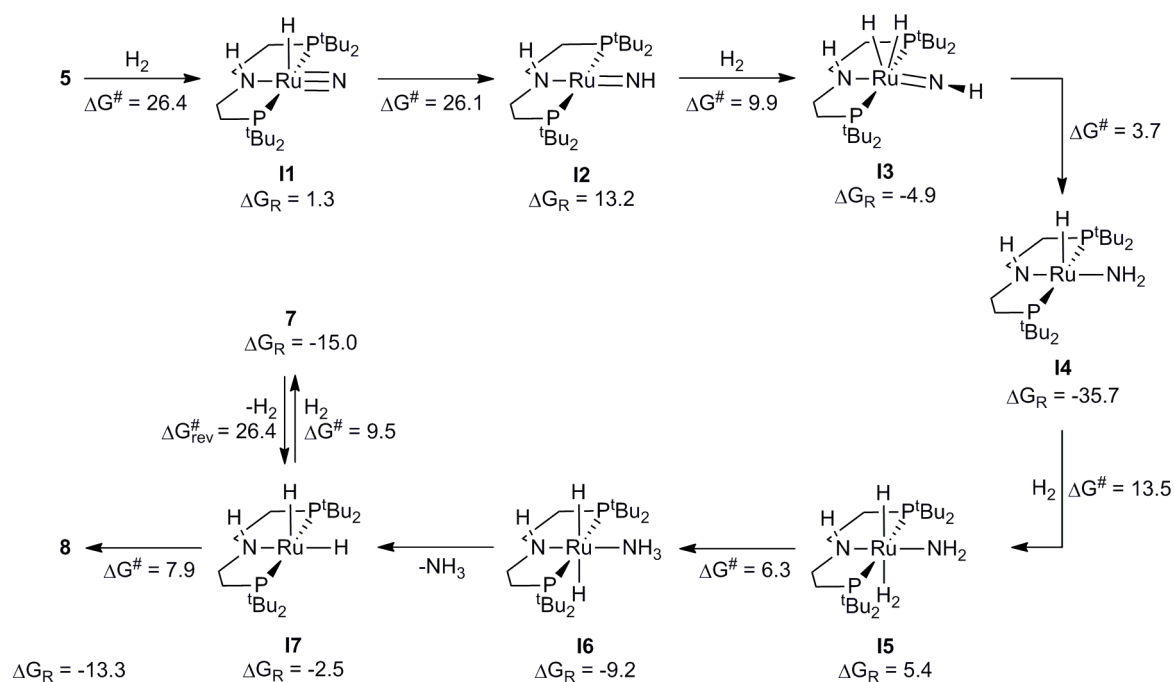
Scheme B-4.1: Computed lowest energy pathway for the hydrogenolysis of **5**; PBE/def2-SVP(PP) relative free energies for the individual steps in kcal·mol^{-1} after standard state correction.

4.4 Conclusions

Four-coordinate complex **2** provides an excellent starting material for the stabilisation of low valent ruthenium complexes with multiply bonded ligands, such as ruthenium(IV) nitride **5**. In contrast to the analogous disilylamido complex **4**, dialkylamide complex **5** exhibits unusual reactivity, such as isocyanate formation by versatile nitride-CO coupling and unprecedented nitride hydrogenolysis to ammonia in high yield at relatively mild conditions.

---

[23] E. Buncel, B. Menon, *J. Am. Chem. Soc.* **1977**, *99*, 4457.

The described reactivity is attributed to two features of the Ru(PNP) platform: (1) The low formal oxidation state of the metal contributes to highly nucleophilic nitride reactivity of **5**. In addition, strong π-donation of the *trans*-amido ligand further increases the nucleophilicity by an unfavourable N-Ru-N 3c-4e π-interaction, giving rise to the bent structure. Relative weakening of Ru≡N bonding is further indicated by infrared spectroscopy. (2) In the initial step of nitride hydrogenolysis, H_2 is heterolytically added across the ruthenium-amido bond. Computations on alternative H_2 addition pathways revealed substantially higher barriers. Hence, pincer ligand cooperativity assists both H_2 activation and reductive proton transfer to the nitride ligand giving rise to the relatively low kinetic barrier of the rate determining initial H_2 activation.

Burger and co-workers have recently demonstrated the partial hydrogenolysis of an electrophilic nitride. Our present study shows, however, that also full hydrogenation of electron rich, nucleophilic nitrides is feasible making use of a cooperating ligand for H_2 activation. While cooperativity of late transition metal amido moieties has been successfully utilised in the catalytic hydrogenation of polar organic multiple bonds,[24] to our knowledge this is the first example for an organometallic example. In the context of this work, it is noteworthy that the metal-pincer motif has been pointed out as a promising platform for N_2 hydrogenation by experimental and computational studies before,[6,25] and ruthenium catalysts are highly active in the heterogeneous *Haber-Bosch* process, as well. This work emphasizes the potential of bifunctional metal-ligand platforms to tune the thermodynamics of M≡N bonding and kinetics of H_2 activation for ammonia generation. We demonstrated the hydrogenation of azide to ammonia in a Ruthenium mediated synthetic cycle according to the overall formal reaction: $HN_3 + H_2 \rightarrow NH_3 + N_2$. Further efforts will be directed towards dinitrogen activation with M(PNP) complexes to enable homogeneous ammonia production form N_2 with H_2 as a hydrogen source.

[24] a) S. E. Clapham, A. Hadzovic, R. H. Morris, *Coord. Chem. Rev.* **2004**, *248*, 2201; b) H. Grützmacher, *Angew. Chem.* **2008**, *120*, 1838; *Angew. Chem. Int. Ed.* **2008**, *47*, 1814.

[25] a) M. Hölscher, M. H. G. Prechtl, W. Leitner, *Chem. Eur. J.* **2007**, *13*, 6636; b) M. Hölscher, W. Leitner, *Chem. Eur. J.* **2010**, *16*, 14266.

4.5 Synthetic and analytical details

Materials and synthetic methods

All experiments were carried out under an atmosphere of argon using Schlenk and glove-box techniques. Solvents were dried over Na/benzophenone/tetraglyme (benzene), Na/benzophenone (THF) and molar sieve (Aceton), distilled under argon and deoxygenated prior to use. Deuterated solvents were obtained from Euriso-Top GmbH, dried over Na/K (d_8-THF, C_6D_6) or CaH_2 (CD_2Cl_2), distilled by trap-to-trap transfer in vacuo, and degassed by three freeze-pump-thaw cycles, respectively. [N(PPh$_3$)$_2$]Cl (Alfa Aesar) and HCl (1M/Et$_2$O, ABCR) were used as purchased. **1**, **2**, and [N(PPh$_3$)$_2$]N$_3$ were prepared according to published procedures.[26]

Analytical methods

Elemental analyses were obtained from the Microanalytical Laboratory of Technische Universität München. The IR spectra were recorded as nujol mulls between KBr plates, UV-Vis spectra on a Thermo Scientific Genesys 6 spectrophotometer with optical plastic liquid transmission cells. NMR spectra were recorded on a Bruker Avance III 400 spectrometer and were calibrated to the residual proton resonance and the natural abundance ^{13}C resonance of the solvent (CD_2Cl_2: $\delta H = 5.32$ and $\delta C = 54.00$ ppm; C_6D_6: $\delta H = 7.16$ and $\delta C = 128.06$ ppm; d_8-THF: $\delta H = 3.58$ and $\delta C = 67.57$ ppm). ^{31}P NMR chemical shifts are reported relative to external phosphoric acid ($\delta = 0.0$ ppm), ^{15}N NMR to external formamid ($\delta = 113.0$ ppm). Signal multiplicities are abbreviated as: s (singlet), d (dublet), t (triplet), q (quartet), m (multiplet), br (broad).

Syntheses

Preparation of [RuN(PNP)] (5). A mixture of **2** (46 mg, 0.093 mmol) and [N(PPh$_3$)$_2$]N$_3$ (53.7 mg, 0.093 mmol) is dissolved in Acetone (5 mL), stirred for 15 min and dried *i. vac.* The solid is extracted trice with pentane (3x 5 mL) and evaporation of the solvent gives **5** as a dark green product. Yield: 34.2 mg (0.072 mmol, 78%). Anal. Calcd. for $C_{20}H_{44}N_2P_2Ru$ (475.59): C, 50.51; H, 9.33; N, 5.89. Found: C, 50.90; H, 9.08; N, 5.40. IR (cm^{-1}) $\tilde{\nu}$ [cm^{-1}] = 976 (s, Ru≡^{14}N), 945 (Ru≡^{15}N). NMR (C_6D_6, r.t., [ppm]) ^{1}H NMR (399.8 MHz): $\delta = 3.17 - 3.09$ (m, 4H, NCH_2), $1.82 - 1.76$ (m, 4H, PCH_2), 1.36 (A$_{18}$XX'A'$_{18}$, N $=\left| ^3J(H,P) + ^5J(H,P) \right| = 13.6$ Hz, 36H, CH_3). ^{13}C{^{1}H} NMR (100.53MHz): d = 61.6 (AXX'A', N

---

[26] a) B. Askevold, M. M. Khusniyarov, E. Herdtweck, K. Meyer, S. Schneider, *Angew. Chem. Int. Ed.* **2010**, *49*, 7566; b) A. Martinsen, J. Songstad, *Acta Chem. Scand., Ser A* **1977**, *31*, 645.

$= \left| {}^2J(C,P) + {}^3J(C,P) \right| = 15.2$ Hz, NCH_2), 35.0 (A$_2$XX'A$_2$', N $= \left| {}^1J(C,P) + {}^3J(C,P) \right| = 12.0$ Hz, C(CH$_3$)$_3$), 29.9 (A$_6$XX'A$_6$', N $= \left| {}^2J(C,P) + {}^4J(C,P) \right| = 7.2$ Hz, CH_3), 25.1 (AXX'A', N $= \left| {}^1J(C,P) + {}^3J(C,P) \right| = 18.6$ Hz, PCH_2). ^{31}P{^{1}H} NMR (161.83 MHz): d = 104.1 (s, P^tBu$_2$). ^{15}N{^{1}H} NMR (40.55 MHz): d = 832.0 (s, P^tBu$_2$). NMR assignments were confirmed by ^{1}H COSY and ^{1}H-^{13}C HMQC NMR spectroscopy. An equimolar mixture of the ^{14}N/^{15}N isotopomers was prepared employing [N(PPh$_3$)$_2$]$^+$[^{15}N^{14}N$_2$]$^-$, which was synthesized from [N(PPh$_3$)$_2$]Cl and Na[1-^{15}N-N$_3$].

Preparation of [Ru(NCO)(CO)(PNP)] (6). A solution of **5** (50 mg; 0,105 mmol) in THF (25 mL) is frozen, evacuated and backfilled with CO. The solution is slowly warmed to r.t. and stirred for 15 min. The color changes via greenish-brown to brick red. The solvent is removed *i. vac.* giving **11** quantitatively. Yield: 54.7 mg (0.103 mmol, 98%). Anal. Calcd. for C$_{22}$H$_{44}$N$_2$O$_2$P$_2$Ru (531.61): C, 49.70; H, 8.34; N, 5.27. Found: C, 49.60; H, 8.48; N, 4.62. IR (cm^{-1}) $\tilde{\nu}$ = 2209 (N=C=O), 1893 (C≡O). NMR (d$_6$-benzene, r.t., [ppm]) ^{1}H NMR (399.8 MHz): δ = 3.00 − 2.82 (m, 2H, NCH_2), 2.68 − 2.56 (m, 2H, NCH_2), 1.45 − 1.53 (m, 4H, PCH_2), 1.22 (A$_{18}$XX'A'$_{18}$, N $= \left| {}^3J_{CP} + {}^5J_{CP} \right| = 18.8$ Hz, 36H, CH_3). ^{13}C{^{1}H} NMR (100.53MHz): d = 213.1 (t, $^2J_{CP} = {}^2J_{CP} = 11.3$ Hz, CO), 132.1 (s, $^3J_{CP} = {}^3J_{CP} = 9.7$ Hz, NCO), 65.9 (AXX'A', N $= \left| {}^2J_{CP} + {}^3J_{CP} \right| = 10.0$ Hz, NCH_2), 35.8 (AXX'A', N $= \left| {}^2J_{CP} + {}^3J_{CP} \right| = 15.8$ Hz, C(CH$_3$)$_3$), 35.5 (AXX'A', N $= \left| {}^2J_{CP} + {}^3J_{CP} \right| = 16.6$ Hz, C(CH$_3$)$_3$), 28.7 (A$_3$XX'A'$_3$, N $= \left| {}^2J_{CP} + {}^4J_{CP} \right| = 4.6$ Hz, CH_3), 28.4 (A$_3$XX'A'$_3$, N $= \left| {}^2J_{CP} + {}^4J_{CP} \right| = 5.2$ Hz, CH_3), 24.2 (AXX'A', N $= \left| {}^1J_{CP} + {}^3J_{CP} \right| = 17.0$ Hz, PCH_2). ^{31}P{^{1}H} NMR (161.83 MHz): d = 112.6 (s, PtBu$_2$). NMR assignments were confirmed by 1H COSY and 1H-13C HMQC NMR spectroscopy.

Preparation of [RuH$_3$(PNP)] (8). THF is trap-to-trap distilled to a mixture of (**1**) (50 mg, 0.094 mmol) and KN(SiMe$_3$)$_2$ (48.9 mg, 0.187 mmol, 2 eq.) at -196 °C, and warmed under an atmosphere of H$_2$ (1 bar). Upon thawing, the color immediately changes to pale yellow. After 30 min at r.t. the solvent is evaporated and the resulting solid extracted with pentane (Three times 10 mL). After removing all volatiles *i. vac.*, the crude product is dissolved in benzene (10 mL). The solvent is sublimed off and the yellow powder evacuated over night affording **8** in high yield. Yield: 35.3 mg (0.076 mmol, 81%). Anal. Calcd. for C$_{20}$H$_{47}$NP$_2$Ru (464.61): C, 51.70; H, 10.20; N, 3.01. Found: C, 51.39; H, 10.57; N, 3.03. IR (cm^{-1}) $\tilde{\nu}$ = 2045 (H, (br)). NMR (C$_6$D$_6$, r.t., [ppm]) ^{1}H NMR (399.8 MHz): δ = 3.46 (A$_2$M$_2$XX', N $= \left| {}^3J(H,P) + {}^5J(H,P) \right| = 26.2$ Hz, 4H, NCH_2), 1.88 (m, 4H, PCH_2), 1.27 − 1.18 (A$_{18}$XX'A'$_{18}$, N $= \left| {}^3J(H,P) + {}^5J(H,P) \right| = 17.8$ Hz, 36H, CH_3), -12.46 (A$_3$XX', N $= \left| {}^2J(H,P) + {}^2J(H,P) \right| = 21.4$ Hz, 3H,

Ru*H*). ^{13}C{^{1}H} NMR (100.53MHz): d = 65.6 (AXX'A', N = |^{2}J(C,P) + ^{3}J(C,P)| = 14.2 Hz, N*C*H$_2$), 34.6 (m, *C*(CH$_3$)$_3$), 29.60 (s, *C*H$_3$), 26.07 (AXX'A', N = |^{1}J(CP) + ^{3}J(C,P)| = 11.4 Hz, P*C*H$_2$). ^{31}P{^{1}H} NMR (161.83 MHz): d = 114.8 (s, *P*^{t}Bu$_2$). NMR assignments were confirmed by ^{1}H COSY and ^{1}H-^{13}C HMQC NMR spectroscopy.

Preparation of [RuH$_4$(HPNP)] (7). A solution of **8** (10 mg, 0.021 mmol) in d$_8$-THF (0.4 mL) is degassed in a J-Young NMR tube and set under 1 bar H$_2$. The color changes to pale yellow affording **7** quantitatively by NMR spectroscopy. Attempted isolation results in partial dehydrogenation and formation of a mixture of **7** and **8**. NMR (d$_8$-THF, r.t., [ppm]) ^{1}H NMR (399.8 MHz): δ = 4.54 (s (br), 1H, N*H*), 3.21 − 3.02 (m, 2H, NC*H$_2$*), 2.22 − 2.12 (m, 2H, NC*H$_2$*), 2.01– 1.97 (m, 2H, PC*H$_2$*), 1.53 − 1.44 (m, 2H, PC*H$_2$*), 1.34 (A$_9$XX'A'$_9$, N = |^{3}J(H,P) + ^{5}J(H,P)| = 11.8 Hz, 18H, C*H$_3$*), 1.26 (A$_9$XX'A'$_9$, N = |^{3}J(H,P) + ^{5}J(H,P)| = 14.8 Hz, 18H, C*H$_3$*), -8.48 (t, *J* = 14.8 Hz, 4H, Ru*H*). ^{13}C{^{1}H} NMR (100.53MHz): d = 56.8 (AXX'A', N = |^{2}J$_{CP}$ + ^{3}J$_{CP}$| = 9.1 Hz, N*C*H$_2$), 34.4 (m, *C*(CH$_3$)$_3$), 32.7 (m, *C*(CH$_3$)$_3$), 31.1 (s (br), *C*H$_3$), 30.9 (s (br), *C*H$_3$), 28.3 (AXX'A', N = |^{1}J$_{CP}$ + ^{3}J$_{CP}$| = 8.1 Hz, P*C*H$_2$). ^{31}P{^{1}H} NMR (161.83 MHz): d = 112.6 (s, *P*^{t}Bu$_2$). NMR assignments were confirmed by ^{1}H COSY and ^{1}H-^{13}C HMQC NMR spectroscopy.

Hydrogenolysis of 5. In a typical experiment, the solution of **5** (8.5 mg; 0.018 mmol) in C$_6$D$_6$ (0.4 mL) is degassed in an NMR tube, set under 1 bar H$_2$ (or D$_2$) and flame sealed or sealed with a Teflon stopcock. The formation of **7** and NH$_3$ at temperatures between 25 - 50 °C was monitored by ^{1}H and ^{31}P NMR spectroscopy. Kinetic parameters from hydrogenolaysis with H$_2$ (or D$_2$) were derived at 298 K by recording ^{31}P NMR spectra in the inverse-gated mode to avoid NOE buildup.

Quantitative analysis of NH$_3$ by the indophenol-method.[27] In a standard procedure, **5** was reacted with H$_2$ in THF at 40 °C until full conversion was obtained by NMR. Subsequently, all volatiles trap to trap distilled into a J-Young flask containing HCL (1M/Et$_2$O, 100 eq. to Ru), warmed to r.t. and stirred for 20 min. All volatiles were removed *i. vac.* and the white residue rinsed with 6-8 aliquots of water into a 50 mL volumetric flask. The samples were analyzed within an hour of preparation. All reagents and NH4Cl standard solutions for calibrations were freshly prepared. The indophenolate absorbance was calibrated within the range of 0.09 to 1.4 (40 to 750 nmol of NH3).

---

[27] A. L. Chaney, E. P. Marbach, *Clinical Chem.* **1962**, *8*, 130.

Reaction of 1 with HCL. HCl (1.0 M in Et$_2$O, 0.02 mL, 0.02 mmol) is added to a solution of **8** (4.7 mg, 0.01 mmol) in THF at r.t.. After 5 min gas evolution is observed and a pale yellow precipitate is formed. The solvent is removed *i. vac.* NMR in CD$_2$Cl$_2$ suggests quantitative formation of [RuCl$_2$(H$_2$)(^{H}PNP^{t}Bu$_2$)]. NMR (CD$_2$Cl$_2$, r.t., [ppm]) ^{1}H NMR (399.8 MHz): δ = 5.54 (s (br), 1H, NH), 3.26 − 3.12 (m, 2H, NCH_2), 2.25 − 2.14 (m, 2H, NCH_2), 2.05 − 1.92 (m, 4H, PCH_2), 1.47 (A$_9$XX'A'$_9$, N = $\left|{}^3J(H,P) + {}^5J(H,P)\right|$ = 12.9 Hz, 18H, CH_3), 1.41 (A$_9$XX'A'$_9$, N = $\left|{}^3J(H,P) + {}^5J(H,P)\right|$ = 11.7 Hz, 18H, CH_3), -10.9 (t, $^2J(H,P)$ = 10.3 Hz, 2H, RuH_2). ^{31}P{^{1}H} NMR (161.83 MHz): s = 63.1 (s, P^tBu$_2$). Heating of the intermediate i. vac. at 60 °C over night leads to elimination of H$_2$ and formation of complex **1** in 75% yield.
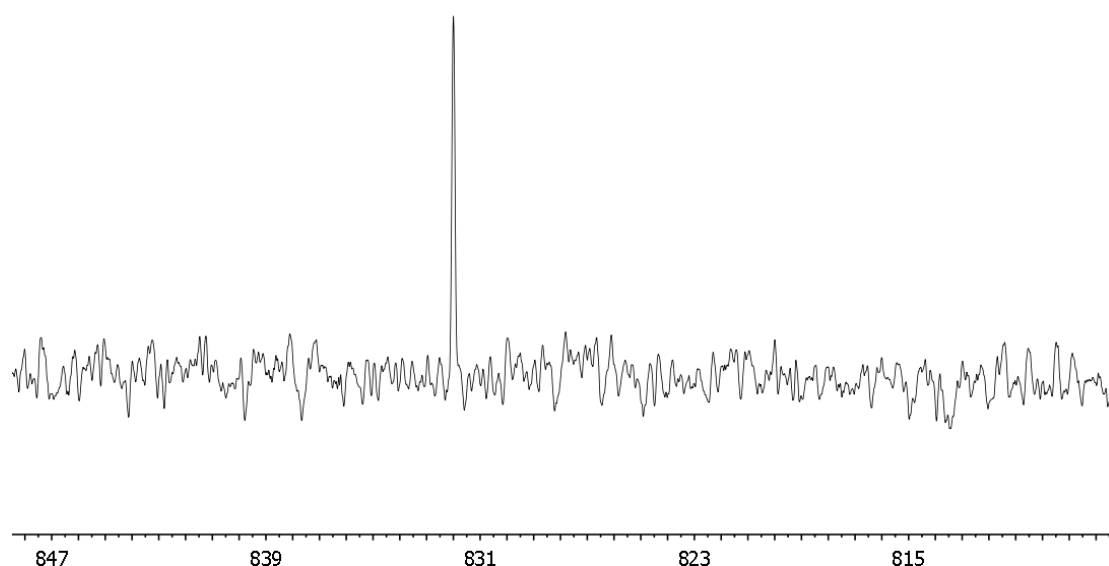
Figure B-4.2: ^{15}N NMR spectrum (THF, r.t.) of complex [RuN(PNP)] (nitride ligand 50 % enriched in ^{15}N).
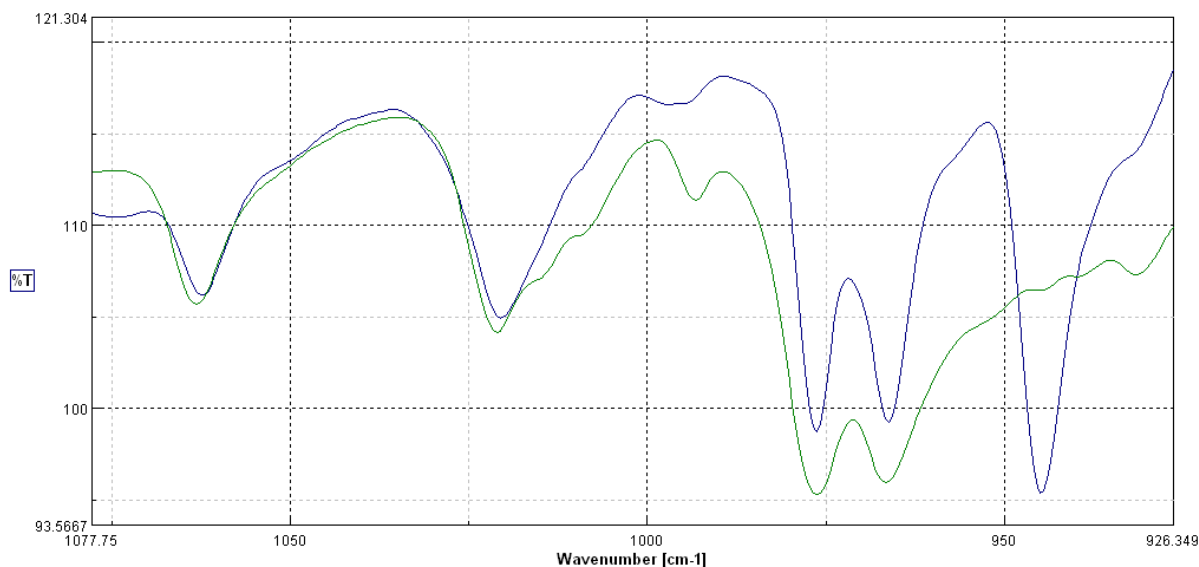
Figure B-4.3: Comparison of the infrared spectra of **5** (green) and $^{14}N/^{15}N$-**5** (blue) in nujol.
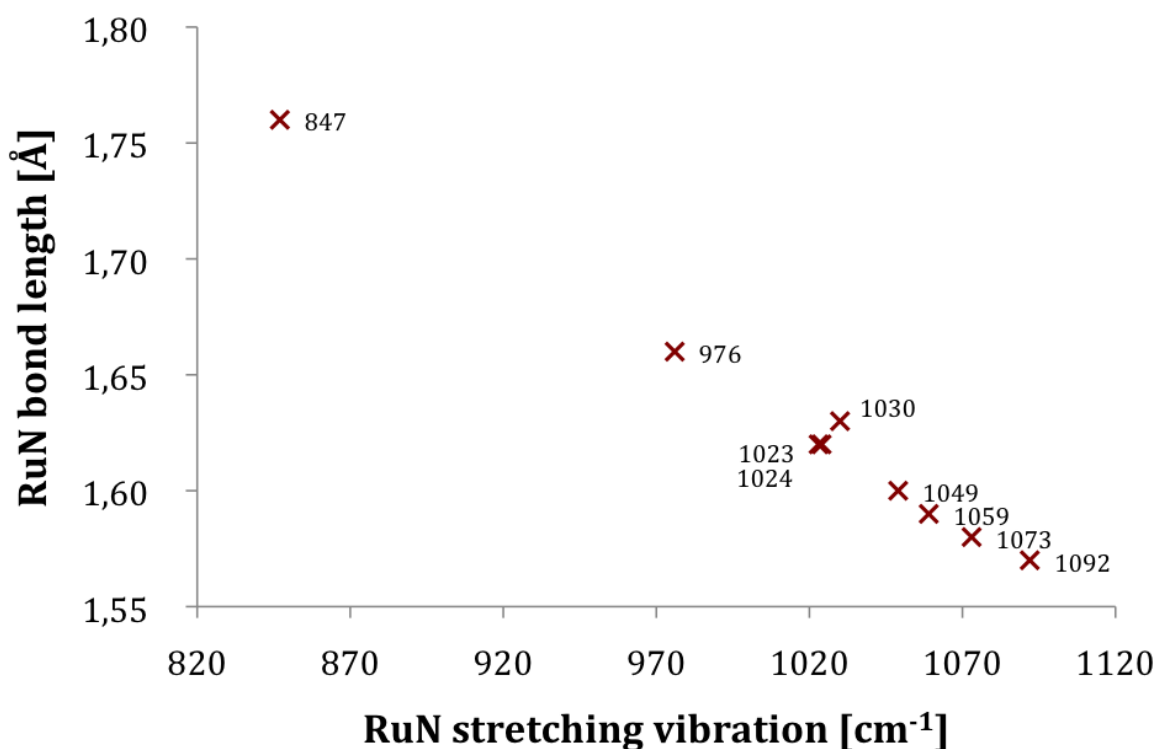
Figure B-4.4: Correlation of Ru≡N stretching vibration *vs.* bond lengths for several terminal ruthenium nitrido complexes reported in the literature compared with complex **5** (976 cm^{-1}, 1.66 Å (average)).[28]

---

[28] a) D. Pawson, W. P. Griffith, *J. Chem. Soc., Dalton Trans.* **1973**, 1315; b) D. Pawson, W. P. Griffith, *Inorg. Nucl. Chem. Lett.* **1974**, *10*, 253; c) F. L. Phillips, A. C. Skapski, *Acta Cryst.* **1975**, *B31*, 2667; d) P. A. Shapley, H. S. Kim, S. R. Wilson, *Organometallics* **1988**, *7*, 928; e) D. Sellmann, M. W. Wemple, W. Donaubauer, F. W. Heinemann, *Inorg. Chem.* **1997**, *36*, 1397; f) M. Magnussen, J. Bendix, *Acta Cryst.* **2003**,
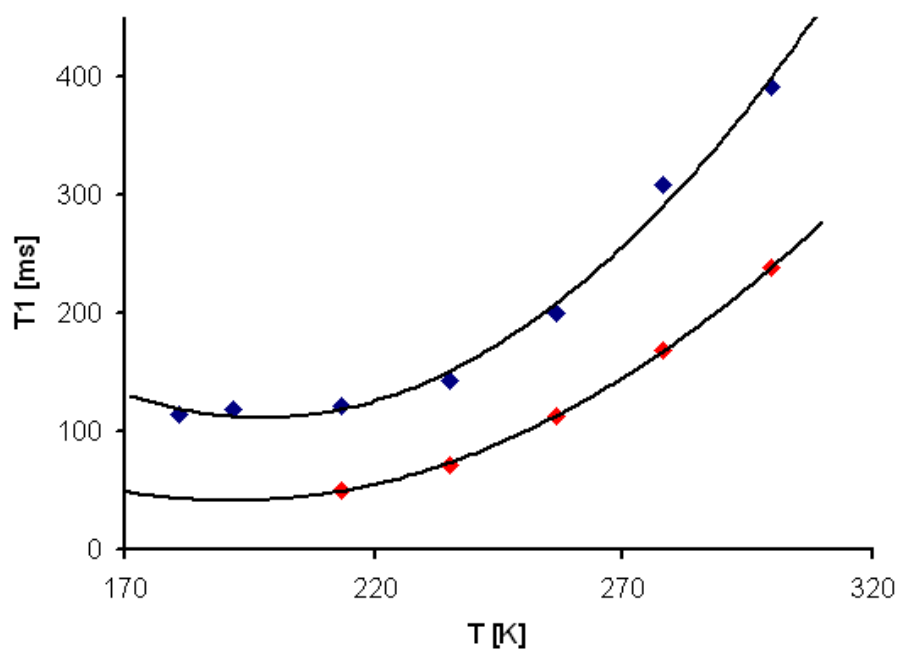
Figure B-4.5: T_1 measurements for the hydride signals of complexes **7** (blue) and **8** (red), respectively (400 MHz).
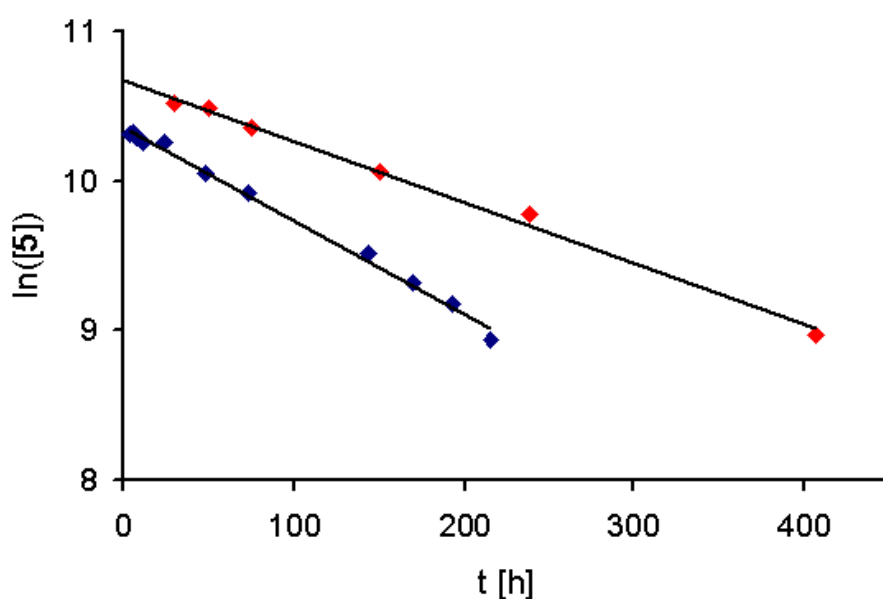
Figure B-4.6: First order kinetic plots for hydrogenolysis of **5** at 298 K in THF with H_2 (blue) and D_2 (red), respectively.

C59, m342; g) G.-S. Fang, J.-S. Huang, N. Zhu, C.-M. Che, *Eur. J. Inorg. Chem.* **2004**, 1341; h) W.-L. Man, T.-M. Tang, T.-W. Wong, T.-C. Lan, M. Chan, W.-Y. Wong, *J. Am. Chem. Soc.* **2004**, *126*, 478; i) A. Walstrom, M. Pink, X. Yang, J. Tomaszewski, M.-H. Baik, K. G. Caulton, *J. Am. Chem. Soc.* **2005**, *127*, 5330; j) J. S. Pap, S. DeBeer George, J. F. Berry, *Angew. Chem. Int. Ed.* **2008**, *47*, 10102; k) A. K. M. Long, R. P. Yu, G. H. Timmer, J. F. Berry, *J. Am. Chem. Soc.* **2010**, *132*, 12228.

4.6 Crystallographic details

General methods

Crystal data and details of the structure determination are presented in Table B-4.1. Suitable single-crystals of **5** and **6** for the X-ray diffraction studies were grown by slow cooling of saturated pentane solutions. The selected crystals were fixed on the top of a glass fiber with perfluorinated ether and transferred into the cold nitrogen flow (Oxford Cryosystems) of the diffractometer. Preliminary examinations and data collection were carried out with an APEX II (Bruker AXS) area detecting system and a rotating anode X-ray source (Bruker AXS, FR591) using graphite-monochromated Mo-K$_\alpha$ radiation (λ = 0.71073 Å). The unit cell parameters were obtained from 9512 (**5**) and 9637 (**6**) reflexes, respectively, by full-matrix least-squares refinements during the scaling procedures.[29] Each crystal was measured with a couple of data sets in rotation scan modus with $\Delta\varphi/\Delta\omega$ = 0.50° (**5**: 5 s per frame, 7383 frames, dx: 60.0 mm and **6**: 20 s per frame, 3495 frames, dx: 60.0 mm). Intensities were integrated and the raw data were corrected for Lorentz, polarization, and, arising from the scaling procedure for latent decay and absorption effects.[30] The structures were solved by a combination of direct methods and difference Fourier syntheses. All non-hydrogen atoms were refined with anisotropic displacement parameters (exceptions see below). Methyl hydrogen atoms were calculated as a part of rigid rotating groups, with d$_{C–H}$ = 0.98 Å and $U_{\mathrm{iso(H)}}$ = 1.5$U_{\mathrm{eq(C)}}$. All other hydrogen atoms were placed in ideal positions and refined using a riding model, with methylene d$_{C–H}$ distances of 0.99 Å, and $U_{\mathrm{iso(H)}}$ = 1.2$U_{\mathrm{eq(C)}}$. Full-matrix least-squares refinements were carried out by minimizing $\Sigma w(F_o^2\text{-}F_c^2)^2$ with the SHELXL-97 weighting scheme[31] and stopped at shift/err < 0.001. The final residual electron density maps showed no remarkable features. Neutral atom scattering factors for all atoms and anomalous dispersion corrections for the non-hydrogen atoms were taken from *International Tables for Crystallography*[32] All calculations were performed with the WINGX system,[33] including the programs DIAMOND,[34] PLATON,[35] SHELXL-97, and SIR92.[36]

---

[29] APEX suite of crystallographic software. APEX 2 Version 2008.4. Bruker AXS Inc., Madison, Wisconsin, USA, **2008**.

[30] SAINT, Version 7.56a and SADABS Version 2008/1. Bruker AXS Inc., Madison, Wisconsin, USA, **2008**.

[31] G. M. Sheldrick, SHELXL-97, University of Göttingen, Göttingen, Germany, **1998**.

[32] International Tables for Crystallography, Vol. C, Tables 6.1.1.4 (pp. 500-502), 4.2.6.8 (pp. 219-222), and 4.2.4.2 (pp. 193-199) (Hrsg.: A. J. C. Wilson), Kluwer Academic Publishers, Dordrecht, The Netherlands, **1992**.

[33] L. J. Farrugia, WINGX (Version 1.70.01 January 2005), *J. Appl. Crystallogr.* **1999**, *32*, 837.

[34] K. Brandenburg,, DIAMOND, Version 3.1d, Crystal Impact GbR, Bonn, Germany, **2006**.

Details: *5*

The nitrogen atom N3 was refined with an isotropic thermal displacement parameter. A disorder over two positions observed for nitride ligand could be resolved and modeled clearly (N2/N3, 0.61(2)/0.39(2)). **6·2(C_4H_8O)**: A disorder over two positions of one of the two solvent molecules C_4H_8O could be resolved and modeled clearly (0.67(1)/0.33(1)).

Crystallographic data (excluding structure factors) for the structures reported in this paper have been deposited with the Cambridge Crystallographic Data Centre as supplementary publication no. CCDC-xxxxxx **(5)** and CCDC-xxxxxx **[6·2(C_4H_8O)]**. Copies of the data can be obtained free of charge on application to CCDC, 12 Union Road, Cambridge CB2 1EZ, UK (fax: (+44)1223-336-033; e-mail: deposit@ccdc.cam.ac.uk).

Table B-4.1: Crystallographic Data for **5** and **6**·2(C_4H_8O).

	5	**6·2(C_4H_8O)**
Formula	$C_{20}H_{44}N_2P_2Ru$	$C_{30}H_{60}N_2O_4P_2Ru$
Fw	475.58	675.81
Color / habit	Blue green / fragment	Red / fragment
Crystal dimensions (mm^3)	$0.25 \times 0.46 \times 0.61$	$0.10 \times 0.25 \times 0.25$
Crystal system	Monoclinic	Monoclinic
Space Group	$P2_1/c$ (no. 14)	$P2_1/c$ (no. 14)
a (Å)	8.4330(3)	8.4996(3)
b (Å)	21.6173(8)	21.0038(7)
c (Å)	13.7382(5)	19.3021(7)
β (°)	107.0112(15)	90.1511(17)
V ($Å^3$)	2394.88(15)	3445.9(2)
Z	4	4
T (K)	123	123
D_{calcd} (g cm^{-3})	1.319	1.303
μ (mm^{-1})	0.794	0.582
F(000)	1008	1440
θ Range (°)	$1.81 - 25.44$	$1.43 - 25.38$

[35] A. L. Spek, PLATON, A Multipurpose Crystallographic Tool, Utrecht University, Utrecht, The Netherlands, **2010**.

[36] A. Altomare, G. Cascarano, C. Giacovazzo, A. Guagliardi, M. C. Burla, G. Polidori, M. Camalli, SIR92, *J. Appl. Crystallogr.* **1994**, *27*, 435.

Index ranges (h, k, l)	±10, ±26, ±16	±10, ±25, ±23
No. of rflns. collected	72830	56334
No. of indep. rflns. / R_{int}	4407 / 0.027	6316 / 0.031
No. of obsd. rflns. [$I_o>2\sigma(I_o)$]	4293	5784
No. of data/restraints/params	4407 / 0 / 238	6316 / 0 / 374
R_1/wR_2 [$I_o>2\sigma(I_o)$][a]	0.0205 / 0.0504	0.0282 / 0.0697
R_1/wR_2 (all data)[a]	0.0211/ 0.0509	0.0317/ 0.0719
GOF (on F^2)[a]	1.077	1.032
Largest diff. peak and hole (e Å^{-3})	+0.99 / -0.69	+0.84 / -0.69

[a] $R_1 = \Sigma(||F_o|-|F_c||)/\Sigma|F_o|$; $wR_2 = \{\Sigma[w(F_o^2-F_c^2)^2]/\Sigma[w(F_o^2)^2]\}^{1/2}$; $GOF = \{\Sigma[w(F_o^2-F_c^2)^2]/(n-p)\}^{1/2}$

4.7 Computational examinations

Methods

DFT calculations were performed on various reaction pathways for the hydrogenolysis of **5** employing the full molecular model of the complex [Ru(N)(PNP)], where PNP = N(CH$_2$CH$_2$P^{t}Bu$_2$)$_2$. Geometry optimizations, analytic harmonic frequency analyses, and intrinsic reaction coordinate (IRC) following calculations were done with the Gaussian 09 program.[37] Unscaled zero-point vibrational energies as well as thermal and entropy corrections were obtained from computed Hessians using the standard procedures implemented in this program and were used to obtain Gibbs free energies, which relate to 298.15 K. We checked the influence of solvent effects using a polarised continuum model (PCM).[38] The results are identical to calculations in the gas phase, which is not surprising considering the uncharged, non-polar nature of the reaction mixture. However, in order to relate quantum chemical results to the reaction/activation free energies, we have to properly

[37] Gaussian 09, Revision **A.02**, M. J. Frisch, G. W. Trucks, H. B. Schlegel, G. E. Scuseria, M. A. Robb, J. R. Cheeseman, G. Scalmani, V. Barone, B. Mennucci, G. A. Petersson, H. Nakatsuji, M. Caricato, X. Li, H. P. Hratchian, A. F. Izmaylov, J. Bloino, G. Zheng, J. L. Sonnenberg, M. Hada, M. Ehara, K. Toyota, R. Fukuda, J. Hasegawa, M. Ishida, T. Nakajima, Y. Honda, O. Kitao, H. Nakai, T. Vreven, J. A. Montgomery, Jr., J. E. Peralta, F. Ogliaro, M. Bearpark, J. J. Heyd, E. Brothers, K. N. Kudin, V. N. Staroverov, R. Kobayashi, J. Normand, K. Raghavachari, A. Rendell, J. C. Burant, S. S. Iyengar, J. Tomasi, M. Cossi, N. Rega, J. M. Millam, M. Klene, J. E. Knox, J. B. Cross, V. Bakken, C. Adamo, J. Jaramillo, R. Gomperts, R. E. Stratmann, O. Yazyev, A. J. Austin, R. Cammi, C. Pomelli, J. W. Ochterski, R. L. Martin, K. Morokuma, V. G. Zakrzewski, G. A. Voth, P. Salvador, J. J. Dannenberg, S. Dapprich, A. D. Daniels, Ö. Farkas, J. B. Foresman, J. V. Ortiz, J. Cioslowski, and D. J. Fox, Gaussian, Inc., Wallingford CT, **2009**.

[38] J. Tomasi, B. Mennucci, and R. Cammi, *Chem. Rev.*, **2005**, 105, 2999.

account for the standard state in solution. Following the clear analysis of Ashcraft et al.,[39] we use 1 mol·L^{-1} as standard reference state in solution (not 0.04 mol·L^{-1}, which would result from the ideal gas standard conditions employed in the thermochemical analysis procedures used within the Gaussian program). Taking account of the standard state concentration change from 0.04 mol·L^{-1} (1 mole per 24.45 litres) ideal gas to 1 mol·L^{-1} ideal solute, the thermodynamic equation relating free energy changes reads

$$\Delta G^{\circ} = \Delta G + RT \, \ln \frac{Q^{\circ}}{Q},$$

where the open circle represents the standard state in solution and Q is the reaction quotient expressing the standard-state concentrations of all reactants and products. In a reaction involving a change in particle count (e.g., A + B → C; with [X]° = (1/24.45) mol·L^{-1} and [X] = 1 mol·L^{-1}), this leads to the expression

$$\Delta G^{\circ} = \Delta G + RT \, \ln \left(\frac{\frac{[C]^{\circ}}{[A]^{\circ}[B]^{\circ}}}{\frac{[C]}{[A][B]}} \right) = \Delta G - RT \, \ln 24.45.$$

At 298.15 K, the correction factor is 1.89 kcal·mol^{-1}. Correspondingly, we subtracted 1.89 kcal·mol^{-1} from free energy differences computed for steps lowering the number of particles involved (e.g., **5** + H$_2$ → **I1**) or added 1.89 kcal·mol^{-1} for reverse cases (e.g., **I6** → **I7** + NH$_3$). Relative free energies of minima and transition states before and after standard state corrections are given in Table B-4.6.

Calculations on the complete set of reaction pathways reported below were performed using the gradient-corrected PBEPBE functional[40] in combination with the def2-SVP[41] double-ζ valence basis set for all atoms. In these calculations we made use of the density fitting approximation[42,43] (def2-SVPfit basis). The 28 core electrons of ruthenium were replaced by the quasi-relativistic effective core potential def2-ECP.[44] This level of DFT is dubbed PBE/def2-SVP(PP) in the following. To assess the accuracy that can be expected for the present class of systems we performed calibration calculations for selected reaction steps based on a smaller molecular model [RuN(PNP′)], in which we replaced the ^{t}Bu groups of the PNP ligand in the ruthenium complexes by H atoms. CCSD(T)[45] reference calculations were

[39] R. W. Ashcraft, S. Raman, W. H. Green, *J. Phys. Chem. B* **2007**, *111*, 11968.

[40] J. P. Perdew, K. Burke, M. Ernzerhof, *Phys. Rev. Lett.* **1996**, *77*, 3865.

[41] F. Weigend and R. Ahlrichs, *Phys. Chem. Chem. Phys.*, **2005**, *7*, 3297.

[42] B. I. Dunlap, *J. Mol. Struct. (Theochem)*, **2000**, *529*, 37.

[43] F. Weigend, R. Ahlrichs, *Phys. Chem. Chem. Phys.*, **2005**, *7*, 3297.

[44] D. Andrae, U. Häußermann, M. Dolg, H. Stoll, H. Preuss, *Theor. Chim. Acta* **1990**, *77*, 123.

[45] K. Raghavachari, G. W. Trucks, J. A. Pople, M. Head-Gordon, *Chem. Phys. Lett.* **1989**, *157*, 479.

performed as single points on the PBE/def2-SVP(PP) geometries with the MOLPRO[46] program package. In these calculations we used Dunning's correlation consistent aug-cc-pVnZ (n = D, T, Q) basis sets[47] on H, C, N, P, and the corresponding aug-cc-pVnZ-PP basis set developed by Peterson et *al*.[48] together with the associated quasi-relativistic effective core potential[48] for Ru; these basis sets are denoted aVnZ in the following. The energies were extrapolated to the complete basis set (CBS) limit using two schemes. Truhlar's formula[49] was used for extrapolation of the double-ζ and triple-ζ results (CBS(D,T)). Note, however, that in his original work, Truhlar derived this scaled extrapolation scheme for the non-augmented cc-pVnZ (n = D, T) series and in systems, which do not contain transition metal atoms. The procedure of Halkier et al.[50] was employed for extrapolation of the triple-ζ and quadruple-ζ correlation energies (CBS(T,Q)); the Hartree–Fock energies corresponding to the largest basis set, i.e., the aVQZ energies, were taken as reference energies in this case. The CCSD(T)/aVnZ Gibbs free energies correspond to single points at the PBE/def2-SVP(PP) geometries, adjusted by standard state corrections as above. Thermal and entropy contributions were taken from the PBE/def2-SVP(PP) results.

Against the extrapolated CCSD(T)/CBS results we also tested the performance of the M06 hybrid functional[51] for the same set of systems. Compared to a number of other promising density functionals, a superior performance was found for M06 in a recent benchmark study[52] on model reactions of a Ru-based Grubbs olefin metathesis catalyst.[53] We employed

[46] MOLPRO, version 2010.1, a package of ab initio programs written by H.-J. Werner, P. J. Knowles, F. R. Manby, M. Schütz, P. Celani, G. Knizia, T. Korona, R. Lindh, A. Mitrushenkov, G. Rauhut, T. B. Adler, R. D. Amos, A. Bernhardsson, A. Berning, D. L. Cooper, M. J. O. Deegan, A. J. Dobbyn, F. Eckert, E. Goll, C. Hampel, A. Hesselmann, G. Hetzer, T. Hrenar, G. Jansen, C. Köppl, Y. Liu, A. W. Lloyd, R. A. Mata, A. J. May, S. J. McNicholas, W. Meyer, M. E. Mura, A. Nicklaß, P. Palmieri, K. Pflüger, R. Pitzer, M. Reiher, T. Shiozaki, H. Stoll, A. J. Stone, R. Tarroni, T. Thorsteinsson, M. Wang, A. Wolf, Cardiff, UK, 2010, see http://www.molpro.net.

[47] a) T. H. Dunning, Jr., *J. Chem. Phys.* **1989**, *90*, 1007; b) D. E. Woon, T. H. Dunning, Jr., *J. Chem. Phys.* **1993**, *98*, 1358.

[48] K. A. Peterson, D. Figgen, M. Dolg, H. Stoll, *J. Chem. Phys.* **2007**, *126*, 124101.

[49] D. G. Truhlar, *Chem. Phys. Lett.*, **1998**, *294*, 45.

[50] A. Halkier, T. Helgaker, P. Jørgensen, W. Klopper, H. Koch, J. Olsen, A. K. Wilson, *Chem. Phys. Lett.*, **1998**, *286* (3–4), 243.

[51] Y. Zhao, D. G. Truhlar, *Theor. Chem. Acc.* **2008**, *120*, 215.

[52] Zhao, Y.; Truhlar, D. G. *J. Chem. Theory Comput.* **2009**, *5,* 324.

[53] Zhao, Y.; Truhlar, D. G. *Theor. Chem. Acc.* **2008**, *120*, 215.

the same basis set recommended in this study, e.g., M3GS,[54] which combines the 6-311+G(2df,2p) basis set for H, C and N,[55,56] 6-311+G(3d2f) for P,[57,58] as well as the quasi-relativistic effective core potential/basis set combination CEP+d3f for Ru.[59,60,61] We performed both, single points based on PBE/def2-SVP(PP) geometries as well as full M06/M3GS optimisations.

The natural population analysis (NPA) was performed using the NBO program version 3.1[62] within the Gaussian 09 software.

Computational Results

Benchmark calculations on the model system [Ru(N)(PNP')] (5'), PNP' = N(CH₂CH₂PH₂)₂. The results of the benchmark calculations with the model system [Ru(N)(PNP')] are given in Table B-4.2. In all CCSD(T) calculations, the T_1 diagnostic does not exceed a value of 0.03, which indicates that the underlying single-reference ansatz is appropriate.[63] According to the deviations in relative energies among the different basis sets employed, the CCSD(T) results are well-converged with the aVTZ basis set. Both extrapolation schemes yield CCSD(T) basis set limit values in very good agreement.

[54] Lynch, B. J.; Zhao, Y.; Truhlar, D. G. *J. Phys. Chem. A* **2003**, *107*, 1384.

[55] R. Krishnan, J. S. Binkley, R. Seeger, J.A. Pople, *J. Chem. Phys.* **1980**, *72*, 650.

[56] M. J. Frisch, J. A. Pople and J. S. Binkley, *J. Chem. Phys.* **1984**, *80*, 3265.

[57] A.D. McLean and G.S. Chandler *J. Chem. Phys.* **1980**, *72*, 5639.

[58] T. Clark, J. Chandrasekhar, G.W. Spitznagel, P.V.R. Schleyer, *J. Comp. Chem.* **1983**, *4*, 294.

[59] W. J. Stevens, M. Krauss, H. Basch, P. G. Jasien, *Can. J. Chem.* **1992**, *70*, 612.

[60] N. Schultz, Y. Zhao, D. G. Truhlar, *J. Phys. Chem. A* **2005**, *109*, 4388.

[61] S. R. Langhoff, L. G. M. Pettersson, C. W. Bauschlicher, Jr. *J. Chem. Phys.* **1987**, *86*, 268.

[62] NBO Version 3.1, E. D. Glendening, A. E. Reed, J. E. Carpenter, and F. Weinhold.

[63] T. J. Lee, P. R. Taylor, *Int. J. Quant. Chem.*, **1989**, *36*, 199.

Table B-4.2: CCSD(T)/ aVnZ//PBE/SVP (n = D,T,Q) results for selected stationary points of the nitride hydrogenolysis path based on the smaller molecular model complex [Ru(N)(PNP′)]; Gibbs free energy differences ΔG°_{298} relative to **5′** (including standard state corrections, *vide supra*).

	aVDZ	aVTZ	aVQZ	CBS(D,T)	CBS(T,Q)
5′	0.0	0.0	0.0	0.0	**0.0**
TS$_{5′\text{-}I1′}$	23.9	25.1	25.0	25.2	**25.0**
I1′	-3.9	-2.5	-2.6	-2.1	**-2.5**
TS$_{I1′\text{-}I2′}$	19.4	20.2	20.1	20.2	**20.0**
I2′	6.4	5.6	5.2	4.8	**4.9**
I7′	-37.4	-38.1	-38.8	-39.5	**-39.4**
7′	-55.8	-55.3	-55.5	-56.5	**-55.9**
8′	-47.5	-47.7	-48.3	-49.0	**-48.9**

Table B-4.3: Deviations[a] of DFT results from CCSD(T)/CBS(T,Q) reference energies for relative Gibbs free energies of the intermediates and transition states.

	$\Delta\Delta G^\circ_{298}$		
Method	PBE/def2-SVP(PP)	M06/M3GS//PBE[b]	M06/M3GS
5′	0.0	0.0	0.0
TS$_{5′\text{-}I1′}$	2.7	0.1	-0.9
I1′	2.3	-2.1	-2.9
TS$_{I1′\text{-}I2′}$	1.4	-2.7	-4.6
I2′	-1.2	0.3	-2.0
7′	-1.2	-7.0	-7.9
8′	0.2	-5.1	-4.8

[a] Obtained as ΔG°_{298}(CCSD(T)/CBS) - ΔG°_{298}(method);

[b] Single point calculations on PBE/def2-SVP(PP) optimized structures.

The PBE/def2-SVP(PP) results show the smallest deviations from the CCSD(T)/CBS(T,Q) reference data, which validates this level of DFT as pleasingly accurate and numerically efficient for the present class of systems. The largest error is below 3 kcal·mol^{-1} and is observed for the first transition state **TS$_{5′\text{-}I1′}$**. As for the second **TS$_{I1′\text{-}I2′}$**, the deviation is

positive, which indicates some "overstabilization" of the transition state. This behavior is well-known for GGA functionals.[64]

The M06 functional with a larger basis set shows somewhat poorer performance. The largest deviation is observed for structure **7′** (-7.0 kcal·mol^{-1}). Full optimization at the M06/M3GS level even slightly increases this error to -7.9 kcal·mol^{-1}.

We conclude that the computationally inexpensive PBE/def2-SVP(PP) level provides results of favourable accuracy with respect to CCSD(T) at the CBS limit. The calculations of the full system were performed using this method.

*Calculations on the full system [Ru(N)(PNP)] (**5**), PNP = N(CH$_2$CH$_2$P^{t}Bu$_2$)$_2$.* In the course of the computations, we found two minima **5** and **5a**, corresponding to the complex [Ru(N)(PNP)] shown in Figure B-4.7. Structure **5** is the lowest-energy minimum, while **5a** corresponds to a local minimum lying 1.7 kcal·mol^{-1} higher in energy than **5**. We located the transition state **TS$_{5\text{-}5a}$** connecting these two minima at 2.9 kcal·mol^{-1} above **5**. The geometry of **5a** is close to square-planar (C$_s$ minimum, close to local C$_{2v}$ symmetry), while **5** relaxes to a distorted geometry (C$_1$ minimum, close to local C$_s$ symmetry). Optimized geometries as well as selected structural parameters of **5** and **5a** are shown in Figure B-4.7 and Table B-4.4 together with the X-ray data. The computed structural parameters of **5** are in good agreement with one of the two conformers found by X-ray diffraction, particularly reproducing the N-Ru-N bending sifficiently well. **5a** shows some discrepancies with the second experimentally derived conformer related to the nitrido position. However, the flat computed N-Ru-N angle bending potential is in the same range as solid state packing forces. Thus, the comparison of the experimental and computational structural data leads us to the conclusion that the PBE/def2-SVP(PP) level of DFT provides realistic geometries for the ruthenium nitride complex [Ru(N)(PNP)].

---

[64] See for example: W. Koch, M. C. Holthausen, *A Chemist's Guide to Density Functional Theory*, Wiley-VCH, Weinheim, **2000**.

5   **5a**
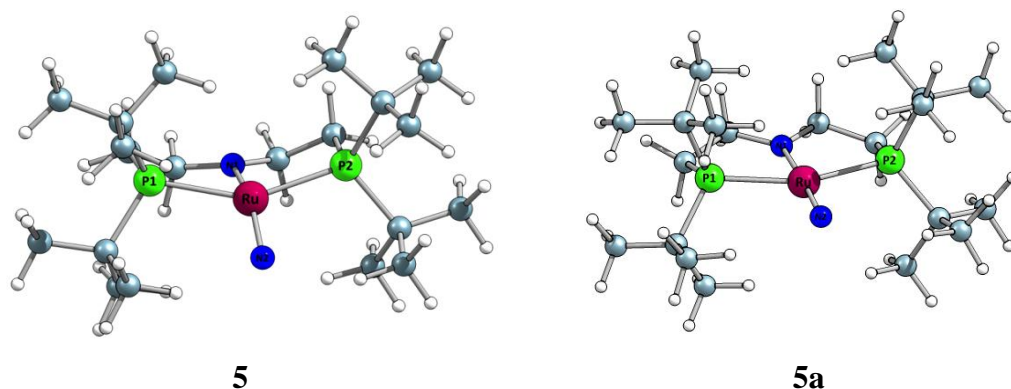
Figure B-4.7: Optimized geometries of the isomers **5** and **5a** of the ruthenium nitride complex [Ru(N)(PNP)].

Table B-4.4: Experimental (X-ray) and optimized (PBE/def2-SVP(PP)) geometries of **5** and **5a**; N_{PNP} – nitrogen of pincer ligand, N – nitrido ligand. Bond lengths are given in Å, angles in degrees

	Exp.	PBE	
	5	**5**	**5a**
Ru-P1	2.3796(4)	2.384	2.378
Ru-P2	2.3724(4)	2.384	2.378
Ru-N_{PNP}	2.051(1)	2.047	2.107
Ru-N	1.688(3); 1.628(4)	1.641	1.657
N_{PNP}-Ru-N	147.3(2); 165.6(3)	145.50	173.45
N_{PNP}-Ru-P1	80.64(4)	81.87	80.64
N_{PNP}-Ru-P2	80.93(4)	81.76	80.64
N-Ru-P1	102.6(1); 100.75	103.74	99.79
N-Ru-P2	101.5(1); 101.06	103.79	99.79
P1-Ru-N_{PNP}-P2	164.10(2)	155.2	171.4
N_{PNP}-Ru-P1-N	146.8(1); 165.4(2)	145.3	173.4

Initial phase of the hydrogenation reactivity of 5.
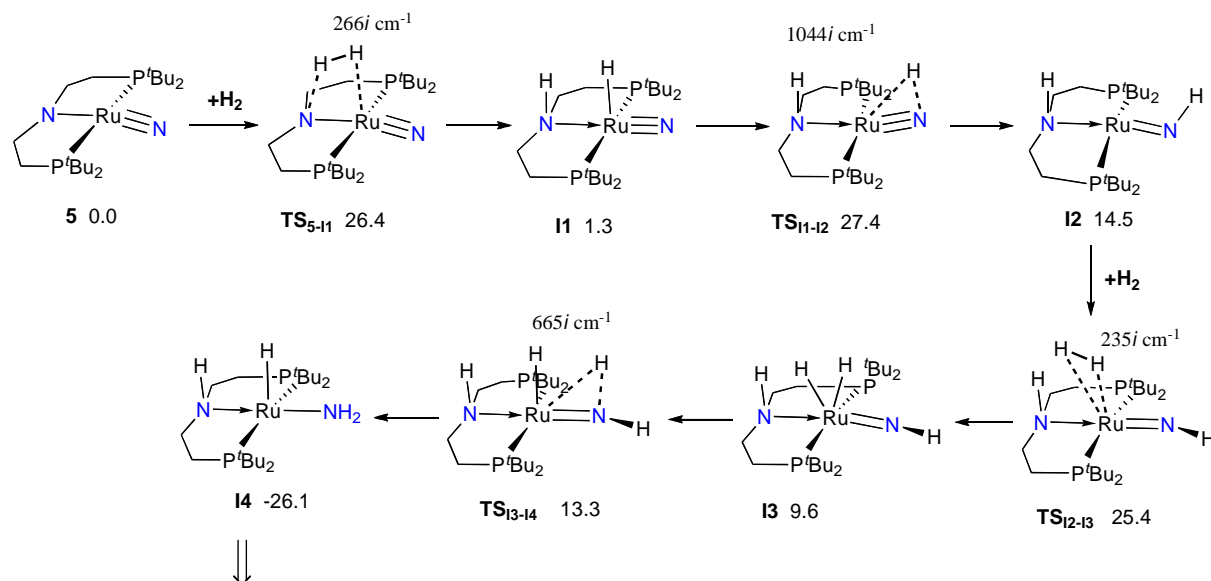
Scheme B-4.2: Part 1 of the nitrido hydrogenolysis of **5** according to DFT calculations; PBE/def2-SVP(PP) relative Gibbs free energies in kcal mol^{-1} after standard state correction.

The computed, energetically most favorable reaction path for the initial hydrogenation reactivity of **5** leading to intermediate **I4** is shown in Scheme B-4.2 (it corresponds to the respective reaction sequence as discussed in the main paper; Scheme B-4.1). Subsequent reaction pathways commencing with **I4** are discussed further below. Commencing our discussion of alternative routes for the initial H$_2$ activation step, we first note that the product of a potential oxidative addition step, **B1**, is substantially higher in energy than **I1**. Further, despite of careful scans of this region of the singlet potential energy surface, we were unable to localize a transition state connecting **B1** with **5**.

Addition of H$_2$ to the terminal nitrido ligand to form **C1** would represent a thermodynamically highly favorable path (ΔG_R = -25.9 kcal mol^{-1}), but the corresponding barrier connected with **TS$_{5\text{-}C1}$** ($\Delta G^{\ddagger}$ = 38.7 kcal mol^{-1}) is preclusively high.
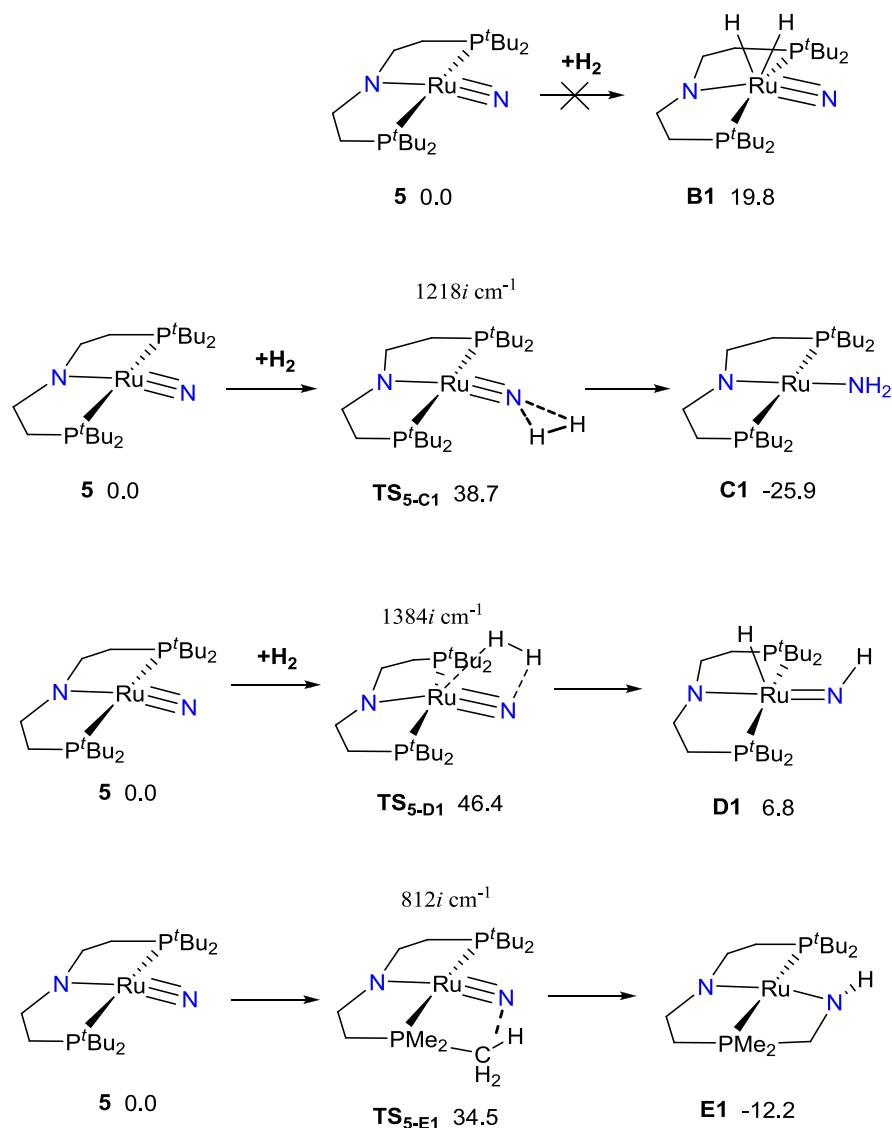
Scheme B-4.3: Alternative pathways for the initial phase of the hydrogenation reactivity of **5**; PBE/def2-SVP(PP) relative Gibbs free energies in kcal mol^{-1} after standard state correction.

Quite interestingly, also the alternative heterolytic H$_2$ activation by addition across the Ru–nitrido bond cannot compete with the reaction path via **TS$_{5\text{-}I1}$** in terms of reaction kinetics ($\Delta G^{\ddagger}$ = 46.4 kcal mol^{-1}). We have analysed NPA partial charges for the reactant **5** and for the transition states of the heterolytic H–H activation across the Ru–N$_{PNP}$ and Ru≡N bonds in **TS$_{5\text{-}I1}$** and **TS$_{5\text{-}E1}$**, respectively (Scheme B-4.4). Clearly, heterolytic splitting is accompanied by a substantial increase of electron density on the N atom involved in the activation, while the corresponding hydrogen atom becomes more positively charged. However, N$_{PNP}$ already in **5** represents the better Lewis base compared to the nitrido N atom and the charge separation of the H$_2$ fragment in transition state **TS$_{5\text{-}I1}$** is less pronounced compared to that in **TS$_{5\text{-}E1}$**. This obviously goes hand in hand with a significantly lower barrier for the former transition state.
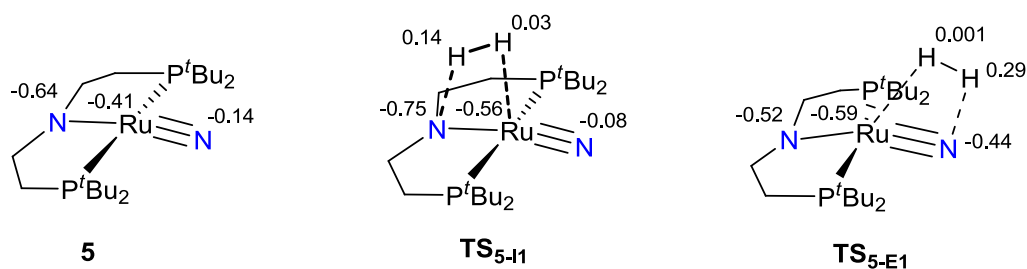
Scheme B-4.4: NPA charges for the reactant **5** and transition states of the heterolytic H–H activation across the Ru–N$_{PNP}$ and Ru≡N bonds in **TS$_{5-I1}$** and **TS$_{5-E1}$**, respectively.

As Chirik *et al.* very recently reported an example for the intramolecular C–H activation of the benzylic positions of the aryl substituents in the putative cobalt nitrido complex[65] we also examined the corresponding intramolecular C–H bond activation of one of the ^{t}Bu-substituents adjacent to the nitrido ligand for the present system. It is quite interesting to note that the resulting intermediate **D1** is actually more stable than **I1** but with an activation barrier of $\Delta G^{\ddagger} = 34.5$ kcal·mol^{-1} via **TS$_{5-D1}$** this path is clearly disfavored kinetically with respect to the path via **TS$_{5-I1}$**.

To conclude this section, we have also examined potential triplet pathways for the initial hydrogenation of **5** (Scheme B-4.5). On the free energy surface, the triplet state of **5** is 18.4 kcal mol^{-1} higher in energy than the singlet state. The corresponding lowest-energy pathway proceeds via the heterolytic H$_2$ activation across the Ru≡N bond. With $\Delta G^{\ddagger} = 30.7$ kcal mol^{-1}, however, also this path cannot compete with the heterolytic H$_2$ activation across the Ru–N$_{PNP}$ bond on the singlet surface. All other triplet paths also lie much higher in energy so that we feel safe to exclude contributions to the experimentally observed reactivity.

---

[65] C. C. Hojilla Atienza, A. C. Bowman, E. Lobkovsky, P. J. Chirik, *J. Am. Chem. Soc.* **2010**, *132*, 16343.
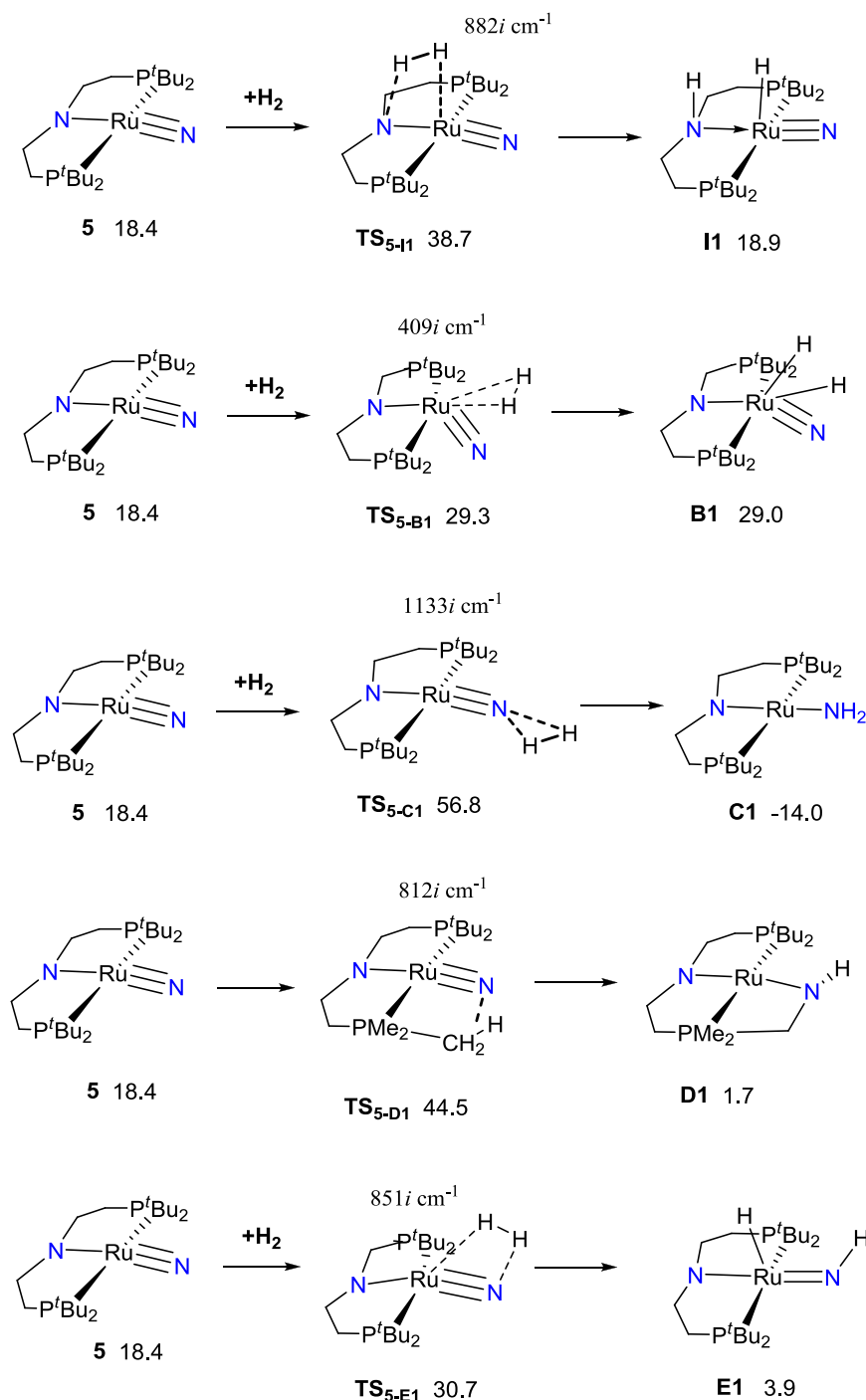
Scheme B-4.5: The hydrogenation pathways of ruthenium nitride complex **5** (triplet surface); PBE/def2-SVP(PP) relative Gibbs free energies in kcal mol^{-1} after standard state correction.

*Reaction pathways commencing with intermediate **I4***. Starting from **I4**, we identified three routes (Scheme B-4.6) among which coordination of a third H_2 molecule initiates the lowest free energy path, i.e., **I4→I5→I6→I7→7(8)**. The other two subroutes have somewhat higher free energy barriers, but as all of them are substantially lower than the initial barrier **TS$_{5-I1}$**, it is likely that all these paths contribute to product formation under the experimental conditions.
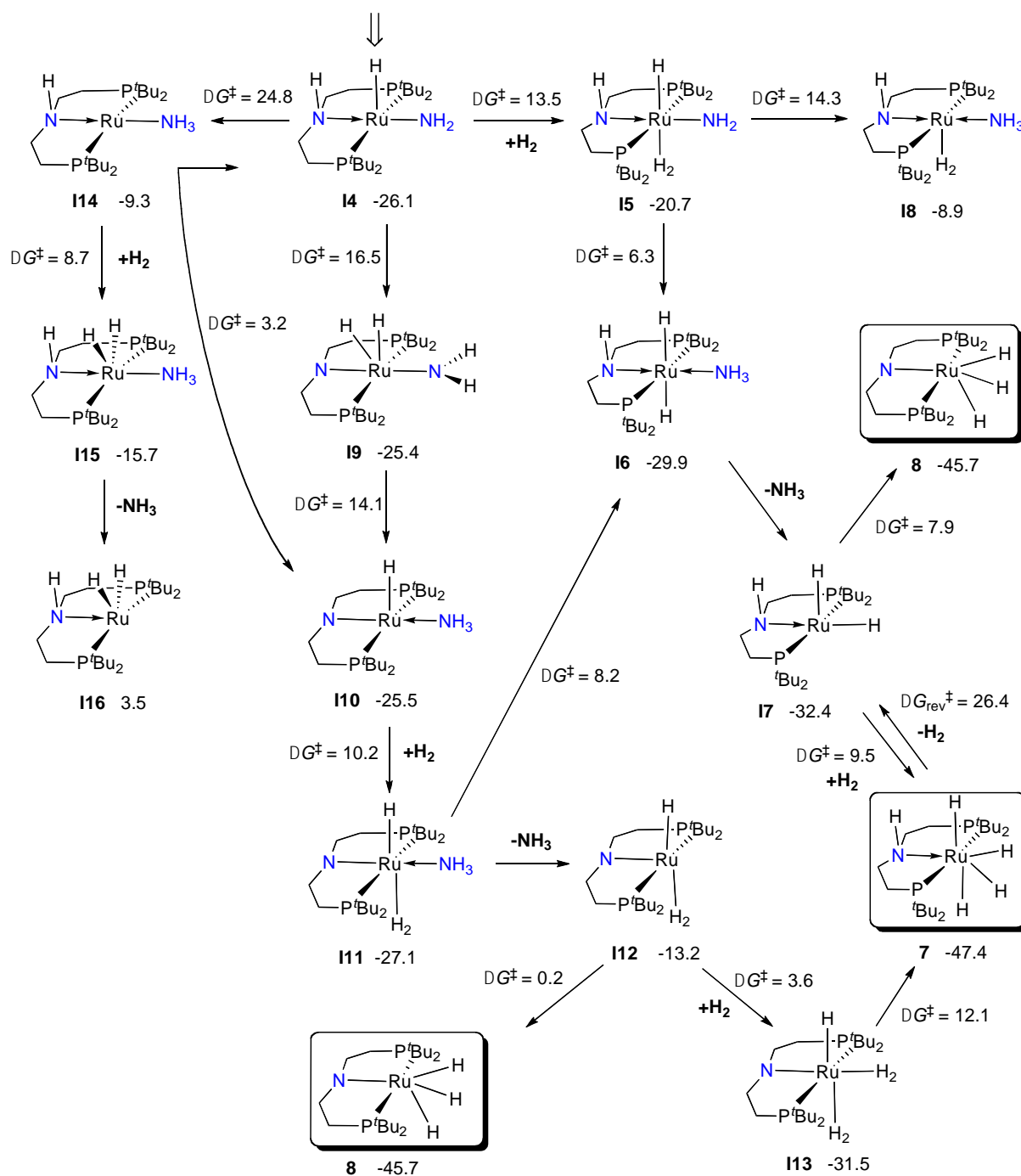
Scheme B-4.6: Part 2 of the nitrido hydrogenolysis of **5**; PBE/def2-SVP(PP) results after standard state corrections. For minima, relative Gibbs free energies are given in kcal mol^{-1} with respect to **5**. For transition states, the activation free energy barriers for the individual reaction steps are given.

Polyhydride complexes 7 and 8: dihydrido versus dihydrogen structures. According to our calculated DFT geometries, both polyhydride structures **7** and **8** bear two H-ligands with a relatively short distance, respectively, and therefore qualify for classification as "compressed" hydride complexes (d_{HH} = 1.3 - 1.6 Å).[66]

7   **8**
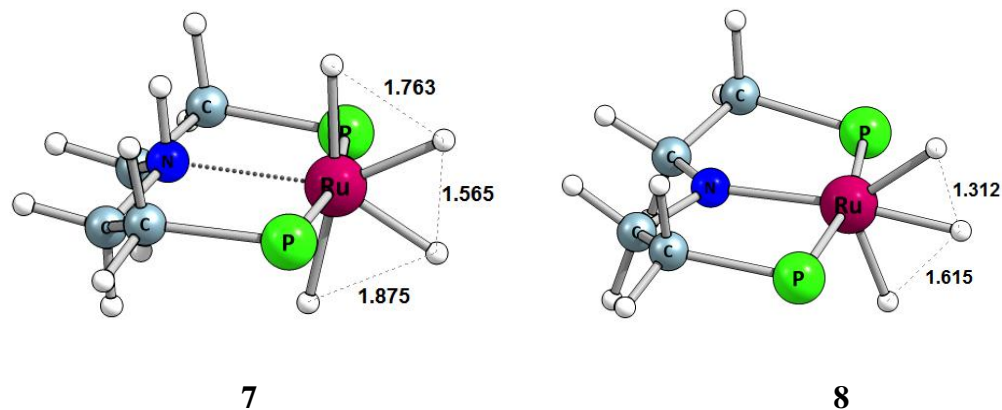
Figure B-4.8: Optimized geometries of the polyhydride complexes **7** and **8**.

KIE calculations. Classical kinetic isotope effects (KIE) were estimated for several transition states based on the respective computed free energy barrier differences (Table B-4.4).[67] The transmission coefficients for tunneling through the potential barrier were estimated using analytic approximation by Truhlar et al.[68] In all cases, however, we obtained transmission coefficients very close to unity and tunneling was not considered further for the computed KIEs. The results are summarized in Table B-4.5.

Table B-4.5: Selected free energy barriers of the hydrogenation reaction with H_2 and D_2.

Molecule	ν_{imag}, cm^{-1}	$\Delta\Delta G^{\neq}_{298}$(H/D), cal·mol^{-1}	k_H/k_D
TS$_{5-I1}$	266i	-10.0	1.02
TS$_{I1-I2}$	1044i	-426.1	1.92
TS$_{I2-I3}$	235i	-135.5	1.23
TS$_{I3-I4}$	665i	-143.1	1.25
TS$_{I4-I5}$	351i	-212.1	1.38
TS$_{I5-I6}$	952i	-436.1	1.95

[66] a) F. Maseras, A. Lledós, E. Clot, O. Eisenstein, *Chem. Rev.* **2000**, *100*, 601. b) G. J. Kubas, *Chem. Rev.* **2007**, *107*, 4152.

[67] B. C. Garrett, D. G. Truhlar, *J. Am. Chem. Soc.* **1980**, *102*, 2559.

[68] R. T. Skodje, D. G. Truhlar, *J. Phys. Chem.* **1981**, *85*, 624.

B Results and discussion

Compilation of computed relative energies.

Table B-4.6: Relative electronic energies (ΔE_e), enthalpies (ΔH°_{298}) and Gibbs free energies (with and without standard state correction, ΔG°_{298} and ΔG_{298}, respectively) of formation of the reactant, intermediates and products of the hydrogenation reaction at the PBE/def2-SVP(PP) level.

Molecule	ΔE_e, kcal·mol^{-1}	ΔH°_{298}, kcal·mol^{-1}	ΔG°_{298}, kcal·mol^{-1}	ΔG_{298}, kcal·mol^{-1}
		Singlet energy surface		
5	0.0	0.0	0	0
TS$_{5-5a}$	2.6	1.9	2.9	2.9
5a	2.5	2.3	1.7	1.7
TS$_{5-I1}$	19.2	19.8	26.4	28.3
I1	-10.2	-5.5	1.3	3.2
TS$_{I1-I2}$	18.3	21.1	27.4	29.3
I2	1.8	7.7	14.5	16.4
TS$_{I2-I3}$	6.4	12.5	25.4	29.2
I3	-13.2	-4.8	9.6	13.4
TS$_{I3-I4}$	-9.6	-1.8	13.3	17.1
I4	-52.5	-41.1	-26.1	-22.3
TS$_{I4-I5}$	-45.4	-33.7	-12.6	-6.9
I5	-55.9	-42.5	-20.7	-15
TS$_{I5-I6}$	-47.6	-35.8	-14.4	-8.7
I6	-68.2	-52.5	-29.9	-24.2
I7	-57.2	-44.0	-32.4	-28.6
TS$_{I7-7}$	-56.9	-41.8	-22.9	-17.2
7	-82.1	-66.4	-47.4	-41.7
TS$_{I7-8}$	-45.2	-35.7	-24.5	-20.7
8	-68.6	-57.7	-45.7	-41.9
TS$_{I4-I9}$	-32.3	-24.7	-9.6	-5.8
I9	-49.7	-40.5	-25.4	-21.6
TS$_{I9-I10}$	-33.1	-25.8	-11.3	-7.5
I10	-51.2	-40.0	-25.5	-21.7
TS$_{I10-I11}$	-47.0	-35.8	-15.3	-9.6
I11	-61.5	-48.7	-27.1	-21.4

I12	-35.3	-24.7	-13.2	-9.4
TS$_{I12\text{-}I13}$	-36.2	-25.2	-9.6	-3.9
I13	-63.1	-49.9	-31.5	-25.8
TS$_{I13\text{-}7}$	-49.8	-38.1	-19.4	-13.7
TS$_{I11\text{-}I6}$	-52.8	-41.3	-18.9	-13.2
TS$_{I4\text{-}I14}$	-26.3	-16.5	-1.3	2.5
I14	-37.7	-24.3	-9.3	-5.5
TS$_{I14\text{-}I10}$	-28.2	-19.4	-6.1	-2.3
TS$_{I14\text{-}I15}$	-34.8	-21.3	-0.6	5.1
I15	-55.1	-39.3	-15.7	-10
I16	-22.5	-8.3	3.5	7.3

		Alternative pathways		

B1	11.6	12.9	19.8	21.7
TS$_{5\text{–}C1}$	31.9	31.8	38.7	40.6
C1	-40.6	-34.2	-25.9	-24
TS$_{5\text{-}D1}$	38.3	35.3	34.5	36.4
D1	-13.3	-12.7	-12.2	-10.3
TS$_{5\text{-}E1}$	37.3	38.1	46.4	48.3
E1	-4.7	-1.0	6.8	8.7

		Triplet energy surface		

5	20.0	19.3	18.4	18.4
TS$_{5\text{–}B1}$	24.9	24.5	29.3	31.2
B1	20.4	22.0	29.0	30.9
TS$_{5\text{–}C1}$	53.3	51.6	56.8	58.7
C1	-24.8	-19.6	-14.0	-12.1
TS$_{5\text{-}D1}$	49.4	46.1	44.5	46.4
D1	2.4	2.3	1.7	3.6
TS$_{5\text{-}E1}$	24.7	24.4	30.7	32.6
E1	-4.4	-1.7	3.9	5.8

5 Learning from the neighbours: improving homogeneous catalysts with functional ligands motivated by heterogeneous and bio-catalysis

This chapter originated the following micro review:

B. Askevold, H. W. Roesky, S. Schneider

ChemCatChem **2012**, *4*, 307.
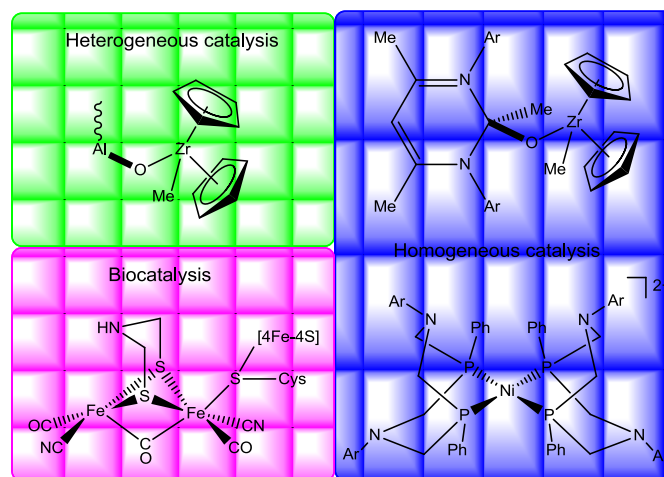
5.1 Introduction

The future shortage of fossil resources requires enhanced efficiency for industrial processes. Catalysis will be a key field for the establishment of novel sustainable feedstock cycles for chemical synthesis.[1,2,3] In addition, reactions associated with conversion and storage of regenerative energy, such as photochemical water splitting or chemical hydrogen storage, demand new reliable and abundant catalysts.[4,5] Approx. 80 % of all industrially synthesized chemicals, worth about 10^{12} US-$ (as of 2007), are presently produced by application of catalysis for one or more reaction steps.[6] Heterogeneous catalysis still represents the lion's share (about 80 % in 2007). The advantages of heterogeneous catalysis, such as high thermal catalyst stability and easy product isolation, are obvious.[7] However, the multiphasic nature of heterogeneous catalysis and the structural and electronic complexity of catalyst surfaces generally render heterogeneous catalysis difficult to study. Therefore, despite tremendous success in creating a higher level of mechanistic understanding catalyst development and improvement remains highly empirical.

This microreview focuses on selected examples for efficient homogeneous catalysis based on functional ligands which were inspired by heterogeneous and metalloenzyme catalysis. The strategies discussed here are not exactly new and cooperative catalysis by the action of either multiple metal centers or metal centers and cooperating ligands was pointed out by many authors as a useful concept to improve catalyst performance.[8] By covering parts of our

[1] H. Arakawa, M. Aresta, J. N. Armor, M. A. Barteau, E. J. Beckman, A. T. Bell, J. E. Bercaw, C. Creutz, E. Dinjus, D. A. Dixon, K. Domen, D. L. DuBois, J. Eckert, E. Fujita, D. H. Gibson, W. A. Goddard, D. W. Goodman, J. Keller, G. J. Kubas, H. H. Kung, J. E. Lyons, L. E. Manzer, T. J. Marks, K. Morokuma, K. M. Nicholas, R. Periana, L. Que, J. Rostrup-Nielson, W. M. H. Sachtler, L. D. Schmidt, A. Sen, G. A. Somorjai, P. C. Stair, B. R. Stults, W. Tumas, *Chem Rev.* **2001**, *101*, 953.

[2] G. W. Huber, S. Iborra, A. Corma, *Chem. Rev.* **2006**, *106*, 4044.

[3] S. R. Collinson, W. Thielemans, *Coord. Chem. Rev.* **2010**, *254*, 1854.

[4] W. E. Piers, *Organometallics*, **2011**, *30*, 13.

[5] N. S. Lewis, D. G. Nocera, *Proc. Nat. Acad. Sci.* **2006**, *103*, 15729.

[6] *Catalysis from A to Z*, Eds. B. Cornis, W. A. Herrmann, M. Muhler, C.-H. Wong, 3rd ed., 2007, Wiley-VCH, Weinheim.

[7] W. A. Herrmann, B. Cornils, *Angew. Chem.* **1997**, *109*, 1074.

[8] Selected reviews on cooperative catalysis: a) E. N. Jacobsen, *Acc. Chem. Res.* **2000**, *33*, 421; b) R. Noyori, T. Ohkuma, *Angew. Chem.* **2001**, *113*, 40; *Angew. Chem. Int. Ed.* **2001**, *40*, 40; c) G. J. Rowlands, *Tetrahedron* **2001**, *57*, 1865; d) M. Shibasaki, N. Yoshikawa, *Chem. Rev.* **2002**, *102*, 2187-2210; e) R. Pascal, *Eur. J. Inorg. Chem.* **2003**, 1813; f) J.-A. Ma, D. Cahard, *Angew. Chem.* **2004**, *116*, 4666-4683; *Angew. Chem. Int. Ed.* **2004**, *43*, 4566; g) Y. J. Park, J.-W. Park, C.-H. Jun, *Acc. Chem. Res.* **2008**, *41*, 222; h) D. H. Paull, C. J.

own recent results and related work, here we want to emphasize some basic principles associated with catalyst design from a more ,inorganic perspective' including topics, such as polymerization of organic and inorganic substrates, and applications relevant to energy conversion and storage.

5.2 Inspiration from heterogeneous catalysis: homogeneous polymerization catalysts with lewis acidic co-ligands

Site isolation represents an important principle for the design of selective heterogeneous catalysts.[9,10] The spatial separation of active sites on support surfaces helps preventing multiple successive or parallel reaction steps that give undesired side products. This is particularly useful for kinetically controlled reactions, such as selective hydrocarbon oxidation,[11] and accounts for some of the extraordinary results with surface immobilized homogeneous catalysts or dendrimer supported catalysis.[12] Grafting of organometallic precatalysts on inorganic supports, such as silica or aluminum oxide, is a well established approach to obtain active-site isolated heterogeneous catalysts.[13] This strategy represents a *bottom-up* approach to unify the advantages of hetereogeneous catalysis with selectivity enhancement through well-defined active sites, as typically found in homogeneous catalysis. A general difficulty, e.g. for surface grafted metallocene polymerization catalysts, arises from the fact that the binding mode of the metal center to one or more surface oxide functional groups is generally hard to predict.[13b] Molecular organometallic species with main group metal oxide ligands, such as siloxanes or calixarenes, can serve as models for surface grafted

Abraham, M. T. Scerba, E. Alden-Danforth, T. Lectka, *Acc. Chem. Res.* **2008**, *41*, 655; i) H. Grützmacher, *Angew. Chem.* **2008**, *120*, 1838; *Angew. Chem. Int. Ed.* **2008**, *47*, 1814; j) D. B. Grotjahn, *Dalton Trans.* **2008**, 6497; k) M. Shibasaki, M. Kanai, S. Matsunaga, N. Kumagai, *Acc. Chem. Res.* **2009**, *42*, 1117; l) R. M. Haak, S. J. Wezenberg, A. W. Kleij, *Chem. Commun.* **2010**, *46*, 2713; m) M. Delferro, T. J. Marks, *Chem. Rev.* **2011**, *111*, 2450; n) L. Ackermann, *Chem. Rev.* **2011**, *111*, 1315.

[9] J. L. Callahan, R. K. Grasselli, *AIChE J.* **1963**, *9*, 755.

[10] J. M. Thomas, *ChemCatChem* **2010**, *2*, 127.

[11] R. K. Grasselli, *Top. Catalysis* **2002**, *21*, 79.

[12] a) C. Copéret, *Pure Appl. Chem.* **2009**, *81*, 585; b) B. Helms, J. M. J. Fréchet, *Adv. Synth. Catal.* **2006**, *348*, 1125.

[13] a) C. Copéret, M. Chabanas, R. P. Saint-Arroman, J.-M. Basset, *Angew. Chem.* **2003**, *115*, 164; *Angew. Chem. Int. Ed.* **2003**, *42*, 156; b) J. R. Severn, J. C. Chadwick, R. Duchateau, N. Friedrichs, *Chem. Rev.* **2005**, *105*, 4073; c) J.-P. Candy, C. Copéret, J.-M. Basset, *Top. Organomet. Chem.* **2005**, *16*, 151; d) B. C. Gates, *Top. Organomet. Chem.* **2005**, *16*, 211.

organometallic catalysts.[14,15] In turn, they can provide highly active molecular catalysts as a *top-down* approach to bridge the gap between heterogeneous and homogeneous catalysis.

Organometallic hydroxides as ligand precursors

Cooperative interactions are often observed in biological systems, where they perform an extraordinary array of catalytic transformations (c.f. chapter 5.3). Thus, appropriate proximity between two different metals in a heterobimetallic complex would allow more efficient chemical transformations. Main group and transition metal hydroxides turned out to be the most appropriate precursors for preparing heterobimetallic M-O-M' precatalysts, which benefit from chemical communication between the oxide linked metal atoms, e.g. by enhancing the Lewis acidity of the catalytic center or providing a binding site for co-catalysts, such as methylalumoxane (MAO). A few prominent examples are listed in Table B-5.1.

Table B-5.1: A Selection of Organometallic Hydroxide Precursors.

Compound	^{1}H NMR δ OH ppm
LAlMe(OH) [16]	0.53
LGaMe(OH) [17]	0.08
LGe(II)OH [18]	1.54
[LCa(OH)]$_2$•2THF [19]	-0.78
(η^5-C$_5$Me$_5$)$_2$ZrMe(OH) [20]	4.2

L = HC(CMeNAr)$_2$, Ar = 2,6-iPr$_2$C$_6$H$_3$

[14] a) R. Murugavel, A. Voigt, M. G. Walawalkar, H. W. Roesky, *Chem. Rev.* **1996**, *96*, 2205; b) E. A. Quadrelli, J. M. Basset, *Coord. Chem. Rev.* **2010**, *254*, 707.

[15] C. Limberg, *Eur. J. Inorg. Chem.* **2007**, 3303.

[16] G. Bai, S. Singh, H. W. Roesky, M. Noltemeyer, H.-G. Schmidt, *J. Am. Chem. Soc.* **2005**, *127*, 3449.

[17] S. Singh, V. Jancik, H. W. Roesky, R. Herbst-Irmer, *Inorg. Chem.* **2006**, *45*, 949.

[18] L.W. Pineda, V. Jancik, H. W. Roesky, D. Neculai, A.M. Neculai, *Angew. Chem.* **2004**, *116*, 1443; *Angew. Chem. Int. Ed.* **2004**, *43*, 1419.

[19] C. Ruspic, S. Nembenna, A. Hofmeister, J. Magull, S. Harder, H. W. Roesky, *J. Am. Chem. Soc.* **2006,** *128*, 15000.

[20] P. M. Gurubasavarj, H. W. Rschoesky, P. M. V. Sharma, R. B. Oswald, V. Dolle, R. Herbst-Irmer, A. Pal, *Organometallics* **2007**, *26*, 3346.

The hydroxides of Table B-5.1 are preferentially prepared by two different methods: Firstly by the hydrolysis with water in stoichiometric amounts at low temperatures shown for LCaN(SiMe$_3$)$_2$•THF and (η^5-C$_5$Me$_5$)$_2$ZrMe$_2$ under the elimination of HN(SiMe$_3$)$_2$ and CH$_4$, respectively; secondly by the hydrolysis of the chloride in the presence of N-heterocyclic carbene given in Scheme B-5.1.
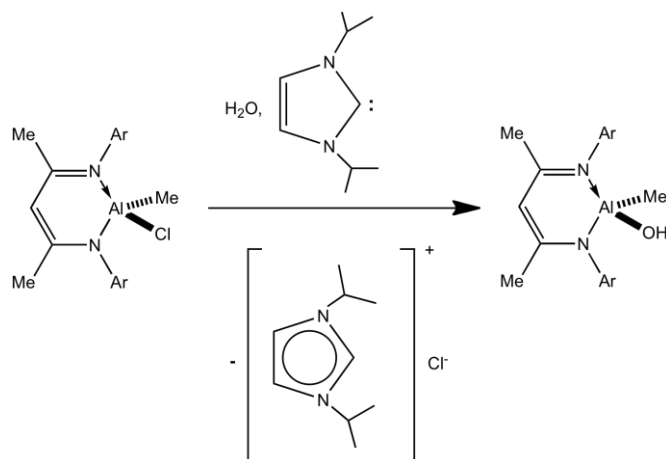
Scheme B-5.1: Preparation of LAlMe(OH), L = HC(CMeNAr)$_2$, Ar = 2,6-iPr$_2$C$_6$H$_3$.

Oxygen bridged heterobimetallic catalysts

The easy access of organometallic hydroxides sets up the possibility to combine a metallocene catalyst and a methylalumoxane cocatalyst. The main objective of this study has been the preparation of compounds with the M-O-Al backbone (M = Zr, Ti) [21] to increase the electrophilic nature at the metal center (M), due to the strong electron withdrawing properties of the bridging oxygen atom. Moreover, compounds with the M-O-Al motif combine the high catalytic activity of group 4 metals in olefin polymerization reactions with the presence of a main group based cocatalyst. The reaction of LAlMe(OH) with organozirconium compounds Cp$_2$ZrMe$_2$ (Cp = C$_5$H$_5$) and Cp$_2$ZrHCl resulted in the formation of LAl(Me)(μ-O)Zr(Me)Cp$_2$ and LAl(Me)(μ-O)Zr(Cl)Cp$_2$ under methane and hydrogen evolution, respectively (Scheme B-5.2).[16]

The molecular structure of these complexes exhibits a bent Zr-O-Al core (158.2(1)° and 155.4(1)°). Both Zr-O-Al compounds are very efficient catalysts for ethylene polymerization. In Table B-5.2 the TOF values for ethylene are listed for LAl(Me)(μ-O)ZrMeCp$_2$ and compared with those of Cp$_2$ZrMe$_2$ and MAO as cocatalyst under similar conditions.

---

[21] P. M. Gurubasavaraj, S. K. Mandal, H. W. Roesky, R. B. Oswald, A. Pal, M. Noltemeyer, *Inorg. Chem.* **2007**, *46*, 1056.
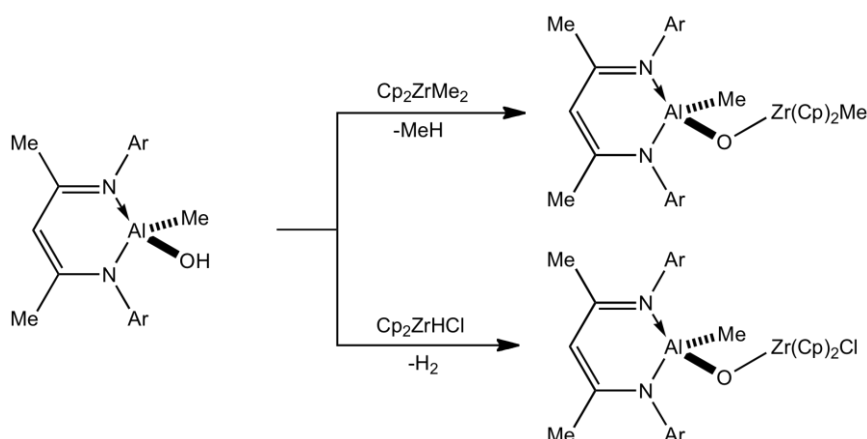
Scheme B-5.2: Preparation of heterobimetallic aluminum-zirconium oxide complexes.

Table B-5.2: TOF ($g_{PE}mol_{cat}^{-1}h^{-1}x10^{-6}$) values for $LAl(Me)(\mu\text{-O})Zr(Me)Cp_2$ and Cp_2ZrMe_2.

Complex	MAO/cat	t/min	PE/g	TOF
$LAl(Me)(\mu\text{-O})Zr(Me)Cp_2$	32	60	0.89	0.05
$LAl(Me)(\mu\text{-O})Zr(Me)Cp_2$	96	30	9.0	0.90
$LAl(Me)(\mu\text{-O})Zr(Me)Cp_2$	176	30	11.9	1.19
$LAl(Me)(\mu\text{-O})Zr(Me)Cp_2$	272	30	12.4	1.24
$LAl(Me)(\mu\text{-O})Zr(Me)Cp_2$	400	30	12.7	1.27
Cp_2ZrMe_2	176	73	7.3	0.52
Cp_2ZrMe_2	272	60	14.6	0.73
Cp_2ZrMe_2	400	37	14.8	1.20

The data of Table B-5.2 clearly show that $LAl(Me)(\mu\text{-O})Zr(Me)Cp_2$ exhibits higher reactivity of the catalytically active species when compared with that of Cp_2ZrMe_2. Moreover, the MAO to catalyst ratio is much lower for $LAl(Me)(\mu\text{-O})Zr(Me)Cp_2$ in comparison to that of Cp_2ZrMe_2. This is an important cost saving factor, and therefore a substantial sustainable component in catalysis.

Another aspect is the increase in stability of half-metallocene complexes; for example, $CpTiMe_3$ (decomp. 30 °C), $Cp*TiMe_3$ (decomp. -80 °C) and $Cp*ZrMe_3$ (decomp. -20 °C) decompose at relatively low temperatures, whereas their reaction products with $LAl(Me)OH$ exhibit high decomposition points, and can be used as catalysts in contrast to their starting

materials[22] [LAl(Me)(μ-O)TiMe$_2$Cp (230 °C), LAl(Me)(μ-O)TiMe$_2$Cp* (235°C), LAl(Me)(μ-O)ZrMe$_2$Cp* (180 °C)]. The decomposition points have increased tremendously.

Finally, two catalytic sites (Ti and Zr) bridged by an oxygen atom can be prepared using Cp*$_2$Zr(Me)OH and Cp*TiMe$_3$ as precursor. The resulting Cp*$_2$Zr(Me)(μ-O)TiMe$_2$Cp* is an effective catalyst for LLDPE (linear low density polyethylene). Both catalytic active sites are competing for ethylene during the polymerization. The use of binuclear polymerization catalysts for to control branching in polyolefins was recently covered in a comprehensive review.[8m]

The molecular oxygen bridged Cp*$_2$Zr(Me)(μ-O)CaN(SiMe$_3$)$_2$•2THF catalyst for hydroamination reactions

The reaction of Cp*$_2$Zr(Me)OH with Ca[N(SiMe$_3$)$_2$]$_2$ resulted in the formation of Cp*$_2$Zr(Me)(μ-O)CaN(SiMe$_3$)$_2$•2THF under elimination of HN(SiMe$_3$)$_2$.[23] The latter complex was used as catalyst for intramolecular hydroamination of unactivated primary and secondary aminoalkenes. The results of kinetic studies unravel that the overall order of the catalytic process is first order, and the reaction rate depends directly upon catalyst concentration for both primary and secondary aminoalkenes. This investigation indicates that the calcium center activates the primary aminoalkenes, and the zirconium center activates the secondary aminoalkenes. This is a rare example where a single catalyst system functions for double activation.

5.3 Bio-inspired homogeneous catalysis: metal-ligand cooperating (MLC) catalysis[24,25]

Many textbook examples for homogeneous catalysis, such as Wilkinson-type olefin hydrogenation, are described in terms of purely metal-centered elementary steps (e.g., H$_2$ oxidative addition, olefin insertion, alkane reductive elimination). Hence, auxiliary ligands,

---

[22] P. M. Gurubasavaraj, H. W. Roesky, B. Nekoueishahraki, A. Pal, R. Herbst-Irmer, *Inorg. Chem.* **2008**, *47*, 5324.

[23] A. Mukherjee, S. Nembenna, T. K. Sen, S. P. Sarish, P. K. Ghorai, H. Ott, D. Stalke, S. K. Mandal, H. W. Roesky, *Angew. Chem.* **2011**, *123*, 4054; *Angew. Chem. Int. Ed.* **2011**, *50*, 3968.

[24] Cooperative reactivity of the metal center and coordinated ligands has been described using several different names (e.g., bifunctional, ambifunctional, or cooperative catalysis).[8] According to the IUPAC recommendation, the frequently used term 'bifunctional catalysis' is correct since two catalyst functional groups are involved in the turn-over limiting step. However, it is not only restricted to metal-ligand cooperativity.[25] Therefore, according to Grützmacher's suggestion, we will use the term metal-ligand cooperating (MLC) catalysis throughout this text to avoid ambiguities.[8i]

[25] P. Müller, *Pure & Appl. Chem.* **1994**, *66*, 1077.

such as arylphosphines are often abbreviated as unspecified 2-electron donors („L_n") in generalized mechanistic schemes, tantamount to chemical innocence. However, in many cases this picture will be grossly oversimplified, as best demonstrated by several metallo-enzymes. There, the first and second coordination spheres around the metal often contain functional groups which simultaneously activate the substrates. A particularly demonstrative example is provided by the enzyme [Fe,Fe]-hydrogenase (*Desulfovibrio desulfuricans*) which catalyzes H_2 production or uptake ($2H^+ + 2e^- \leftrightarrows H_2$) at the diiron subcluster of the active site (Figure B-5.1a).[26,27] Experimental and theoretical studies suggest that the dithiolate bridge contains an amine functional group which acts as a Brønsted base, deprotonating a dihydrogen ligand in the H–H bond heterolysis step (Figure B-5.1b).[28] As a bioinspired analogue, homogeneous nickel electrocatalysts with functional 1,5-diaza-3,7-diphosphinocyclooctane ligands were reported to approach catalytic rates in H_2 oxidation/production close to the biological example.[29] Covalent linking of such a catalyst to multiwalled carbon nanotubes and deposition of this material on a membrane afforded the assembly of an electrolysis half-cell which produces H_2 in acidic condition with high turn-over numbers at very low overpotential (Figure B-5.1c).[30]

[26] Selected Reviews: a) G. J. Kubas, *Chem. Rev.* **2007**, *107*, 4152; b) P. M. Vignais, B. Billoud, *Chem. Rev.* **2007**, *107*, 4206; c) J. C. Fontecilla-Camps, A. Volbeda, C. Cavazza, Y. Nicolet, *Chem. Rev.* **2007**, *107*, 4273; d) J. C. Gordon , G. J. Kubas, *Organometallics* **2010**, *29*, 4682.

[27] Y. Nicolet, C. Piras, P. Legrand, C. E. Hatchikian, J. C. Fontecilla-Camps, *Structure* **1999**, *7*, 13.

[28] a) Y. Nicolet, A. L. de Lacey, X. Vernède, V. M. Fernandez, E. C. Hatchikian, J. C. Fontecilla-Camps, *J. Am. Chem. Soc.* **2001**, *123*, 1596; b) H.-J. Fan, M. B. Hall, *J. Am. Chem. Soc.* **2001**, *123*, 3828; c) B. E. Barton, M. T. Olsen, T. B. Rauchfuss, *J. Am. Chem. Soc.* **2008**, *130*, 16834; d) A. Silakov, B. Wenk, E. Reijerse, W. Lubitz, *Phys. Chem. Chem. Phys.* **2009**, *11*, 6592.

[29] M. Rakowski DuBois, D. L. DuBois, *Acc. Chem. Res.* **2009**, *42*, 1974.

[30] A. Le Goff, V. Artero, B. Jousselme, P. D. Tran, N. Guillet, R. Métayé, A. Fihiri, S. Palacin, M. Fontecave, *Science* **2009**, *326*, 1384.
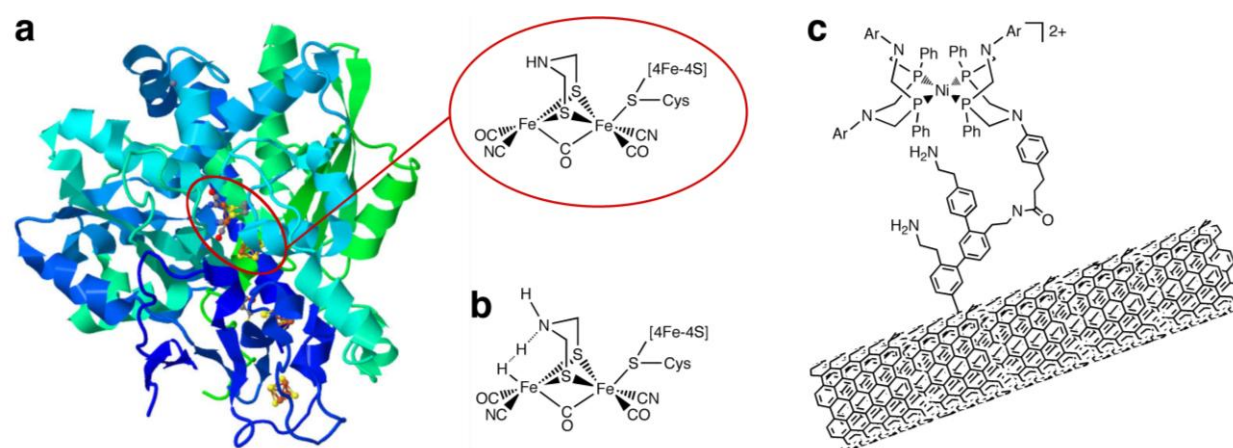
Figure B-5.1: Ribbon diagram of the structural model for [Fe,Fe]-H$_2$ase from *Desulfovibrio desulfuricans* from single-crystal X-ray diffraction (PDB: 1HFE) and proposed structure for the active center (a); proposed mechanism for the H$_2$ heterolysis step (b); bioinspired nickel electrocatalyst for H$_2$ oxidation/production (c).

Amido complexes of electron rich metals: prototype MLC catalysts

Electron rich ($d^6 - d^{10}$) transition metal complexes with amido ligands are particularly well suited for cooperative ligand reactivity, owing to the high *N*-centered basicity.[31] Heterolytic H$_2$ splitting with metal amides was pioneered by Fryzuk using disilylamido complexes.[32] Around 10 years later, the extraordinary activities and selectivities (C=O over C=C hydrogenation) in ketone direct hydrogenation with H$_2$ (DH) and transfer hydrogenation (TH) catalyzed by ruthenium(II) complexes with primary amine ligands (the '*NH-effect*')[8b,33] were attributed to metal-ligand-cooperative H$_2$ activation (Scheme B-5.3, *Step III*) and outer-sphere transfer to the substrate (Scheme B-5.3, *Step II*).[34,35] As a possible alternative to concerted

[31] a) H. E. Brzynda, W. Tam, *Chem. Rev.* **1988**, *88*, 1163; b) M. D. Fryzuk, C. D. Montgomery, *Coord. Chem. Rev.* **1989**, *95*, 1; b) M. D. Roundhill, *Chem. Rev.* **1992**, *92*, 1. (c) R. G. Bergman, *Polyhedron* **1995**, *14*, 3227; d) J. R. Fulton, A. W. Holland, D. J. Fox, R. G. Bergman, *Acc. Chem. Res.* **2002**, *35*, 44; e) T. B. Gunnoe, *Eur. J. Inorg. Chem.* **2007**, 1185.

[32] a) M. D. Fryzuk, P. A. McNeil, *Organometallics* **1983**, *2*, 355; b) M. D. Fryzuk, P. A. McNeil, *Organometallics* **1983**, *2*, 682; c) M. D. Fryzuk, P. A. McNeil, S. J. Rettig, *Organometallics* **1985**, *4*, 1145; d) M. D. Fryzuk, P. A. McNeil, S. J. Rettig, *Organometallics* **1986**, *5*, 2469; e) M. D. Fryzuk, P. A. McNeil, S. J. Rettig, *J. Am. Chem. Soc.* **1987**, *109*, 2803.

[33] W. P. Hems, M. Groarke, A. Zanotti-Gerosa, G. A. Grasa, *Acc. Chem. Res.* **2007**, *40*, 1340.

[34] a) K. Abdur-Rashid, S. E. Clapham, A. Hadzovic, J. N. Harvey, A. J. Lough, R. H. Morris, *J. Am. Chem. Soc.* **2002**, *124*, 15104; b) C. A. Sandoval, T. Okhuma, K. Muñiz, R. Noyori, *J. Am. Chem. Soc.* **2003**, *125*, 13490.

[35] a) S. E. Clapham, A. Hadzovic, R. H. Morris, *Coord. Chem. Rev.* **2004**, *248*, 2201; b) K. Muñiz, *Angew. Chem.* **2005**, *117*, 6780; *Angew. Chem. Int. Ed.* **2005**, *44*, 6622; c) J. S. M. Samec, J.-E. Bäckvall, P. G.

transfer to the substrate, experimental evidence for an alkoxide intermediate which eliminates the alcohol under basic conditions was also presented.[36]
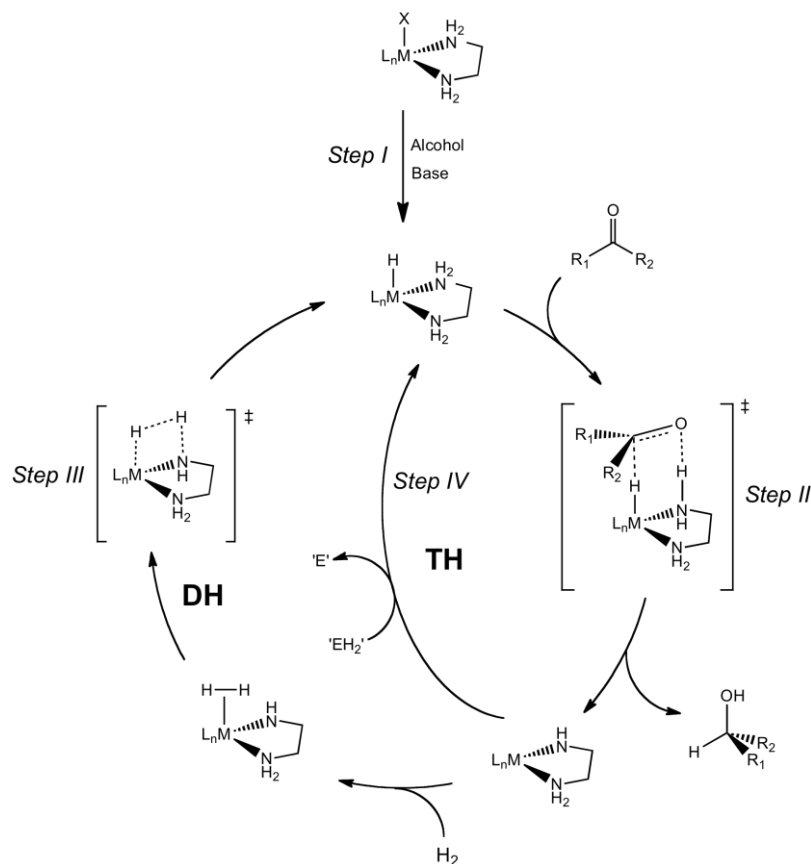
Scheme B-5.3: Proposed catalytic cycles of direct hydrogenation (DH) and transfer hydrogenation (TH) of ketones with Noyori-type bifunctional catalysts. Typical 'EH$_2$' sacrificial hydrogen donors are 2-propanol or formiate.

Based on experimental and theoretical results, Brønsted-acid and -base assistance for H$_2$-heterolysis, e.g. by water, alcohols, or alkoxides, was proposed.[37,38,39,40,41] For example, the

Andersson, P. Brandt, *Chem. Soc. Rev.* **2006**, *35*, 237; d) T. Ikariya, A. J. Blacker, *Acc. Chem. Res.* **2007**, *40*, 1300; e) M. Ito, T. Ikariya, *Chem. Commun.* **2007**, 5134.

[36] a) R. J. Hamilton, S. H. Bergens, *J. Am. Chem. Soc.* **2006**, *128*, 13700; b) R. J. Hamilton, S. H. Bergens, *J. Am. Chem. Soc.* **2008**, *130*, 11979.

[37] a) R. Hartmann, P. Chen, *Angew. Chem.* **2001**, *113*, 3693; *Angew. Chem. Int. Ed.* **2001**, *40*, 3581; b) M. Ito, M. Hirakawa, K. Murata, T. Ikariya, *Organometallics* **2001**, *20*, 379; c) V. Rautenstrauch, X. Hoang-Cong, R. Churland, K. Abdur-Rashid, R. H. Morris, *Chem. Eur. J.* **2003**, *9*, 4954; d) W. Baratta, K. Siega, P. Rigo, *Chem. Eur. J.* **2007**, *13*, 7479; e) A. Hadzovic, D. Song, C. M. MacLaughlin, R. H. Morris, *Organometallics* **2007**, *26*, 5987; f) A. Friedrich, M. Drees, J. Schmedt auf der Günne, S. Schneider, *J. Am. Chem. Soc.* **2009**, *131*, 17552.

trans-dihydride complex [Ru(H)$_2$(PMe$_3$){HN(CH$_2$CH$_2$P^{i}Pr$_2$)}] (**1**) exhibits rapid hydride/proton exchange of the *syn*-H–Ru–N–H hydride but not of the *anti*-H–Ru–N–H hydride with H$_2$O.[37f] The stereoselectivity was attributed to a water mediated proton shuttle mechanism for the hydride/amine-dihydrogen/amide-equilibrium (Scheme B-5.4). Model DFT calculations confirm that the reverse reaction (H$_2$ heterolysis) is strongly accelerated ($\Delta\Delta G^\ddagger$ = 8.2 kcal/mol) and becomes almost barrierless ($\Delta G^\ddagger_{H_2O}$ = 2.5 kcal/mol) upon H$_2$O catalyis. Hence, only minute contributions to the kinetic barrier result from rearrangement of the first coordination sphere around the metal. Note that the coordination number of the metal center is changed by one only, as opposed to two for H$_2$ oxidative addition.
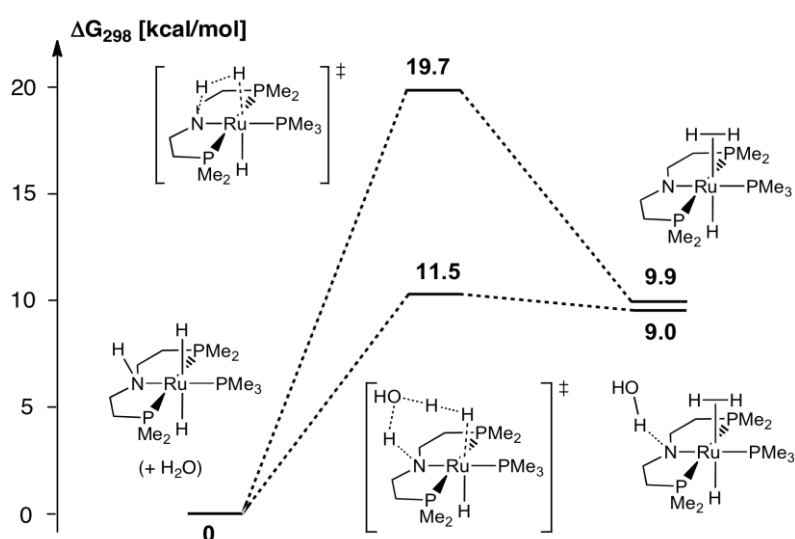
Scheme B-5.4: Computed free energy profile for H$_2$ heterolysis at a ruthenium(II) amide complex with and without water catalysis.[37f]

In recent years, a wide variety of MLC hydrogenation catalysts with primary or secondary amine ligands was established.[33,34,42,43] Some of them were also successfully employed for

[38] a) C. Hedberg, K. Källström, P. I. Arvidsson, P. Brandt, P. G. Andersson, *J. Am. Chem. Soc.* **2005**, *127*, 15083; b) D. H. Ess, C. K. Schauer, T. J. Meyer, *J. Am. Chem. Soc.* **2010**, *132*, 16318.

[39] C. P. Casey, J. B. Johnson, S. W. Singer, Q. Cui, *J. Am. Chem. Soc.* **2005**, *127*, 3100.

[40] Z. A. Heiden, T. B. Rauchfuss, *J. Am. Chem. Soc.* **2009**, *131*, 3593.

[41] M. Zimmer-De Iuliis, R. H. Morris, *J. Am. Chem. Soc.* **2009**, *131*, 11263.

[42] R. H. Morris, *Chem. Soc. Rev.* **2009**, *38*, 2282.

[43] Selected recent examples: a) W. Baratta, G. Chelucci, E. Herdtweck, S. Magnolia, K. Siega, P. Rigo, *Angew. Chem.* **2007**, *119*, 7795; *Angew. Chem. Int. Ed.* **2007**, *46*, 7651; b) D. Amoroso, T. W. Graham, R. Guo, C.-W. Tsang, K. Abdur-Rashid, *Aldrichim. Acta* **2008**, *41*, 15; c) A. Mikhailine, A. J. Lough, R. H. Morris, *J. Am. Chem. Soc.* **2009**, *131*, 1394; d) S. D. Phillips, J. A. Fuentes, M. L. Clarke, *Chem. Eur. J.* **2010**, *16*, 8002; e) T. Irrgang, D. Friedrich, R. Kempe, *Angew. Chem. Int. Ed.* **2011**, *123*, 2231; *Angew. Chem. Int. Ed.*

the reverse reaction, i.e. the oxidation of alcohols by acceptorless dehydrogention to give H_2 and ketones, aldehydes, or dehydrocoupling products (e.g. esters), or for alcohol functionalizations based on the ,borrowing hydrogen' methodology.[44,45,46] The large amount of mechanistic work renders this an interesting case to discuss MLC catalyst design. The primary or secondary alkylamine functional groups often used give rise to highly basic alkylamido ligands upon catalyst activation (Scheme B-5.3, *Step I*). Chelating ligands help to suppress amide β-hydrogen elimination.[31] Imine formation was, in fact, found to account for catalyst decomposition in the absence of H_2.[47] Conformational flexibility of the chelating ligand assists in stabilizing both the pyramidal (amine) and planar (amido) geometries around the nitrogen atom. The highly organized transition state for hydride and proton transfer (Scheme B-5.3, *Step II*) contributes to the high stereoselectivities obtained with several chiral, non-racemic catalysts. Hence, a near co-planar H-M-N-H *syn*-arrangement should be favorable and is in fact stabilized by intramolecular M-H⋯H-N dihydrogen bonding.[48]
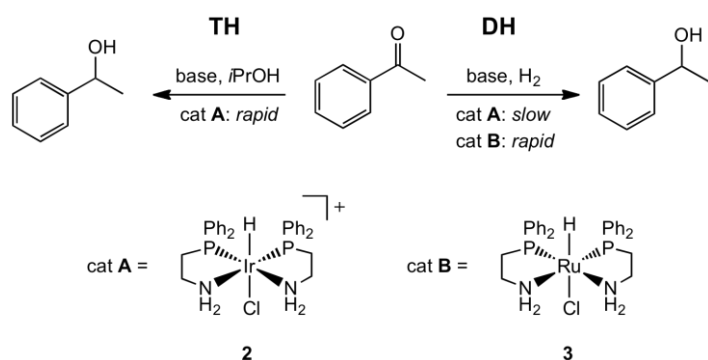
Scheme B-5.5: [MHCl(Ph$_2$PCH$_2$CH$_2$NH$_2$)$_2$]$^{0/+}$ (M = Ir, Ru) as precatalysts for ketone TH and DH.

2011, *50*, 2183.

[44] a) J. Zhao, J. F. Hartwig, *Organometallics* **2005**, *24*, 2441; b) N. Andrushko, V. Andrushko, P. Roose, K. Moonen, A. Börner, *ChemCatChem* **2010**, *2*, 640; c) M. Bertoli, A. Choualeb, A. J. Lough, B. Moore, D. Spasyuk, D. G. Gusev, *Organometallics* **2011**, *30*, 3479; d) M. Bertoli, A. Choualeb, D. G. Gusev, A. J. Lough, Q. Major, B. Moore, *Dalton Trans.* **2011**, *40*, 8941; e) M. Nielsen, A. Kammer, D. Cozzula, H. Junge, S. Gladiali, M. Beller, *Angew. Chem.* **2011**, *123*, 9767; *Angew. Chem. Int. Ed.* **2011**, *50*, 9593.

[45] A. Friedrich, S. Schneider, *ChemCatChem* **2009**, *1*, 72.

[46] a) M. H. S. A. Hamid, P. A. Slatford, J. M. J. Williams, *Adv. Synth. Catal.* **2007**, *349*, 1555-1575; b) T. D. Nixon, M. K. Whittlesey, J. M. J. Williams, *Dalton Trans.* **2009**, 753.

[47] R. Abbel, K. Abdur-Rashid, M. Faatz, A. Hadzovic, A. J. Lough, R. H. Morris, *J. Am. Chem. Soc.* **2005**, *127*, 1870.

[48] R. H. Crabtree, P. E. M. Siegbahn, O Eisenstein, A. L. Rheingold, T. H. Koetzle, *Acc. Chem. Res.* **1996**, *29*, 348.

However, not all precatalysts with this structural motif operate *via* this mechanism. Some compounds are active catalysts for TH, but not for DH. For example, cationic $[IrHCl(Ph_2PCH_2CH_2NH_2)_2]^+$ (**2**), which strongly resembles the ruthenium DH precatalyst $[RuHCl(Ph_2PCH_2CH_2NH_2)_2]$ (**3**), is an efficient TH but not DH catalyst for ketones (Scheme B-5.5).[49] For both systems, the *trans*-dihydride complexes [M-*trans*-$(H)_2(Ph_2PCH_2CH_2NH_2)_2]^n$ (M = Ru, n = 0; M = Ir, n = +1 (**4**)) are anticipated to be the active species transfering H_2 to the substrate. The lack of H_2 activation by the resulting Ir as opposed to the Ru amido complex can be explained with weak $Ir-H_2$ binding to this intermediate imposing a large barrier on the route of heterolytic H_2-splitting.[50] In the light of the highly active analogous ruthenium or some neutral iridium direct hydrogenation catalysts[51] it is tempting to attribute weaker $M-H_2$ bonding for the cationic Ir complex to the charge critically reducing $Ir{\rightarrow}H_2$ back bonding.[26a]
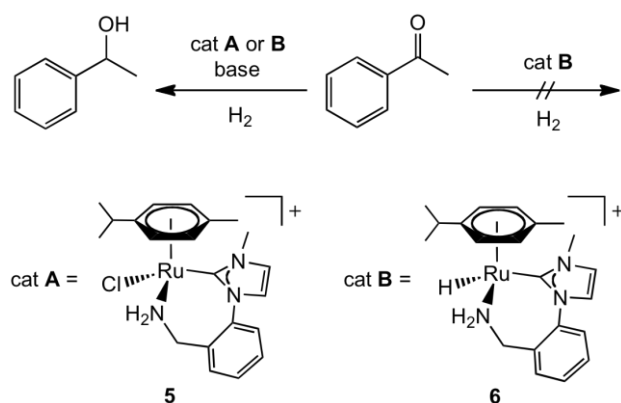
Scheme B-5.6: Hydrogenat. of acetophenone with *N*-heterocyclic carbene complexes **5** and **8**.

N-Heterocyclic carbene complex $[(p\text{-cymene})RuCl(CN(Me)CHCHN(C_6H_4\text{-}o\text{-}NH_2))]^+$ (**5**, Scheme B-5.6) is active in TH and DH of ketones upon activation with base.[52] However, the corresponding hydride **6**, which resembles Noyori's outer-sphere catalyst $[(p\text{-cymene})RuH(p\text{-}MeC_6H_4SO_2NCH_2CH_2NH_2)]$ (**7**), fails to transfer H_2 to the substrate in the absence of a base (Scheme B-5.6).[52b] This lack of direct hydrogen transfer excludes an outer-sphere mechanism for the carbene precatalyst **5** and points towards lower hydride nucleophilicity attributable to the cationic charge as compared with **7**. Many active catalyst species for outer-

[49] a) L. Dahlenburg, R. Götz, *Inorg. Chim. Acta.* **2004**, *357*, 2875; b) K. Abdur-Rashid, R. Guo, A. J. Lough, R. H. Morris, D. Song, *Adv. Synth. Catal.* **2005**, *347*, 571.

[50] R. Puchta, L. Dahlenburg, T. Clark, *Chem. Eur. J.* **2008**, *14*, 8898.

[51] X. Chen, W. Jia, R. Guo, T. W. Graham, M. A. Gullons, K. Abdur-Rashid, *Dalton Trans.* **2009**, 1407.

[52] a) W. W. N. O, A. J. Lough, R. H. Morris, *Organometallics* **2009**, *28*, 6755; b) W. W. N. O, A. J. Lough, R. H. Morris, *Organometallics* **2011**, *30*, 1236.

sphere H_2-transfer to the substrate carry strong σ-donor ligands particularly in *trans*-position to the transferred hydride which labilize M-H bonding.[26a,53] For example, out of the possible stereoisomers for [Ru(H)$_2$(PPh$_3$)$_2$(1,2-(*R,R*)-diaminocyclohexane)] (**8**) the *trans*-dihydride complex was shown to be the catalytically active isomer (Figure B-5.2).[47] This trend was further demonstrated in a DFT examination of ketone DH with model catalysts [Ru-*trans*-(HX)(H$_2$NCMe$_2$CMe$_2$NH$_2$)-*cis*-(PH$_3$)$_2$]$^{n+}$ (n = 0: X = H, Cl, OR; n = 1: CO, NCMe).[54] Both weak field ligands in *trans* position and cationic charge result in reduced hydricity and therefore high barriers to H_2 transfer to the substrate.[55]
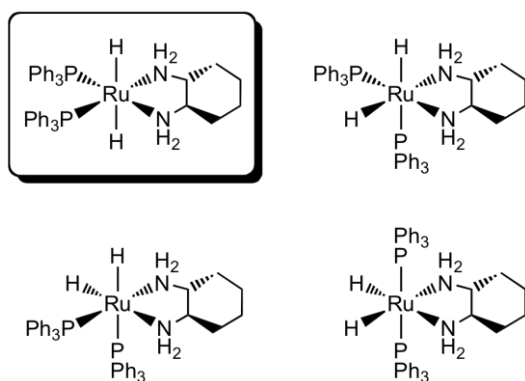
Figure B-5.2: Experimentally observed stereoisomers of **8** with the active H_2-transfer species marked by frame.

These examples suggest that basic principles for catalyst design can be extracted considering simple, well established trends for bond energies. The turn-over frequency of a catalytic cycle can be estimated by determining the energetic span of the reaction steps, i.e., the difference of the highest to the lowest free energy point on the reaction coordinate.[56] Hence, the catalytic rates are diminished both by strong ground state stabilization (e.g. for **6**) and destabilization (e.g. for **5**) of intermediates. This interpretation resembles a fundamental rule in heterogeneous catalysis known as 'Sabatier's principle', which predicts that the best catalyst for a given reaction will have an 'intermediate' binding strength for substrate

[53] A. Albinati, V. I. Bakhmutov, K. G. Caulton, E. Clot, J. Eckert, O. Eisenstein, D. G. Gusev, V. V. Grushin, B. E. Hauger, W. T. Klooster, T. F. Koetzle, R. K. McMullan, T. J. O'Loughlin, M. Pelissier, J. S. Ricci, M. P. Sigalas, A. B. Vymenits, *J. Am. Chem. Soc.* **1993**, *115*, 7300.

[54] Z. Chen, Y. Chen, Y. Tang, M. Lei, *Dalton Trans.* **2010**, *39*, 2036.

[55] H. Jacobsen, H. Berke in *Recent Advances in Hydride Chemistry* (Eds. M. Peruzzini, R. Poli), Elsevier, Amsterdam, **2001**, p 89-116.

[56] S. Kozuch, C. Amatore, A. Jutand, S. Shaik, *Organometallics* **2005**, *24*, 2319.

molecules, intermediates, and products on the surface.[57,58] In homogeneous catalysis, this principle was recently emphasized for molecular proton reduction electrocatalysts ($2\,H^+ + 2e^- \rightarrow H_2$).[29,59] Minimal overpotentials will be accomplished if H_2 addition to the catalyst is thermoneutral ($\Delta G_r = 0$), which is in fact the case for [Fe,Ni]-hydrogenase.[60] These purely thermodynamic considerations neglect differences in activation energies. However, for related systems with moderate heats of reaction, a Brønsted-Evans-Polanyi type relationship provides a reasonable first approximation to estimate relative reaction barriers.[61]

[57] a) P. Sabatier, *Ber. Dtsch. Chem. Ges.* **1911**, *44*, 1984; b) J. K. Nørskov, T. Bligaard, J. Rossmeisl, C. H. Christensen, *Nature Chem.* **2009**, *1*, 37.

[58] a) A. A. Balandin, *Adv. Catal.* **1969**, *19*, 1; b) T. Bligaard, J. K. Nørskov, S. Dahl, J. Matthiesen, C. H. Christiansen, J. Sehested, *J. Catal.* **2004**, *224*, 206.

[59] J. L. Dempsey, B. S. Brunschwig, J. R. Winkler, H. B. Gray, *Acc. Chem. Res.* **2009**, *42*, 1995.

[60] M. T. M. Koper, E. Bouwman, *Angew. Chem.* **2010**, *122*, 3810; *Angew. Chem. Int. Ed.* **2010**, *49*, 3723.

[61] R. I. Masel, *Chemical Kinetics and Catalysis*, **2001**, Wiley, New York.
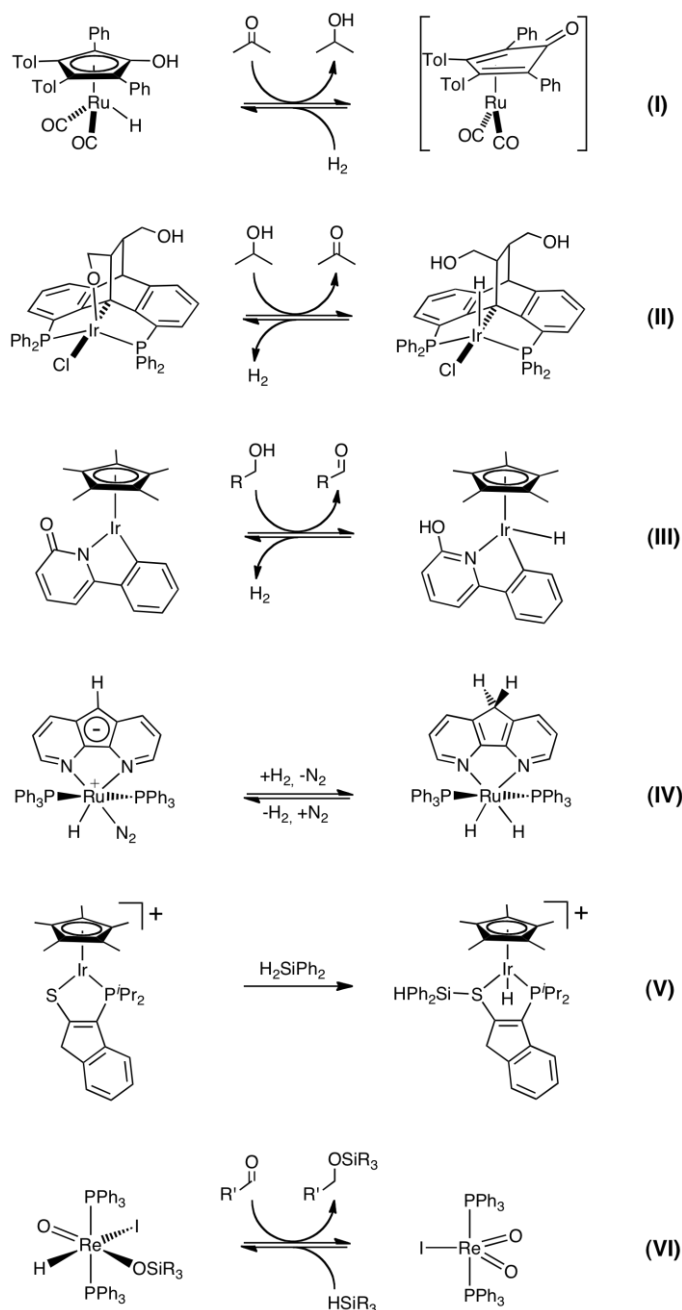
Scheme B-5.7: Representative examples for metal-ligand cooperative bond activation and catalysis.

Comparison with other MLC platforms

Shvo's catalyst, $[\{(\eta^5\text{-}C_4Ph_4O)_2(\mu\text{-}H)\}Ru_2(CO)_4(\mu\text{-}H)]$, was introduced for DH, TH, and acceptorless dehydrogention of polar functional groups as early as the mid 1980's. Detailed examinations provided strong evidence for a Ru-H/O-H metal-ligand cooperative mechanism, which comprises H_2 heterolysis by addition to putative, unsaturated intermediate $[(\eta^4\text{-}OC_5R_4)Ru(CO)_2]$ (Tol = p-tolyl) and subsequent transfer to the substrate (Scheme B-5.7,

I).[39,62] The scope and mechanistic aspects of reactions catalyzed by Shvo's catalyst were recently covered by a comprehensive review.[63] Other hydrogenation or dehydrogenation catalysts which presumably rely on M-H/O-H cooperativity are also known, such as a recently reported pincer-type iridium catalyst with a hydroxyalkyl tether (Scheme B-5.7, **II**) or iridium hydroxypyridine piano-stool catalysts (Scheme B-5.7, **III**).[64,65] Apart from amides or alkoxides, several other basic functional groups, such as carbanions (Scheme B-5.7, **IV**)[66] or carbenes (Scheme B-5.14),[100,101] thiolates (Scheme B-5.7, **V**),[67] phosphines (Scheme B-5.15)[106] or oxo ligands (Scheme B-5.7, **VI**),[68] are also capable of serving as proton (silyl) acceptors in H_2 (silane) activation and hydrogenation (hydrosilylation) reactions, respectively. Similarly, the high activities of Pd- and Ru-acetate catalysts in aryl cross-coupling by C–H direct arylation were attributed to carboxylate cooperativity in the C-H activation step which was very recently discussed in an excellent review.[8n]
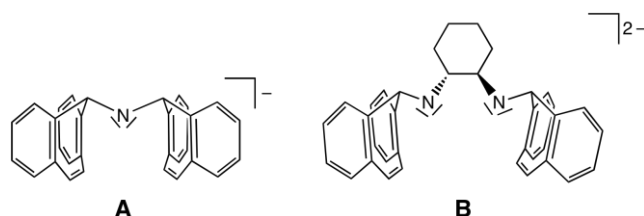
Figure B-5.3: Cycloheptatrienylamido-based pincer ligands.

These examples demonstrate the rapidly growing structural variety of MLC building blocks and the broad applicability of MLC catalysis. Hence, a comprehensive discussion of the numerous MLC catalyst motifs is beyond the scope of this account. However, two systems will be pointed out below owing to their interesting structural features and excellent catalytic performance.

[62] C. P. Casey, S. W. Singer, D. R. Powell, R. K. Hayashi, M. Kavana, *J. Am. Chem. Soc.* **2001**, *123*, 1090.

[63] B. L. Conley, M. K. Pennington-Boggio, E. Boz, T. J. Williams, *Chem. Rev.* **2010**, *110*, 2294.

[64] S. Musa, I. Shaposhnikov, S. Cohen, D. Gelman, *Angew. Chem.* **2011**, *123*, 3595; *Angew. Chem. Int. Ed.* **2011**, *50*, 3533.

[65] a) K. Fujita, N. Tanino, R. Yamaguchi, *Org. Lett.* **2007**, *9*, 109-111; K. Fujita, T. Yoshida, Y. Imori, R. Yamaguchi, *Org. Lett.* **2011**, *13*, 2278.

[66] E. Stepowska, H. Jiang, D. Song, *Chem. Commun.* **2010**, *46*, 446.

[67] K. D. Hesp, R. McDonald, M. J. Ferguson, M. Stradiotto, *J. Am. Chem. Soc.* **2008**, *130*, 16394.

[68] K. A. Nolin, J. R. Krumper, M. D. Pluth, R. G. Bergman, F. D. Toste, *J. Am. Chem. Soc.* **2007**, *129*, 14684.
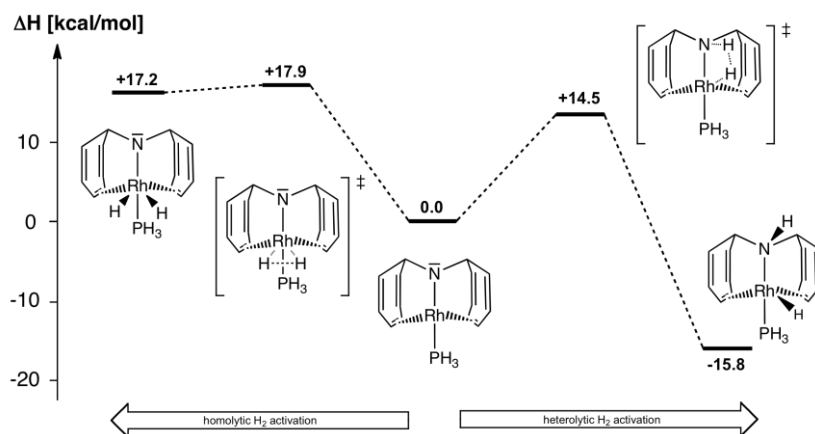
Scheme B-5.8: Computed reaction enthalpies for homolytic vs. heterolytic H_2 addition to **9**.

Grützmacher's group established rhodium(I) and iridium(I) MLC catalysts for C=O and C=N DH and TH with chelating cycloheptatrienylamido-based CNC pincer ligands (Figure B-5.3).[69,70] The use of olefinic auxiliary ligands might be somewhat counter-intuitive, but some chelating olefins have been demonstrated to be surprisingly inert towards hydrogenation.[71] Both the amide $[Rh\{N(C_{15}H_{11})_2\}(PPh_3)]$ and the corresponding amine complex with a *syn*-coplanar H-Rh-N-H moiety are active precatalysts for ketone DH with similar activities indicating a cooperative mechanism. Oxidative addition of H_2 to the metal center of model complex $[Rh\{N(C_7H_7)_2\}PPh_3]$ (**9**) was calculated to be endothermic by $\Delta H_r \approx$ +17 kcal/mol,[70a] attributable to the stereochemical rigidity of the chelating ligand (Scheme B-5.8). For comparison, oxidative additon of H_2 to $[RhCl\{P(C_6H_4\text{-}4\text{-}CH_3)_3\}_2L]$ (L = $P(C_6H_4\text{-}4\text{-}CH_3)_3$, $S(CH_2)_4$) is exothermic by around 11 kcal/mol.[72] In contrast, hydrogen addition across the covalent Rh-N bond is downhill by $\Delta H_r \approx$ -16 kcal/mol *via* direct [2+2] cycloaddition. The entropic contribution to the free energy of reaction (TΔS at 298 K) can be

[69] a) T. Büttner, F. Breher, H. Grützmacher, *Chem. Commun.* **2004**, 2820; b) P. Maire, F. Breher, H. Grützmacher, *Angew. Chem.* **2005**, *117*, 6483; *Angew. Chem. Int. Ed.* **2005**, *44*, 6325; c) T. Büttner, J. Geier, G. Frison, J. Harmer, C. Calle, A. Schweiger, H. Schönberg, H. Grützmacher, *Science* **2005**, *307*, 235.

[70] a) P. Maire, T. Büttner, F. Breher, P. Le Floch, H. Grützmacher, *Angew. Chem.* **2005**, *117*, 6477; *Angew. Chem. Int. Ed.* **2005**, *44*, 6318; b) P. Maire, F. Breher, H. Schönberg, H. Grützmacher, *Organometallics* **2005**, *24*, 3207; c) T. Zweifel, J.-V. Naubron, T. Büttner, T. Ott, H. Grützmacher, *Angew. Chem.* **2008**, *120*, 3289; *Angew. Chem. Int. Ed.* **2008**, *47*, 3245; d) T. Zweifel, D. Scheschkewitz, T. Ott, M. Vogt, H. Grützmacher, *Eur. J. Inorg. Chem.* **2009**, 5561; e) M. Trincado, H. Grützmacher, F. Vizza, C. Bianchini, *Chem. Eur. J.* **2010**, *16*, 2751.

[71] a) P. Maire, S. Deblon, F. Breher, J. Geier, C. Böhler, H. Rüegger, H. Schönberg, H. Grützmacher, *Chem. Eur. J.* **2004**, *10*, 4198; b) C. Defieber, H. Grützmacher, E. M. Carreira, *Angew. Chem.* **2008**, *120*, 4558; *Angew. Chem. Int. Ed.* **2008**, *47*, 4482.

[72] R. S. Drago, J. G. Miller, M. A. Hoselton, R. D. Farris, M. J. Desmond, *J. Am. Chem. Soc.* **1983**, *105*, 444.

estimated to be around 8-10 kcal/mol.[73] Hence, this reaction is exoergic by only a few kcal/mol in accord with the requirements for an efficient catalyst. Note that the nitogen atoms in the respective amido complexes are pyramidalized as a consequence of the NCN ligand geometry and the absence of suitable orbitals on the Rh^I center for N→M π-donation. This geometric feature thermodynamically and kinetically favours H_2 addition with little rearrangement of the first ligand sphere.
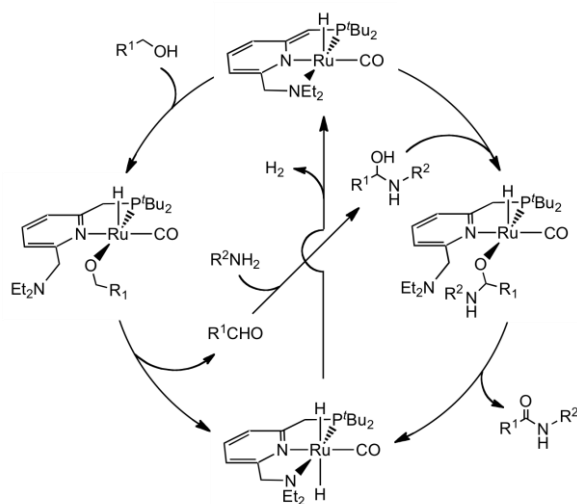
Scheme B-5.9: Proposed mechanism for the dehydrocoupling of alcohols and amines to amides catalyzed by pyridine based pincer complexes.

Milstein and co-workers developed a class of M-H/C-H MLC catalysts with pyridine based pincer ligands, $[MH(CO)Cl\{NC_5H_3\text{-}2\text{-}CH_2PR_2\text{-}6\text{-}CH_2ER'_2\}]$ (R = ^{i}Pr, ^{t}Bu; ER'$_2$ = NEt$_2$, P^{i}Pr$_2$; M = Ru, Fe), which are highly active in carbonyl group DH and acceptorless alcohol dehydrocoupling.[74,75] The versatile benzylic deprotonation of these pincer ligands to give a 'dearomatized' amido complex has been demonstrated for several metal complexes,[76,77] and

[73] L. A. Watson, O. Eisenstein, *J. Chem. Educ.* **2002**, *79*, 1269.

[74] a) J. Zhang, G. Leitus, Y. Ben-David, D. Milstein, *J. Am. Chem. Soc.* **2005**, *127*, 10840; b) J. Zhang, G. Leitus, Y. Ben-David, D. Milstein, *Angew. Chem.* **2006**, *118*, 1131; *Angew. Chem. Int. Ed.* **2006**, *45*, 1113; c) C. Gunanathan, Y. Ben-David, D. Milstein, *Science* **2007**, *317*, 790; d) B. Gnanaprakasam, J. Zhang, D. Milstein, *Angew. Chem.* **2010**, *122*, 1510; *Angew. Chem. Int. Ed.* **2010**, *49*, 1468; e) R. Langer, G. Leitus, Y. Ben-Davis, D. Milstein, *Angew. Chem.* **2011**, *123*, 2168; *Angew. Chem. Int. Ed.* **2011**, *50*, 2120.

[75] a) D. Milstein, *Top. Catal.* **2010**, *53*, 915; b) C. Gunanathan, D. Milstein, *Acc. Chem. Res.* **2011**, *44*, 588.

[76] J. I. van der Vlugt, J. Reek, *Angew. Chem.* **2009**, *121*, 8990-9004; *Angew. Chem. Int. Ed.* **2009**, *48*, 8832.

[77] a) E. Ben-Ari, G. Leitus, L. J. W. Shimon, D. Milstein, *J. Am. Chem. Soc.* **2006**, *128*, 15390; b) J. I. van der Vlugt, M. Lutz, E. A. Pidko, D. Vogt, A. L. Spek, *Dalton Trans* **2009**, 1016; c) J. I. van der Vlugt, E. A. Pidko, D. Vogt, M. Lutz, A. L. Spek, *Inorg. Chem.* **2009**, *48*, 7513.

reversible addition of H_2 across the metal and the pincer backbone was proposed as decisive step for catalysis (Scheme B-5.9). These results demonstrate that the functional group on the ligand relevant for cooperative reactivity does not have to be directly bound to the metal center and can be even more 'remote' as recently demonstrated with a related acridine based PNP pincer complex.[78]
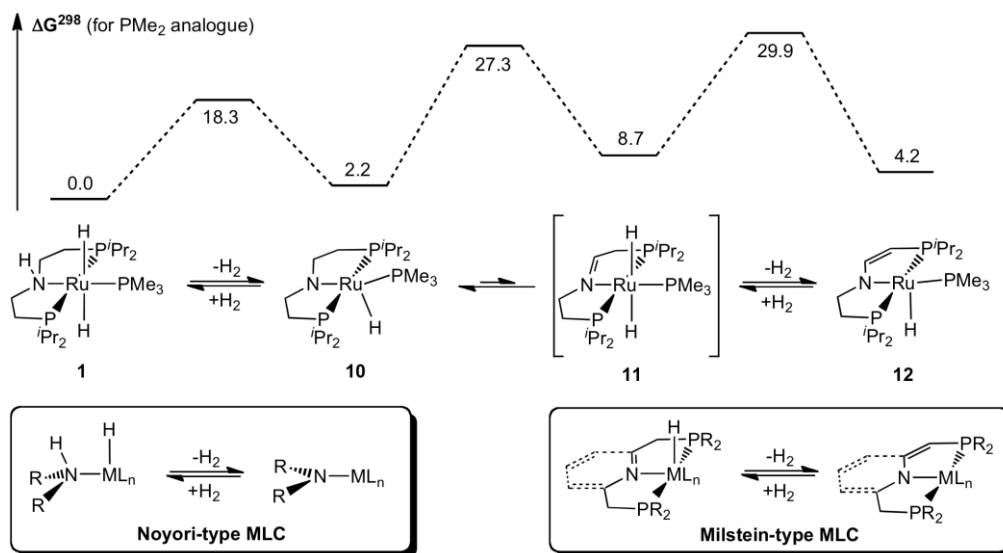
Scheme B-10.5: H_2 elimination equilibria of amine (**1**), amido (**10**), imine (**11**) and enamido (**12**) complexes and comparison with other MLC platforms. Ground and transition state free energies are given for the PMe_2 truncated model in kcal/mol relative to amine complex **1**.

Aromaticity of the pincer backbone is, however, not a prerequisite for these proton shift reactions. Amine complex **1** reversibly eliminates H_2 both from the Ru-H/N-H moiety and from the pincer backbone, respectively (Scheme B-5.10).[79] Hence, the bis(phosphinoethane)amine M(PNP) fragment both exhibits typical reactivity for Noyori-type MLC catalysts and represents an aliphatic analogue of Milstein's system. Ruthenium, osmium and iridium complexes with this ligand were used as catalysts for ketone DH and TH,[51,43b,80,81] acceptorless alcohol dehydrogenation and dehydrocoupling,[44b,e,82] borane-

---

[78] a) C. Gunanathan, L. J. W. Shimon, D. Milstein, *J. Am. Chem. Soc.* **2009**, *131*, 3146; b) C. Gunanathan, B. Gnanaprakasam, M. A. Iron, L. J. W. Shimon, D. Milstein, *J. Am. Chem. Soc.* **2010**, *132*, 14763.

[79] M. Käß, A. Friedrich, M. Drees, S. Schneider, *Angew. Chem.* **2009**, *121*, 922; *Angew. Chem. Int. Ed.* **2009**, *48*, 905.

[80] Z. E. Clarke, P. T. Maragh, T. P. Dasgupta, D. G. Gusev, A. J. Lough, K. Abdur-Rashid, *Organometallics* **2006**, *25*, 4113.

[81] S. Schneider, J. Meiners, B. Askevold, *Eur. J. Inorg. Chem.* DOI: 10.1002/ejic.201100880.

amine dehydrocoupling,[79,96] and borane-amine hydrolysis.[83] Mechanistic examinations of the dual H_2 elimination/addition sequence suggest that the imine complex **11** is an unstable intermediate towards both migrative imine insertion and hydrogen loss.[84] The latter is relatively slow. However, for a related Ir^I diphosphinopyridine complex water catalyzed proton transfer from the ligand backbone to the hydride ligand was shown to substantially lower this barrier.[85]
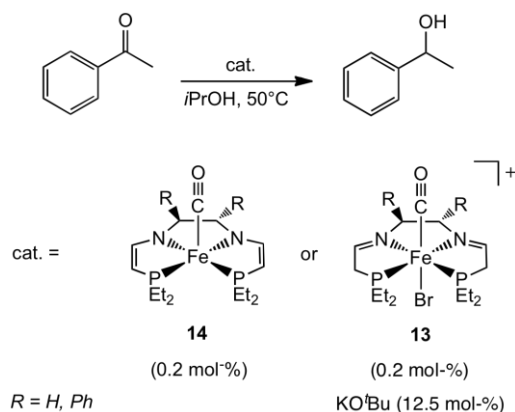
Scheme B-5.11: TH of acetophenone with iron(II) imine and enamido catalysts **13** and **14**.

Morris described ketone TH with the iron diimine precatalyst **13** after activation with base (Scheme B-5.11).[86] In turn, the isolable bisenamido complex **14** exhibits the same catalytic rates without base.[87] These results suggest a yet elusive hydrido imine species as intermediate for H_2 transfer from 2-propanol to the substrate. However, conversion of both precatalysts to an amine catalyst species under catalytic conditions which undergoes an amine/amide based catalytic cycle cannot be fully excluded at this point. Milstein reported that iron complex [FeBr(CO)H{NC$_5$H$_3$-2,6-(CH$_2$PiPr$_2$)$_2$}] is a highly efficient precatalyst for DH of aryl ketones (0.05 mol-% cat., 4 atm. H_2, 25°C) upon activation with base (0.1 mol-% KOtBu).[74e] A MLC mechanism was proposed based on PNP ligand reversible de-/aromatization. Similarly, Casey and co-workers used an iron(II) analogue of Shvo's MLC

[82] a) M. Bertoli, A. Choualeb, A. J. Lough, B. Moore, D. Spasyuk, D. G. Gusev, *Organometallics* **2011**, *30*, 3479; b) M. Bertoli, A. Choualeb, D. G. Gusev, A. J. Lough, Q. Major, B. Moore, *Dalton Trans.* **2011**, *40*, 8941.

[83] T. W. Graham, C.-W. Tsang, X. Chen, R. Guo, W. Jia, S.-M. Lu, C. Sui-Seng, C. B. Ewart, A. Lough, D. Amoroso, K. Abdur-Rashid, *Angew. Chem.* **2010**, *122*, 8890; *Angew. Chem. Int. Ed.* **2010**, *49*, 8708.

[84] A. Friedrich, M. Drees, M. Käß, E. Herdtweck, S. Schneider, *Inorg. Chem.* **2010**, *49*, 5482.

[85] M. A. Iron, E. Ben-Ari, R. Cohen, D. Milstein, *Dalton Trans.* **2009**, 9433.

[86] P. O. Lagaditis, A. J. Lough, R. H. Morris, *Inorg. Chem.* **2010**, *49*, 10057.

[87] P. O. Lagaditis, A. J. Lough, R. H. Morris, *J. Am. Chem. Soc.* **2011**, *133*, 9662.

catalyst, [Fe{η^5-C$_5$OH-2,5-(SiMe$_3$)$_2$-3,4-(CH$_2$)$_4$}H(CO)$_2$], for chemoselective ketone DH.[88] These examples emphasize that the MLC concept can be instrumental to establish efficient catalysts using more sustainable base metals, like iron. Their preference both for higher spin states and for formal 1-electron rather than 2-electron (e.g. oxidative addition / reductive elimination) redox chemistry generally results in fundamentally different reactivity compared with the precious metals. In analogy to hydrogenase (see above), the strong field ligands used in these examples (e.g. CO) stabilize an electronic low spin configuration, which is critical to enable H$_2$ binding to the metal. Furthermore, the MLC H$_2$-addition/elimination reactions result in no net change of the formal metal oxidation state throughout the catalytic cyle. A conceptually related approach is provided by the use of redox non-innocent ligands for catalysis.[89] They can stabilize catalytic intermediates by intramolecular metal-ligand electron transfer to attenuate high oxidation state changes of the metal. Chirik's pyridine diimine iron complexes, which catalyze hydrogenation, hydrosilylation, and olefin cyclization reactions, are particularly impressive examples.[90] However, the discussion of this concept is beyond the scope of this review.

Beyond organic synthesis: MLC catalysts for sustainable catalysis

MLC catalysts, most prominently Noyori-Moris-, Shvo-, and Milstein-type catalysts, have been extensively utilized in the past 10 years for organic synthesis, particularly the chemo- and stereoselective functionalization of polar functional groups (e.g. ketones, imines, esters, alcohols, amines) via hydrogenation and, in reverse, by dehydrogenative coupling reactions. These applications were discussed in several comprehensive review articles and book chapters.[8b,33,35,63,75,76,91] MLC catalysis is therefore particularly attractive for the transformation of polar, 'inorganic' molecules in the context of sustainable catalysis, e.g. for CO$_2$ conversion, water splitting, or chemical hydrogen storage. Although this distinction is not mechanistically justified, the general lack of comprehensive coverage provides sufficient motivation for a discussion of this work in the succeeding sections.

[88] C. P. Casey, H. Guan, *J. Am. Chem. Soc.* **2009**, *131*, 2499.

[89] Recent highlight articles: a) P. J. Chirik, K. Wieghardt, *Science* **2010**, *327*, 794; b) W. I. Dzik, J. I. van der Vlugt, J. N. H. Reek, B. de Bruin, *Angew. Chem.* **2011**, *123*, 3416; *Angew. Chem. Int. Ed.* **2011**, *50*, 3356.

[90] a) S. C. Bart, E. Lobkovsky, P. J. Chirik, *J. Am. Chem. Soc.* **2004**, *126*, 13794; b) M. W. Bouwcamp, A. C. Bowman, E. Lobkowsky, P. J. Chirik, *J. Am. Chem. Soc.* **2006**, *128*, 13340; c) S. C. Bart, K. Chlopek, E. Bill, M. W. Bouwcamp, E. Lobkovsky, F. Neese, K. Wieghardt, P. J. Chirik, *J. Am. Chem. Soc.* **2006**, *128*, 13901.

[91] *Bifunctional Molecular Catalysis*, Eds. T. Ikariya, M. Shibasaki, **2011**, Springer, Heidelberg.

Dehydrogenation of borane-amines: hydrogen storage and materials synthesis.

Among the numerous small molecules with high hydrogen content that were proposed as safe hydrogen vectors for chemical H_2 storage, borane-amine adducts, particularly parent ammoniaborane (H_3N-BH_3, AB), were arguably studied most extensively.[92] Besides hydrogen storage, controlled borane-amine dehydrocoupling potentially offers access to novel inorganic polymers and B-N-ceramics.[93] The polarization of protic and hydridic *N-* and *B-* terminal hydrogen substituents, respectively, suggests an analogy with polar functional groups, such as alcohols (rather than isoelectronic ethane), and therefore the suitability of MLC alcohol dehydrogenation catalysts for AB functionalization.
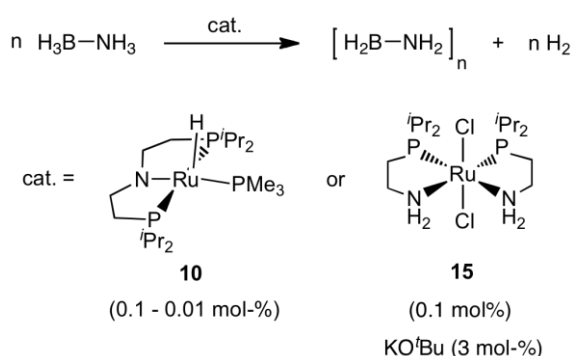
Scheme B-5.12: Dehydrocoupling of ammonia borane with Noyori-type MLC catalysts.

Fagnou and Schneider independently reported that [$RuCl_2(H_2NCH_2CH_2PiPr_2)_2$] (**15**) / KO*t*Bu (30 equiv.) or **10** (without base) catalyse the release of H_2 (1 equiv.) from AB solutions with high activities (TOF = ~20 s^{-1}) and turn over numbers (TON > 3000) at room temperature (Scheme B-5.12).[79,94] ^{11}B-MQ-MAS analysis of the AB dehydrocoupling product obtained with **10** suggests formation of linear polyaminoborane H_3N-[H_2B-H_2N]$_n$-BH_3, isoelectronic with polyethylene.[95] Likewise, dehydrocoupling of monosubstituted MeH_2N-BH_3 produces linear poly-*N*-methylaminoborane MeH_2N-[H_2B-$MeHN$]$_n$-BH_3 of high molecular mass.[96] Dehydrocoupling of Me_2HN-BH_3 with **10** gives aminoborane dimer

[92] a) F. H. Stephens, V. Pons, R. T. Baker, *Dalton Trans.* **2007**, 2613; b) C. W. Hamilton, R. T. Baker, A. Staubitz, I. Manners, *Chem. Soc. Rev.* **2009**, *38*, 279; c) N. C. Smythe, J. C. Gordon, *Eur. J. Inorg. Chem.* **2010**, 509; d) A. Staubitz, A. P. M. Robertson, I. Manners, *Chem. Rev.* **2010**, *110*, 4079.

[93] a) T. J. Clark, K. Lee, I. Manners, *Chem. Eur. J.* **2006**, *12*, 8634; b) A. Staubitz, A. P. M. Robertson, M. E. Sloan, I. Manners, *Chem. Rev.* **2010**, *110*, 4023.

[94] N. Blaquiere, S. Diallo-Garcia, S. I. Gorelsky, D. A. Black, K. Fagnou, *J. Am. Chem. Soc.* **2008**, *130*, 14034.

[95] A. Friedrich, *PhD Thesis*, Technische Universität München, **2010**.

[96] A. Staubitz, M. E. Sloan, A. Robertson, A. Friedrich, S. Schneider, P. J. Gates, J. Schmedt auf der Günne, I. Manners, *J. Am. Chem. Soc.* **2010**, *132*, 13332.

$[Me_2N-BH_2]_2$, with linear diborazane $Me_2HN-H_2B-Me_2N-BH_3$ as intermediate.[97] Baker recently used $[RuCl_2(H_2NCH_2CH_2PtBu_2)_2]$ as catalyst for H_2-release from mixtures of AB and *N-sec*-butylamineborane.[98]

Based on DFT calculations, Fagnou proposed a mechanism with release of free H_2N-BH_2 by concerted H^+/H^- transfer from AB to an in situ formed ruthenium amido species and subsequent turn over limiting H_2 elimination from the resulting hydrido amine complex (Scheme B-5.13). In fact, high N-H/D and B-H/D kinetic isotope effects were found for precatalyst **10**, indicative of concerted proton and hydride bond cleavage in the rate determining step.[79] Furthermore, using amine complex **1** as precatalyst comparable TOF's are obtained,[97] while precatalyst $[Ru(H)_2PMe_3\{MeN(CH_2CH_2PiPr_2)_2\}]$ with a tertiary amine ligand exhibits considerably slower dehydrocoupling rates.[95] However, some observations remain unaccounted for by this mechanism: The slow experimental and calculated rates for H_2-loss from **1** are incongruent with the rapid catalytic borane-amine dehydrogenation.[37f,84] Furthermore, the rate law for AB dehydrogenation with **10** exhibits first order dependence in substrate but should be zeroth order according to Fagnou's mechanism.
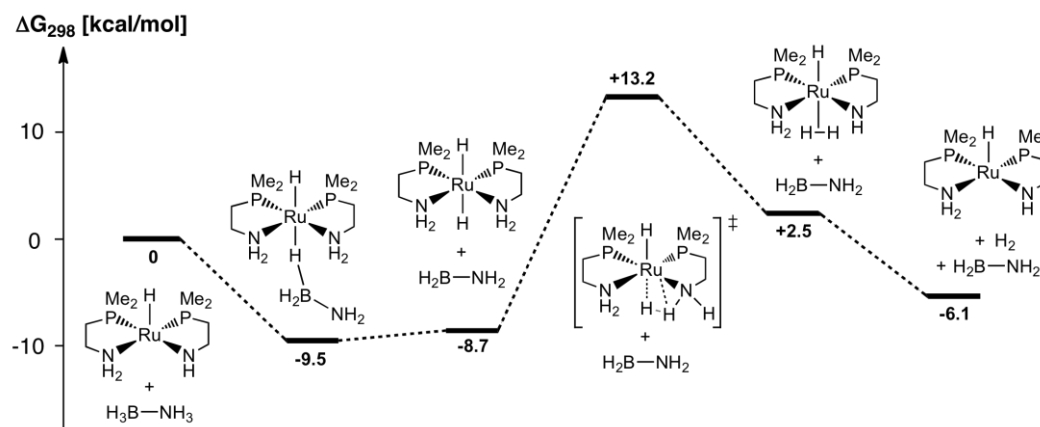
Scheme B-5.13: Proposed mechanism for cooperative AB dehydrogenation with ruthenium amides.

Baker and co-workers reported the dehydrocoupling of AB to give more than 2.5 equiv. H_2 and polyborazylene using 5 mol-% $Ni(COD)_2$ with 2 equiv. of Enders' *N*-heterocyclic carbene (NHC), [CN(Ph)NC(Ph)N(Ph)], as catalyst at 60 °C.[99] In a theoretical study, Yang and Hall proposed the unusual cooperativity of the carbene ligand acting as a proton relay in the

[97] A. Friedrich, M. Drees, S. Schneider, *Chem. Eur. J.* **2009**, *15*, 10339.

[98] S. S. Mal, F. H. Stephens, R. T. Baker, *Chem. Commun.* **2011**, *47*, 2922.

[99] R. J. Keaton, J. M. Blacquiere, R. T. Baker, *J. Am. Chem. Soc.* **2007**, *129*, 1844.

catalytic cycle.[100] Detailed computational examinations by Musgrave and co-workers suggested a slightly modified overall mechanism (Scheme B-5.14) but confirmed the cooperative behaviour of the carbene ligand in the N–H activation step.[101] Alternatively, off-metal H_2 transfer from AB to free carbene and subsequent nickel catalyzed dehydrogenation of the 2,3-dehydro-1,2,4-triazolidine NHC geminal hydrogenation product provides an energetically competitive pathway.[102] However, this kind of NHC-cooperativity in proton transfer reactions might be more common given that NHC's are popular ligands in DH and TH (see also Scheme B-5.20).[103]
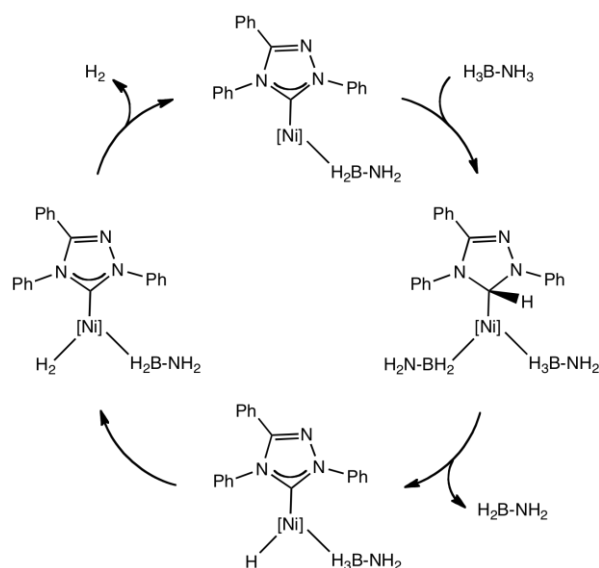
Scheme B-5.14: Simplified catalytic cycle proposed for Ni/carbene catalyzed AB dehydrogenation.

Conley and Williams used Shvo's catalyst (5 mol-%) to release 2.0 equiv. H_2 and borazine from AB at 70 °C.[104] The authors reported a rate law which is independent on substrate and first order in catalyst, attributed to a MLC mechanism with turn-over limiting O-H/Ru-H dihydrogen elimination. Other multifunctional catalysts for amine-borane dehydrogenation include frustrated Lewis-pairs.[105] In a related approach, Wass and co-workers reported the

[100]X. Yang, M. B. Hall, *J. Am. Chem. Soc.* **2008**, *130*, 1798.

[101]P. M. Zimmerman, A. Paul, C. B. Musgrave, *Inorg. Chem.* **2009**, *48*, 5418.

[102]P. M. Zimmerman, A. Paul, Z. Zhang, C. B. Musgrave, *Angew. Chem.* **2009**, *121*, 2235; *Angew. Chem. Int. Ed.* **2009**, *48*, 2201.

[103]S. Díez-González, N. Marion, S. P. Nolan, *Chem. Rev.* **2010**, *109*, 3612.

[104]B. L. Conley, T. J. Williams, *Chem. Commun.* **2010**, *46*, 4815.

[105]a) A. J. M. Miller, J. E. Bercaw, *Chem. Commun.* **2010**, *46*, 1709; b) Y. Guo, X. He, Z. Li, Z. Zou, *Inorg. Chem.* **2010**, *49*, 3419.

rapid H_2 release from $R_2HN–BH_3$ (R = H, Me, ^{i}Pr) catalyzed by the zirconocene complexes $[(C_5R_5)_2Zr(OC_6H_4$-o-$P^tBu_2)][B(C_6F_5)_4]$ (R = H, Me) and the formation of polyaminoborane $(H_2NBH_2)_n$ (with minor amounts of borazine), diaminoborane $(Me_2NBH_2)_2$, and aminoborane $^iPr_2NBH_2$, respectively.[106] These complexes are far superior to the previously reported group 4 catalysts for borane-amine dehydrogenation.[107] H_2 heterolysis was also demonstrated, giving hydrido phosphonium complex $[(C_5Me_5)_2Zr(H)(OC_6H_4$-$o$-$PH^tBu_2)]^+$ by hydrogen splitting across the weak interaction of the metal center with the hemilabile phosphorous ligand. Based on this observation and deuterium labeling experiments a MLC mechanism was proposed (Scheme B-5.15).
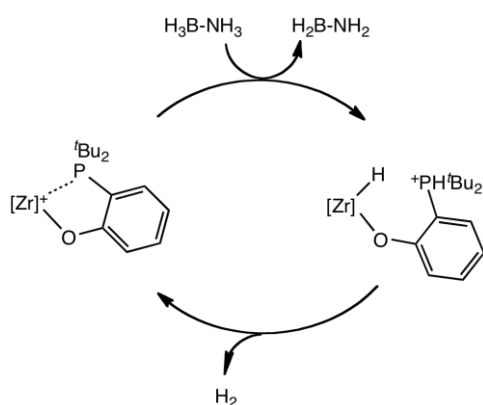
Scheme B-5.15: Proposed mechanism for AB dehydrogenation with group 4 MLC catalysts ([Zr] = $(C_5R_5)_2Zr$; R = H, Me).

Hydrogenation of CO_2 and N_3^-: cooperative formiate, methanol, and ammonia generation

Chemical transformations which make use of the greenhouse gas CO_2 are highly desirable goals.[108] As an entry to sustainable synthesis or chemical energy storage with this C_1 building block, CO_2 hydrogenation is an attractive reaction, if the hydrogen is not of fossil origin but arises from sustainable sources, such as water electrolysis. However, this reaction faces several challenges, particularly with respect to selectivity for the hydrogenation

[106]A. M. Chapman, M. F. Haddow, D. F. Wass, *J. Am. Chem. Soc.* **2011**, *133*, 8826.

[107]a) T. J. Clark, C. A. Russel, I. Manners, *J. Am. Chem. Soc.* **2006**, *128*, 9582; b) D. Pun, E. Lobkovsky, P. J. Chirik, *Chem Commun.* **2007**, 3297; c) M. E. Sloan, A. Staubitz, T. J. Clark, G. C. Lloyd-Jones, I. Manners, *J. Am. Chem. Soc.* **2010**, *132*, 3831.

[108]a) P. G. Jessop, T. Ikariya, R. Noyori, *Chem. Rev.* **1995**, *95*, 259; b) W. Leitner, *Angew. Chem.* **1995**, *107*, 2391; *Angew. Chem. Int. Ed. Engl.* **1995**, *34*, 2207; c) P. G. Jessop, F. Joo, C.-C. Tai, *Coord. Chem. Rev.* **2004**, *248*, 2425; d) T. Sakakura, J.-C. Choi, H. Yasuda, *Chem. Rev.* **2007**, *107*, 2365; e) M. R. DuBois, D. L. DuBois, *Acc. Chem. Res.* **2009**, *42*, 1974; f) C. Federsel, R. Jackstell, M. Beller, *Angew. Chem.* **2010**, *122*, 6392; *Angew. Chem. Int. Ed.* **2010**, *49*, 6254.

products HCO_2H, CO, or CH_3OH. Turn over frequencies for the hydrogenation to formic acid with benchmark catalyst $[RuXY(PMe_3)_4]$ (X, Y = H, Cl, OAc) and other catalysts are enhanced in the presence of water, alcohol, and amines.[109,110] These observation sparked speculations about ROH or R_3NH^+ to serve as proton donor in an ionic mechanism aiding concerted H^+/H^- transfer to CO_2 and/or H_2 heterolysis.[108c] Initial attempts to utilize ligand cooperation by tethering an amine as an internal base to a CpRu complex exhibited only limited success.[111] Hazari and co-workers recently reported the particularly efficient (TON up to 348000; TOF up to 18670 h^{-1}) hydrogenation of CO_2 to formiate in basic, aqueous solution using an iridium formiate MLC catalyst (Scheme B-5.16).[112] The authors proposed the concerted outer-sphere transfer of H^+/H^- to the substrate, analogous to Noyori-type ketone hydrogenation, as turn-over limiting step of the catalytic cyle. They further emphasized a correlation of hydride *trans*-ligand labilization with the thermodynamic driving force for outer-sphere hydride transfer, as similarly pointed out for Noyori-type hydrogenation (see above).
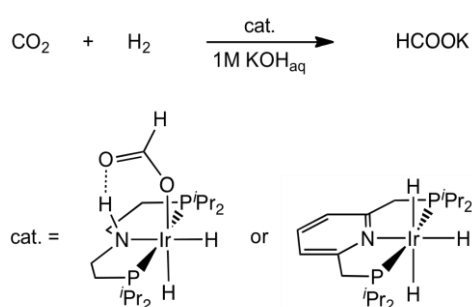
Scheme B-5.16: Hydrogenation of CO_2 to formiate with iridium catalysts.
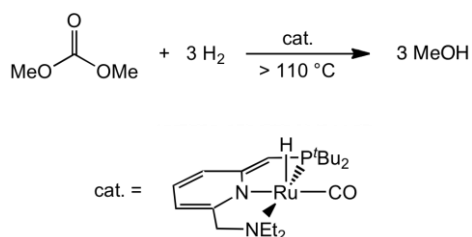
Scheme B-5.17: Hydrogenation of dimethylcarbonate to methanol catalyzed by a dearomatized PNN pincer complex.

[109]a) P. G. Jessop, T. Ikariya, R. Noyori, *Nature* **1994**, *368*, 231; b) P. G. Jessop, Y. Hsiao, T. Ikariya, R. Noyori, *J. Am. Chem. Soc.* **1996**, *118*, 344; c) P. Munshi, A. D. Main, J. C. Linehan, C.-C. Tai, P. G. Jessop, *J. Am. Chem. Soc.* **2002**, *124*, 7963.

[110]C. P. Lau, S. M. Ng, G. Jia, Z. Lin, *Coord. Chem. Rev.* **2007**, *251*, 2223.

[111]H. S. Chu, C. P. Lau, K. Y. Wong, *Organometallics* **1998**, *17*, 2768.

[112]T. J. Schmeier, G. E. Dobereiner, R. H. Crabtree, N. Hazari, *J. Am. Chem. Soc.* **2011**, *133*, 9274.

Pyridine based PNP complex [Ir(H)$_3${NC$_5$H$_3$-2,6-(CH$_2$PiPr$_2$)$_2$}] is a highly active catalyst for CO_2 hydrogenation to formate, as well (Scheme B-5.16).[113] The authors proposed a mechanism with cooperative behaviour of the pincer backbone benzylic CH_2 group by de-/aromatization. On the contrary, two independent computational studies of the reaction suggest that deprotonation of a dihydrogen complex intermediate by external base (OH$^-$) should be kinetically favoured over intramolecular H_2 heterolysis.[114] Further experimental data will be necessary to confirm or exclude the originally proposed MLC mechanism. However, Milstein and co-workers most recently presented the quantitative hydrogenation (40 atm H_2; 145 °C) of dimethylcarbonate O=C(OMe)$_2$ to methanol with a dearomatized PNN pincer complex (TON = 2500) in the absence of base (Scheme B-5.17).[115] Reversible H_2 addition to the catalyst gives dihydride [Ru(H)$_2$(CO){NC$_5$H$_3$(CH$_2$P^{t}Bu$_2$)(CH$_2$NEt$_2$)}], which in turn hydrogenates dimethylcarbonate in the absence of H_2 stoichiometrically by backbone dearomatization, hence supporting a MLC mechanism. This reaction provides an unprecedented example for the selective, homogeneous hydrogenation of a CO_2 derivative beyond formic acid. In comparison, benchmark CO_2-hydrogenation precatalyst [RuCl(OAc)(PMe$_3$)$_4$] failed to catalyze the hydrogenation of methylcarbonate MeOCO$_2^-$.[109b]
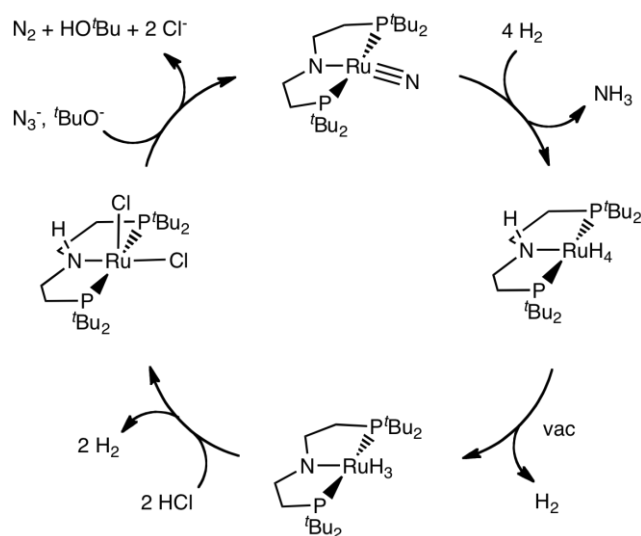

Scheme B-5.18: Synthetic cycle for the hydrogenation of azide to ammonia mediated by [RuCl$_2${HN(CH$_2$CH$_2$PtBu$_2$)$_2$}].

[113]R. Tanaka, M.Yamashita, K. Nozaki, *J. Am. Chem. Soc.* **2009**, *131*, 14168.

[114]a) M. S. G. Ahlquist, *J. Mol. Catal. A* **2010**, *324*, 3-8; b) X. Yang, *ACS Catal.* **2011**, *1*, 849.

[115]E. Balaraman, C. Gunanathan, J. Zhang, L. J. W. Shimon, D. Milstein, *Nature Chem.* **2011**, *3*, 609.

A synthetic cycle for the hydrogenation of azide to ammonia and dinitrogen ($HN_3 + H_2 \rightarrow NH_3 + N_2$) was recently demonstrated (Scheme B-5.18).[116] [RuCl$_2$\{HN(CH$_2$CH$_2$PtBu$_2$)$_2$\}] gives d^4 nitrido complex [RuN\{N(CH$_2$CH$_2$PtBu$_2$)$_2$\}] in the presence of azide and base. The decisive step in the cycle is defined by hydrogenolysis of the terminal nitrido ligand to ammonia. Kinetic measurements and DFT calculations indicate the two initial steps, i.e. addition of H$_2$ across the Ru-amido bond and the subsequent first proton transfer to the nitrido ligand, to be rate determining. This reaction is of interest in the context of Haber-Bosch model chemistry. However, reactivity of nitrido complexes with H$_2$ is rarely observed,[117] emphasizing the benefits of MLC catalysts. Notably, strongly related nitride complex [RuN\{N(SiMe$_2$CH$_2$PtBu$_2$)$_2$\}] was reported not to react with H$_2$.[118]
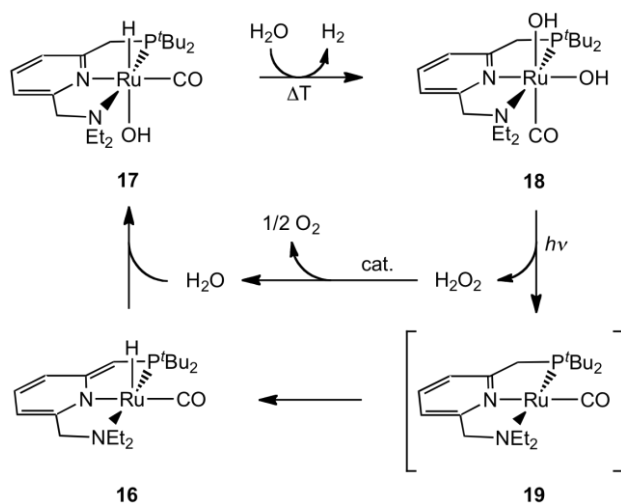
Scheme B-5.19: Proposed mechanism for stepwise thermal and photochemical water splitting with a ruthenium MLC complex.

[116]B. Askevold, J. T. Nieto, S. Tussupbayev, M. Diefenbach, E. Herdtweck, M. C. Holthausen, S. Schneider, *Nature Chem.* **2011**, *3*, 532.

[117]a) S. D. Brown, M. P. Mehn, J. C. Peters, *J. Am. Chem. Soc.* **2005**, *127*, 13146; b) J. Schöffel, A. Y. Rogachev, S. DeBeer George, P. Burger, *Angew. Chem.* **2009**, *121*, 4828; *Angew. Chem. Int. Ed.* **2009**, *48*, 4734.

[118]a) A. Walstrom, M. Pink, X. Yang, J. Tomaszewski, M.-H. Baik, K. G. Caulton, *J. Am. Chem. Soc.* **2005**, *127*, 5330; b) A. Walstrom, H. Fan, M. Pink, K. G. Caulton, *Inorg. Chim. Acta* **2010**, *363*, 633.

Cooperative water splitting and organometallic fuel-cells: MLC catalysts for energy conversion

Milstein and co-workers utilized MLC catalysts for water splitting with successive thermal H_2 generation and photochemical generation of O_2 (Scheme B-5.19).[119] Dearomatized complex **16** adds water across the metal and the ligand backbone to form hydroxo complex **17** which releases H_2 upon solvolysis with additional water. Computational studies suggest rate determining formation of an intermediate dihydrogen complex in this step after proton transfer from the benzylic position of the ligand backbone to the hydride of **17**.[120] Irradiation of the dihydroxo complex **18** at $\lambda > 320$ nm in the presence of H_2O resulted in the detection of O_2 and recycling of the hydroxy hydride complex. $^{16/18}$O-labelling suggests intramolecular O–O bond formation. Reductive H_2O_2 elimination and formation of **19** was proposed to proceed on the triplet spin surface in terms of two-state-reactivity.[120b,121] Instead of the originally proposed formation of **16** prior to H_2O addition, oxidative proton transfer from the 'amine-arm' to the metal might be kinetically favoured for this step.[120b] Although this cycle produced O_2 only in stoichiometric amounts it can be of high relevance for future catalyst design: Instead of H_2O activation by multiple metal centers, monometallic MLC platforms can also effectively activate water using the cooperating ligand as an intramolecular proton relay.[122]

[119]S. W. Kohl, L. Weiner, L. Schwartsburd, L. Konstantinovski, L. J. W. Shimon, Y. Ben-David, M. A. Iron, D. Milstein, *Science* **2009**, *324*, 74.

[120]a) J. Li, Y. Shiota, K. Yoshizawa, *J. Am. Chem. Soc.* **2009**, *131*, 13584; b) X. Yang, M. B. Hall, *J. Am. Chem. Soc.* **2010**, *132*, 120.

[121]a) D. Schröder, S. Shaik, H. Schwarz, *Acc. Chem. Res.* **2000**, *33*, 139; b) R. Poli, J. Harvey, *Chem. Soc. Rev.* **2003**, *32*, 1.

[122]D. G. H. Hetterscheid, J. I. van der Vlugt, B. de Bruin, J. N. H. Reek, *Angew. Chem.* **2009**, *121*, 8324; *Angew. Chem.* **2009**, *48*, 8178.

Llobet, Albrecht, and co-workers presented efficient catalysts with a chelating, abnormal triazolidene ligand, $[Ru(CNMe)_4\{CN(R)NN(CH_3)C–C_5H_4N\}][OTf]_2$ (R = Me, Et, ^{i}Pr, Ph), for the oxidation of water to O_2 with sacrificial Ce^{IV} as oxidizing agent.[123] Chemical stability of the ligand is indicated by the absence of CO_2 side product from oxidative degradation. Most importantly, these catalysts are highly superior to sterically comparable normal imidazolidene complex $[Ru(CNMe)_4\{CN(CH_3)CHCHN–C_5H_4N\}]^{2+}$ with respect to TON and TOF. The improved catalytic performance of the mesoionic triazolidene as compared with imidazolidene based complexes was attributed to possible ligand cooperativity by tautomeric activation of a coordinated water ligand (Scheme B-5.20).
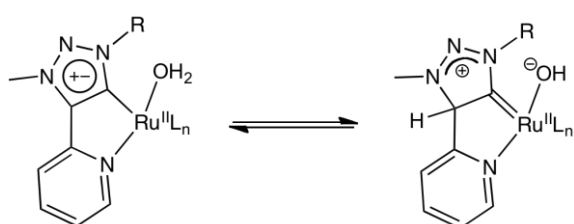

Scheme B-5.20: Proposed tautomerization of water with mesoionic abnormal triazolidene ligands.

Grützmacher and co-workers reported the oxidation of alcohols in the presence of water, methanol, or amines under TH or aerobic conditions to give the corresponding carbonic acid, methyl esters, and amides, respectively.[124] Besides the synthetic utility, these oxidations can drive an alcohol based fuel cell. Deposition of $[Rh(OTf)\{HN(C_{15}H_{11})_2\}(PPh_3)]$ (OTf$^-$ = $OSO_2CF_3^-$) onto a conductive carbon support enabled the development of an organometallic fuel cell (OMFC).[125] In the anodic reaction of the OMFC, ethanol is oxidized to acetic acid. Electrochemical examinations and homogeneous model reactions suggest that the molecular catalyst stays structurally intact and operates via a MLC dehydrogenation mechanism (Scheme B-5.20).

[123]L. Bernet, R. Lalrempuia, W. Ghattas, H. Mueller-Bunz, L. Vigara, A. llobet, M. Albrecht, *Chem. Commun.* **2011**, *47*, 8058.

[124]a) T. Zweifel, J.-V. Naubron, H. Grützmacher, *Angew. Chem.* **2009**, *121*, 567; *Angew. Chem. Int. Ed.* **2009**, *48*, 559; b) S Annen, T. Zweifel, F. Ricatto, H. Grützmacher, *ChemCatChem* **2010**, *2*, 1286; c) M. Trincado, K. Kühnlein, H. Grützmacher, *Chem. Eur. J.* **2011** (DOI: 10.1002/chem.201101084).

[125]S. P. Annen, V. Bambagioni, M. Bevilacqua, J. Filippi, A. Marchionni, W. Oberhauser, H. Schönberg, F. Vizza, C. Bianchini, H. Grützmacher, *Angew. Chem.* **2010**, *122*, 7387; *Angew. Chem. Int. Ed.* **2010**, *49*, 7229.
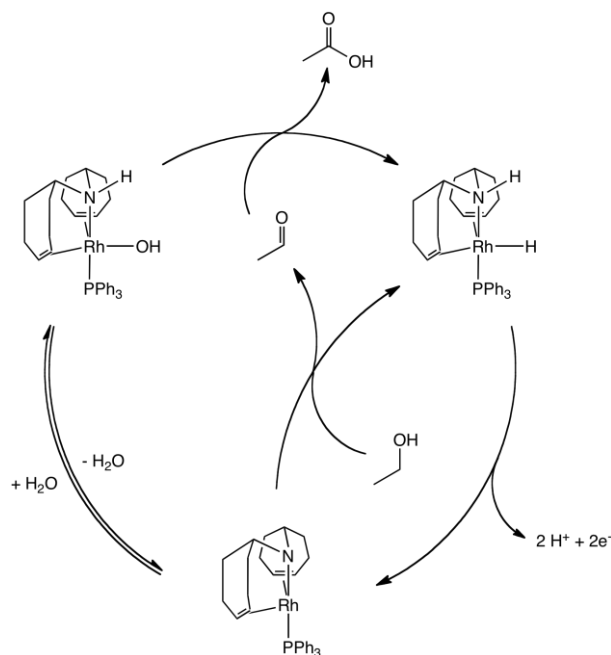
Scheme B-5.20: Proposed mechanism for anodic ethanol oxidation with an MLC-based organometallic fuel cell. The chelating ligand abbreviates CNC ligand **A** (Figure B-5.3).

5.4 Concluding remarks

In this review we tried to emphasize the benefit of applying concepts across the traditional borders of homogeneous, heterogeneous, and bio-catalysis. Selected examples were presented that demonstrate how the design of functional ligands can enhance catalyst performance and afford new catalytic transformations, particularly in the context of challenges provided by sustainable feedstocks. Many other exciting examples of ligand cooperativity, e.g. the rapidly growing use of redox non-innocent ligands in catalysis,[89] could not be covered. Instead, we tried to emphasize some guidelines for functional ligand design.

The synthesis of molecular aluminum hydroxy compounds provides easy access to oxo-bridged heterobimetallic assemblies, e.g. by linking them to metallocene precatalysts. Such compounds do not only provide homogeneous models for isolated transition metal sites on solid oxide supports of heterogeneous catalyts but exhibit high catalytic activity, e.g. in homogeneous olefin polymerization or hydroamination. The enhanced catalytic activity is attributed to the Lewis acidity of the functional alumoxide ligands and the formation of a potential binding site for other Lewis acidic activators, such as MAO.

MLC catalysts have found widespread use for polar functional group transformations through heterolytic bond activation reactions. Hence, their reactivity makes them particularly interesting in the context of renewable feedstock functionalization. Hydrogenation and dehydrogenation (dehydrocoupling) reactions using MLC catalysts were examined most

extensively. However, other catalytic reactions with MLC catalysts were reported as well. For example, rhodium thiolate complexes catalyze ketone hydrosilylation attributed to cooperative Si–H splitting along the covalent Rh–S bond.[67] Given the mechanistic similarities of H–E (E = H, Si, C) activation by late transition metals through M··H–E σ-complexes,[126] selective C–H bond functionalizations with MLC catalysts provide an important goal for further developments. In fact, the stoichiometric addition of sp^3, sp^2, and sp C-H bonds across covalent M–N bonds is well known.[127]

Catalytic activities for new MLC platforms remain difficult to predict. H–E addition across the MLC fragment will increase the metal coordination number by one as compared with two for 'traditional' metal centered oxidative addition. Hence, kinetic barriers arising from ligand sphere rearrangement can be attenuated. In case of hydrogenation reactions, the examples discussed here suggest that the thermochemistry of H_2 addition generally allows for the estimation of trends. Thermoneutral addition/elimination provides the ideal situation to avoid excessive stabilization or destabilization of intermediates, expressed in a wide span of the catalytic potential energy surface. Hence, within a given series of related catalysts qualitative trends can be estimated from the parameters which strongly influence M–H bond energies, such as metal oxidation state, charge, or the ligand in *trans*-position to the formed M–H bond. If no other steps with particularly high kinetic barriers dominate the overall catalytic rate, these guidelines will hold true for other H–E functionalization reactions as well. Finally, the addition of H–E across the MLC framework proceeds without a change in the formal oxidation state of the metal center. With the smaller tendency of the 3*d* vs. 4*d* and 5*d* metals to engage in 2-electron redox reactions, such as oxidative addition / reductive elimination, the use of cooperating ligands can be instrumental in achieving a highly desirable goal, i.e. the more sustainable use of earth-abundant base metal catalysts in the future.[89]

---

[126] a) G. J. Kubas in *Metal Dihydrogen and σ-Bond Complexes* (Ed. J. P. Fackler), Kluwer Academic / Plenum Publishesr, New York, **2001**; b) R. Perutz, S. Sabo-Etienne, *Angew. Chem.* **2007**, *119*, 2630; *Angew. Chem. Int. Ed.* **2007**, *46*, 2578.

[127] a) D. Rais, R. G. Bergman, *Chem. Eur. J.* **2004**, *10*, 3970; b) A. N. Walstrom, L. A. Watson, M. Pink, K. G. Caulton, *Organometallics* **2004**, *23*, 4814; c) Y. Feng, M. Lail, N. A. Foley, T. B. Gunnoe, K. A. Barakat, T. R. Cundari, J. L. Petersen, *J. Am. Chem. Soc.* **2006**, *128*, 7982; d) D. Conner, K. N. Jayaprakash, T. R. Cundari, T. B. Gunnoe, *Organometallics* **2004**, *23*, 2724.

C Summary

This work aimed at the synthesis and characterization of late transition metal complexes with rare coordination geometries and oxidation states. The resulting electronic structures usually facilitate exceptional reactivities. Therefore, the coordination chemistry of ruthenium and iridium complexes with the ethylene bridged HPNP ligand was examined, which offered the possibility for versatile ligand functionalization by deprotonation or oxidative backbone dehydrogenation and provided thus synthetic access to amido, imido, enamido and dienamido late transition metal complexes. The π-basicity of the PNP fragment has a profound influence on the electronic structure in the synthesized electronically and coordinatively unsaturated complexes and allowed the electronic fine-tuning by simple oxidative dehydrogenation of the backbone and thus control of the ground state spin multiplicity. The strong π-basicity is furthermore responsible for ligand centered nucleophilicity and enables this type of ligand to participate in metal-ligand cooperativity.

The examination of d^6-d^8 dialkylamido PNP complexes by Schneider and co-workers already yielded important information about N$\rightarrow$M π-bonding in late transition metal complexes and allowed the introduction and utilization of this type of ligand in bifunctional catalysis.[1] Among others, it was already demonstrated that Iridium(I) amido complexes [IrL{PNP^{iPr}}] (L = CO, COE and C_2H_4) could be obtained by deprotonation of [IrL{HPNP^{iPr}}], which are thermally relatively robust towards β-H elimination. A very electron-rich Ir{PNP} fragment in the dialkylamido complexes was expressed by a large hypsochromic shift of the C-O stretching vibration in [Ir(CO)(PNP^{iPr})] ($\Delta \nu = 68$ cm^{-1}) and the large olefin ^{13}C NMR spectroscopic high-field shifts in [Ir(olefin)(PNP^{iPr})] ($\Delta\delta C_2H_4 = 22.1$ ppm; $\Delta\delta COE = 20.8$ ppm).[2]

Within this work, it was shown that the ligand *trans* to the nitrogen atom further exhibits a profound effect on the amine pK_a value, which varies over more than 7 orders of magnitude (in dmso) within the series L = CO [pK_a = 14.9(3)], COE [pK_a = 16.0(4)], PMe$_3$ [pK_a = 22.0(1)]. This trend could be rationalized by a N$\rightarrow$Ir$\rightarrow$L *push-pull*-interaction that stabilizes the N-Ir π^* orbital (HOMO) if the trans-Ligand L is a π-acceptor ligand (e.g. CO or olefins). A high nucleophilicity of the amido group towards C-nucleophiles was observed in

[1] a) A. Friedrich, Bifunctional *Transition Metal Amido Complexes: Cooperative H2 Activation and Catalytic Dehydrogenation, disertation*, TU München, 2010; b) J. Meiners, A. Friedrich, E. Herdtweck, S. Schneider, *Organometallics* **2009**, *28*, 633.

[2] A. Friedrich, R. Ghosh, R. Kolb, E. Herdtweck, S. Schneider, *Organometallics* **2009**, *28*, 708.

[Ir(PMe$_3$)(PNP^{iPr})], which is analog to reported [PdCl(PNP^{iPr})]. Therefore, the nitrogen atom attacked selectively MeOTf without formation of a possible iridium(III)methyl complex.[3]

The molecular structure and reactivity of transition metal complexes is strongly determined by the spin multiplicity. In principle, metal ions with a d^6 electronic configuration can develop a low-spin (S = 0), intermediate-spin (S = 1) and a high-spin (S = 2) configuration. A square-planar coordination geometry (D_{4h}) results in splitting of the d-orbital manifold into nonbonding d_{xy} (b_{2g}) and d_{xz}, d_{yz} (e_g), weakly antibonding d_{z^2} (a_{1g}), and antibonding $d_{x^2-y^2}$ (b_{1g}) orbitals. In case of 3d ions, a high-spin configuration was reported for Fe^{II} and Co^{II} complexes coordinated by weak-field ligands.[4] An intermediate-spin (S = 1, $(xy,yz,z^2)^5(xz)^1(x^2-y^2)^0$) is expected in d^6 ions for stronger ligand fields (Scheme C-1, A), as observed in Ferrous complexes like iron(II)porphyrinato and iron(II)bis(dithiolato).[5,6] However, examples of the heavier analogues are particularly rare and the few reported show an intermediate spin ground state (Scheme C-1, B). Nevertheless, the first square planar ruthenium(II) complex with a low spin configuration was reported within this work. The steric bulk of the ^{t}Bu-groups of the PNP pincer ligand enforces a square-planar coordination geometry, while the strong N→Ru π-donation of the dialkylamido PNP ligand destabilises the d$_{xz}$ orbital favouring a low-spin configuration (S = 0, $(xy,yz,z^2)^6(xz)^0(x^2-y^2)^0$) by overcompensation of the spin pairing energy (Scheme C-1, C). Remarkably, ^{1}H and ^{31}P NMR spectra of the diamagnetic complex exhibit unusual, temperature depending chemical shifts for the PNP pincer backbone protons and the phosphor atoms. The observation was rationalized by population of an excited, energetically low-lying triplet state. A numerical fitting of the NMR spectroscopic data allowed to estimate the thermodynamic parameters of the singlet-triplet transition ($\Delta H = 10.6 \pm 0.3$ kJ mol^{-1}; $\Delta S = 4.2 \pm 0.8$ J mol^{-1} K^{-1}) which is in good agreement with DFT calculations.

[3] A. N. Marziale, E. Herdtweck, J. Eppinger, S. Schneider, *Inorg. Chem.* **2009**, *48*, 3699.

[4] S. A. Cantalupo, S. R. Fiedler, M. P. Shores, A. L. Rheingold, L. H. Doerrer, *Angew. Chem.* **2012**, 124, 1024; *Angew. Chem. Int. Ed.* **2012**, *51*, 1000.

[5] a) B. W. Dale, R. J. P. Williams, C. E. Johnson, T. L. Thorp, *J. Chem. Phys.* **1968**, *49*, 3441; b) H. Goff, G. N. La Mar, C. A. Reed, *J. Am. Chem. Soc.* **1977**, *99*, 3641.

[6] K. Ray, A. Begum, T. Weyhermüller, S. Piligkos, J. van Slageren, F. Neese, K. Wieghardt, *J. Am. Chem. Soc.* **2005**, *127*, 4403.
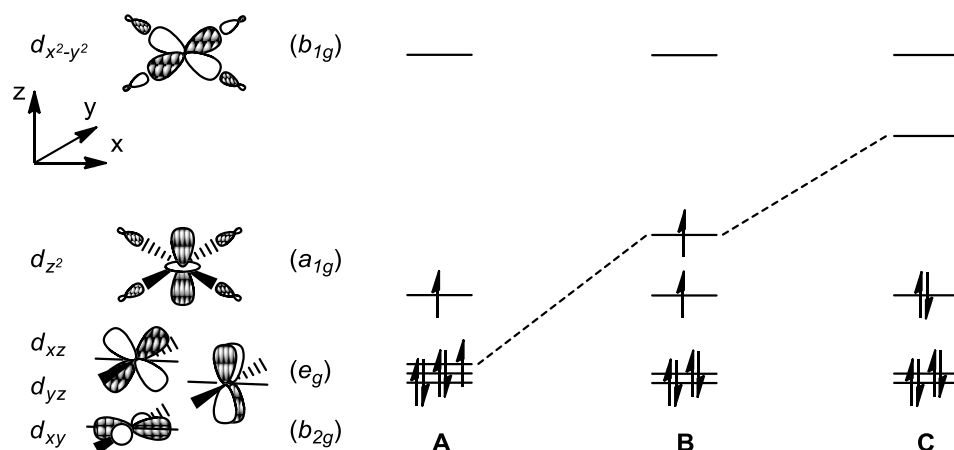
Scheme C-1: Qualitative *d*-orbital splitting of square-planar d^6 complexes with pure σ-donor ligands (A), with one weak π-donor ligand (B), and one strong π-donor ligand (C), respectively.

The exchange of the dialkylamido pincer ligand by Caulton's weaker N→Ru π-donating disilylamido ligand results in a diverse ground state spin multiplicity.[7] The strong N→Ru π-donation of the dialkylamido pincer ligand could be likewise reduced by dehydrogenation of either or both PNP pincer ethylene bridges to vinyl substituents (Scheme C-2), by acting of these as π-acceptors and thus favouring an intermediate spin ground state. NMR spectroscopic and SQUID magnetometry data of the paramagnetic complexes were in agreement with two unpaired electrons at room temperature. However, $\chi_M T$ dropped at low temperature to near zero indicating a nonmagnetic ground state. Fitting of the magnetic data to a zero-field-splitting (ZFS) spin-hamiltonian (SH) model resulted in considerable high positive axial ZFS parameters for the enamido ($D = +392$ cm^{-1}) and the dienamido ($D = +232$ cm^{-1}) complex. The resulting positive axial ZFS parameter indicated that the spin triplet ground state is further split into the non-magnetic $| S = 1, M_S = 0 \rangle$ microstate and the Kramer's doublet $| S = 1, M_S = \pm 1 \rangle$ at higher energies. A gradual spin-transition instead of ZFS could be excluded by an invariant Ru-N distance [1.994(2) Å] and N-Ru-Cl angle (180.0 °) in the molecular structure of the dienamido complex over a wide temperature range (30 – 200K) determined by single crystal X-ray diffraction. The fine-tuning of the electronic properties by simple dehydrogenation of the chelate backbone bridges towards corresponding enamido and dienamido ligands thus allowed to control the ground state spin multiplicity.

[7] L. A. Watson, O. V. Ozerov, M. Pink, K. G. Caulton, *J. Am. Chem. Soc.* **2003**, *125*, 8426.
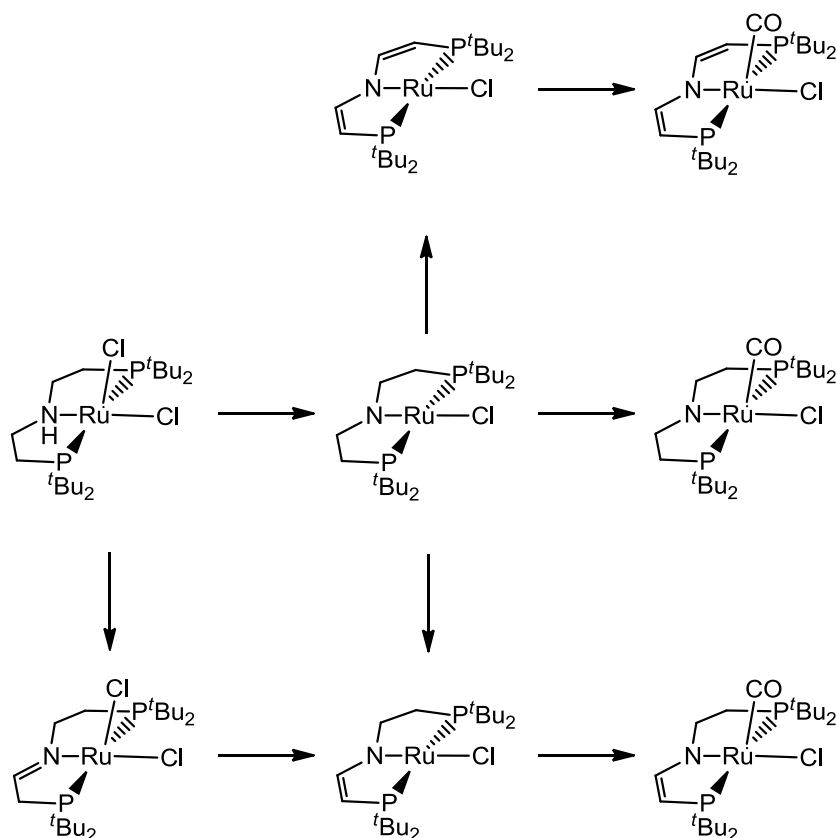
Scheme C-2: Overview of square-planar ruthenium dialkylamido PNP complexes and related five-coordinated carbonyl complexes.

CO stretching vibrations of the related five-coordinated carbonyl complexes allowed the preliminary scaling of the electronic effects of backbone dehydrogenation (Scheme C-2). The obtained CO stretching vibrations were observed in a relatively narrow range within less than 30 cm^{-1} (ν_{CO} = 1888 cm^{-1} for amido, ν_{CO} = 1896 cm^{-1} enamido and ν_{CO} = 1916 cm^{-1} for dienamido ruthenium complex). The obtained shift of the stretching vibration reflects the electronic influence of backbone dehydrogenation: oxidative ligand backbone functionalization reduces the N→Ru electron donation, owing to the stabilization of the N-lone-pair by C(p)-N(p) overlap.

The coordinatively and electronically highly unsaturated 14 VE complexes were shown as suitable platforms for the stabilization of multiply bonded ligands. The corresponding Ru^{IV} nitride could be obtained in high yields via salt metathesis with PPN-Azide and N$_2$ elimination (Scheme C-3). This rare example of a terminal nitrido complex with a d^n-electron count n > 2 exhibits a larger Ru≡N distance and lower stretching vibrations in comparison to Caulton's terminal nitride with related disilylamido PNP ligand ($\Delta d_{Ru≡N}$ = 0.06 Å and $\Delta\nu_{Ru≡N}$ = 54 cm^{-1}), indicating weaker bonding. This was attributed to the stronger π-donor ability of

the dialkylamido PNP ligand.[8] However, both molecular structures exhibit a considerable deviation from planarity by N-Ru-N angle bonding as a consequence of the trans-configuration of two π-donors (nitride and amide). A high nucleophilicity of the nitrido ligand was demonstrated on the one hand by lack of reactivity towards phosphanes and on the other hand by unusual N-C coupling with π-acidic CO (Scheme C-3). The selective formation of the isocyanato complex is contrary to Carlton's related nitrido complex. This observed reactivity can possibly be assigned to the stronger nucleophilic character of the nitride ligand.[9]
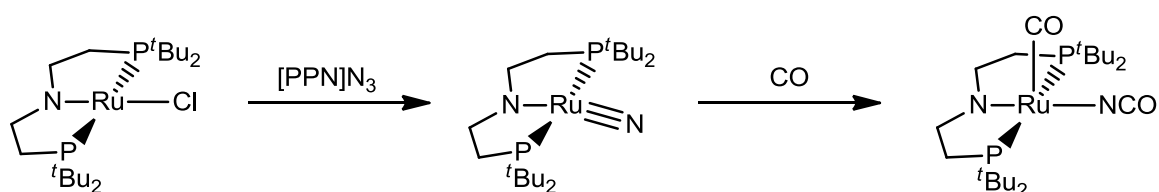
Scheme C-3: Synthesis of Ru^{IV} nitride and N-C coupling with π-acidic CO.

The functionalization of dinitrogen under mild conditions still represents a major challenge. Nitrido complexes could serve herein as model compounds to examine ammonia formation for N_2 hydrogenation at ambient conditions en route to a highly desirable homogeneous catalyst. Terminal nitrides (including Caulton's) are besides few reported examples surprisingly inert towards hydrogen.[9,10] Therefore, only partial M-N bond hydrogenolysis had been reported and no example existed for stochiometric hydrogenolysis of a nitrido ligand with H_2 to ammonia.[11] The presented Ru^{IV} nitride with dialkylamido PNP pincer ligand reacts in contrast readily at relative mild conditions (50 °C, 1 bar H_2) to polyhydride [RuH$_4$(HPNP^{t}Bu$_4$)] and unprecedented formation of ammonia in 85% yields (Scheme C-4).

[8] A. Walstrom, M. Pink, X. Yang, J. Tomaszewski, M.-H. Baik, K. G. Caulton, *J. Am. Chem. Soc.* **2005**, *127*, 5330.

[9] A. Walstrom, H. Fan, M. Pink, K. G. Caulton, *Inorg. Chim. Acta* **2010**, *363*, 633.

[10] M. P. Shaver, M. D. Fryzuk, *Adv. Synth. Catal.* **2003**, *345*, 1061.

[11] S. D. Brown, M. P. Mehn, J. C. Peters, *J. Am. Chem. Soc.* **2005**, *127*, 13146; b) J. Schöffel, A. Y. Rogachev, S. DeBeer George, P. Burger, *Angew. Chem.* **2009**, *121*, 4828; J. Schöffel, A. Y. Rogachev, S. DeBeer George, P. Burger, *Angew. Chem. Int. Ed.* **2009**, *48*, 4734.
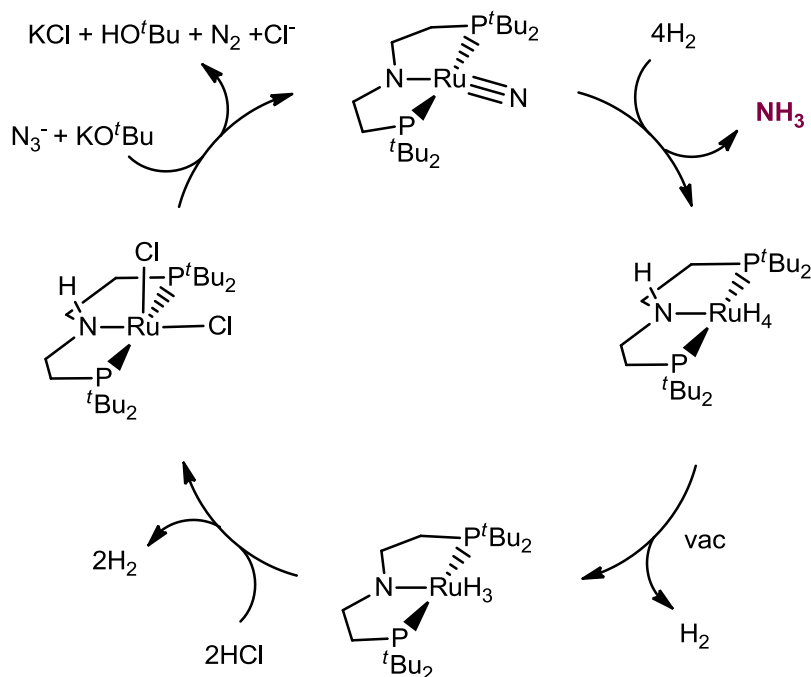
Scheme C-4: Synthetic cycle for the hydrogenation of azide to ammonia.

The yield of ammonia increased at lower reaction temperatures, however at the expense of smaller rates. Preliminary mechanistic examinations suggested pseudo first-order kinetics ($k_{298} = 5.1 \times 10^{-3}$ h^{-1} ± 0.1) and a kinetic isotope effect (KIE) of $k_H/k_D = 1.3 \pm 0.2$. Moreover, the kinetic measurements and computational calculations assigned the initial heterolytic hydrogen splitting across the Ru-amido bond and the subsequent first proton transfer to the nitrido ligand as rate determining, followed by stepwise proton transfer reactions to the nitride via amido and amine intermediates. The observed reactivity was attributed to two features of the Ru(PNP) platform: (1) The low formal oxidation state of the metal center in combination with the mentioned strong π-donation of the *trans*-amido ligand (with its unfavourable N-Ru-N 3c-4e π-interaction) contribute to a high nucleophilicity of the nitride ligand and induce a weakening of the Ru≡N bond. (2) Metal-ligand cooperative H$_2$ activation accelerates the reaction. Computational studies revealed that the pincer ligand cooperativity assists both H$_2$ activation and reductive proton transfer to the nitride ligand giving rise to a relatively low kinetic barrier of the rate determining initial H$_2$ activation. Recycling of the hydrido ruthenium complex [RuH$_4$(*H*PNP^{tBu})] by protonolysis followed by reaction with base and azide afforded the starting material in high yields. Overall, a synthetic cycle for hydrogenation of azide to NH$_3$ was presented (Scheme C-4). It was thus demonstrated, that the full hydrogenation of electron rich, nucleophilic nitrides is feasible, making use of a cooperative ligand for H$_2$ activation. Although this cooperativity of late transition-metal

amido moieties was already successfully applied in the catalytic hydrogenation of polar organic multiple bonds,[12] this is the first example of an organometallic substrate.

The strong π-basicity of the dialkylamido PNP ligand accounts for a ligand centered nucleophilicity. This type of ligand is thus an ideal building block to achieve metal-ligand cooperativity in stoichiometric bond activation reaction, exemplified by efficient hydrogenation of an organometallic substrate. The π-basicity of the nitrogen atom furthermore affects the electronic structure of coordinatively and electronically unsaturated ruthenium complexes. The versatile adjustment of π-donation of the PNP ligand by backbone functionalization enables the control of ground state spin multiplicity, thus will be an interesting goal for future developments if the adjustable electronic structure of these compounds can be translated into diverse reactivity, as well.

---

[12] a) S. E. Clapham, A. Hadzovic, R. H. Morris, *Coord. Chem. Rev.* **2004**, *248*, 2201; b) H. Grützmacher, *Angew. Chem.* **2008**, *120*, 1838; *Angew. Chem. Int. Ed.* **2008**, *47*, 1814.

D Zusammenfassung

Ziel der Arbeit war die Synthese und Charakterisierung von späten Übergangsmetall-komplexen in seltenen Koordinationsgeometrien und Oxidationsstufen. Die resultierenden ungewöhnlichen elektronischen Strukturen ermöglichen zumeist außergewöhnliche Reaktivität. Dafür wurde die Koordinationschemie von Ruthenium und Iridium Komplexen mit ethylenverbrückten amino HPNP Liganden untersucht. Dieser bietet vielfältige Möglichkeiten zur Funktionalisierungen durch Deprotonierung oder oxidative Dehydrierung des Ligandenrückgrats und eröffnet dadurch einen synthetischen Zugang zu Amido-, Imido-, Enamido- und Dienamido-Komplexen von späten Übergangsmetallen. Die starke π-Basizität des PNP-Fragments beeinflusst maßgeblich die elektronische Struktur der dargestellten elektronisch und koordinativ ungesättigten Komplexe. Die Dehydrierung des Ligandenrückgrats ermöglicht die elektronische Feinabstimmung der Donorstärke und folglich die Kontrolle der Spinmultiplizität im Grundzustand. Des Weiteren ist die π-Basizität verantwortlich für eine ligand-zentrierte Nucleophilie und ermöglicht es diesen Ligandentypen in Metall-Ligand Kooperativität zu partizipieren.

Die Untersuchung von d^6-d^8 dialkylamido PNP Komplexen von Schneider *et al.* lieferte bereits wichtige Informationen über die M-N π-Bindung in späten Übergangsmetall-komplexen und erlaubte die Einbeziehung und Verwendung dieses Ligandentyps in der bifunktionellen Katalyse.[1] Es wurde unter anderem gezeigt, dass Iridium(I)amido Komplexe [IrL{PNP^{iPr}}] (L = CO, COE oder C_2H_4) durch Deprotonierung von [IrL{HPNP^{iPr}}] erhalten werden können, welche sich als relativ robust gegenüber β-H Eliminierung erwiesen. Ein stark elektronenreiches Ir(PNP) Fragment in den dialkylamido Komplexen manifestierte sich einerseits aufgrund einer großen hypsochromen Verschiebung der C-O Streckschwingung bei [Ir(CO)(PNP^{iPr})] ($\Delta\nu = 68$ cm^{-1}) und andererseits durch eine starke Hochfeldverschiebung der Olefinsignale im ^{13}C NMR Spektrum bei [Ir(olefin)(PNP^{iPr})] ($\Delta\delta C_2H_4 = 22.1$ ppm; $\Delta\delta COE = 20.8$ ppm).[2]

In der vorliegenden Arbeit konnte gezeigt werden, dass der Ligand in *trans*-Stellung zum Stickstoffatom ebenfalls einen entscheidenden Einfluss auf die elektronischen Eigenschaften und somit den pK_a Wert von Übergangsmetall-Amido-Komplexen besitzt, welcher im Bereich von 7 Größenordnungen (in DMSO) innerhalb der Serie L = CO [pK_a = 14.9(3)], COE [pK_a = 16.0(4)], PMe$_3$ [pK_a = 22.0(1)] variiert. Der vorliegende pK_a-Trend konnte anhand einer

---

[1] a) A. Friedrich, Bifunctional *Transition Metal Amido Complexes: Cooperative H2 Activation and Catalytic Dehydrogenation, disertation*, TU München, 2010; b) J. Meiners, A. Friedrich, E. Herdtweck, S. Schneider, *Organometallics* **2009**, *28*, 633.

[2] A. Friedrich, R. Ghosh, R. Kolb, E. Herdtweck, S. Schneider, *Organometallics* **2009**, *28*, 708.

N→Ir→L *push-pull*-Interaktion erklärt werden, welche das N-Ir π^* Orbital (HOMO) stabilisiert, wenn der *trans*-ständige Ligand ein π-Akzeptor ist (z.B. CO oder Olefine). Wie bereits für [PdCl(PNP$^{i\text{Pr}}$)] berichtet,[3] wurde weiterhin eine hohe Nucleophilie des Amids in [Ir(PMe$_3$)(PNP$^{i\text{Pr}}$)] gegenüber C-Nucleophilen festgestellt. Daher greift das Stickstoffatom selektiv Methyltriflat ohne Bildung eines Iridium(III)methyl-Komplexes an.

Die molekulare Struktur und Reaktivität von Übergangsmetallkomplexen ist maßgeblich von der Spinmultiplizität bestimmt. Metallkomplexe mit einer d^6 Konfiguration können prinzipiell eine low-spin (S = 0), intermediate-spin (S = 1) oder eine high-spin (S = 2) Konfiguration ausbilden. Eine quadratisch-planare Koordinationsgeometrie (D_{4h}) resultiert in einer Aufspaltung der *d*-Orbitale in nichtbindende d_{xy} (b_{2g}) als auch d_{xz}, d_{yz} (e_g), schwach antibindende d_{z^2} (a_{1g}), und antibindende $d_{x^2-y^2}$ (b_{1g}) Orbitale. Im Falle von 3*d* Metallen wird eine high-spin Konfiguration für Fe^{II} und Co^{II} mit schwachen Ligandenfeld erhalten.[4] Für d^6 Komplexe mit stärkeren Ligandfeld (Schema C-1, A) wird dagegen ein intermediate spin (S = 1, $(xy,yz,z^2)^5(xz)^1(x^2-y^2)^0$) erwartet, beispielsweise in Eisen(II)porpyrinato- und Eisen(II)bis(dithiolato)-Komplexen. Im Gegensatz dazu sind Beispiele der schweren Homologen sehr selten und die wenigen in der Literatur beschriebenen weisen eine intermediate-spin Konfiguration auf (Schema C-1, B). Ungeachtet dessen wurde in dieser Arbeit der erste quadratisch-planare Ruthenium(II) Komplex mit einer low-spin Konfiguration vorgestellt. Während die sterisch anspruchsvollen ^{t}Bu-Gruppen eine quadratisch planare Anordnung stabilisiert, destabilisiert die starke N→Ru π-Donation des dialkylamido PNP Liganden das d_{xz} Orbital und begünstigt eine low-spin Konfiguration (S = 0, $(xy,yz,z^2)^6(xz)^0(x^2-y^2)^0$) (Schema C-1, C) durch Überkompensation der notwendigen Spinpaarungsenergie. Bemerkenswerterweise zeigen ^{1}H und ^{31}P NMR Spektren der diamagnetischen Verbindung ungewöhnliche, temperaturabhängige chemische Verschiebungen der PNP Rückgrat-Protonen und der Phosphoratome. Die Beobachtung wurde mit der Besetzung eines angeregten, energetisch niedrig liegenden Triplett-Zustandes erklärt. Ein numerisches Fitten der NMR spektroskopischen Daten als Funktion der Temperatur ermöglichte es die thermodynamischen Parameter des Singulett-Triplett-Übergangs (ΔH = 10.6 ± 0.3 kJ mol^{-1}; ΔS = 4.2 ± 0.8 J mol^{-1} K^{-1}) abzuschätzen, was anhand von DFT Rechnungen bekräftigt werden konnte.

[3] A. N. Marziale, E. Herdtweck, J. Eppinger, S. Schneider, *Inorg. Chem.* **2009**, *48*, 3699.

[4] S. A. Cantalupo, S. R. Fiedler, M. P. Shores, A. L. Rheingold, L. H. Doerrer, *Angew. Chem.* **2012**, 124, 1024; *Angew. Chem. Int. Ed.* **2012**, *51*, 1000.

$d_{x^2-y^2}$ (b_{1g})

d_{z^2} (a_{1g})

d_{xz} d_{yz} (e_g)

d_{xy} (b_{2g})

A **B** **C**
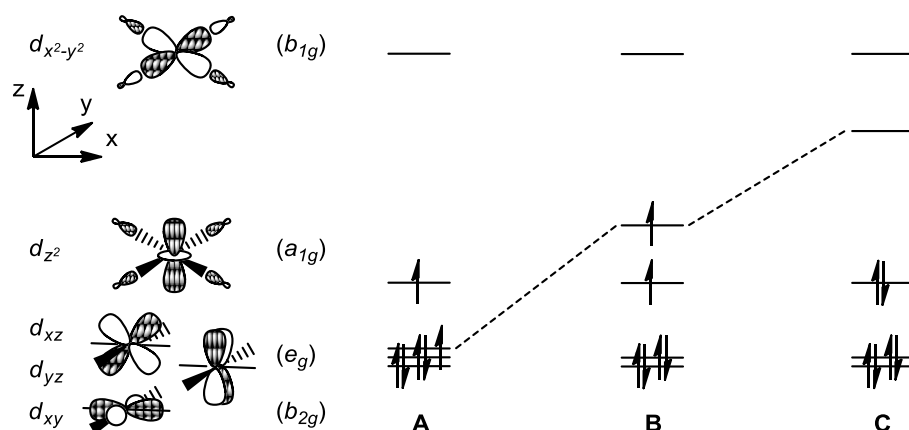
Schema D-5: Qualitatives *d*-Orbitalschema von quadratisch-planaren d^6 Komplexen mit reinem σ-Donor Liganden (A), mit einem schwachen π-Donor Ligand (B), und einem starken π-Donor Liganden (C).

Der Austausch des dialkylamido gegen den disilylamido Liganden von Caulton mit einem schwächeren N→Ru π-Donor resultiert in einer unterschiedlichen Spinmultiziplität (S = 1).[5] Die N→Ru π-Donorstärke des dialkylamido PNP Liganden konnte ebenfalls durch Dehydrierung von einer oder beiden Ethylenbrücken des PNP-Rückgrats zu Vinyl-Substituenten (Schema C-2) verringert werden, da diese als π-Akzeptoren fungieren. Infolge dessen wird ebenfalls ein intermediate spin Grundzustand favorisiert. NMR spektroskopische und SQUID magnetische Daten der paramagnetischen Komplexe stehen in Einklang mit zwei ungepaarten Elektronen bei Raumtemperatur. $\chi_M T$ fällt jedoch bei niedrigen Temperaturen auf nahezu Null ab, was für einen nichtmagnetischen Grundzustand spricht. Durch Fitten der magnetischen Daten mit einem Spin-Hamiltonian-Modell wurde eine beachtliche, positive axiale Nullfeldaufspaltung (ZFS) beim Enamido (D = +392 cm^{-1}) und beim Dienamido (D = +232 cm^{-1}) Komplex erhalten. Dies deutet auf eine weitere Aufspaltung des Spin Triplett Grundzustand in den nichtmagnetischen $|S = 1, M_S = 0\rangle$ Mikrozustandes und dem Kramer Doublett $|S = 1, M_S = \pm1\rangle$ bei höherer Energie hin. Ein gradueller Spinübergang anstelle einer Nullfeldaufspaltung konnte anhand der Invarianz in der Ru-N Bindungslänge [1.994(2) Å] als auch im N-Ru-Cl Winkel (180.0 °) in der Molekülstruktur des Dienamido Komplexes im Einkristall über einen breiten Temperaturbereich (30 − 200K) ausgeschlossen werden. Die Feinabstimmung der elektronischen Eigenschaften durch einfache Dehydrierung des

[5] L. A. Watson, O. V. Ozerov, M. Pink, K. G. Caulton, *J. Am. Chem. Soc.* **2003**, *125*, 8426.

Liganden-Rückgrats zu den entsprechenden Enamido und Dienamido Liganden ermöglichte folglich die Kontrolle der Spinmultiziplität.
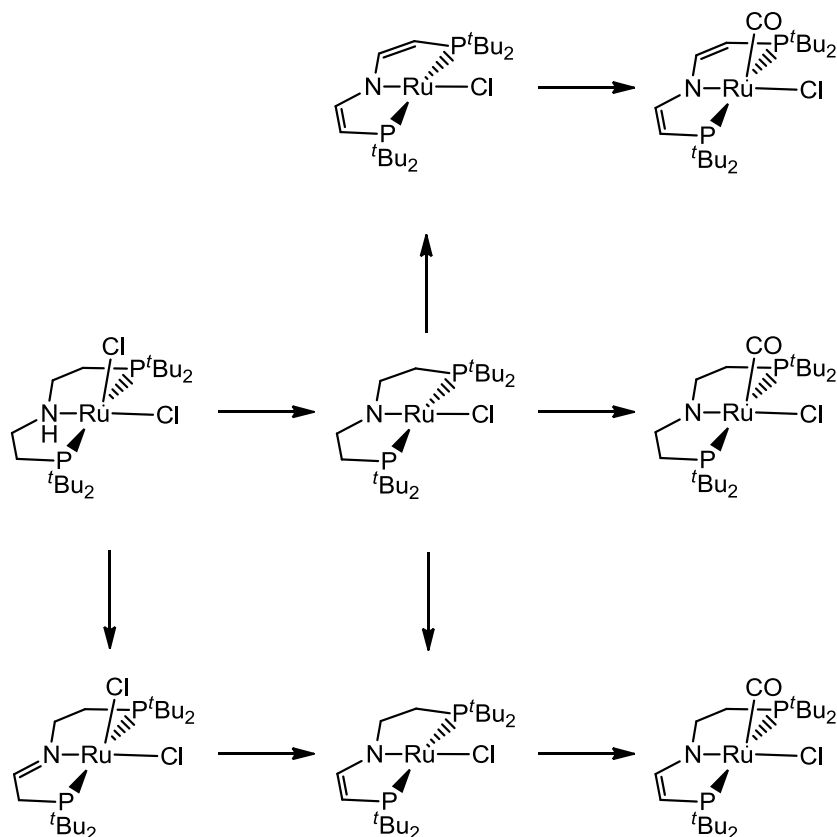
Schema D-6: Übersicht über quadratisch planaren Ruthenium dialkylamido PNP Komplexe und verwandte fünffach-koordinierte Carbonyl-Komplexe.

Anhand der CO-Streckschwingungen der zugehörigen fünffach-koordinierten Carbonyl-Komplexe konnte der elektronische Einfluss der Rückgrat-Dehydrierung abgeschätzt werden (Schema D-2). Die korrespondierenden CO Streckschwingungen treten dabei in einem sehr engen Bereich mit weniger als 30 cm^{-1} auf (ν_{CO} = 1888 cm^{-1} für den Amido-, ν_{CO} = 1896 cm^{-1} für den Enamido- und ν_{CO} = 1916 cm^{-1} für den Dienamido-Rutheniumkomplex). Die erhaltene Verschiebung der Streckschwingung reflektiert den Einfluss der Rückgrat-Dehydrierung: die oxidative Funktionalisierung des Liganden reduziert die N→Ru Elektronendonation, welche auf die Stabilisierung des freien Elektronenpaares am Stickstoff durch eine Überlappung der C(p)-N(p)-Orbitale zurückgeführt werden kann.

Die koordinativ und elektronisch ungesättigten 14 VE Komplexe konnten als geeignete Plattform für die Stabilisierung von Liganden mit Mehrfachbindung eingesetzt werden. Das entsprechende Ru[IV]-Nitrid konnte in hohen Ausbeuten via Salzmetathese nach anschließender N_2 Eliminierung erhalten werden (Schema C-3). Dieses seltene Beispiel für einen terminalen Nitrido-Komplex mit einer d[n]-Elektronenzahl von n > 2 weist eine größere Ru≡N Bindungslänge und schwächere Streckschwingungen als der vergleichbare Komplex von Caulton mit disilyamido PNP Liganden auf ($\Delta d = 0.06$ Å and $\Delta\nu_{Ru\equiv N} = 54$ cm^{-1}). Dies suggeriert eine schwächer Bindung, welche anhand der stärkeren π-Donorfähigkeit des dialkylamido PNP Ligand erklärt werden kann.[6] Beide Molekülstrukturen weisen jedoch eine beachtliche Abwinklung der N-Ru-N Bindung aufgrund der *trans*-Konfiguration von zwei π-Donoren auf. Eine hohe Nucleophilie des Nitrido Liganden konnte einerseits anhand der Inertheit gegenüber Posphanen und andererseits anhand einer ungewöhnlichen N-C Kupplung mit π-aciden CO (Schema D-3) nachgewiesen werden. Die selektive Bildung des Isocyanato-Komplexes ist gegensätzlich zu Caultons terminalen Nitrid. Die beobachtete Reaktivität liegt möglicherweise im schwächeren nucleophilen Charakter des Nitrido Liganden begründet.[7]
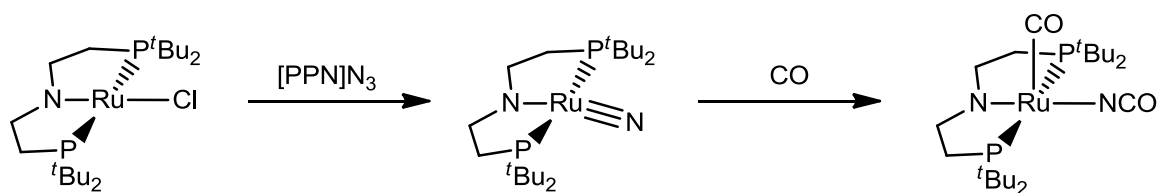
**Schema D-7:** Synthese des Ru[IV]-Nitrids und N-C-Kupplung mit π-aciden CO.

Die Funktionalisierung von Stickstoff unter milden Bedingungen stellt nach wie vor eine große Herausforderung dar. Nitrido-Komplexe können dabei als Modellverbindungen für die Untersuchung der Hydrierung von N_2 zu Ammoniak unter milden Bedingungen auf dem Weg zu einem homogen Katalysator dienen. Terminale Nitride, insbesondere Caultons, sind abgesehen von wenigen Ausnahmen erstaunlich inert gegenüber Wasserstoff.[9,8] Folglich wurde nur über eine teilweise M-N Bindungshydrolyse berichtet und kein Beispiel für die

[6] A. Walstrom, M. Pink, X. Yang, J. Tomaszewski, M.-H. Baik, K. G. Caulton, *J. Am. Chem. Soc.* **2005**, *127*, 5330.

[7] A. Walstrom, H. Fan, M. Pink, K. G. Caulton, *Inorg. Chim. Acta* **2010**, *363*, 633.

[8] M. P. Shaver, M. D. Fryzuk, *Adv. Synth. Catal.* **2003**, *345*, 1061.

stöchiometrische Hydrolyse eines Nitrido Liganden mit H_2 zu Ammoniak beschrieben.[9] Im Gegensatz dazu reagiert das vorgestellte Ru^{IV}-Nitrid mit dialkylamido PNP Liganden bereits bei relativ milden Bedingungen (50 °C, 1 bar H_2) zu dem Polyhydrid-Komplex [RuH_4(HPNP^{t}Bu$_4$)] unter der Bildung von Ammoniak in hohen Ausbeuten von 85% (Schema D-4).
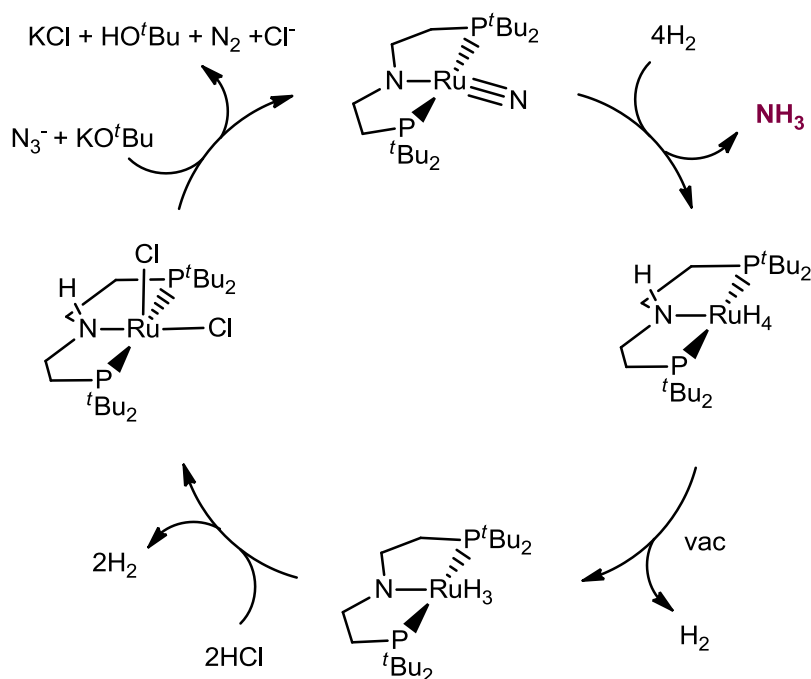
Schema D-8: Synthetischer Zyklus für die Hydrierung von Azid zu Ammoniak.

Die Ausbeute an Ammoniak steigt bei niedrigerer Reaktionstemperatur, jedoch zu Lasten einer langsameren Reaktion. Vorläufige mechanistische Studien sprechen für eine Reaktion Pseudo-Erster Ordnung (k_{298} = 5.1 x 10^{-3} h^{-1} ± 0.1) und einem kinetischen Isotopeneffekt (KIE) von k_H/k_D = 1.3 ± 0.2. Des Weiteren weisen die kinetischen Messungen und DFT Studien darauf hin, dass die initiale, heterolytische Spaltung von Wasserstoff entlang der Ruthenium-Amido-Bindung und der erste Protonentransfer zum Nitrido Ligand als geschwindigkeitsbestimmende Schritte darstellt, gefolgt von der stufenweisen Protonentransferreaktion des Nitrids via Imido-, Amido-, und Amino-Intermediaten. Aufgrund der beobachteten Reaktivität wurde der Ru(PNP) Plattform zwei Besonderheiten zugesprochen: (1) Die niedrige formale Oxidationsstufe des Metallzentrums in Kombination mit der erwähnten π-Donation des Amido Liganden in *trans*-Stellung (mit seiner ungünstigen

[9] a) S. D. Brown, M. P. Mehn, J. C. Peters, *J. Am. Chem. Soc.* **2005**, *127*, 13146; b) J. Schöffel, A. Y. Rogachev, S. DeBeer George, P. Burger, *Angew. Chem.* **2009**, *121*, 4828; c) J. Schöffel, A. Y. Rogachev, S. DeBeer George, P. Burger, *Angew. Chem. Int. Ed.* **2009**, *48*, 4734.

N-Ru-N 3z-4e π-Wechselwirkung) tragen zu einem hohen nucleophilen Charakter des Nitrido Liganden bei und verursachen eine Schwächung der Ru≡N Bindung. (2) Die Metall-Ligand kooperative H_2 Aktivierung beschleunigt die Reaktion. DFT Studien offenbaren, dass der Pinzetten-Ligand sowohl die H_2 Aktivierung als auch den reduktiven Protonentransfer zum Nitrido Liganden unterstützt, was sich wiederum in einer niedrigen Barriere für die geschwindigkeitsbestimmende H_2-Aktivierung widerspiegelt. Das Recycling des Polyhydrido-Ruthenium Komplexes [RuH$_4$(*H*PNP^{tBu})] über die Reaktion mit Salzsäure gefolgt von Azid und Base ermöglichte die Rückgewinnung des Eduktes in hohen Ausbeuten. Insgesamt konnte somit ein synthetischer Zyklus für die Hydrierung von Azid zu Ammoniak vorgestellt werden (Schema D-4). Folgloch konnte gezeigt werden, dass die vollständige Hydrierung von elektronenreichen, nucleophilen Nitriden unter Einbeziehung eines koopeartiven Liganden für die H_2-Aktivierung möglich ist. Obwohl diese Kooperativität von späten Übergangsmetallkomplexen mit funktionellen Amido-Gruppen bereits erfolgreich in der katalytischen Hydrierung von polaren organischen Mehrfachbindungen eingesetzt wurde, [10] ist dies das erste Beispiel für ein metallorganisches Substrat.

Die starke π-Basizität des dialkylamido PNP Liganden führt zu einer ligandenzentrierten Nucleophilie. Dieser Ligandtyp stellt daher einen idealen Baustein dar, welcher Metall-Ligand Kooperativität in der stöchiometrischen Bindungsaktivierung ermöglicht. Diese konnte in der effizienten Hydrierungen von metallorganischen Substraten angewendet werden. Die π-Basizität des Stickstoffatoms beeinflusst weiterhin die elektronische Struktur von koordinativ und elektronisch ungesättigten späten Übergangsmetallkomplexen. Die vielfältige Funktionalisierung des Rückgrats ermöglicht die Kontrolle der Spinmultiziplität des Grundzustandes und stellt daher ein interessantes Ziel für zukünftige Entwicklungen dar, vor allem wenn die steuerbare elektronische Struktur in eine unterschiedliche Reaktivität übersetzt werden kann.

---

[10] a) S. E. Clapham, A. Hadzovic, R. H. Morris, *Coord. Chem. Rev.* **2004**, *248*, 2201; b) H. Grützmacher, *Angew. Chem.* **2008**, *120*, 1838; *Angew. Chem. Int. Ed.* **2008**, *47*, 1814.

E List of publications

List of publications

1 Journal publications

(1)   **"**A Square-Planar Ruthenium(II) Complex with a Low-Spin Configuration."

B. Askevold, M. M. Kushniyarov, E. Herdtweck, K. Meyer, S. Schneider, *Angew. Chem.* **2010**, 122, 7728-7731; *Angew. Chem. Int Ed.* **2010**, 49, 7566-7569.

(2)   "Ammonia formation by metal–ligand cooperative hydrogenolysis of a nitrido ligand."

B. Askevold, J. Torres Nieto, S. Tussupbaysev, M. Diefenbach, E. Herdtweck, M.C. Holthausen, S. Schneider *Nature Chem.* **2011**, *3*, 532-537.

(3)   "Cooperative Aliphatic PNP Amido Pincer Ligands – Versatile Building Blocks for Coordination Chemistry and Catalysis."

S. Schneider, J. Meiners, B. Askevold, *Eur. J. Inorg. Chem.* **2012**, 412-429.

(4)   "Learning from the Neighbours: Improving Homogeneous Catalysis with Functional Ligands Motivated by Heterogeneous and Biocatalysis."

B. Askevold, H. W. Roesky, S. Schneider, *ChemCatChem*, **2012**, *4*, 307-320.

(5)   "Closed-Shell and Open-Shell Square-Planar Iridium Nitrido Complexes."

M. G. Scheibel, B. Askevold, F. W. Heineman, E. J. Reijerse, B. d. Bruin, S. Schneider, *Nature Chem.*, **2012**, *accepted*.

2 Oral presentations

(1)   "Four-coordinate Ru(II) amido PNP-pincer complexes."

2010, 240th ACS National Meeting Boston, USA.

(2)   "Square-planar ruthenium-platforms: Unusual spin-states and nitride ligand hydrogenolysis to ammonia."

2011, Koordinationschemie-Treffen Stuttgart, Germany.

(3)   Eletron-rich nitrido complexes of ruthenium and iridium,

2011, WEB, Erlangen, Germany

F Curriculum Vitae

Personal Information

Name	Björn Birger Askevold
Date of Birth:	05.07.1982
Place of birth	Starnberg, Germany

Education

08/1989 – 07/1993	Elementary School Feldafing
08/1993 – 07/2002	Gymnasium Starnberg
	Participation on international Student Exchange Program „La Villette" in Paris, France
	Student Program at Alexanders International School in London, England
	Diploma: Abitur

Civil Service

09/2002 – 06/2003	Bavarian Red Cross Institution Starnberg
	Ambulance Driver

Medical Training

07/2003 – 09/2003	Ambulance Officer

University

10/2003 – 10/2006	Technical University Munich
	Bachelor Degree Chemistry
10/2006 – 11/2008	Technical University Munich
	Master Degree Chemistry
	Supervisor Dr. Eppinger at the chair of inorganic chemistry Prof. Dr. Herrmann
01/2009 – 05/2012	PhD in organometallic chemistry at the Technical University Munich, supervised by Prof. Dr. Schneider at the chair of Prof. Dr. Herrmann
	Funding from NANOCAT, part of Elitenetzwerk Bayern
	Member of TUM graduate school
	Participation at Minerva school for alternative energy 2011, Nazareth, Israel

Internship

03/2005 – 04/2005	Internship at Linde AG in Höllriegelskreuth „Analysis of special gases"
03/2006 – 04/2006	Research Internship at the National University of Singapore Prof. Dr. Jaenicke „Oxidation of Benzene"

08/2006 – 09/2006	Research Internship at the Eidgenössischen Universität Zürich, Switzerland, Prof. Dr. Nesper „Synthesis and positioning of Nanotubes"
10/2007 – 11/2007	Internship at Südchemie AG in Richards Bay, South Africa „Commission of a new production line"
10/2008 – 12/2008	Internship at Südchemie AG in Heufeld „Synthesis of WGS catalysts"
10/2011 – 11/2011	Internship at ECKART GmbH in Hartenstein „Optical properties of CVD particles"